Universitat Internacional de Catalunya
Facultat de Ciències Bàsiques

Tesis doctoral

Role of CPT1C in breast cancer development and chemoresistance.

Helena Muley Vilamú

UNIVERSITAT INTERNACIONAL DE CATALUNYA

FACULTAT DE MEDICINA

DEPARTAMENT DE CIÈNCIES BÀSIQUES

Role of CPT1C in breast cancer development and chemoresistance

Helena Muley Vilamú

Sant Cugat del Vallès, 2021

UNIVERSITAT INTERNACIONAL DE CATALUNYA

FACULTAT DE MEDICINA

DEPARTAMENT DE CIÈNCIES BÀSIQUES

Role of CPT1C in breast cancer development and chemoresistance

Memòria presentada per Helena Muley Vilamú per optar al títol de doctor per la Universitat Internacional de Catalunya.

Treball realitzat en el Departament de Ciències Bàsiques de la Universitat Internacional de Catalunya, sota la co-direcció de les doctores Núria Casals Farré i Rut Fadó Andrés.

Programa de Doctorat en Ciències de la Salut de la Universitat Internacional de Catalunya.

Sant Cugat del Vallès, 2021.

Núria Casals Farré

Directora de tesi

Rut Fadó Andrés

Co-directora de tesi

Helena Muley Vilamú

Doctoranda

ACKNOWLEDGMENTS

(AGRADECIMIENTOS)

AGRADECIMIENTOS

Echo una mirada a atrás y se me llena la boca solo de agradecimiento. Al trasladarme a la prehistoria de esta tesis, aparece una primera persona, que es Núria. Aparecí yo cual paracaidista en la UIC y además en doble caída, y a pesar del aterrizaje abrupto, Núria me dio la oportunidad de embarcarme en este doctorado, en el mundo de la investigación y en esta pequeña gran universidad. Ella, Josep, María, Javi… cuando aún Ciencias Básicas habitaba entre la pecera y el búnker, entre el lado claro y el lado oscuro me dieron siempre una incondicional acogida y me introdujeron en esta familia de Ciencias Básicas de la UIC.

Rosi, Marta Palomo y Xavi fueron los primeros en echarme una mano en el laboratorio. De ellos aprendí las primeras técnicas y a manejarme de nuevo entre pipetas. Siempre tuvieron una disposición de ayuda incluso para acabarme algún experimento cuando tenía que irme corriendo a trabajar a la farmacia de avinguda del Paral·lel los primeros meses de incorporación.

Llegó el momento de empezar la travesía de la tesis, iba a pisar el sendero con más doctorandos. Por todo el tiempo compartido y lo vivido, Cris, María y Abril han sido piezas clave para vivir esta tesis con sentido del humor, incluso disfrutándola tanto dentro como fuera del laboratorio. Las “marxes pel Montseny” con el fiel Tro incluido, barbacoas, cenas, comidas en el kebab… A Abril debo agradecerle en concreto su ayuda y consejos en algunas técnicas en cáncer que en nuestro grupo no utilizábamos… Enseguida, otros rostros sonrientes fueron apareciendo: Èlia, Leire, Bego… con esos partidos de pádel de expertas-aficionadas, Núria M incluso en las horas y días más intempestivos. A la pregunta: ¿Hay alguien allí? Difícilmente uno se iba sin respuesta…, “Reye” la gran compañera del FACs, Bárbara una gran teacher de un último experimento de la tesis.... Al poco tiempo, apareció “Fosqui”, conocida también por “pilas duracell y duran y duran”, para vivir la vida con intensidad por contagio ;), y ¡Andrea! facilitando siempre todo para poder hacer los últimos experimentos de la tesis e implicándose 100% en la causa. Y cómo no, las nuevas incorporaciones del laboratorio Cris enseñándome uno de los últimos experimentos de la tesis y compartiendo también recorridos montañeros (Mura, el Puig…) Y, Rocío, Anna, Jesús, Xavi, Sebas, Ana, Blanca… siempre dando ánimos en esta etapa final de la tesis. Los más veteranos siempre han estado dispuestos a echar una mano cuando hacía falta: Miguel, Laura (mano a mano en cultivos), Miguel, Mariana, Pau, Marta Pérez, Samu, Bob, Eva… También ¡Vero! “tante grazie”! y a ¡Erola y Tatiana! animando en las comidas en que coincidíamos. Y tantos más de la UIC con los que me cruzo habitualmente en el laboratorio y en los largos pasillos de la UIC y que los recorren con una

sonrisa de oreja a oreja incluso con mascarilla. A todos ellos les agradezco mucho su ayuda y compañía de estos años.

Me gustaría hacer una mención especial a mis dos co-directoras. Bea M. me co-dirigió solo el primer curso y medio de tesis ya que tuvo que desplazarse a Pamplona por motivos familiares. Pero la distancia no fue motivo para dejar de estar pendiente y cercana. A los pocos meses de estar trabajando en el CIMA (Centro de Investigación Médica Aplicada), sabiendo lo complicada que estaba siendo mi tesis, Bea me abrió la posibilidad de ir al CIMA a hacer unos experimentos que serían clave para seguir adelante con la tesis. Los hice en el grupo de Fernando Lecanda, al que también estoy muy agradecida. Bea es una anfitriona de bandera, es una persona que consigue generar alrededor un gran clima de confianza en cuestión de minutos. Ella, con Patxi e Irati, me hicieron ¡los mejores "tour's" gastronómicos e artísticos por Pamplona! En el CIMA también encontré otro lugar donde se trabaja con intensidad, pero con gusto ¡por el buen ambiente que se respira! Allí Susana, las Cris'es, Haritz, Montse, Luís… me acogieron como una más. Gracias también a esta primera estancia ¡tuve la suerte de conocer a Karmele! Se dejó invitar a dar un seminario a la UIC y allí ella me abrió las puertas a una segunda estancia en el CIMA también muy enriquecedora. Le agradezco mucho su gran apoyo en esta etapa final de la tesis.

De Rut, mi segunda co-directora, debo decir que me siento muy afortunada de haberle tenido como co-directora. Debo destacar el mérito que tuvo embarcarse a codirigir la tesis ya comenzada. De forma incondicional siempre ha estado disponible para ayudar incluso en días y horas en que no tendría por qué haberlo estado. He aprendido mucho de ella. También agradezco su sinceridad y claridad a pesar de que exigir y corregir siempre cuesta, y más a veces cuando el de enfrente se pone farruco.

En este final de la tesis, debo agradecer también a la Dra. Ariadna Tibau, incluso en tiempos de pandemia, teniendo poco tiempo por la dedicación a su familia y a sus pacientes oncológicos en el hospital, se ha revisado toda la parte clínica de la tesis, aparte de resolverme dudas siempre que lo necesitaba.

Y por supuesto, un papel primordial y fundamental en los agradecimientos lo ocupa mi familia, todas aquellas personas que cuando volvía a casa me recibían con una sonrisa preguntándome y animándome, compartiendo alegrías y penas de la tesis, aprendiéndose el nombre impronunciable de "Carnitina palmitoil transferasa 1C", arrimando más el hombro para que yo pudiera dedicarle el extra de tiempo del final de tesis, y mis padres, mis hermanos, mis cuñados… Y tantas amigas que han seguido tan de cerca cada paso de la

tesis. Aquí estáis presentes muchísimas personas a las que espero poder agradeceros pronto de palabra si aún no lo he hecho.

Como dice el proverbio africano “Si quieres ir rápido ve solo, si quieres llegar lejos ve acompañado”. Gracias a Dios he podido recorrer este camino del segundo modo. Cuando uno ha recibido tanto, le vienen ganas de agradecer, pero sobretodo de intentar devolver lo recibido. Esto me lo tomo como tarea de vida y por tanto en *lei motiv* para la etapa que se abre a continuación.

ABSTRACT

ABSTRACT

Carnitine palmitoyl transferase 1 (CPT1) are enzymes that catalyze the conversion of long-chain acyl-CoA to acyl-carnitines, to transport long-chain fatty acids across intracellular membranes. CPT1C isoform is highly different respect the other CPT1 isoforms. It is located in the endoplasmic reticulum of cells, rather than in mitochondria, and it does not have catalytic activity. An animal model deficient in CPT1C and the interactions described between CPT1C and other proteins have related CPT1C with major functions as cognition, motor function, and energy homeostasis.

In 2011, it was first showed that CPT1C was overexpressed in many human cancers conferring them higher cell survival and tumor growth under conditions of metabolic stress, like hypoxia or glucose deprivation. Several publications have confirmed the crucial role of CPT1C in cancer development.

The aim of our work was to study whether CPT1C promoted proliferation, migration, invasion and chemotherapy resistance in breast cancer cells, using triple-negative cancer MDA-MB-231 cells as a model. Several assays showed that CPT1C silencing increases cell proliferation and cell invasion; however, it does not impair cell migration. Interestingly, CPT1C silencing also increases cell survival to doxorubicin or paclitaxel treatment, in several breast cancer cell lines. This effect was explained by a reduced drug influx, as demonstrated in doxorubicin uptake assays in CPT1C-silenced MDA-MB-231 cells.

Doxorubicin is a drug that enter cell mainly through passive diffusion and this drug transport is highly dependent on plasma membrane lipid composition. For this reason, we performed a lipid analysis of plasma membrane enriched fractions of MDA-MB-231 cells by liquid chromatography-high resolution mass spectrometry (LC-HRMS). We confirmed that, under CPT1C silencing, there is a lipid plasma membrane remodeling giving rise a more rigid membrane and thus, less permeable to drugs.

All these results match with the Kaplan-Meier Plotter and ROC plotter analysis that correlates lower expression of CPT1C in HER2-positive and triple-negative human breast tumors with worse prognosis and lower pathological complete response, pointing out CPT1C as a novel tumor prognostic marker in the treatment of breast cancer.

PRESENTATION

(PRESENTACIÓN)

PRESENTACIÓN

Mi interés por la investigación despertó en los últimos años de la carrera de farmacia, donde tuve la oportunidad de realizar dos asignaturas optativas dedicadas exclusivamente al trabajo de laboratorio y colaborar con tesis sobre Química farmacéutica. De allí surgió mi interés en hacer un doctorado. Gracias a una amiga conocí el grupo de investigación liderado por la Dra. Núria Casals en la Universitat Internacional de Catalunya. Un grupo focalizado mayoritariamente en el ámbito de las neurociencias. La investigación llevada a cabo en el grupo, el buen ambiente que se respiraba en la institución y la posibilidad de adquirir también experiencia en docencia universitaria fueron parte de las motivaciones que me llevaron a embarcarme en este proyecto de tesis.

Estas tres motivaciones han seguido presentes a lo largo de toda la tesis. Sin embargo, los vaivenes en la temática han añadido emoción al proceso. Inicialmente, el proyecto de tesis se basó en el estudio de una de las funciones de CPT1C en el ámbito de las neurociencias. Se trataba de estudiar cómo esta proteína podía regular la síntesis de ceramidas a través de una potencial proteína interactora, la neutral esfingomielinasa 1. Después de prácticamente un año, decidimos abandonar el proyecto al no confirmarse la interacción. No obstante, esa temporada pude aprender varias técnicas interesantes, como hacer clonajes, mutagénesis dirigidas, ensayos de FRET (transferencia de energía de resonancia de Förster), immunoprecipitación y click-chemistry.

De este modo, a finales del primer año, la tesis viró al ámbito del cáncer. Un campo nuevo en el grupo, pero que tenía en común con el proyecto anterior a la proteína de estudio, la CPT1C. Esta proteína, que está presente solo en neuronas, se demostró por primera vez en 2011 que se encontraba también en células cancerosas. ¿Qué ventajas debía conllevar CPT1C para que células normales de cualquier tejido del organismo optaran por expresar esta proteína al transformarse en cancerosas? La idea era explorar el mecanismo de resistencia llevado a cabo por CPT1C en situaciones de estrés metabólico como ausencia de glucosa e hipoxia en distintos tipos de células cancerosas (especialmente pulmón, pero también colon y mama). Este tipo de resistencia ya había sido demostrada por Zaugg et al., pero faltaba abordar el mecanismo implicado.

Después de algunos resultados preliminares, decidimos estudiar el papel de CPT1C en el cáncer de mama. Este tipo de tumor se desarrolla en un microambiente altamente enriquecido en lípidos, por lo que una proteína como CPT1C, que interviene en el metabolismo lipídico, podría tener especial interés. Por otra parte, vimos que un modelo de inhibición podía ser

más adecuado que el de sobrexpresión ya que las células cancerosas en general ya sobreexpresan CPT1C. A su vez, consideramos interesante explorar otros ámbitos del cáncer como la migración, invasión y quimioresistencia. Este proyecto no llegó a consolidarse hasta junio de 2018, es decir, finalizando el 2º año de tesis. Fue en gran parte gracias a mi anterior co-directora de tesis que se desplazó por trabajo al CIMA (Centro de Investigación Médica Aplicada), en Pamplona. Fue ella quién me sugirió ir al CIMA a utilizar el sistema RTCA xCELLigence para analizar proliferación, migración, invasión y quimioresistencia en líneas cancerosas de mama en el grupo del Dr. Fernando Lecanda. El resultado de esa estancia, de pocas semanas, supuso un respiro al darme por fin los primeros resultados consistentes de la tesis. A partir de entonces, se trató de confirmar esos resultados mediante otras técnicas. En los 2 últimos años he tratado de profundizar en el mecanismo de resistencia observado. Una segunda estancia de 2 meses, y gracias a la ayuda de la Dra. Karmele Valencia, me permitió reproducir el fenotipo de resistencia en mamosferas y colaborar en un experimento in vivo.

El fenotipo de quimioresistencia identificado en esta tesis nos sorprendió desde el principio, También gracias al feed-back de la Dra Valencia que nos dio su parecer después de invitarle a dar un seminario en nuestra universidad. Ella nos apuntó el potencial interés clínico de estos resultados. A raíz de esta reunión iniciamos un proyecto de colaboración con el Dr. Miguel Ángel Carrasco, jefe del servicio de Anatomía Patológica del Hospital General de Catalunya. El objetivo de este proyecto era el estudio de la expresión de CPT1C en muestras tumorales de pacientes de cáncer de mama y relacionarlo también con respuesta a quimioterapia. Una de las reuniones que tuvimos con uno de los médicos oncólogos especialistas en cáncer de mama del hospital nos animó aún más en este proyecto ya que manifestó el gran interés que podía tener para su práctica clínica disponer de un marcador más que predijera si un tumor iba a responder o no a un tratamiento de quimioterapia. No obstante, surgió una dificultad técnica que nos obligó a abandonar el proyecto. Al no existir un buen anticuerpo en el mercado anti-CPT1C para inmunohistoquímica, la única opción posible era analizar la expresión de CPT1C por WB. Esto suponía hacer una desparafinización y posterior extracción proteica de las muestras tumorales parafinadas. Después de varios intentos de puesta a punto, sumado a la poca calidad del único anticuerpo de CPT1C disponible en el mercado en ese momento, tuvimos que abandonar esta proyecto.

Visto en perspectiva, la evolución de esta tesis y en línea con lo que comentaba en los agradecimientos, veo sobre todo lo positivo que me ha supuesto esta trayectoria. Es cierto que la tesis ha venido más decorada por intentos fallidos que por logros. No obstante, cada nuevo intento ha conllevado un crecimiento en resiliencia, en paciencia, en capacidad de

autocrítica, en disfrutar del proceso, y no solo en el resultado, y en recordar qué es lo más importante en la vida. A su vez, el hecho de estar en un grupo de investigación especializado en neurociencias y no en cáncer, de forma más imperativa me ha llevado a buscar recursos y aprender nuevas técnicas, también a veces de una forma más autónoma. Es cierto que trabajando así uno avanza mucho más lento debido a la dificultad añadida, pero, en cierto modo, te obliga a crecer más en esa búsqueda activa. No obstante, como ya he apuntado en los agradecimientos, esta búsqueda activa hubiera sido estéril si tantas personas, como otros doctorandos del grupo del Dr. Clotet especializado en cáncer, del grupo de la Dra. Casals, investigadores del CIMA y por supuesto, mi co-directora y directora de tesis no me hubieran echado una mano como tan generosamente han hecho constantemente y siempre que se lo he pedido.

En relación a la búsqueda activa, cabe mencionar lo mucho que me ha aportado la redacción de la review escrita y publicada durante la tesis. Es algo que me propusieron mis directoras de tesis. Supuso muchas horas de trabajo, pero el haber leído tanto alrededor de esta temática me ha dado ideas, me ha permitido ser más crítica, diseñar nuevos experimentos y, por tanto, en ocasiones llevar un papel más activo en el proyecto.

Otra experiencia interesante de esta tesis ha sido la asistencia a dos congresos internacionales. El primero se celebró en Ischia y se focalizó en el estudio de mecanismos de endocitosis. Allí presenté un póster y fue una primera toma de contacto con la experiencia de intercambiar ideas con grupos de investigación de todo el mundo. Un poco más retador fue el segundo congreso sobre metástasis en cáncer, ya que allí se me ofreció la oportunidad de impartir mi primera comunicación oral en un congreso internacional. Esta vez asistí con la Dra. Núria Casals. Allí pudimos también entrar en contacto y establecer alguna colaboración con otros grupos de cáncer de España.

En resumen, la mochila de experiencias enriquecedoras de esta tesis termina bien cargada. Las dificultades iniciales de la tesis me han permitido introducirme en el ámbito de investigación del cáncer, que me ha parecido apasionante. A su vez, aunque a largo plazo, la posible implicación clínica de este campo de estudio ha sido un plus añadido a la motivación presente a lo largo de la tesis.

TABLE OF CONTENTS

TABLE OF CONTENTS

ABBREVIATIONS

ABBREVIATIONS

ACC	acetyl-CoA carboxylase
µg	microgame
µl	microliter
µM	micromolar
2-AG	2-arachidonoylglycerol
ABHD6	serine hydrolase α/β-hydrolase domain 6
AMPAR	α-amino-3-hydroxyl-5-methyl-4-isoxazole-propionate-type glutamate receptor
AMPK	AMP-activated protein kinase
ATP	adenosine triphosphate
BMP	bis(monoacylglycero)phosphate
BSA	bovine serum albumine
CDK	cyclin-dependent kinase
CE	cholesteryl ester
Cer	ceramide
CFA	cyclophosphamide
CFP	cyan fluorescent protein
Chol	cholesterol
CL	cardiolipin
CME	clathrin-mediated endocytosis
CavME	caveolae-mediated
CIE	clathrin- and caveolin independent
CREB	cAMP response element-binding protein
DEPC	diethylpyrocarbonate
DFS	disease free survival
DG	diacylglycerol
dhCer	dihydroceramide
dhSM	dihydrosphingomyelin
DMEM	dulbecco's modified Eagle medium
DMFS	distant metastasis–free survival
DNA	deoxyribonucleic acid
D-PDMP	D-threo-1-Phenyl-2-decanoylamino-3-morpholino-1-propanol
DTT	dithiothreitol
DTX	docetaxel
E.Coli	Escherichia coli
EDTA	ethylenediaminetetraacetic acid
EGFR	epidermal growth factor receptor
EMT	epithelial–mesenchymal transition
ER	endoplasmic reticulum
ERRα	estrogen-related receptor α
EV	empty vector
FACS	fluorescence-activated cell-sorting
FAO	fatty acid oxidation
FAS	fatty acid synthase

FRET	fluorescence resonance energy transfer
GFP	green fluorescent protein
GluA1	α-amino-3-hydroxy-5-methyl-4-isoxazolepropionic acid
GOLPH 3	golgi phosphoprotein 3
H	trastuzumab
HEPES	4-(2-hydroxyethyl)-1-piperazineethanesulfonic acid
HER2	human epidermal growth factor 2
HexCer	hexosylceramide
HR	hormone receptor
HR	hazard ratio
IgG	immunoglobuline G
ILVs	intraluminal vesicles
Kbp	kilo-base pair
ko	knock-out
LB	lysogeny broth
Lcb	long chain base biosynthesis protein
LC-HRMS	liquid chromatography-high resolution mass spectrometry
LDLR	low density lipoprotein receptor
LDs	lipid droplets
LEs	late endosomes
LPC	lysophosphatidylcholine
LPE	lysophosphatidylethanolamine
MAG	monoacylglycerol
MBCD	methyl-beta-cyclodextrin
MCD	malonyl-CoA decarboxylase
ml	mililiter
mM	milimolar
mRNA	messenger ribonucleic acid
mTOR	mammalian target of rapamycin
MTS	3-(4,5-dimethylthiazol-2-yl)-5-(3-carboxymethoxyphenyl)-2-(4-sulfophenyl)-2H-tetrazolium inner salt
MTT	3-(4,5-dimethylthiazol-2-yl)-2,5-diphenyltetrazolium bromide
NCBI	national center for bitechnology information
ORP	oxysterol binding related proteins
OS	overall survival
OSBP	oxysterol-binding protein
P	pertuzumab
PAGE	polyacrylamide gel electrophoresis
PC	phosphatidylcholine
PCR	polymerase chain reaction
PDAC	pancreatic ductal adenocarcinoma
PE	phosphatidylethanolamine
PFA	paraformaldehyde
PG	phosphatidylglycerol
PGC-1β	peroxisome proliferator-activated receptor gamma coactivator-1-beta
PI	phosphatidylinositol
PI(4)P	phosphatidyl-inositol-4-phosphate

PITP	phosphatidylinositol transfer protein
PM	plasma membrane
PO4	phosphoric acid
PPARα	peroxisome proliferator-activated receptor alpha
PR	progesterone receptor
PS	phosphatidylserine
PVDF	polyvinylidene difluoride
RFS	relapse-free survival
RNA	ribonucleic acid
ROI	region of interest
rpm	revolution per minute
RT	room temperature
SAC1	phosphatidylinositol-3-phosphatase
SDS	sodium dodecyl sulphate
SLC	solute carrier
SM	sphingomyelin
T	taxane
TAE	tris acetate-EDTA
TAG	triglycerides
TBS-T	tris-buffered saline-tween
TfR	transferrin receptor
TGN	trans Golgi Network
TM	transmembrane
TNBC	triple-negative breast cancer
VAP	VAMP-associated protein
vs	versus
WT	wild-type
YFP	yellow fluorescent protein

INTRODUCTION

INTRODUCTION

1. The protein CPT1C

1.1. Expression, activity and molecular structure

Carnitine palmitoyl transferase 1's (CPT1) proteins are enzymes that catalyze the conversion of long-chain acyl-CoA to acyl-carnitines, to transport long-chain fatty acids across mitochondrial membranes. This protein family includes three members: CPT1A, CPT1B and CPT1C. CPT1C was the last member of the CPT1 family to be discovered [1]. Although CPT1C exhibits high sequence similarity to CPT1A and CPT1B is a protein highly different respect them. CPT1C is a neuronal specific isoform and it has been reported to be also expressed in cancer cells and stem cells, while CPT1A and CPT1B are mainly present in liver and muscle, respectively. In addition, CPT1C is located in the endoplasmic reticulum (ER), rather than in mitochondria (Fig. 1).

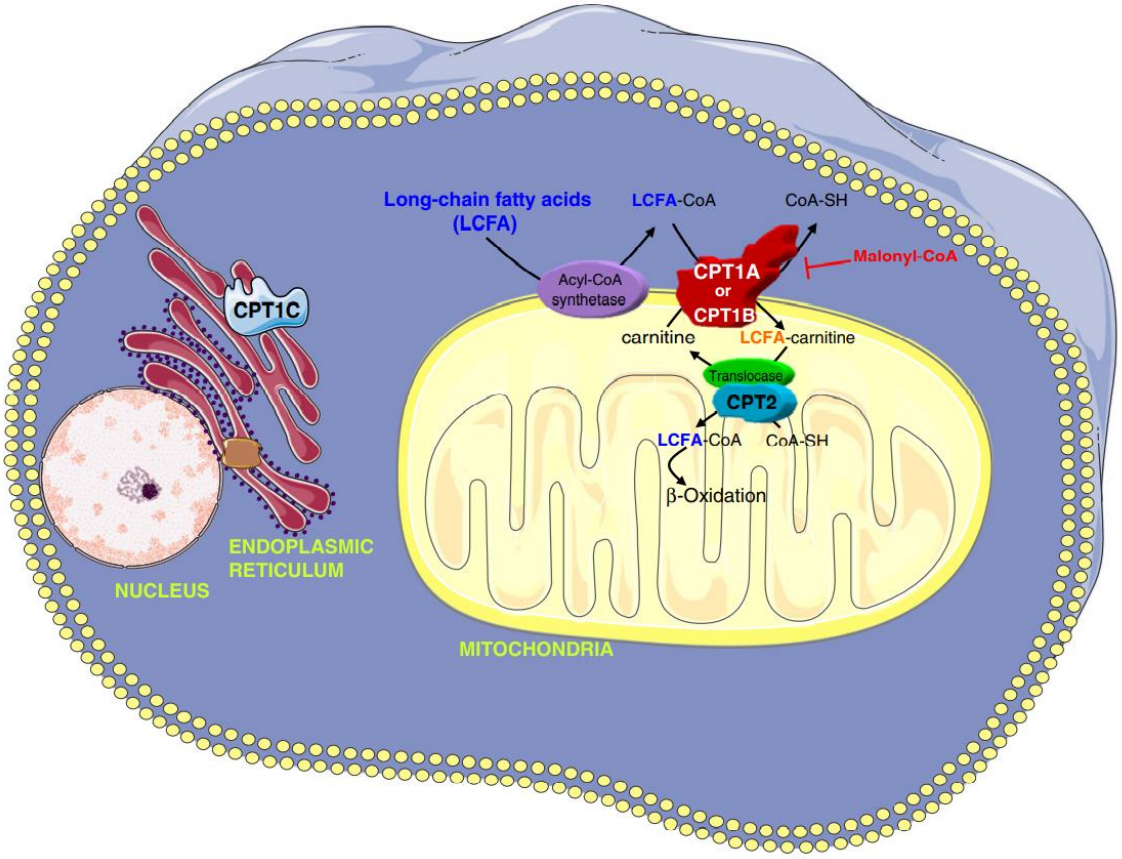

Fig. 1. Carnitine acyltransferases. CPT1 proteins catalyze the reversible transesterification of acyl-CoA esters and carnitine to form acyl-carnitine esters and coenzyme A. CPT1A and CPT1B are located in the outer mitochondrial membrane. The acyl-carnitines formed are transported through membranes into the mitochondria to be β-oxidized. Malonyl-CoA regulates fatty acid oxidation by inhibiting CPT1A and CPT1B. CPT1C is located in the ER membrane and has minimal activity (extracted from [2]).

All the CPT1's are transmembrane proteins with an N- and C-terminal cytosolic domains (Fig. 2). Nevertheless, in CPT1C the C-terminal region is around 30 residues longer than the other members [2], which indicates that this extra long C-terminus may have a potential role in its diverging physiological functions. Furthermore, CPT1C has been demonstrated to have very low catalytic activity. However, CPT1C preserves a strong ability to bind malonyl-CoA as CPT1A [3], and it has been demonstrated to be a sensor of malonyl-CoA in neurons [4]. Our group has demonstrated the hypothesis that CPT1C regulates the function of its interactors depending on malonyl-CoA levels.

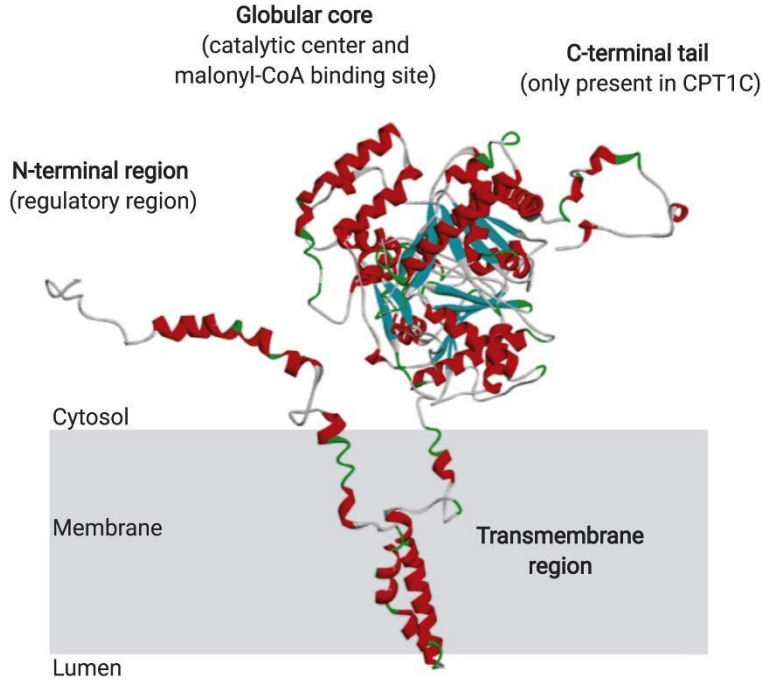

Fig. 2. Representation model of CPT1 proteins. CPT1 proteins contain the following regions: a N-terminal regulatory domain, which switches between two different conformations depending on malonyl-CoA binding; two transmembrane domains that anchor the protein to the outer mitochondrial membrane (CPT1A and CPT1B) or to the ER (CPT1C); the protein is always facing the cytosol; the globular core that comprises the catalytic center and the malonyl-CoA binding site; and a C-terminal tail of about 30 residues, which is only present in CPT1C (extracted from [4]).

The CPT1C interactors described so far are the following proteins: GluA1 (α-amino-3-hydroxy-5-methyl-4-isoxazolepropionic acid, AMPA) subunit receptor [5,6], protrudin [7], SAC1 (Suppressor of Actin 1; phosphatidylinositol-4-phosphatase) [8] and ABHD6 (serine hydrolase α/β-hydrolase domain 6) [9]. The interactions described between CPT1C and some of these proteins have related CPT1C with major functions in mice and humans.

1.2. Physiological functions

The ubiquitous expression of CPT1C in the central nervous system explains the diversity of brain physiological functions in which it is involved. The development of a CPT1C knock-out (KO) mouse has enabled to learn the role of this protein in energy homeostasis, cognition, and motor function (Fig. 3).

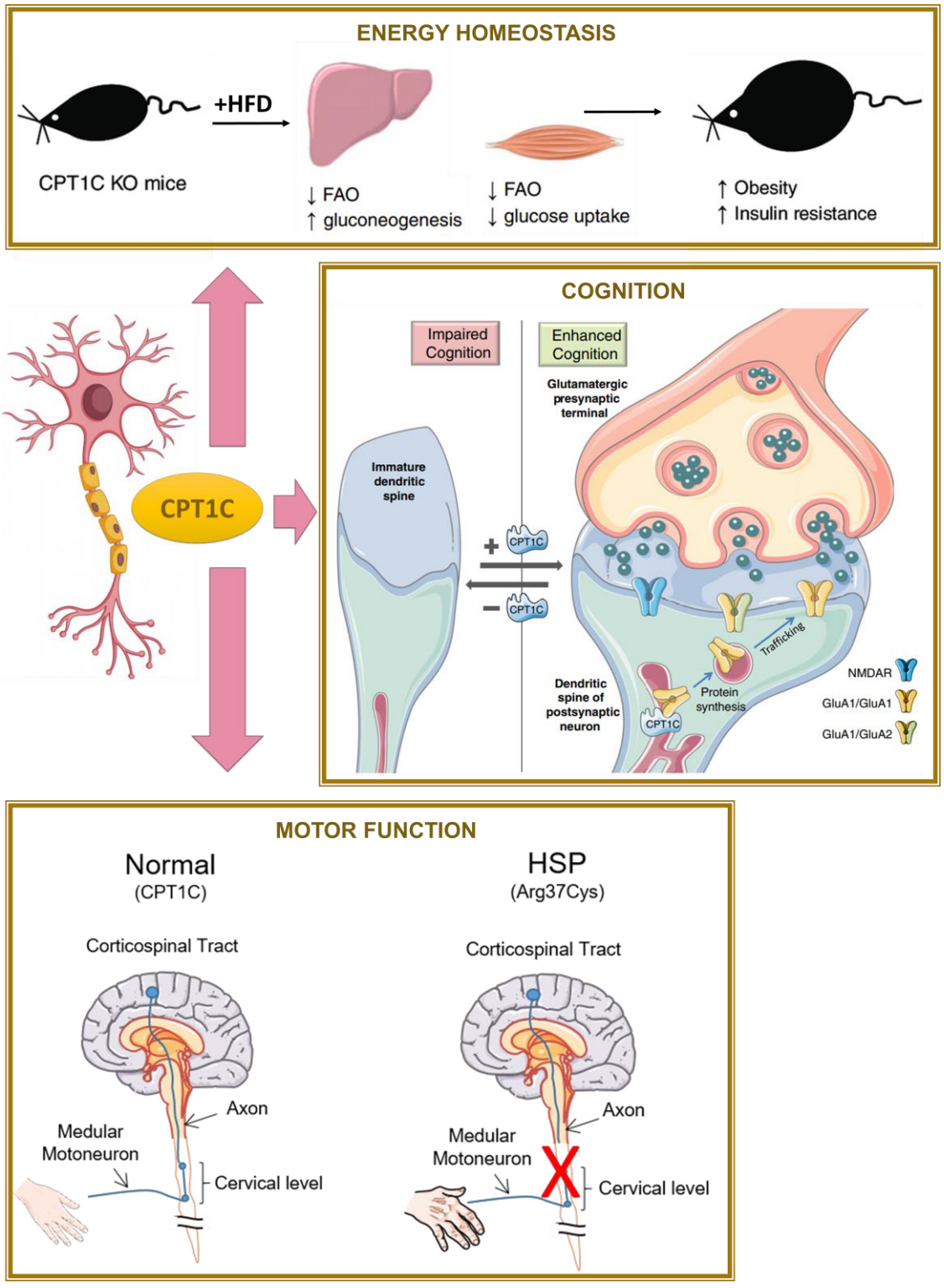

Fig. 3. CPT1C roles at cellular and physiological levels. Illustrative examples of CPT1C involvement in the regulation of energy homeostasis, cognition and motor function. CPT1C KO mice fed with high fat diet show reduced fatty acid oxidation in muscle and liver and impaired glucose homeostasis, resulting in an obese phenotype with insulin resistance. CPT1C expression is required for efficient spine maturation, AMPAR subunits GluA1 and GluA2 synthesis, GluA1 trafficking to the plasma membrane, and enhanced cognition. Indeed, there is a correlation between CPT1C deficiency, immature filopodia in hippocampal neurons, and impaired cognition. Finally, a mutation in CPT1C as the genetic cause of a pure form of the autosomal dominant hereditary spastic paraplegia exemplify CPT1C role in motor function (figure modified from [2], [10]).

In 2006, Wolfgang and colleagues described that CPT1C KO-mice showed no apparent developmental abnormalities but manifested a reduction in body weight and a decreased daily food intake, pointing to an involvement of CPT1C in appetite control. Despite CPT1C KO-mice showed a reduced food intake, when fed a high fat diet they were more susceptible to obesity gaining more body weight than WT-mice [3]. Moreover, these animals exhibited more severe insulin resistance, with elevated hepatic gluconeogenesis and decreased glucose uptake in skeletal muscle [11]. In addition, CPT1C KO mice had a deteriorated leptin-induced brown adipose tissue thermogenesis under high fat diet, which favors obesity development [12]. CPT1C-KO mice had also an impaired fasting-induced FAO (fatty acid oxidation) and enhanced glycolysis under hypoglycemia [13]. These findings indicated an important regulatory contribution of hypothalamic CPT1C in peripheral lipid metabolism.

On the other hand, the involvement of CPT1C on memory consolidation and learning processes has also been demonstrated. CPT1C KO genotype shows a delayed spatial learning which has been associated with poor maturation of neuronal dendritic spines [14]. This cellular phenotype has appeared as a consequence of CPT1C direct modulation of α-amino-3-hydroxyl-5-methyl-4-isoxazole-propionate-type glutamate receptors (AMPARs) trafficking [15]. These are ionotropic glutamate receptors that mediate the majority of excitatory synaptic transmissions in the mammalian central nervous system. CPT1C, interacting with the GluA1 AMPARs, regulates their synaptic and total surface expression and total amount [15], [16]. GluA1 recruitment to the plasma membrane (PM) is required to promote synaptic formation and maturation during learning acquisition. Therefore, GluA1 modulation by CPT1C correlates with the deteriorated learning phenotype in CPT1C KO mice.

Finally, it should be noted a role of CPT1C in motor function. Neurological tests on CPT1C KO mice revealed impaired coordination and gait, severe muscle weakness, and reduced daily locomotor activity. This impaired motor function has been associated with the role of CPT1C in ceramide metabolism in neurons. Ceramide and sphingosine levels which are lipid factors necessary for the development and survival of neurons are reduced in brain motor regions of CPT1C KO mice [17]. The first disease-causing CPT1C mutation described in humans to date

is consistent with this motor phenotype. A recent study by Rinaldi et al. has identified a mutation in CPT1C as the genetic cause of a pure form of autosomal dominant hereditary spastic paraplegias in an Italian family [10]. This is an inherited neurological disorder characterized by length-dependent axonopathy of corticospinal motor neurons, resulting in lower-extremity spasticity and weakness [2,13]. Related with this, Palomo-Guerrero et al. confirmed CPT1C interaction with protrudin. Protrudin is an ER integral membrane protein that mediates microtubule-based transport of late endosomes (LEs) or lysosomes, which is crucial for proper neuronal axon growth. CPT1C appeared as a nutrient protein sensor (malonyl-CoA sensor) that promotes or arrest LE/Lys transport depending on the cell metabolic status. This sensing is crucial for proper regulation of axon growth in cortical neurons and give clues for the understanding of hereditary spastic paraplegias [7].

1.3. CPT1C interactors

As it has been previously mentioned, CPT1C has been found as a great interactor of several proteins and these protein interactions have explained large part of the physiological functions of CPT1C (Fig. 4). Among the four interactors of CPT1C described, SAC1 and ABHD6 are of special relevance. Both proteins have been related with pathological cancer processes.

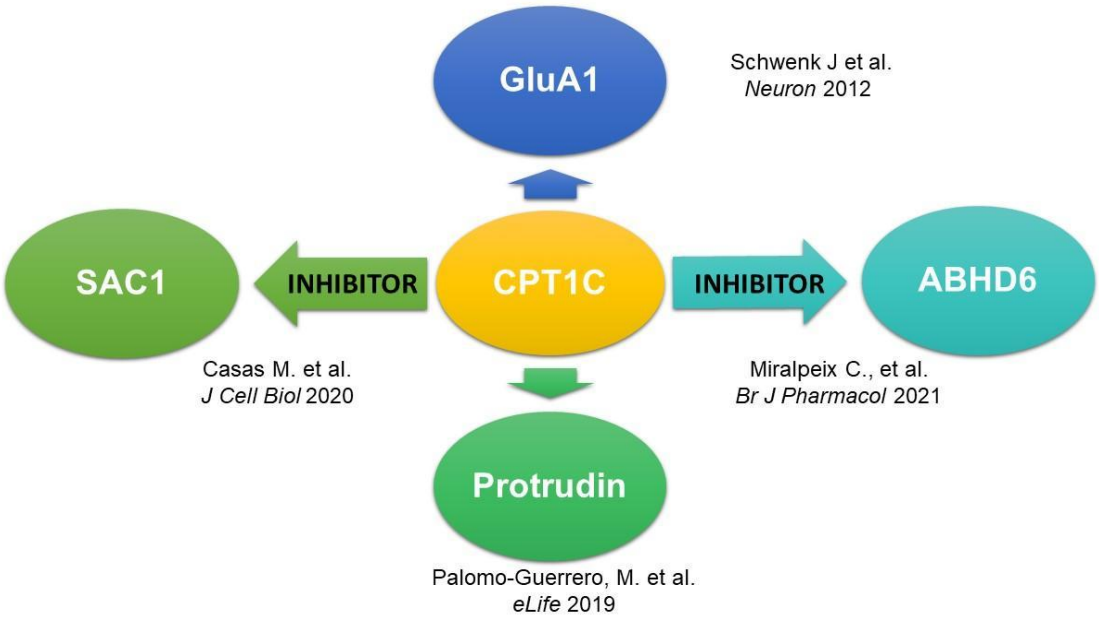

Fig. 4. CPT1C and some of its protein interactors. In the recent years, it has been demonstrated that CPT1C modulates the catalytic activity of SAC1 and ABHD6, the function of protrudin and the transport of GluA1.

1.3.1. SAC1

SAC1 or phosphatidylinositol-4-phosphatase is an ubiquitously expressed protein that is present at ER and Golgi membranes. In different cellular compartments, SAC1 tightly regulates phosphatidyl-inositol-4-phosphate (PI(4)P) levels by dephosphorylating PI(4)P into phosphatidylinositol (PI). PI(4)P is crucial for the vesicular secretory pathway of the Golgi system and for the transport of cholesterol (Chol) and other phospholipids between different organelles and also between the ER and the PM [18]. PI4P levels have also been involved in the control of autophagy flux and of mitochondrial fission [19].

1.3.1.1. SAC1 and lipid homeostasis

SAC1 has a significant influence in sphingolipid biosynthesis, phospholipid homeostasis and Chol transport.

Sphingolipids are remarkably diverse and with crucial roles in apoptosis, cell cycle regulation, cell motility, differentiation, adhesion and as structural components of cellular membranes. De novo sphingolipid biosynthesis begins in the ER with the serine palmitoyltransferases (Lcb1 and Lcb2) activity that condenses serine and palmitoyl-coenzyme A to form long-chain bases. These species can be acylated or hydroxylated to form ceramides, which are further modified to generate complex sphingolipids through Golgi compartment. SAC1 activity in the ER contributes directly and indirectly in the sphingolipid biosynthesis pathway [20].

Regarding to phospholipid homeostasis, SAC1 modulates particularly phosphatidylserine (PS) and phosphatidylcholine (PC) biosynthesis and distribution through intracellular membranes. SAC1 activity facilitates the continuous exchange of PS for PI4P. PS enrichment at the PM (against its concentration gradient), requires PI4P hydrolysis. Without SAC1-mediated PI4P metabolism, PS cannot be transferred to the PM and accumulates at the ER, ceasing PS production. In addition, PC biosynthesis is elevated in SAC1-depleted cells also because of the shared biosynthesis pathway between both phospholipids (reviewed by [20]).

It has also been attributed to SAC1 a primary role in modulating Chol transport to PM. In vivo and in vitro studies suggest that the ER-bound oxysterol-binding protein (OSBP) is a PI4P-dependent Chol transporter. In ER-Golgi membrane contact sites OSBP transfers Chol from ER to trans-Golgi, and PI4P in the opposite direction. The gradient of PI4P between the two membranes is required, and the ER-anchored SAC1 helps in maintaining the PI4P gradient by PI4P degradation [18] (Fig. 5).

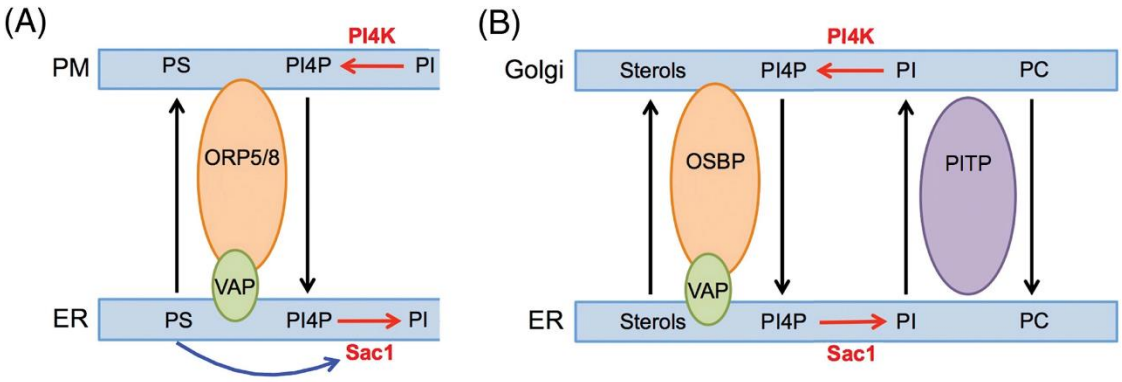

Fig. 5. Role of SAC1 at membrane contact sites. A. ER-PM contact sites. ORP5/8-VAP protein complex exchanges PS and PI4P between the ER and PM. At the ER, PS activates SAC1 to dephosphorylate PI4P and replenish PI. This constitutes a feedback mechanism, which regulates PS production and exchange. B. ER-Golgi contact sites. OSBP-VAP protein complex exchanges sterols and PI4P between the ER and Golgi. At the ER, SAC1 dephosphorylates PI4P to produce PI. PI is transferred back to the Golgi in a manner dependent on PITP, which exchange PI for PC (extracted from [20]).

1.3.1.2. SAC1 and cancer

SAC1 expression is altered in some cancers and it is related to tumor staging and disease development. For example, in breast cancer tissue, moderate overexpression of SAC1 is detected in early-stage tumors but expression afterwards decreases in more advanced tumors which tend to be more invasive and metastatic. This suggests that loss of SAC1 correlates with a more aggressive phenotype (reviewed by [21]).

In terms of cancer development mechanism, loss of SAC1 expression or activity promotes PI4P-dependent secretion or augmented trafficking of cell surface proteins that regulate cell adhesion and motility. A PI(4)P effector, Golgi phosphoprotein 3 (GOLPH 3), drives cell migration by promoting Golgi reorientation and directional protein trafficking to the leading edge. This partly explains how reduced SAC1 expression results in increased trafficking of the pro-metastatic glycoproteins CD44 to the cell surface together with ezrin proteins which are required for focal adhesion integrity (Fig. 6; [22]). The formation of focal adhesions is a critical step for developing the invasive – metastatic phenotype of cancer cells. In addition, SAC1 depletion promotes an abnormal localization of cell–cell adhesion proteins as E-cadherin and β-catenin and peripheral actin cytoskeleton, which are essential for epithelial–mesenchymal transition (EMT) program. EMT is a process that enables metastatic dissemination of the cancer cells including the capability for self-renewal [23].

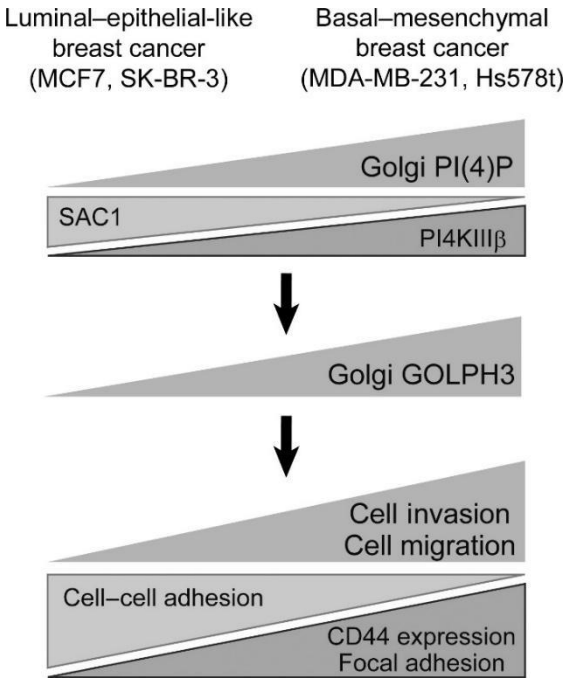

Fig. 6. Schematic representation of regulatory cross-talk between Golgi PI(4)P, CD44 expression, and cell adhesion in breast cancer cell invasion and motility. Changes in the Golgi PI(4)P levels altered the expression and localization of CD44, focal adhesion formation, cell–cell adhesion formation, cell migration/invasion, and metastasis in breast cancer cell lines. Localization of the PI(4)P effector Golgi phosphoprotein 3 (GOLPH3) at the Golgi was predicted to cause these phenotypes (extracted from [22]).

1.3.2. ABHD6

One of the last protein interactors that has been established for CPT1C is ABDH6. In our group, Miralpeix C. et al. demonstrated that CPT1C acts as a negative regulator of ABHD6 activity depending on the sensing of malonyl-CoA. When CPT1C binds malonyl-CoA, ABHD6 activity decreases, whereas when CPT1C does not detect malonyl-CoA levels, ABHD6 activity is restored. These results indicate that CPT1C act as a metabolic sensor that regulates ABHD6 activity [9].

1.3.2.1. ABHD6 enzyme

ABHD6 is an ubiquitously expressed membrane lipase. This protein has multiple functions depending on its tissue and cellular localization. It controls the cellular levels of monoacylglycerol (MAG) species as 2-AG (2-arachidonoylglycerol) by hydrolysis of these substrates. In fact, ABHD6 has been described as a key enzymatic regulator of endocannabinoid signaling with high expression in the brain. Furthermore, ABHD6 hydrolyzes lysophospholipids, including lysophosphatidylcholine (LPC), lysophosphatidic acid, and bis(monoacylglycero)phosphate (BMP), which is highly abundant in intraluminal vesicles. BMP favors the formation of ILVs (intraluminal vesicles) in LEs and it plays an important role

in lipid digestion and sorting. LEs can fuse to the PM and release ILVs into the extracellular space, these released ILVs are known as exosomes, which are key players in some pathological processes such as cancer. ILV's BMP can form a stable docking platform for luminal acid hydrolases. Accordingly, it has been shown that BMP stimulates the activity of lysosomal acid lipase. This latter enzyme is responsible for triglyceride (TAG) and cholesteryl ester (CE) degradation in lysosomes. Furthermore, BMP is thought to play an important role in endosomal Chol sorting. Through BMP hydrolase activity, ABHD6 participates in the late endosomal/lysosomal lipid sorting machinery (Fig. 7) [24]. LEs are a key route for cellular distribution of LDL-derived Chol to the PM and other intracellular compartments. In these organelles, it has been demonstrated that selective perturbation of BMP-rich membranes is involved in the regulation of intracellular transport of Chol [25].

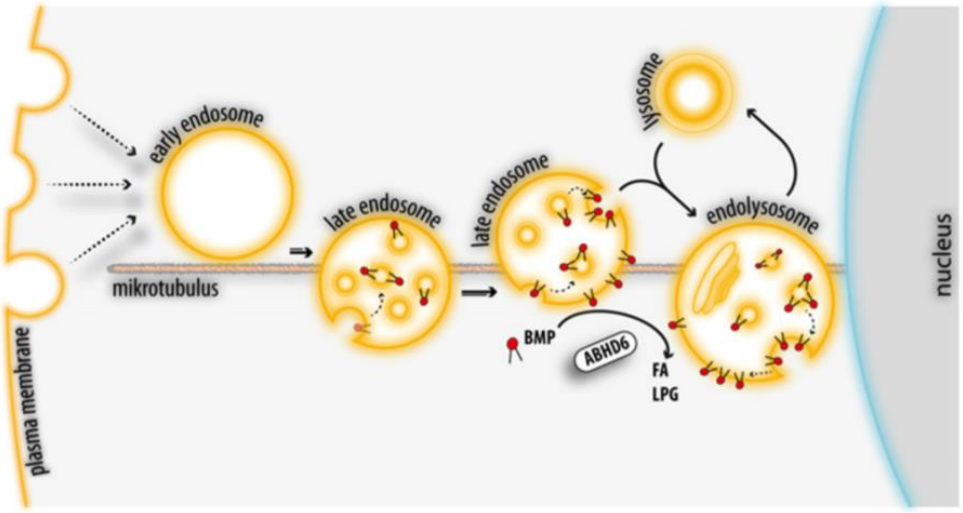

Fig. 7. Role of ABHD6 in the late endosomal/lysosomal pathway. The conversion of early endosomes into LEs involves the formation of BMP-containing (ILVs). LEs finally fuse with lysosomes to form endolysosomes. BMP is resistant to acid hydrolysis and forms stable membrane structures within acidic organelles, promoting lipid digestion and sorting. BMP-rich ILVs of LE and endolysosomes can fuse with the limiting membrane, allowing the export of ILV contents. After fusion, BMP appears on the limiting membrane and is degraded by ABHD6 into lysophosphatidylglycerol and free fatty acids [26].

1.3.2.2. ABHD6 and cancer

ABHD6 is more expressed in tumor cells than in normal cells. For example, ABHD6 has an extremely high level of expression in U2OS (bone), PC-3 (prostate), Jurkat cancer cells and Ewing tumors [27]. It also has been found highly expressed in pancreatic ductal adenocarcinoma (PDAC) which is one of the cancers with higher rate of metastasis and worse prognostic. ABHD6 inhibitors in mouse and human PDAC tumors and in cell lines were able to reduce cancer cell proliferation in vitro, and tumor metastasis in vivo [28]. In addition, endogenous 2-AG (an ABHD6 substrate) has anti-invasive properties in prostate carcinoma.

Finally, RNAseq data and screening of differential genes in liver tumours, has pointed ABHD6 as a potential marker of hepatocellular carcinoma prognosis [24].

Recently, Tang and colleagues described the metastatic role of ABHD6 in human lung cancer [29]. Cancer cells require increased MAG lipolysis catalyzed by monoacylglycerol lipases to promote cancer pathophysiology, including melanoma, ovarian, breast, prostate, nasopharyngeal, and hepatic cancers. In non-small-cell lung carcinoma cell lines, ABHD6 appeared as the primary MAG lipase. ABHD6 has been significantly associated with advanced tumor node metastasis stage and has a negative impact on the overall survival of NSCLC patients. In agreement with this, ABHD6 silencing reduces migration and invasion of NSCLC cells in vitro as well as metastatic seeding and tumor growth in vivo [29].

ABHD6 substrate BMP has been involved in sensitivity to chemotherapy drugs in vitro. The frequently used inhibitor of glycosphingolipid biosynthesis called D-threo-1-Phenyl-2-decanoylamino-3-morpholino-1-propanol (D-PDMP) modulates the structure of the BMP membrane in a pH-dependent manner. Several publications have highlighted the interesting characteristic of D-PDMP in chemosensitization of multidrug resistant cancer cells. As an example, D-PDMP chemosensitizated the neuroblastoma Neuro-2a cancer cells to paclitaxel. This happened as a subsequent consequence of the BMP structure membrane impairment which inhibited the degradation of LDL and thus decreased PM Chol levels [30]. Moreover, in macrophage cancer cell lines, BMP levels were increased in LEs through dioleoyl-phosphatidylglycerol (18:1/18:1-PG) treatment also decreasing Chol transport to PM [31].

Not only SAC1 and ABHD6 proteins have been related with cancer processes, but also CPT1C itself.

2. CPT1C and cancer

Cells have the ability to adapt its metabolism to support rapid proliferation, continuous growth, and survival in aggressive conditions. Cancer cells have an increased adaptive phenotype to maintain both viability and uncontrolled proliferation. They reprogram their metabolism to be provided with energy and biosynthetic intermediates that are requested to preserve their integrity from hypoxic and adverse environment. The first example of metabolic reprogramming is the Warburg effect, which is defined as an increase in the rate of glucose uptake and preferential production of lactate, independently from oxygen availability. In addition to glycolysis, cancer cells can take advantage of other metabolic strategies such as FAO to obtain energy. Fatty acids can adequately fuel cancer cells, since mitochondrial FAO produces much more ATP per mole than oxidation of nutrients, such as glucose or amino acids. In this context, recent findings have suggested that proteins involved in the transport of

fatty acids from cytosol to mitochondria as CPT1s could be considered key for the metabolic adaptation of cancer cells.

2.1. CPT1C expression in cancer cell lines and tumors

In 2011, Zaugg and colleagues identified CPT1C as a gene frequently expressed in tumors. They showed the unusual expression of CPT1C in many breast cancers, and that CPT1C mRNA was overexpressed in 13 of 16 lung cancers compared to normal tissues. Afterwards, CPT1C mRNA expression studies in a wide array of tumor types showed that CPT1C is highly expressed in brain cancers and several sarcomas (Fig. 8; [32]). Interestingly, hematopoietic malignancies which hold greater access to nutrients, have the lowest levels of CPT1C mRNA [32].

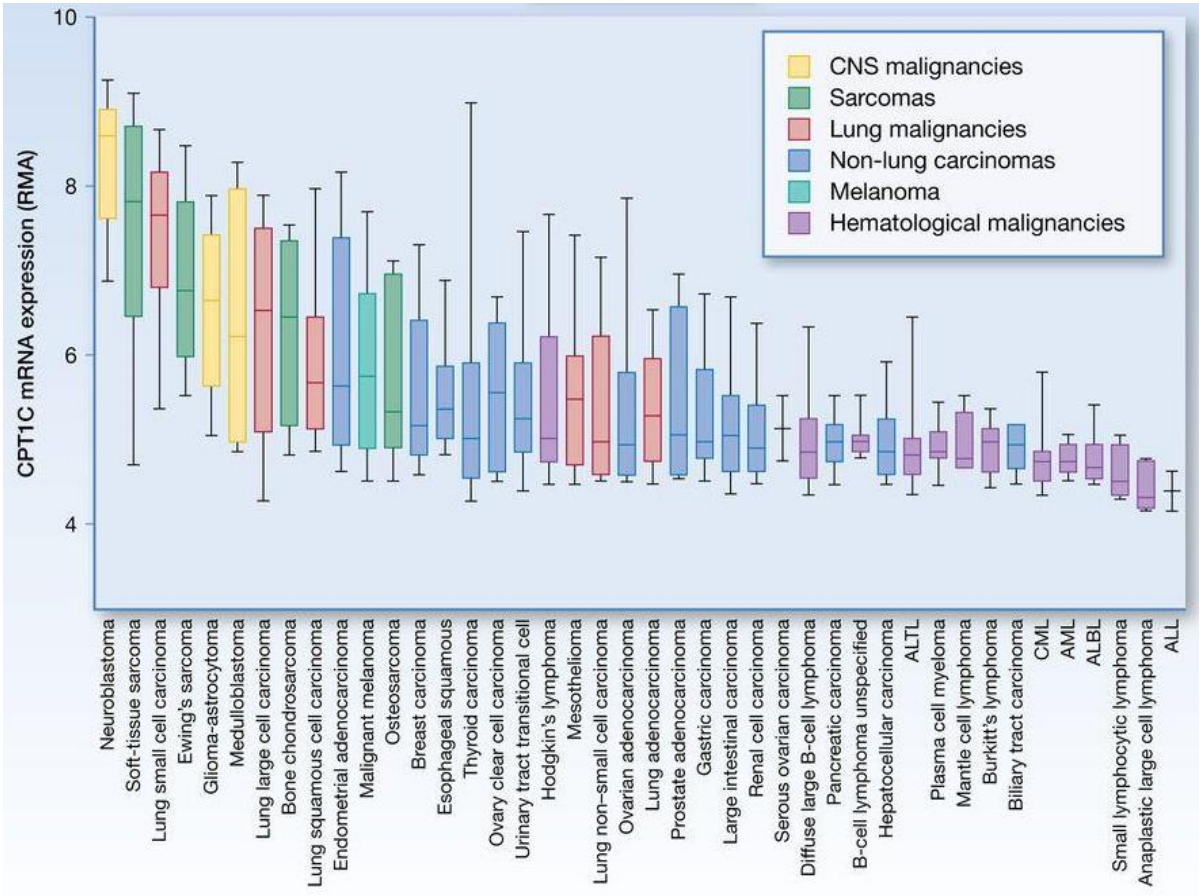

Fig. 8. CPT1C mRNA is expressed in a wide range of human malignancies. Data collected from the cancer cell line encyclopedia expression analysis show that CPT1C is preferentially expressed in cell lines from central nervous system malignancies, sarcomas, and lung cancers, and is less present in cell lines derived from hematologic malignancies. CML, chronic myelogenous leukemia; AML, acute myelogenous leukemia; ALL, acute lymphoblastic leukemia (extracted from [32]).

2.2. CPT1C as a prognostic marker

Several publications have given to CPT1C expression a prognostic value in different cancer types. The work of Nath A. and Chan C., has defined CPT1C, among the five genes stronger associated with EMT program and poor survival across multiple cancers. The progression of EMT and cancer stem cell-like features in tumors confer resistance to therapeutics and are associated with poor prognosis [33]. A poor prognosis has also been attributed to CPT1C expression, in specific studies of different types of cancer. Recently, high expression of CPT1C has been significantly associated with poor overall (OS) and disease free survival (DFS) of gastric patients [34]. In addition, a colorectal cancer gene signature based on stromal and immune microenvironment cell scores has established CPT1C expression as a risk factor of colorectal cancer. Other studies have related CPT1C expression to different cancer staging's. For example, Cirillo A. et al., found in glioblastoma patients that the grade of tumor malignancy was associated with CPT1C expression. Thus, gliomas of grade II had higher levels of CPT1C compared to grade IV (the most malignant) [35]. However, CPT1C expression and tumor staging are related in an inverse manner in bladder cancer. Kim WT. et al. found decreased CPT1C expression in tumor tissues compared to control ones and at the same time, they noted that in non-muscle invasive bladder cancers CPT1C expression was significantly lower than in muscle invasive bladder cancer [36].

A more advanced stage of a tumor (with worse prognosis) is directly correlated with its metastatic potential. The next table summarize how is the relation of the expression of CPT1C and its protein interactors with metastatic features (Table 1). Based on the literature published and mentioned above, we distinguish between metastatic characteristics demonstrated at in vitro, in vivo or patient level. The table shows that SAC1 and ABDH6 proteins correlate with metastasis in an opposite manner. Instead, CPT1C expression is differently related with metastatic processes depending on the cancer tissue.

RELATION BETWEEN PROTEIN EXPRESSION AND METASTATIC FEATURES			
Protein	**In vitro metastatic features (ex. EMT, migration…)**	**In vivo metastases**	**Metastatic tumors (advanced stages)**
CPT1C	**High CPT1C** expression in high migrating papillary thyroid carcinoma cell lines [37].	**High CPT1C** expression correlates with more metastasis in neurofibromatosis type I tumor model [38].	**High CPT1C** expression in MIBC[c] [36].
			High CPT1C expression correlates with EMT in many human tumors [33].
			Low CPT1C expression in higher grade glioblastoma tumors [35].
SAC1	**SAC1 depletion** increases migration and EMT markers in human breast cancer cell lines [22,23,39].	**Low SAC1 activity** (high PI4P) increases lung metastases in breast cancer xenograft mice [39].	**Decreased SAC1** expression in advanced (stages III and IV) human breast cancer tissues [39].
ABHD6	**High ABHD6** expression in highly metastatic PDAC[a] and NSCLC[b] cell lines [24,29].	**High ABHD6** expression related with metastases in PDAC and NSCLC xenograft mice [24,29].	**ABHD6** expression **increased** in NSCLC advanced tumor node metastasis [24].

Table 1. Relation between expression of CPT1C, SAC1 and ABHD6 with metastasis in vitro, in vivo and in patients. Data published in recent literature are shown. [a]PDAC, [b]Non Small-Cell Lung Cancer (NSCLC), [c]Muscle Invasive Bladder Cancers (MIBC).

2.3. CPT1C and signaling pathways

The carnitine palmitoyl transferase 1 (CPT1) enzymes promote FAO by catalyzing the conversion of long-chain acyl-CoA to acyl-carnitines, to make possible the transport of long-chain fatty acids into the mitochondria. However, due to the localization of CPT1C in the ER and negligible catalytic activity, CPT1C does not promote FAO in HEK cells or neurons. Despite that, most of the published cancer literature has explored the role of this protein in relation to FAO and few of them have directly measured it.

As previously mentioned, Zaugg et al. described for the first time the role of CPT1C in cancer. They demonstrated that p53 directly activates CPT1C expression under different stress insults in multiple cancer cell lines, but not in all of them. In murine sarcomas, elevated expression of CPT1C was accompanied with highly upregulated p53 and p21 protein levels. At the same time this CPT1C expression correlated inversely with mammalian target of rapamycin (mTOR) pathway activation which is frequently up-regulated in human lung tumors. They also found that tumor cells constitutively expressing CPT1C show increased FAO, ATP production, and resistance to glucose deprivation or hypoxia [40]. Conversely, cancer cells lacking CPT1C produce less ATP, have mitochondrial dysfunction, are more sensitive to hypoxia and glucose deprivation [41], and have increased lipid droplets levels and impaired fatty acid levels. In

xenograft tumors, they proved that CPT1C expression can be induced by hypoxia or glucose deprivation and is partly regulated by AMPKα. In summary, they proposed the p53–AMPK–CPT1C axis in cancer cells for sensing and responding to metabolic stress, something that often occurs in solid tumors which contain regions of poor oxygenation and nutrient availability [38,40].

As outlined before, in some cancers CPT1C is overexpressed in a p53-independent manner. This concerns lung cancer, as p53 is either mutated or present at very low levels in these malignancies. An alternative pathway for CPT1C expression induction proposed in breast cancer cell lines is the CREB/PGC-1b/ERRα route. Under 2-deoxyglucose, a glycolytic inhibitor, treatment, via AMPK activation, the cAMP response element-binding protein (CREB) is phosphorylated and activated, and the expression of nuclear peroxisome proliferator-activated receptor gamma coactivator-1-beta (PGC-1β) and estrogen-related receptor a (ERRα) proteins are promoted, leading to augmented mitochondrial biogenesis and expression of FAO genes including peroxisome proliferator-activated receptor alpha (PPARα) and CPT1C. According to this, recently, PPARα and ERRα have been included among the direct activators of CPT1C transcription in PANC-1 prostate cancer cells and MDA-MB-231 breast cancer cells [42,43]. Once again, CPT1C appears included in the metabolic reprogramming by which cancer cells survive metabolic stress associated in this case with glycolysis inhibition [44] (Fig. 9).

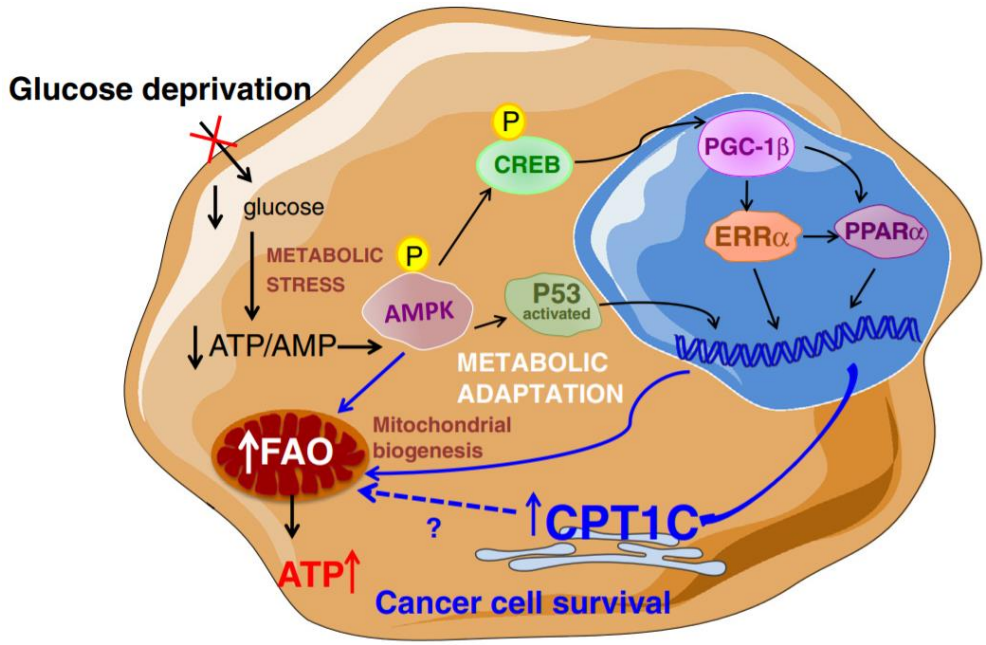

Fig. 9. Regulators of CPT1C expression in cancer cells. Glucose deprivation induces metabolic stress and activation of AMPK. CPT1C expression might be activated via the AMPK/PGC-1β pathway and in a p53-dependent manner, thus contributing to metabolic adaptation and cancer cell survival. This metabolic adaptation could also happen in a p53-independent manner. cAMP response element-

binding protein (CREB); Peroxisome proliferator-activated receptor gamma, coactivator 1 beta (PGC-1β), Estrogen receptor-related receptor alpha (ERRα); Peroxisome proliferator-activated receptor alpha (PPARα) [2].

In summary, there is an interesting signaling pathway that somehow relates CPT1C and FAO in cancer cells. However, the effects seen in FAO under CPT1C expression modulation seems to be as an indirect consequence since as we have commented CPT1C is mainly present in the ER and it lacks carnitine palmitoyl transferase activity.

2.4. CPT1C and senescence

Cellular senescence is a multidimensional and highly heterogeneous status consisting of usually irreversible growth arrest, resistance to apoptotic stimuli, persistent DNA damage, elevated lysosomal activity, deregulated metabolism, and elevated secretion of chemokines, cytokines and growth factors. The cell cycle is arrested depending on the cyclin-dependent kinase (CDK) inhibitors p16 and p21 which are often regulated by p53 and their elevated expression are considered markers for senescence detection [45]. In the past few years, CPT1C has been identified as a novel biomarker and key regulator of cancer cell senescence through mitochondria-associated metabolic reprograming. Silencing of CPT1C in different tumor cell lines was sufficient to trigger cellular senescence, induce mitochondrial dysfunction, cause senescence-like growth suppression, suppress cell survival under metabolic stress, and inhibit tumorigenesis in vivo. On the contrary, gain-of-function of CPT1C reversed cell senescence and enhanced mitochondrial function. Regarding to mitochondrial morphology, in CPT1C-dependent senescent cells, there was an increase in the presence of swollen mitochondria exhibiting loss of internal cristae density and abnormal membrane structures [41]. In MDA-MB-231, senescent role of CPT1C has been located downstream PPARα, in a p53-independent manner. CPT1C silencing effect in proliferation has been partly explained by the capacity of CPT1C to modulate c-Myc expression. CPT1C knockdown remarkably downregulates c-Myc and consistently, activates the cell cycle inhibitor p27 and suppresses the expression of the cell cycle inducers cyclin D1, cyclin A1 and cyclin E1 [46].

2.5. CPT1C and lipid homeostasis

Deregulation of lipid metabolism is crucial for malignant transformation in tumors as breast cancer. The bulk of fatty acids produced in cancer cells is mainly used to generate phospholipids, specially glycerophospholipids [47]. Phospholipids contain an alcohol (glycerol or sphingosine), fatty acids, and phosphoric acid (PO4). They are subdivided into glycerophospholipids (when the alcohol is glycerol) and sphingophospholipids (when the alcohol is sphingosine) [48] (Fig. 10).

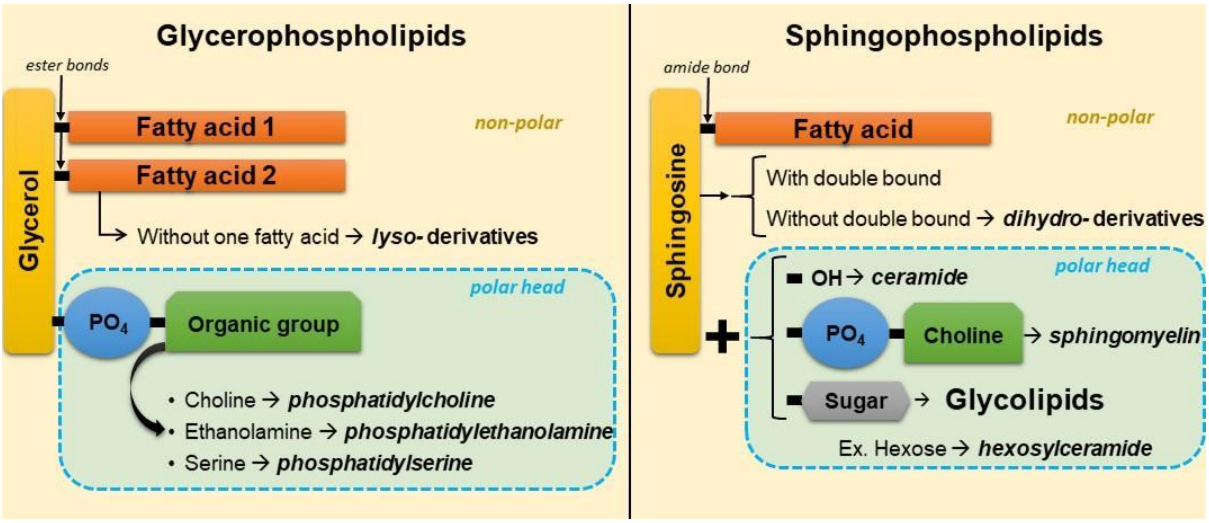

Fig. 10. Schematic representation of glycerophospholipids and sphingophospholipids structure.

Glycerophospholipids are the primary components of cellular membranes. Depending on the amino alcohol, the glycerophospholipid could be PC, phosphatidylethanolamine (PE), or PS. Glycerophospholipids show great diversity in the composition of their fatty acids, which differ in carbon chain length and the double-bond number (saturation degree). The saturation degree and length of glycerophospholipid acyl chains are important determinants of many membrane characteristics such as fluidity and permeability.

Apart from fatty acid saturation, the size and/or the hydration status of the polar head group of glycerophospholipids have been shown to alter membrane fluidity (Fig. 11). According to head group shape, PC increases membrane fluidity as the choline head group is large, resulting in a relatively similar area of head group compared to fatty acyl chains. By contrast, PE reduces fluidity as ethanolamine is slightly smaller. In addition, the head group hydration status of PC was suggested to be more hydrated than PE, which prevents the tight packing of adjacent hydrophobic lipids [49]. Moreover, PE is a hydrogen donor and can form hydrogen bonds with the anionic phosphate–oxygen of the adjacent phospholipid, thus restricting lipid movement. Altogether, this explains why the PC/PE ratio directly correlates with membrane fluidity [50].

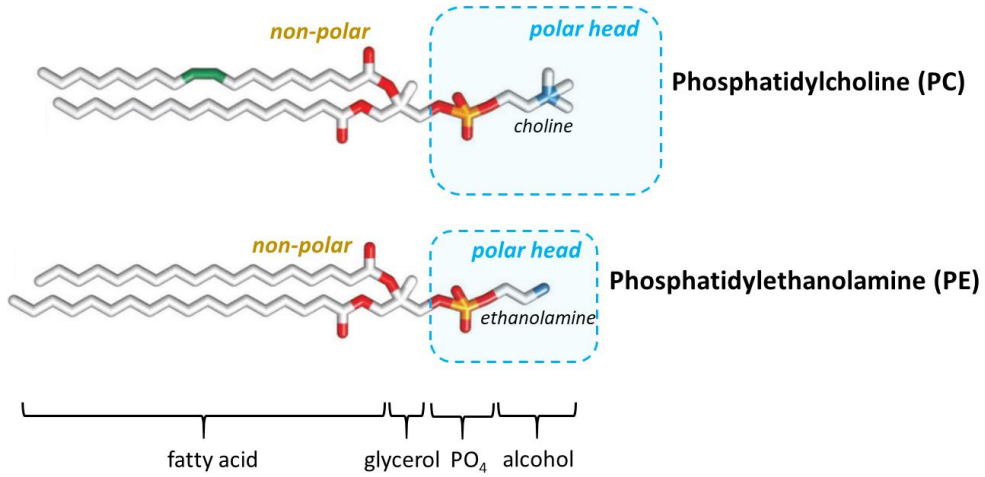

Fig. 11. Schematic representation of PC and PE structure modified from [51].

In each glycerophospholipid molecule, one of the two fatty acids can be hydrolyzed by phospholipase A2, resulting in lysoderivatives formation as LPCs and lysophosphatidylethanolamines (LPEs). In cells, lysoglycerophospholipid concentration is low compared to their corresponding phospholipids. By contrast, this concentration is high in interstitial fluids and plasma [52]. Additionally, their amphipathic characteristics allows some of them to be secreted extracellularly and act as important signaling molecules [48].

CPT1C expression has been related to marked changes in cellular lipid composition and localization patterns (Table 2).

LIPIDOMICS of CPT1C-silenced or CPT1C- KO cell lines	
INCREASED levels of:	**DECREASED levels of:**
LD [38,46,53]	
linoleic, arachidonic, docosotetraenoic acids [40]	oleic acid [40]
TAG [53,46]	PC/PE ratio [53,46]
SM	DG [53,46]
fatty acids	PG [53,46]
oxidized fatty acids	CL [53,46]

Table 2. Comparison of cellular content of lipid species in cell lines after CPT1C knockdown. The cell lines used were murine embrionic stem cells [40] and the human cancer cell lines PANC-1 (pancreatic) [53,46] and A549 (lung) [53], MDA-MB-231 (breast) [53], and HCT116 (colon) [53].

Zaugg et al. demonstrated in CPT1C KO murine embryonic stem cell line a higher presence of lipid droplets presence, increased levels of linoleic, arachidonic, and docosotetraenoic acids, and decreased levels of oleic acid [40]. The same increasing effect in lipid droplets (LDs) has been found in CPT1C-depleted human cancer cell lines, accompanied by increased levels of TAGs and sphingomyelin (SM) and decreased levels of cardiolipins (CL), PC/PE ratio, PCs, LPEs, diacylglycerols (DG) and phosphatidylglycerols (PG) [53,46]. However, in several cancer cell lines, CPT1C expression was not related with changes in ceramide levels [53]. A more recent lipidomic analysis was carried out in CPT1C siRNA-treated cancer cells and revealed increased fatty acid, and lipid peroxidation levels [53]. The excess of fatty acids prevents lipid maintenance without being oxidized and it has been directly related with the mitochondrial dysfunction seen in CPT1C-depleted cancer cells. After CPT1C knockdown, also DGAT1 and DGAT2 mRNAs involved in TAG synthesis were increased, while PNPLA2 and LIPE mRNAs encoding TAG hydrolytic enzymes were decreased, suggesting that knockdown of CPT1C promotes the synthesis of TAG and inhibits its hydrolysis, resulting in the accumulation of TAG in cells, as it was previously published [53].

2.6. CPT1C and chemoresistance

According to the role of CPT1C under stress conditions, some studies have demonstrated the effect of different chemotherapy drugs in CPT1C expression. For example, CPT1C expression in 5-fluorouracil (5-FU)- and cisplatin (CDDP)-resistant gastric cancer cells is increased respect their parental cell lines [54]. The same effect in CPT1C expression via p53 has been found in HCT116 colon cancer cell lines under 5-FU treatment [38]. In pancreatic cancer PANC cell line, a 24h treatment with 0.7 μM doxorubicin (DOX) (a positive p53 agonist) treatment induced CPT1C mRNA upregulation [55]. An opposite effect in CPT1C expression has been revealed in ovarian cancer cell lines. Vert et al. compared gene expression in OVCAR-8 cells with its multi-drug resistant equivalent cell line, NCI/ADR-RES cells. This one is 509.3-fold and 228.6-fold more resistant to DOX and paclitaxel, respectively, compared to the original sensitive-cell line. Microarray-derived transcriptional profiling used to identify differentially expressed genes between both cell lines placed CPT1C among the top 20 downregulated genes in NCI/ADR-RES cells [56].

All the information related to CPT1C and cancer described above reveals a broad role of this protein in cancer metabolic reprogramming and in turn demonstrates its varied, even sometimes, opposite function, depending on the tumor tissue and stage. However, the multiple tumorigenic processes related with CPT1C, revealed this protein as a promising target in cancer research. As CPT1C is a protein directly related with lipid metabolism, and the highly

frequent breast cancer tumors develop in a crucial lipid environmental context, we explored the role of CPT1C in this tumor.

3. Breast cancer and chemotherapy resistance

Breast cancer is the most common cancer in women and the second leading cause of death due to cancer among women globally. New statistics published in 2019 suggest that 30% of women will develop breast cancer in their lifetime and 15% of them will die from it [57]. Even though breast cancer incidence has increased in recent decades, death rates have decreased due to better screening methods, diagnosis and treatment.

3.1. Breast cancer types

Breast cancers are characterized into three major subtypes according to the presence or absence of molecular markers for estrogen receptor (ER) or progesterone receptor (PR) and human epidermal growth factor 2 (HER2). They are hormone receptor (HR) positive/HER2 negative (HR+/HER2-; 70% of patients), HER2 positive (HR +/-/HER2+; 15–20%), and triple-negative breast cancers (TNBCs, HR-/HER2-; 15%). TNBC recur more frequently and the median overall survival for metastatic patients is approximately 1 year compared to 5 years for the other two subtypes (Fig. 12) [58].

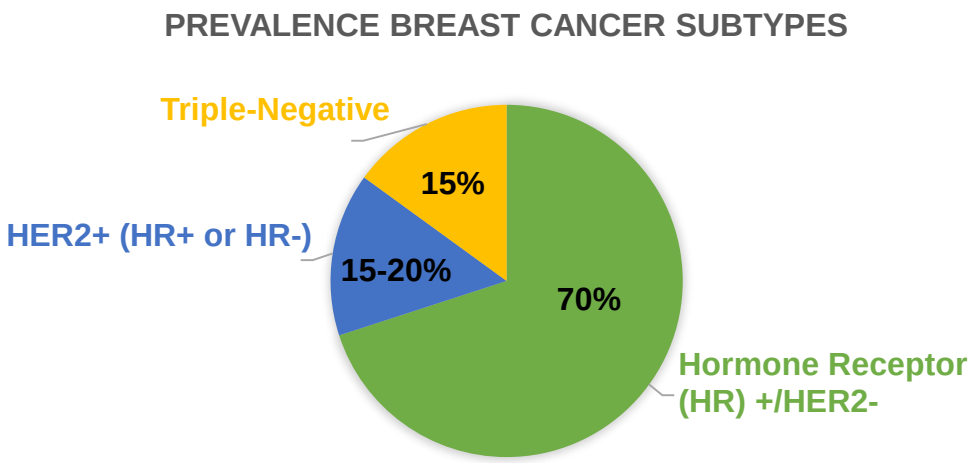

Fig. 12. Prevalence for the 3 Breast Cancer Subtypes. Represented by percentage of breast cancer cases (%) in USA indicated in [58].

3.2. Chemotherapy in breast cancer

Despite metastatic disease remains the leading cause of death in breast cancer patients, over 94% of breast cancer patients do not have detectable metastases at diagnosis [58]. For non-metastatic breast cancer, local therapy consists of surgical resection and sampling or removal of axillary lymph nodes, and often postoperative radiation. Systemic therapy may

be preoperative (neoadjuvant), postoperative (adjuvant), or both. The main goals in these patients are tumor eradication and prevention of recurrence and metastasis. For metastatic breast cancer, the same basic systemic therapy is used (neoadjuvant/adjuvant approaches), since local therapy (surgery and radiation) is only carried out for palliative purposes. The main goals here are prolonging life and relieving symptoms (Table 3) [58].

	Hormone Receptor (HR) +/HER2-	HER2+ (HR+ or HR-)	Triple-Negative
Pathological definition	≥1% of tumor cells stain positive for estrogen receptor or progesterone receptor proteins	Tumor cells stain strongly (3+) for HER2 protein or HER2 gene is amplified in tumor cells. Approximately half of HER2+ tumors are also HR+	Tumor does not meet any pathologic criteria for positivity of estrogen receptor, progesterone receptor, or HER2
Prognosis: stage I (5-year breast cancer–specific survival), %	≥99	≥94	≥85
Prognosis: metastatic (median overall survival)	4-5 years	5 years	10-13 months

Table 3. Pathological definition and prognosis for the 3 Breast Cancer Subtypes. Prognosis estimated from nearly 44,000 patients with breast cancer enrolled in the California Cancer Registry (2005-2008); stage I breast cancer defined by the American Joint Committee on Cancer staging manual anatomic staging table, 8th edition. Represented by percentage of breast cancer cases (%). Prognosis of metastasis listed is from time of diagnosis of metastatic breast cancer (adapted from [58]).

Depending on their receptor signature, the three breast cancer subtypes have distinct neoadjuvant/adjuvant treatments, such as hormonal agents and cytotoxic chemotherapy either simultaneously or consecutively. For ER-positive or PR-positive breast cancer, the use of endocrine agents, like tamoxifen, to downregulate HR signaling is the first systemic therapy and in some cases, chemotherapy alongside endocrine therapy. Patients with amplified or overexpressed HER2 benefit from targeted therapy, including anti-HER2 antibodies, such as trastuzumab, and small-molecule tyrosine kinase inhibitors, combined with chemotherapy, such as DOX (also called adriamycin), paclitaxel, docetaxel (DTX), cyclophosphamide (CFA) and/or carboplatin. Since the specific molecular pathophysiology of TNBC remains poorly

understood, the only systemic therapy with demonstrated efficacy in TNBC patients is chemotherapy, such as DOX/CFA, DOX/CFA/ paclitaxel or DTX/CFA regimens. As such, chemotherapy remains an essential treatment for preventing recurrence in many patients with stage I-III breast cancer regardless of the subtype (Table 4) [58].

Hormone Receptor (HR) +/HER2-	HER2+ (HR+ or HR-)	Triple-Negative
Endocrine therapy (all patients): • Tamoxifen, letrozole, anastrozole, or exemestane • Oral therapy • 5-10 years **Chemotherapy (some patients):** • Adriamycin/cyclophosphamide (AC) • Adriamycin/cyclophosphamide/ paclitaxel (AC-T) • Docetaxel/cyclophosphamide (TC) • Intravenous therapy • 12-20 weeks	**Chemotherapy plus HER2-targeted therapy (all patients):** • Paclitaxel/trastuzumab (TH) • Adriamycin/cyclophosphamide/ paclitaxel/trastuzumab ± pertuzumab (AC-TH±P) • Docetaxel/carboplatin/trastuzumab ± pertuzumab (TCH±P) • Intravenous therapy • 12-20 weeks of chemotherapy; 1 year of HER2-targeted therapy **Endocrine therapy (if also hormone receptor positive)** • Tamoxifen, letrozole, anastrozole, or exemestane • Oral therapy • 5-10 years	**Chemotherapy (all patients):** • AC • AC-T • TC • Intravenous therapy • 12-20 weeks

Table 4. Therapeutic Options for the 3 Breast Cancer Subtypes. Typical systemic therapies for non-metastatic disease (agents, route and duration) reviewed in [58].

3.3. Chemoresistance mechanisms

One of the main causes of chemotherapy failure, and a major concern in breast cancer treatment, is chemoresistance. Cancer cells can activate a great variety of mechanisms to avoid the cytotoxic effects of drugs. They can decrease influx or increase efflux of drugs, activate apoptosis-evading/survival pathways, or enhance DNA repair mechanisms [59]. Decrease influx is included among the first chemoresistance mechanisms in terms of time. It

is the opening cellular drawback faced by chemotherapy drugs. There are many current molecular strategies in study in order to overcome this uptake-based chemoresistance mechanism, especially in the nanoparticle emerging field.

3.4. Uptake-based chemoresistance mechanisms

Drug's lipid solubility, size, degree of ionization and other physicochemical properties determine the way in which drugs penetrate cells. There are different pathways for drug uptake: diffusion across the PM, transference by transporters, and endocytosis (summarized in Fig. 13).

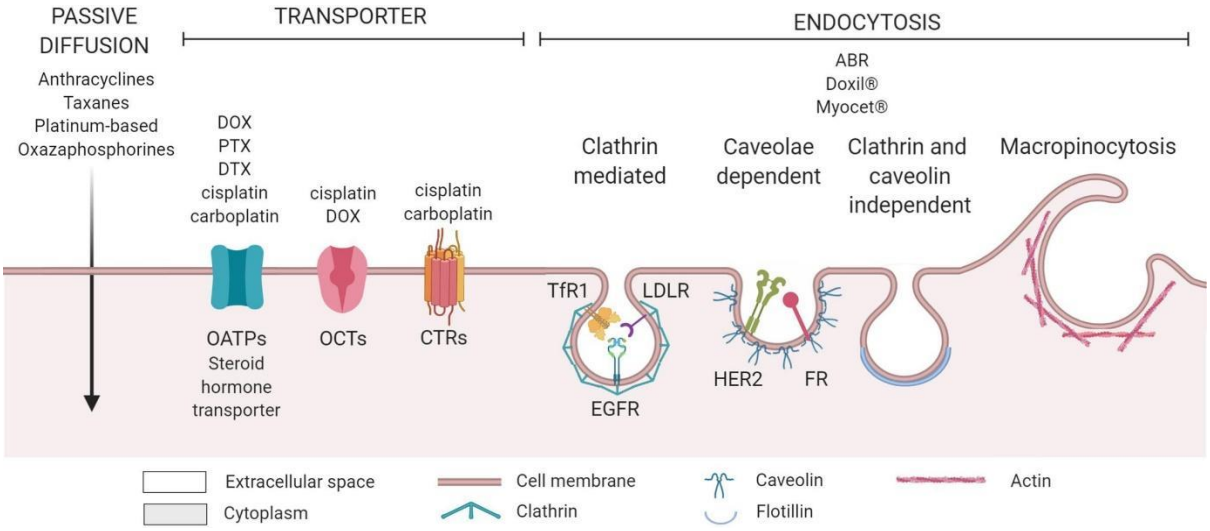

Fig. 13. Schematic overview of drug uptake pathways in breast cancer chemotherapy. Several pathways exist for cellular entry of breast cancer chemotherapy drugs: passive diffusion, PM transporters and endocytosis. Endocytosis can be clathrin-mediated (CME), caveolae-mediated (CavME), clathrin- and caveolin independent (CIE) or through macropinocytosis. One same drug could enter a cell through different mechanisms. The transport mechanisms for the most used drugs in breast cancer treatment are indicated (image published in [60]).

3.4.1. Diffusion across the PM

The PM is the first barrier for therapeutic agents to enter cells. Most cancer chemotherapeutics are weak bases with pKa values between 7.4 and 8.2 and are hydrophobic in neutral form. It is therefore assumed that they traverse the cell membrane by passive diffusion [61]. Passive transport occurs by diffusion through a continuous concentration gradient but also by passive 'flip-flop' mechanism. Cell membranes are dynamic structures where

specific phospholipid species are distributed asymmetrically. Three types of proteins maintain the asymmetry between the two leaflets of the plasma bilayer: flippases, floppases and scramblases. Flippases are type-IV P-type ATPases that catalyze the movement of phospholipids from the extracellular leaflet to the cytosolic leaflet, floppases are ATP-Binding Cassette (ABC)-transporters that move phospholipids in the reverse direction, and scramblases that translocate lipids bidirectionally between leaflets without the help of ATP [62]. A normal asymmetric cell PM maintains zwitterionic lipids such as PC and SM prevalent in the outer leaflet, and phospholipids containing amine (PE) or serine (PS) in the inner leaflet. However, in cancer cells, this asymmetry is deregulated meaning that cells often expose PS in the outer membrane resulting in a negative surface charge, which correlates with a more acidic pH of extracellular media. Metabolic changes that cancer cells go through (increased anaerobic glycolysis) also reduce extracellular pH. The low pH can influence the ionization state of drugs and therefore their transport across the lipid bilayer (Fig. 14) [63].

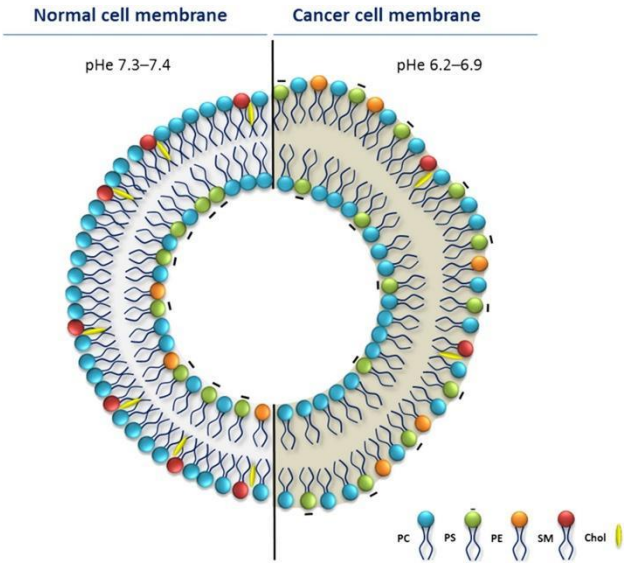

Fig. 14. Schematic representation of lipid composition and extracellular pH in normal and tumor cells. Normal membranes exhibit an outer leaflet mainly composed by zwitterionic PC and SM, while anionic PS along with most of the PE are usually present in the inner leaflet. By contrast, cancer cells loss this asymmetric distribution exposing negatively charged PS on the surface of their membranes. Since the flippase aminophospholipid translocases maintain the distribution of both PE and PS, evidences demonstrated that PE is also located in the membrane's outer leaflet in some cancer cells (extracted from [63]).

Lipid composition changes can also modulate the transmembrane passive diffusion of drugs due to changes in rigidity/fluidity properties of the PM. For example, membrane fluidity is influenced by Chol content and the degree of lipid unsaturation [64]. It is well known that cancer cells undergoing malignant transformation suffer genetic alterations that lead to changes in

lipid composition of PM. This is one of the most frequent causes of drug uptake-based chemoresistance [61].

3.4.2. PM transporters

Many drugs are hydrophilic and diffuse through lipid membranes very slowly. However, they can enter cells through solute carrier (SLC) transporters, as OATPs and OCTs. SLC transporters are a family of more than 300 proteins that facilitate the transport of specific substrates, such as amino acids, sugars, organic cations, anions, phosphates, nucleosides, metals and water-soluble vitamins, and mediate the uptake of drugs with similar structures. The efficacy of chemotherapy may be also dependent on the relative activity of these transporters in normal tissues and cancer tissues [65]. OATPs transport a large number of amphipathic substrates, including steroid hormones. This transporter family is important for the proliferation of hormone-dependent cancers, such as breast and prostate cancer [66]. In fact, OATP1A2, OATP1B1, OATP1B3, OATP2B1 have an increased expression in malignant breast tissue compared with normal tissue [66]. Interestingly, the expression levels of these transporters change in a cell line–dependent manner under chemotherapy treatment [66]. Namely, OCT1, OCT2, OCT3, OCTN2 and OCT6 have strong expression in tumor cells [67]. OCTs mediate the transport of various organic cations, weak bases, and some neutral compounds across PMs. OCTN1-2 and OCT6 are important for the transport of major drugs in breast cancer therapy. For example, DOX, a widely used anticancer drug in breast cancer, is transported by OCT6 [65].

3.4.3. Endocytosis-based pathways

Endocytosis is a cellular process for the uptake of macromolecules, such as proteins and lipids, through their engulfment and sequestration into a vesicle derived from the PM. This mechanism is essential for nutrients, synaptic neurotransmitter recycling, receptor signaling, etc. Endocytosis can be broadly divided into pinocytosis (cell drinking) and phagocytosis (cell eating). Pinocytosis is commonly involved in the internalization of fluids and molecules by small vesicles, whereas phagocytosis is the process whereby cells such as monocytes/macrophages, neutrophils and dendritic cells engulf large particles [68]. Pinocytosis, the main endocytic pathway in breast cells, can be constitutive, or receptor-mediated and highly regulated (Fig. 15).

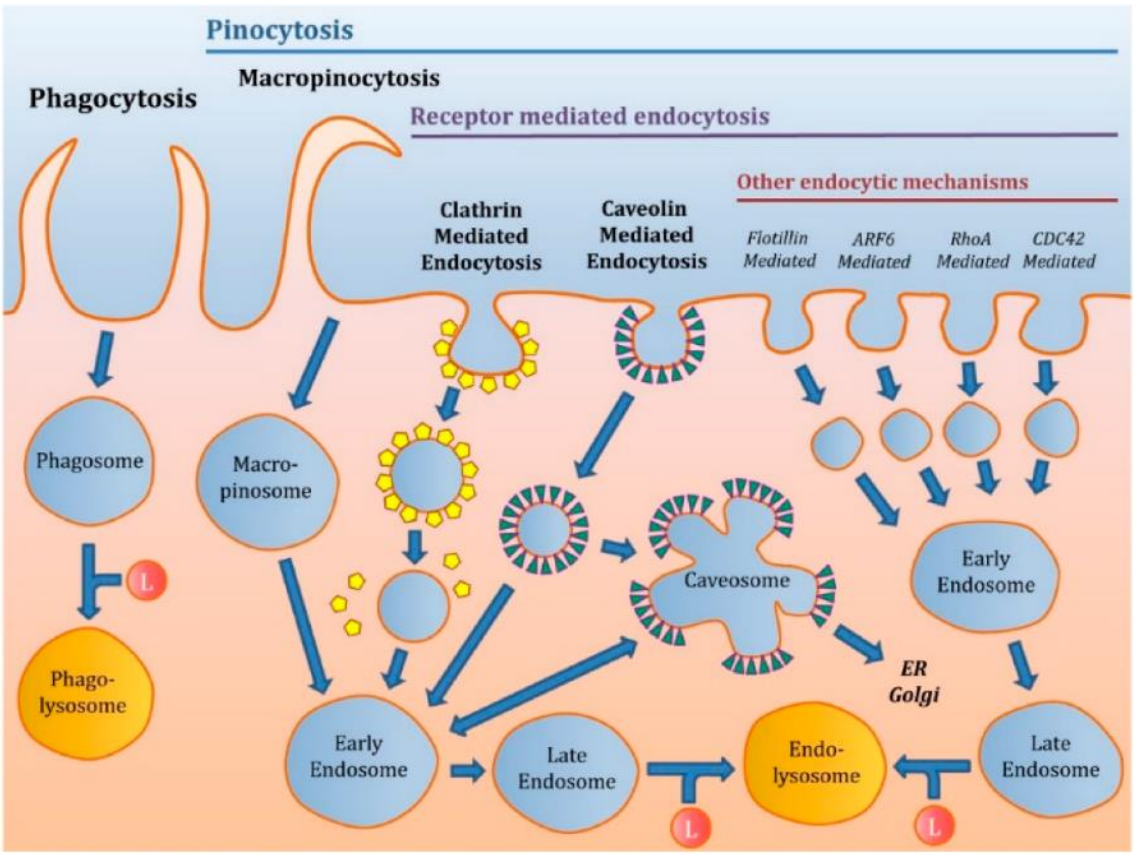

Fig. 15. Main energy-dependent uptake endocytic pathways of the cell. Macropinocytosis forms macropinosomes that could finally join the early endosomes. Clathrin-mediated endocytosis (CME) and caveolin mediated endocytosis (CavME) are the main receptor-mediated endocytosis processes. Other endocytic receptor-mediated endocytosis mechanisms as flotillin, ARF6, RhoA, or CDC42 that mediated endocytosis are also present in the cell. Frequently, the final fate of endosome vesicles is to fuse with lysosomes (extracted from [69]).

Taking advantage of the overexpressed levels of some transmembrane receptors in cancer cells, many drugs have been developed as drug-ligand complexes in recent years. When the ligand recognizes its specific receptor in the cancer cell PM, it is internalized thereby facilitating drug uptake. Therefore, endocytosis is the main route for the uptake of nanoparticles NPs and, in some cases, for free-drug uptake [70]. There are 4 major types of pinocytosis:

3.4.3.1. Clathrin-mediated endocytosis (CME)

Clathrin-mediated endocytosis is the main endocytic route in eukaryotic cells and it is the most studied and well-characterized endocytic mechanism. It is the principal route of internalization of receptor-bound macromolecules. CME has a central role in nutrient uptake, cell signaling, adhesion, migration, morphogenesis and neurotransmission. The endocytosis of cargo receptors can be stimulated by ligand binding, as in epidermal growth factor receptor (EGFR), or can be constitutively internalized, as in transferrin receptor (TfR), or low density

lipoprotein receptor (LDLR) [71]. Since TfR, EGFR and LDLR are highly expressed in breast tumors [72], they are candidates to decorate NPs to enhance their uptake through CME.

3.4.3.2. Caveolae-mediated endocytosis (CavME)

Caveolae-mediated endocytosis is a clathrin-independent endocytic process which involves bulb-shaped, 50–100 nm PM invaginations called caveolae. These are detergent resistant, highly hydrophobic membrane domains, enriched in Chol and sphingolipids. Caveolae formation is driven by integral membrane proteins called caveolins and cytosolic coat proteins called cavins. Caveolin-1 (Cav-1), the most common caveolin, is overexpressed in breast cancer and it is associated with increased invasion, metastasis, poor prognosis and chemotherapy resistance [73]. The commercially available nanotherapeutic Abraxane® (ABR), an albumin-bound form of paclitaxel, is taken up by cancer cells through CavME [70]. HER2 is amplified or overexpressed in approximately 20% of breast cancers [58] and it is found in caveolae domains. On the other hand, the folate receptor, which is overexpressed in multiple cancer types including breast carcinoma, is internalized by both CME and CavME. In recent years, NPs tagged to specific ligands of HER2 and folate receptor have been developed for breast cancer treatment with promising results [72].

1.4.3.3. Clathrin- and caveolin-independent endocytosis (CIE)

Clathrin- and caveolin-independent endocytosis comprises a small percentage of the total cellular endocytic flux. The endocytic vesicles/tubules involved in CIE have no specific coat. This uptake does not necessarily require binding to specific cell-surface receptors. CIE involves lipid rafts, which are Chol and sphingolipid-rich domains within the PM [74]. Interestingly, breast cancer stem cells, which are thought to be the major cause of chemoresistance [75], have a higher rate of CIE than differentiated breast cancer cells. CIE is classified on the basis of GTPase effectors: Arf6-dependent, flotillin-dependent, Cdc42-dependent, and RhoA-dependent [76]. Flotillin-1, one of the GTPases that mediates CIE, is highly expressed in breast cancer and correlates with poorer patient survival [77]. Nanomedicine can also take advantage of this pathway.

3.4.3.3. Macropinocytosis

Macropinocytosis is a non-specific cellular uptake mechanism that is characterized by engulfment of extracellular fluids and solutes through large actin-stabilized PM extensions. Macropinocytosis thus enables the uptake of different macromolecules including albumin, extracellular proteins, exosomes, necrotic cell debris and exogenous solutes like drugs, and it is sensitive to receptor regulation [78]. Depending on the cell type, macropinocytosis is mainly

constitutive or induced. Macropinosomes can have two intracellular fates: recycling to the cell surface for cargo release back into the extracellular space, or trafficking to lysosomes, where the macromolecular cargo will be broken down into their monomeric constituents, thereby creating an intracellular source of nutrients [79]. Since macropinocytosis is an efficient and rapid form of endocytosis, it is not surprising that cancer cells have exploited it to replenish scarce nutrients for sustained proliferation [80]. Interestingly, prostate and breast cancer cells utilize macropinocytosis to translocate the growth factor receptor EGFR from the PM into the nucleus for further cellular proliferation [81]. The fact that macropinosomes can reach the nucleus can be very advantageous in nanomedicine since most of chemotherapeutic drugs need to reach the nucleus to perform their cytotoxic effects. Macropinocytosis has been exploited for the targeted delivery of anti-cancer therapeutics. Synthetic conjugates comprising any combination of small chemicals, lipids, proteins, genetic materials, and chemical scaffolds can be developed to form NPs that can then be internalized into target cells by this route [82]. One example is the albumin-bound form of paclitaxel, ABR, one of the FDA-approved drugs for treating multiple cancers, which is internalized by macropinocytosis, in addition to CavME. Conjugates with non-albumin carriers, such as paclitaxel poliglumex (PPX), comprising paclitaxel and polyglutamic acid polymers, have also been successful for metastatic breast cancer treatment [83].

3.5. Drug uptake and chemoresistance in the main breast cancer drugs

Inherent and/or acquired resistance to chemotherapy is a major challenge to developing feasible targeted strategies for breast cancer. Numerous studies describe how breast cancer resistance is caused by alterations in activation/inhibition of distinct signaling pathways (survival, apoptosis, autophagy, cell cycle, etc.) [59], as well as mutations or changes in the expression of specific proteins (hormone and growth receptors, transcription factors, etc). Moreover, it has been clearly demonstrated that the expression of many members of the drug efflux ABC transporter family, such as the P-glycoprotein (P-gp), also known as multidrug resistance protein 1 (MRP1), or the breast cancer resistance protein (BCRP), is greatly increased in resistant breast cancer cells [84]. Nevertheless, the role of drug uptake in de novo or acquired resistance is less well understood and needs further research, in order to obtain better dose–response outcomes and reduce toxic side effects.

3.5.1. Anthracyclines

Anthracyclines are highly effective chemotherapy drugs used in treating a broad range of malignancies. The mechanisms that contribute to the cytotoxic effect of these drugs are DNA intercalation, inhibition of topoisomerase II and the generation of free oxygen radicals

(Fig. 16). The major adverse effect of anthracyclines is cardiotoxicity in cumulative doses. The two most commonly used anthracyclines in breast cancer are doxorubicin (DOX) and epirubicin (EPI), a semisynthetic derivative of DOX [85].

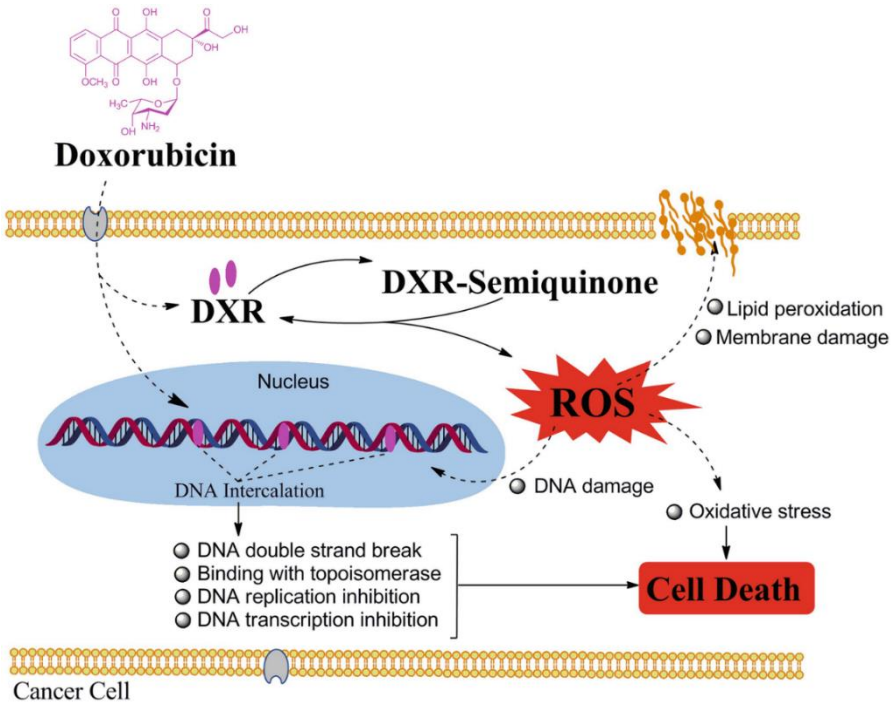

Fig. 16. Molecular structure and mechanisms of DOX-mediated cell death. The primary mechanism of action of DOX involves the drug's ability to intercalate within DNA base pairs, causing breakage of DNA strands and inhibition of both DNA and RNA synthesis. It also inhibits the enzyme topoisomerase II, causing DNA damage and induction of apoptosis and it causes free radical-mediated oxidative damage to DNA (extracted from [86]).

EPI has similar effect to DOX in tumors but it has a lower toxicity. In breast carcinoma treatment, DOX is one of the most efficacious drugs in both early and late stage tumors [87]. Nevertheless, DOX is the subject of several drug resistance mechanisms that are not well understood, some of them related to drug uptake. It is well known that DOX and the rest of anthracyclines can create electrostatic and hydrophobic interactions with cell membranes, enabling them to enter cells by passive diffusion. Once inside, they are rapidly distributed and retained in the nucleus due to their lipophilic nature and DNA binding capacity. Comparative studies between DOX resistant breast cancer cell lines and the parental ones have demonstrated that changes in lipid PM composition promote multi-drug resistance by impairing drug uptake. DOX-resistant MCF7 breast cancer cells have higher concentrations of SM and Chol than the sensitive ones entailing a more rigid and less permeable PM [88] (Fig. 17).

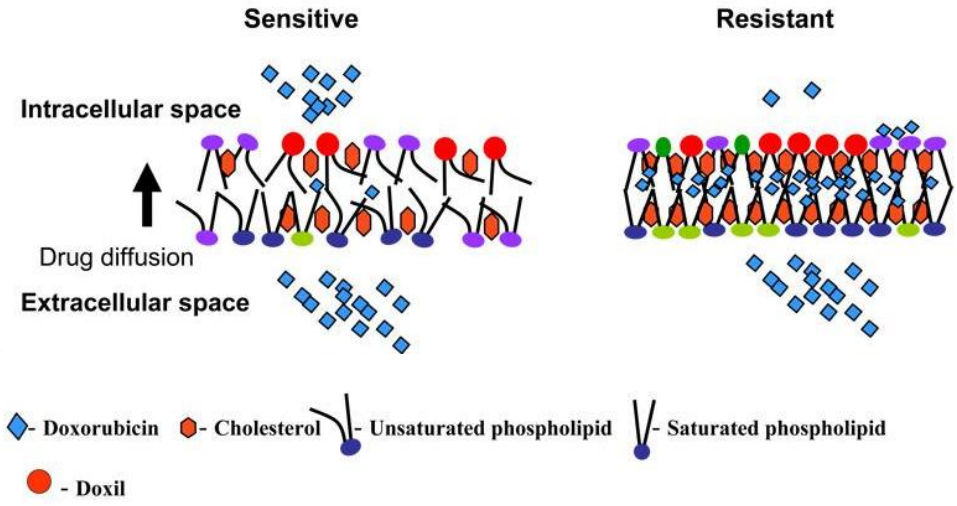

Fig. 17. Drug uptake in sensitive and resistant cells. Representation of the influence of lipid packing density and fluidity of sensitive and resistant cell membrane lipids on drug diffusion across the lipid bilayer. Low lipid packing density and high fluidity arrangement of the lipids of sensitive cells allow the drug to diffuse freely across the bilayer without interaction. In contrast, high lipid packing density and low fluidity of resistant cells and the hydrophobic nature of resistant membrane lipids hinders free drug diffusion and favors drug-lipid interaction, trapping the drug in membrane lipids (extracted from [88]).

DOX establishes a strong hydrophobic interaction with resistant cell membranes, which causes the drug to be trapped in the lipid bilayer. Palmitate abundance is also increased in the PM of resistant cells. Fatty acid synthase has been demonstrated to be highly expressed in the drug-resistant breast cancer cell line MCF7/AdVp3000, increasing palmitate content, which modulates the transversal mobility of membrane components and disrupts DOX uptake [89]. Moreover, changes in cytosolic pH due to a higher activity of the proton pump vacuolar-type ATPase and the proton transporters can affect the packing of lipids and decrease the transverse movement of DOX [90]. Furthermore, weak bases like DOX can be protonated in an acidic extracellular environment leading to ion-trapping and reduced drug uptake [91]. The modified lipid composition of the PM of MCF7/ADR breast cancer resistant cells not only impairs passive diffusion, but also endocytosis (Fig. 18) [88]. Endocytosis is a crucial uptake mechanism for commercial DOX-nanoparticle drugs, such as Doxil® (pegylated liposomal) and Myocet® (non-pegylated liposomal), and also for free DOX [87]. Moreover, in cancer cells, the increased rigidity of the endosome membrane prevents drug escape into the cytoplasm, while leading the vesicles to the late endosomal/lysosomal pathway, rather than the recycling pathway, hence disrupting the continuous endocytosis [88].

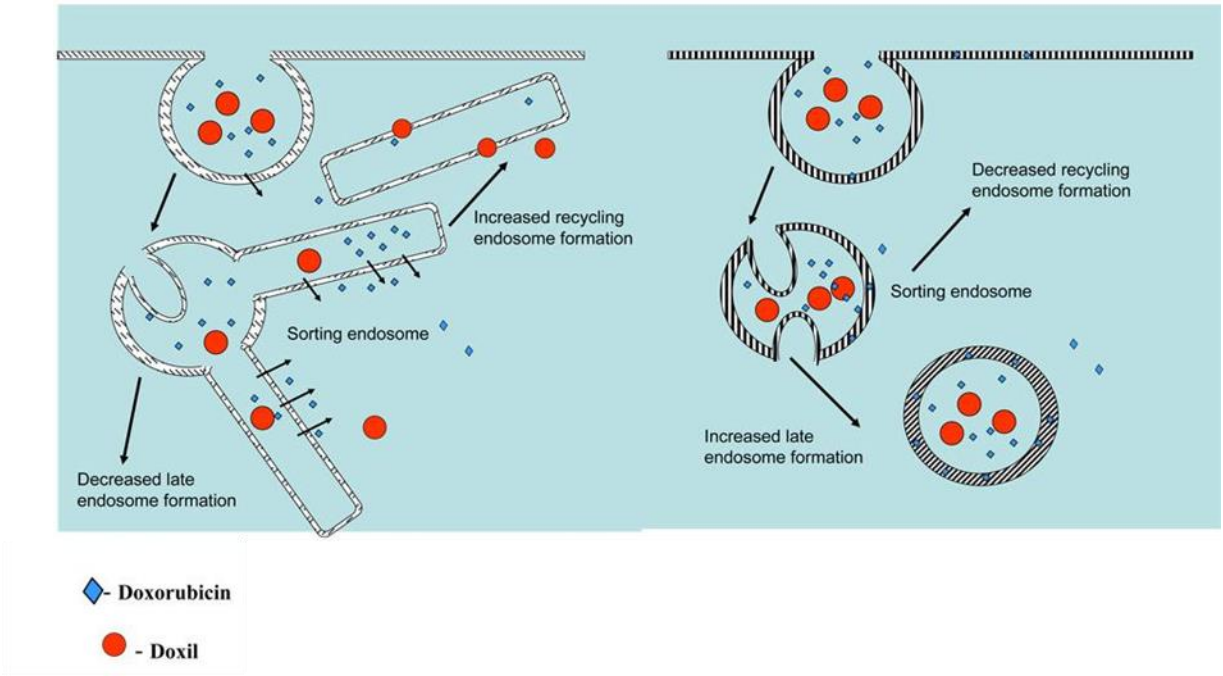

Fig. 18. Mechanism of drug transport in sensitive and resistant cells. Pathways of drug transport in sensitive (left) and resistant (right) cells. Drug or Doxil preferentially follow the pathway of sorting endosomes to recycling endosomes in sensitive cells as against sorting endosomes to LEs/lysosomes in resistant cells. This effect could be due to the low membrane fluidity of resistant cells vs. that of sensitive cells and also due the difference in drug interaction with resistant and sensitive cell membrane lipids. DOX interacts with the membrane lipids of resistant cells but not that of sensitive cells (extracted from [88]).

The third main pathway for DOX uptake is through the organic cation transporter OCT6. This high affinity carnitine transporter is expressed in a variety of cancer cell lines and has been involved in anthracycline resistance [65].

3.5.2. Taxanes

Taxanes are cytotoxic chemotherapy agents that act as mitotic inhibitors disrupting microtubule function (Fig. 19). A combination of taxanes and anthracyclines remains the standard neoadjuvant chemotherapy in breast cancer. Adding a taxane drug to standard chemotherapy improves survival in early breast cancer. However, the use of taxanes leads to increased risk of some side effects, such as febrile neutropenia and neuropathy. Two main taxane drugs are available in breast cancer treatment: paclitaxel and DTX.

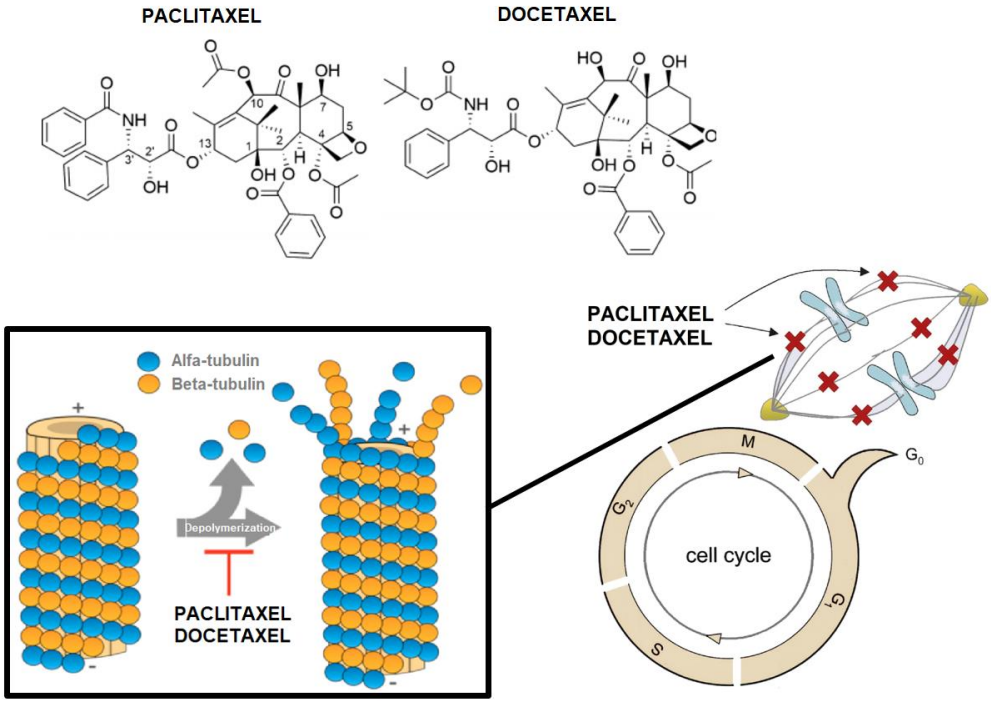

Fig. 19. Molecular structure and mechanism of action of taxanes. Illustration of how taxanes as paclitaxel and docetaxel prevent cell division by inhibiting microtubules depolymerization (modified from [92,93]).

Several mechanisms of chemoresistance related to taxane uptake have been described. Taxanes enter cells through rapid passive diffusion, due to their hydrophobicity [94]. Therefore, similar to what happens in anthracyclines, higher levels of PM Chol present in some multi-drug resistant cell lines will impair drug uptake. Another important mechanism of taxane resistance involves the membrane transporter OATP1B3, which is expressed in 50% of breast tumors, and correlates with better prognosis [95]. Both paclitaxel and DTX are substrates of this transporter [66]. Since paclitaxel resistant breast cancer cell lines show OATP1B3 downregulation compared to sensitive cell lines, OATP1B3 expression is used as a prediction marker of paclitaxel sensitivity in patients [96]. Four nanoformulations containing paclitaxel are currently available for breast cancer therapy: ABR, Genexol®, Nanoxel® and Lipusu® [87]. These nanoformulations enter cancer cells through endocytosis and several mechanisms of resistance have been described. For example, a proteomic analysis comparing ABR sensitive and resistant cancer cells has identified several proteins involved in the regulation of actin cytoskeleton function (which is critical for macropinocytosis) [97]. On the other hand, plastin-3 (PLS3) expression, a protein involved in endocytosis, was increased in cisplatin-resistant human cancer cell lines compared to their cisplatin-sensitive counterparts [98]. Coherently, PLS3 downregulation increased paclitaxel sensitivity in MDA-MB-231 breast cancer cells [99]

through endocytosis modulation. On the other hand, it has been demonstrated that ABR resistant cell lines have decreased Cav1 expression, a crucial component of CavME [73].

Many other proteins and mechanisms must be present in resistance to doxorubicin and paclitaxel. Greater knowledge of these would facilitate their approach.

More detailed information related to drug uptake-based chemoresistance in breast cancer treatment is contained in the recent published literature review: Muley H, Fadó R, Rodríguez-Rodríguez R, Casals N. Drug uptake-based chemoresistance in breast cancer treatment. Biochem Pharmacol. 2020.

HYPOTHESES

HYPOTHESES

1. The first hypothesis is that CPT1C, which is a protein involved in cancer cell metabolic adaptation, its expression can be a prognosis marker in human breast cancers.
2. The second hypothesis is that CPT1C is involved in proliferation, migration, invasion and chemoresistance processes specially in relation to lipid metabolism in human breast cancer cells.

OBJECTIVES

OBJECTIVES

General objective

To explore the association between CPT1C expression and breast cancer prognosis and to study the role of CPT1C in proliferation, migration, invasion and chemoresistance in breast cancer cells.

Specific objectives

1. To explore in survival databases, the relationship between CPT1C expression and human breast cancer prognosis.
2. To study whether CPT1C silencing can impair cell proliferation, migration and invasion processes in breast cancer cells.
3. To figure out whether CPT1C silencing is involved in chemoresistance in breast cancer cells.
4. To elucidate the molecular mechanism by which CPT1C regulates this chemoresistance.

METHODOLOGY

METHODOLOGY

1. Cellular biology

1.1. Cell lines and cell culture

1.1.1. Cell lines maintenance

All the human breast cancer (MDA-MB-231, MCF7, BT-474 and MDA-MB-468), neuroblastoma (SH-SY5Y), glioblastoma (U-87 MG) and HEK293T cell lines were cultured in Dulbecco's Modified Eagle's Medium (DMEM) (41966 Gibco) supplemented with 10% fetal bovine serum (FBS-12A Capricorn), and 100 U/ mL penicillin and 100 µg/mL streptomycin (15140122 ThermoFisher). Cells were maintained at 37°C in 5% CO2 humidified air. Two passages per week with a 10 dilution factor were conducted in all stable cell lines. These were used within 1 month after thawing of frozen aliquots and were authenticated on the basis of viability, recovery, growth, and morphology by ATCC on 24th September, 2018. The cells were tested for mycoplasma contamination using EZ-PCR™ Mycoplasma Detection Kit (20-700-20 BI). TP53 status of breast cancer cell lines are specified in Table 5.

TP53 STATUS IN HUMAN BREAST CANCER CELL LINES				
Cell line	**Mutated status**	**DNA variant**	**Prediction**	**Activity**
MCF7	Wild-type	Wild-type	Normal	Active
BT-474	Mutated	c.853G>A	Damaging	Inactive
MDA-MB-231	Mutated	c.839G>A	Damaging	Inactive
MDA-MB-468	Mutated	c.818G>A, c.524G>A	Damaging	Inactive

Table 5. p53 mutation status in different human breast cancer cell lines (extracted from [100]).

1.1.2. Plasmids for stable cell lines

Human cancer cell lines cells expressing silencing CPT1C-shRNA or SAC1-shRNA were generated using lentiviral infection. shLVTHM1-CPT1C (shCPT1C_1) and shLVTHM2-CPT1C (shCPT1C_2) plasmids were engineered with the pLVTHM vector (12247 Addgene) at UIC by Dr. Xavier Roa-Mansergas [101] expressing CPT1C-specific shRNA's (sequence 5′-GAAAUCCGCUGAUGGUGAA-3′ and 5′-GACAAAUCCUUCACCCUAA-3′ respectively). Conversely, the construct to silence SAC1, psiLVRU6MP-SAC1 (shSAC1) was purchased in tebu-bio containing the silencing sequence 5′-GTAGCAAATCACATGGATG-3′ [8].

Human cancer cell lines expressing CPT1C were generated using lentiviral infection. pWPI-CPT1C plasmid, which contains the murine CPT1C in the pWPI vector (12254 Addgene), was constructed by Dra. Macarena Pozo [13].

All plasmids were generated carrying the GFP (green fluorescent protein) as an expression control. The vectors were packaged into lentiviral particles in HEK293T cells.

1.1.3. Production of lentiviral infected cells

Lentivirus infection for CPT1C or SAC-1 overexpression or silencing was performed in different cell lines. The whole procedure was conducted under Biosafety level-2 hoods. Lentivirus infection was performed at different Multiplicity of Infection (MOI) ranging from 7 to 30 depending on the cell line.

1.1.4. Cell lines freezing

After checking by flow cytometry that almost 100% of infected cancer cells were GFP-positive, cells were mixed with medium containing 10% DMSO in cell-cryotubes. Then, vials were immediately transferred to cell freezing container (5100-0001 Thermo-Fisher) and placed in a -80°C freezer for at least 24 h. Few days later, frozen cells were transferred to liquid nitrogen (-196°C) for storage.

1.1.5. Cell lines thawing

Cells were very quickly thawed in a 37°C water bath and mixed with culture medium. After centrifugation, cell pellets were resuspended and added to flask (or dish) already containing cell culture medium. Minimum two passages after thawing were done before any of the experimental procedures.

1.1.6. 3D culture

Growth factor-reduced Matrigel (GFR Matrigel; 356231 BD Biosciences 9,1 mg/mL) was removed from −20°C storage and thawed slowly at 4°C. Culture media was mixed at 1:1 ratio with Growth Factor Reduced Matrigel. Mix containing 32 µl was added to each well of a 96-well opaque (136101 Thermo Scientific) or clear plate and incubated at 37°C for 30 min. 2,000 cells/well of MDA-MB-231 or 10,000 cells/well of BT-474 in 10% matrigel medium were added on top of the coating and maintained in culture for 4 days. Pictures of the spheres were taken at day 4, 5 and 6 with × 10 magnification using an inverted microscope (Leica).

1.2. Cell proliferation assays

1.2.1. 3-(4,5-dimethylthiazol-2-yl)-5-(3-carboxymethoxyphenyl)-2-(4-sulfophenyl)-2H-tetrazolium inner salt (MTS)

To evaluate the proliferation rate of MDA-MB-231 cells, the CellTiter 96 AQueous Non-radioactive Cell Proliferation Assay, MTS (G5421 Promega) was used according to the manufacturer's protocol. Briefly, 1,000 MDA-MB-231 cells/well were incubated in 96-well plates for 24, 48 or 72 h. Upon completion of the experiment, cell medium was replaced by complete medium with Cell Titer 96 AQueous One (MTS) solution. After 1 h incubation at 37°C, 5% CO2, absorbance was measured at 490 nm and 650 nm. All absorbance values were normalized with the absorbance values from day 0. Test was performed in six replicates per condition.

1.2.2. Bromodeoxyuridine (BrdU) incorporation assay

For cell proliferation analysis, an enzyme-linked immunosorbent assay (ELISA) (cell proliferation Elisa BrdU (5-bromo-2-deoxyuridine) 11647229001, Roche Applied Science) was applied. 10^5 cells/ml were seeded in 96-well plates in complete medium and incubated overnight to allow attachment. Cells were then incubated for 2 h with 1 µM BrdU labeling solution. After fixing the cells and denaturating DNA, cells were labeled with anti-BrdU-peroxidase solution for 2 h. Cells were washed, incubated with tetramethyl-benzidine substrate for 5 min and immune complexes were detected by measuring the absorbance at 370 nm. All tests were performed at least in triplicates in 3 independent experiments.

1.2.3. Colony formation assay

1.2.3.1. Procedure

For colony-formation assay, 1,500 MDA-MB-231 for 9 days, MCF7 for 9 days, BT-474 for 5 weeks and MDA-MB-468 cells for 7 days were plated in 6-well plates. The medium was changed every 3 days. At indicated time, cells were methanol-fixed at -20°C for 15 min followed by PBS washings. The image of each well were kept after staining with 0.5% crystal violet in water with 25% methanol for 30 min and three PBS washings. All tests were performed in at least three replicates and tests were repeated four times.

1.2.3.2. ImageJ "Colony formation" macro development and analysis

Colony formation analysis was conducted using the open-source Fiji ImageJ software (https://imagej.net/Fiji/Downloads, version 2.0, National Institute of Health, Bethesda, MD, USA). The ImageJ step-by-step protocol used in this study for image analysis is shown in Figure 19. First, individual color images were imported into ImageJ by selecting the *File option* followed by the dropdown *Open option* (Fig. 20A). On the opened images, a generated macro was automatically applied for all the experiments. The macro included the next steps. After

uploading color images the background was subtracted in *Process/Subtract Background* checking a rolling ball radius of 1 and light background (Fig. 20B). Then, the local contrast of the image was enhanced selecting *Process/Enhance Local Contrast (CLAHE).* In this method, the parameters were chosen as followed: block size (127), histogram bins (256) and max slope (3), and mask and fast unchecked (Fig. 20C). Finally, the image was converted to black and white in *Process/Binary/Make binary* (Fig. 20D) and for cutting apart particles that touch, *Binary options/Watershed* was selected (Fig. 20E). The white area represents the area of the colonies. At that point, an oval selection was manually made around the inner part of the well. The *Analyze Particles* macro was run by first selecting the *Analyze option* and then the macro *Analyze Particles*. Thereafter, maximum and minimum values for the size and circularity of the objects (size: 150–∞ and circularity: 0.10–1.00) were selected and particles of edges were checked for being excluded. Once all parameters from the *Analyze Particles* macro were setup, the automated analysis was run. After running the analysis, ImageJ generated a new image displaying the particles that were identified (Fig. 20F). The following output variables were taken: total number of identified colonies, the total colony area (in pixels), the average size of each colony (in pixels), and the percentage of colony area per well surface.

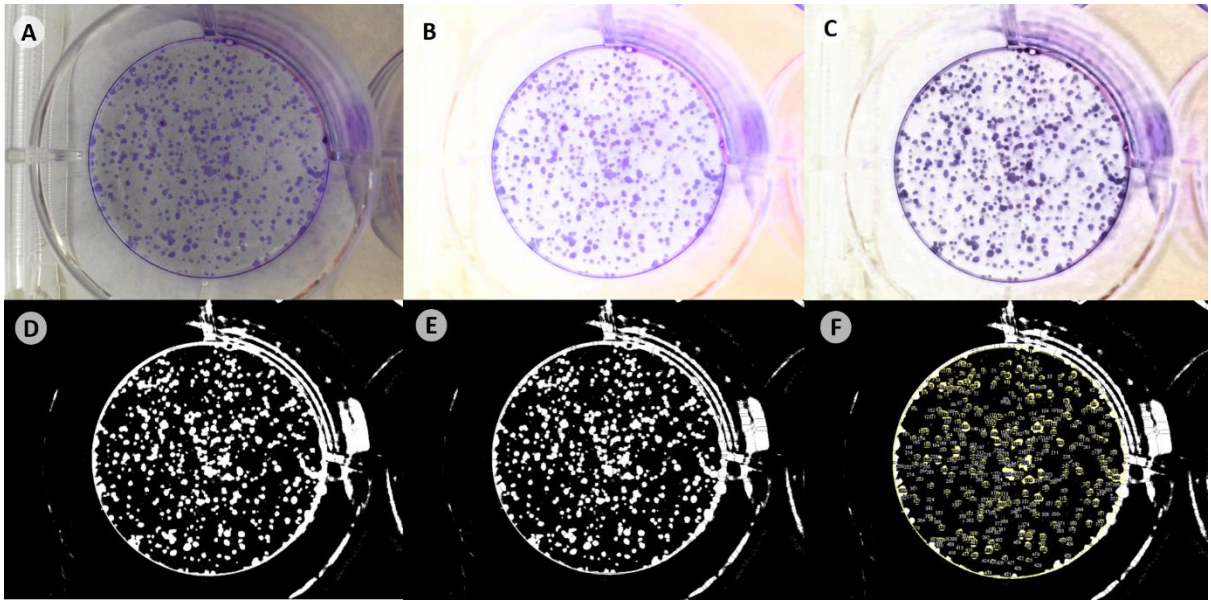

Fig. 20. "Colony formation.ijm" macro was developed for automatic analysis of colony formation assays. Colony formation analysis was conducted using the open-source Fiji ImageJ software. The ImageJ step-by-step protocol used in this study for image analysis is shown. First, individual color images were imported into ImageJ (A). The macro included the next steps: background subtraction (B), local contrast enhancement (C), binary image creation (D) and running of "Watershead" (E). An oval selection was manually made around the inner part of the well and the Analyze Particles macro was run.

1.2.4. xCELLigence DP Real-Time Cell Analyzer (RTCA) proliferation assay

xCELLigence RTCA label-free technology continuously monitors live cell number by changes in impedance measured through gold electrodes fused to the bottom surface of culture plates. In the presence of an electrically conductive solution, the presence of cells on top of the plates affects the ionic environment at the electrode/solution interface, leading to an increase in electrode impedance. The more cells that are attached on the electrodes, the larger the increases in electrode impedance. Electrode impedance is displayed as a dimensionless parameter called Cell Index (CI) values.

A total of 7,500 MDA-MB-231 cells/well were seeded into E-plate 16 (5469830001, ACEA Biosciences). Experiments were carried out using the RTCA DP instrument (Roche Diagnostic GmbH, Germany) which was placed in a humidified incubator maintained at 37°C with 5% CO2. The slope of the curve of cell index measured over time can be related to the proliferation velocity of tumor cells. Cell indices were measured every 10 min for up to 48 h with the RTCA software (version 2.0, Roche Diagnostics). All tests were performed in duplicates and tests were repeated four times.

1.3. Cell migration assays

1.3.1. xCELLigence DP Real-Time Cell Analyzer (RTCA) migration assay

Real-time cell analysis (RTCA) of migration was performed on the xCELLigence DP device essentially as described in the supplier's instruction manual. Briefly, cells are added to the upper chamber of a two-chamber device separated by a porous membrane (the CIM-plate 16). Cells attach and migrate directly through the pores to the bottom side of the membrane (where the electrodes reside). The cell index represents the capacity for cell migration, and the slope of the curve can be related to the migration velocity of tumor cells. The cell index thus reflects the tumor cell's migratory capacity. MDA-MB-231 cells were incubated overnight with serum-free medium in non-confluent 6-wells plate. Then, 80,000 cells/well were suspended in culture medium without FBS and then seeded on the top chamber according to the manufacturer's manual. Culture medium containing 10% FBS was used as a chemoattractant in the bottom chamber. Cell indices were measured every 10 min for up to 48 h with the RTCA software. All tests were performed with at least duplicates and repeated three times.

1.3.2. Wound healing assay

MDA-MB-231 cells were incubated overnight with serum-free medium in non-confluent 6-wells plate. From there, 10^6 MDA-MB-231 cells/well were seeded on 6-well plates and incubated overnight. Adherent cell monolayers were scratched with a 10-µl pipette tip and

washed twice with PBS. Cells were cultured in 0,5% FBS DMEM for 16h. Images were taken at 0 h and 16 h, using an Olympus CKX41 inverted microscope under 10x objective lens. Four sequential photos were taken for each well to keep the whole gap. Cell migration was assessed by monolayer gap closure (Cell area (16 h) – Cell area (0 h)), embedded by ImageJ software with a wound healing tool macro (Montpellier RIO Imaging, CNRS, Montpellier, France). All tests were performed in six-replicates and tests were repeated four times.

1.3.3. Transwell migration assay

After an overnight incubation with serum-free medium in non-confluent 6-wells plate, 50,000 MDA-MB-231 cells were seeded in serum-free medium conditions in Corning® Costar® Transwell® cell culture inserts (CLS3464 Sigma-Aldrich). Culture medium containing 10% FBS culture was used as a chemoattractant in the lower chamber. After incubation in standard conditions (37°C, 5% CO2), the medium was removed at 14 h. The cells in the upper chamber were washed twice with cold PBS and methanol-fixed for 15 min at -20°C. After washing with cold PBS, the nuclei were stained with Hoechst for 5 min at RT (room temperature). Once PBS-washed, the non-migrated cells (out of focus) and the migrated cells (focused) were observed through Hoechst staining under an Olympus CKX41 inverted microscope). Captured images (10 random fields/well) were analyzed automatically and also manually, counting the percentage of migrated cells using ImageJ. All the experiments were performed in triplicate and tests were repeated two times.

1.4. Cell invasion assays

1.4.1. Gelatin degradation invasion assay

1.4.1.1. Procedure

An invasion assay with EMD QCM™ Gelatin Invadopodia kit (ECM671 Millipore) was performed similarly as described in the supplier's instruction manual. In brief, at RT, 12mm coverslips were coated with poly-L-lysine for 20 min, washed three times with PBS, and cross-linked 15min with a solution of glutaraldehyde. Coverslips were again washed three times in PBS and then incubated with a pre-warmed gelatin mixture (Cy3-Gelatin and unlabelled gelatin) dissolved in PBS for 10 min. Before plating cells, dishes were washed in PBS three times, disinfected for 30 min in 70% ethanol, washed and incubated in normal culture medium for 30 min to quench residual free aldehydes. Cells were plated at a density of 38,000 cells/well on these dishes for 40 h before processing. Following fixation in 3,7% PFA for 30min and PBS washings, cells were permeabilizated in 0.25% TritonX100 and blocked in 2% BSA. Then, cells were stained with FITC-phalloidin (2 µg/mL) and DAPI (1 µg/mL) in fluorescent staining

buffer (DPBS with 2% blocking serum and 0.25% Triton X-100) for 1 h at RT. After two PBS washings, slides were mounted in Fluoromount Aqueous Mounting Medium (F4680 Sigma-Aldrich). Images were collected using a Nikon Ti-E inverted microscope under 20x objective lens. Gelatin degradation was measured by quantifying the total area of non-fluorescent pixels per cell using two automatic macros generated in ImageJ for cell counting (nuclei detection by DAPI with Hoechst nucleus macro.ijm) and for gelatin degradation quantification (black area detection by Cy3 with Red gelatin macro.ijm). 10 random fields were imaged per condition, and each independent experiment was performed in quadruplicate and averaged. The experiment was performed twice.

1.4.1.2. ImageJ gelatin degradation analysis macro development and analysis

1.4.1.2.1. Red gelatin macro.ijm development

Gelatin degradation analysis was conducted using a generated macro in ImageJ. The ImageJ step-by-step protocol used in this study for image analysis is shown in Figure 20. First, individual color images were imported into ImageJ by selecting the *File option* followed by the dropdown *Open option* (Fig. 21A). On the opened images, a generated macro was automatically applied for all the experiments. The macro included the next steps. First of all, on the uploaded color images the background was subtracted in *Process/Subtract Background* selecting a rolling ball radius of 50 and light background (Fig. 21B). Then, an *Auto Threshold* was applied by *Moments* method in *Image/Adjust/Auto Threshold* (Fig. 21C) followed by thresholding to convert each color image into a binary image (*Image/Adjust/Threshold*) (Fig. 21D). The *Analyze Particles* macro was run by first selecting the *Analyze option* and then the macro *Analyze Particles*. Thereafter, maximum and minimum values for the size and circularity of the objects (size: 1–∞ and circularity: 0.00–1.00) were selected. Once all parameters from the *Analyze Particles* macro were setup, the automated analysis was run. After running the analysis, ImageJ generated a new image displaying the particles that were identified (Fig. 21E). Total gelatin degradated area was the output variable analyzed.

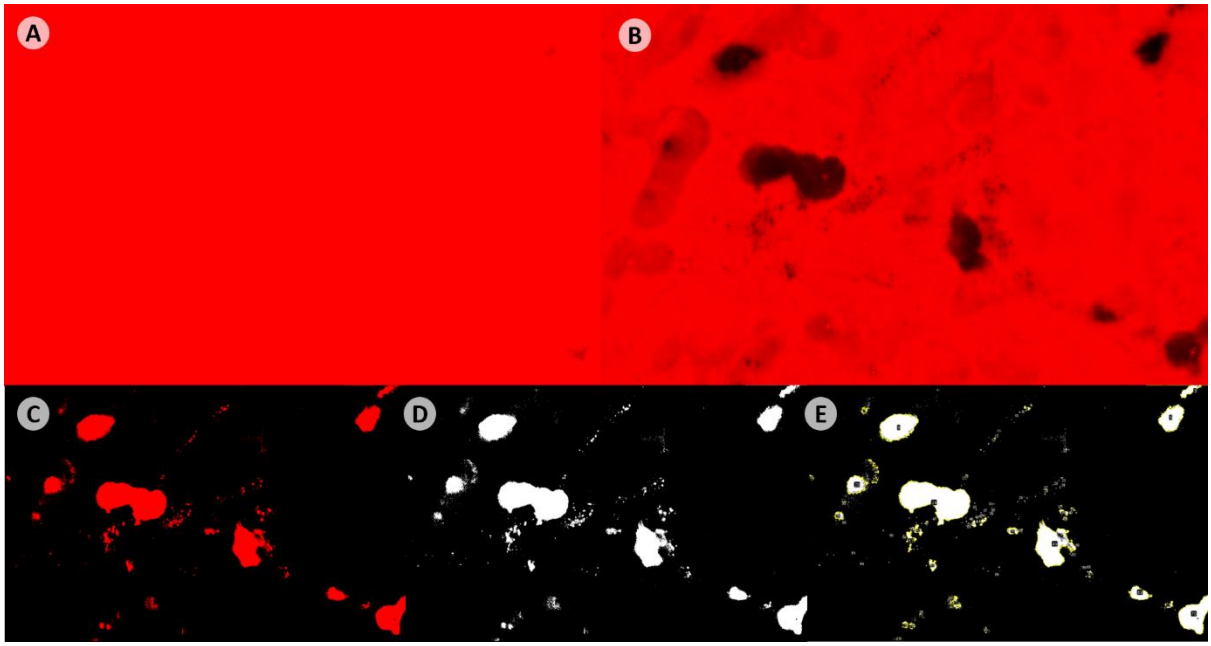

Fig. 21. "Gelatin degradation.ijm" macro was developed for automatic analysis of red gelatin degradation assays. Gelatin degradation analysis was conducted using a generated macro in ImageJ. The ImageJ step-by-step protocol used in this study for image analysis is shown. First, individual color images were imported into ImageJ (A). The macro included the next steps: subtraction of background (B), an Auto Threshold (C) followed by conversion to binary image (D). Then, Analyze Particles macro generated a new image displaying the particles that were identified (E) and a separate Summary window provided the output variable: total gelatin degraded area.

1.4.1.2.2. Hoescht nucleus macro.ijm development

Cell counting in each field was conducted using another generated macro in ImageJ. The ImageJ step-by-step protocol used in this study for image analysis is shown in Figure 21. Individual color images were imported into ImageJ by selecting the *File option* followed by the dropdown *Open option* (Fig. 22A). On the opened images, a generated macro was automatically applied for all the experiments. The macro included the next steps. First, on the uploaded color images the contrast was enhanced with a 0.3% of saturation in *Process/Enhance* (Fig. 22B). Then, each color image was converted into a binary image in *Process/Binary/Make binary* (Fig. 22C) and finally the holes were filled and cutted apart particles that touch, selecting inside *Binary options Fill Holes* (Fig. 22D) and *Watershed* (Fig. 22E). The Analyze Particles macro was run by first selecting the Analyze option and then the macro Analyze Particles. Thereafter, maximum and minimum values for the size and circularity of the objects (size: 40–∞ and circularity: 0.00–1.00) were selected. Once all parameters from the Analyze Particles macro were setup, the automated analysis was run. After running the analysis, ImageJ generated a new image displaying the particles that were identified (Fig. 22F). The number of particles were taken as output variable.

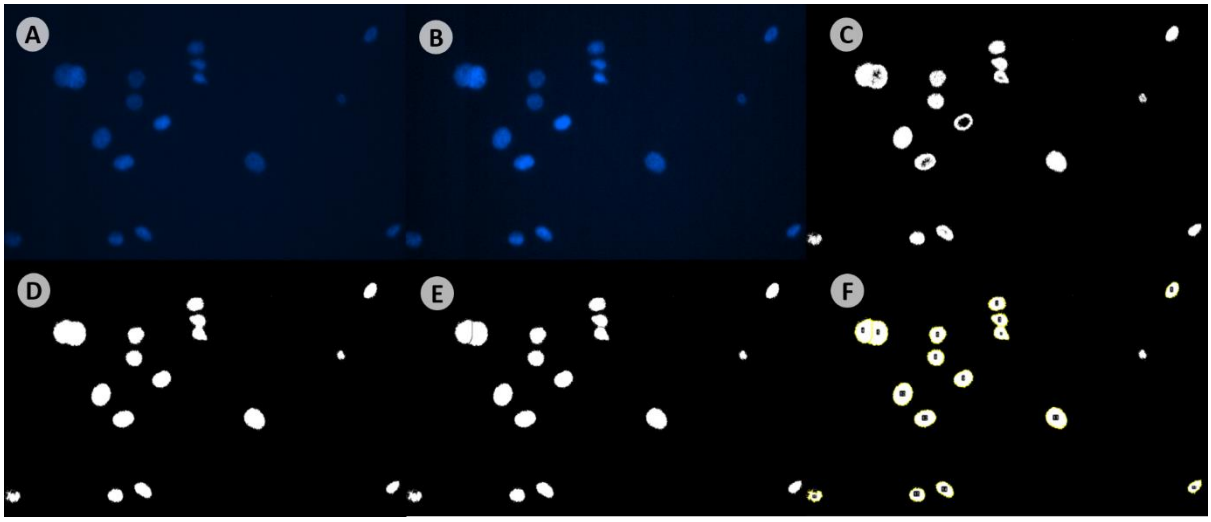

Fig. 22. "Hoescht nucleus macro.ijm" was developed for automatic analysis of red gelatin degradation assays. Gelatin degradation analysis was conducted using a generated macro in ImageJ. The ImageJ step-by-step protocol used in this study for image analysis is shown. First, individual color images were imported into ImageJ (A). The macro included the next steps: contrast enhancement (B), conversion to binary image (C) followed by running of "Fill holes" (D) and "Watershead (E). Then, Analyze Particles macro generated a new image displaying the particles that were identified (F).

1.4.2. xCELLigence DP Real-Time Cell Analyzer (RTCA) invasion assay

Real-time cell analysis (RTCA) invasion assay was performed similarly than migration assay described above, except that the surface of the upper chamber was previously covered with a monolayer of 50µl Growth factor-reduced Matrigel (diluted 1:40 with serum-free medium as detailed by Roche in the application notes). Cell indices were measured every 10 min for up to 48 h with the RTCA software.

1.5. Cell cytotoxicity assay

1.5.1. Chemicals and reagents treatments

Doxorubicin hydrochloride (DOX, 44583), paclitaxel (T7402) and KT182 (SML1248) were purchased from Sigma-Aldrich.

1.5.2. 3-(4,5-dimethyl-2-thiazolyl)-2,5-diphenyl-2-H-tetrazolium bromide (MTT) assay

25,000 cells/well were seeded in quadruplicate in 48-well plates for MTT assay. After an overnight incubation, cells were treated with drugs (or vehicle) at indicated times and doses. Upon completion of the experiment, cells of each well were incubated with 10 µl MTT reagent (M2128 Sigma-Aldrich) at 37°C for 2h. Then, the medium was removed and formazan crystals were dissolved in 100 µl DMSO and plates were read in Multi-Detection Microplate

Reader Synergy™HT (Biorad). Absorbance was measured at 570 nm. Percentage of viable cells were calculated normalizing by non-treated cells in order to abolish proliferation-related differences.

1.5.3. CellTiter-Glo® Luminescent Cell Viability Assay

Cell viability was evaluated with the Cell Titer-Glo®Luminescent Cell Viability Assay (G7572 Promega). White 96-well plates (136101 Thermo Scientific) were needed for these experiments. 4 days after seeding, 3D cultured cells were treated with drugs (or vehicle) at indicated times and doses. 100 µl of CellTiter-Glo reagent was then added to each well at RT for 30 min. ATP luminescence intensity was measured using the GloMax® 20/20 Luminometer. Percentage of viable cells was calculated normalizing by non-treated cells.

2. Microbiology

2.1. Escherichia Coli strain and growing conditions

The Escherichia coli (E. Coli) strain used in this project for pET28/His6-mCherry-D4 plasmid propagation was BL21. BL21 from a frozen glycerol stock were grown in 5 ml of autoclaved LB liquid broth without antibiotics overnight at 37°C.

2.2. Competent E.coli BL21 preparation

A total volume of 50 µl of the saturated BL21 culture was allowed to grow exponentially in 5 ml of LB for 2 h at 37°C. Then, cells were centrifuged at 4,000 rpm for 5 min at 4°C. Supernatant was discarded and pellet was gently resuspended in 2.5 mL of ice cold 50mM $CaCl_2$. Suspension was kept on ice for 20 min. After that, cells were centrifuged at 4,000 rpm for 5 min at 4°C. Supernatant was discarded and pellet was gently resuspended in 500 µl of ice -cold 50mM $CaCl_2$. Cell suspension was ready for transformation.

2.3. Bacterial transformation

A total volume of 100 µl of competent BL21 cells was gently mixed with 0.5 µl of pET28/His6-mCherry-D4 plasmid solution (RIKEN BioResource Research Center; RDB14300; 25 ng/µl) in a transformation tube on ice. Same protocol was followed without DNA for the negative control. Mixture was placed on ice for 30 min and heat shock was made at exactly 42°C for exactly 45 sec. Sample was placed on ice for 2 min and 400 µl of SOC (0.5% yeast extra, 2% triptona, 10mM NaCl, 2.5mM KCl, 10mM $MgCl_2$ $6H_2O$, 10mM $MgSO_4$ $7H_2O$) was added the mixture at RT. Tube was placed at 37°C for 1 h with vigorous shaking. All the mixture was spread onto a LB agar plate (Luria Agar Cat. 1552.00) with kanamycin (11815-024 Gibco) for plasmid selection. Selection plate was incubated overnight at 37°C.

2.4. Plasmid extraction and detection

Plasmid extraction was performed from 4 colonies to check pET28/His6-mCherry-D4 presence. Miniprep DNA Purification Kit (A1330 Promega) was used according to manufacturer's instructions. Then, DNA was digested with ApaI restriction enzyme (R0114 New England BioLabs) according to manufacturer's instructions. Next, digested DNA was run in an agarose gel electrophoresis. pET28/His6-mCherry-D4 plasmid was detected at the expected size: 6.3 kbp.

2.5. Protein purification

mCherry-D4 protein was purified similarly to manufacturer's instructions and as following[102]. One BL21 transformed colony where it has been confirmed pET28/His6-mCherry-D4 plasmid presence was transferred to 10 mL of LB broth with kanamycin and incubated for 16 h at 37°C under agitation. Pre-culture was transferred to a 5 L conical flask containing 1 L of LB broth with kanamycin and was incubated at 37°C under agitation. When the optical density at 600 nm has reached 0.4–0.6 (approximately 4 h), the culture was cooled down to 18°C. Isopropyl-β-D-thiogalactopyranoside (IPTG, A4773 Panreac) was added to a final concentration of 0.4 mM and the culture was incubated under agitation for 16 h at 18°C. The culture medium was transferred to centrifugation tubes and pelleted by centrifugation at 3,500g for 15 min. Then, the supernatant was discarded and cell pellet was resuspended in 20 mL of lysis buffer (50 mM NaH2PO4/Na2HPO4, 300 mM NaCl, 10 mM imidazole, pH 8.0) complemented with pepstatin (P5318 Sigma), leupeptin (108976 Calbiochem), benzamidine (B6506 Sigma) and PMSF (P7626 Sigma). Lysate was sonicated for 10 min (40% amplitude, on/off cycles 10s/20s, UP 50H) on ice alternating with agitation and centrifuged twice at 3,500g for 15 min at 4°C and the supernatant was kept. Then, it was centrifuged twice at 11,000g for 30 min at 4°C and the supernatant was kept. 300 µl of Nickel-charged affinity resin (11540656 Invitrogen) was transferred to an 1,5 ml-tube and washed three times with 1 ml of lysis buffer with subsequent centrifugation for 1 min at 1000 rpm at RT. Nickel-charged affinity resin was added to supernatant and mixture was further incubated for 1 h with 360º rotation at 4ºC. Supernatant was centrifuged for 2 min at 1000 rpm at 4ºC. Then, pellet with resin was kept and washed 3 times with 15 ml of buffer lysis with a subsequent centrifugation for 2 min at 1000 rpm at 4ºC. After washings, 600 µl of elution buffer (20 mM NaH_2PO_4/Na_2HPO_4, 250 mM imidazole, pH 7.4) was added into resin pellet and mixture was incubated for 20 min with 360º rotation at 4ºC. Membrane of a centrifugal filter was first equilibrated by adding 5 mL of phosphate buffer (PB, 20 mM NaH_2PO_4/Na_2HPO_4 pH 7.4) and it was centrifuged for 10 min at 3500 g. Next, the liquid was discarded. Supernatant probe was added to the ultrafiltration unit

and it was spun at 4500 g for 30 min in a fixed-angle rotor. The flow-through was discarded. 7 mL of PB buffer was added and spun at 4500 g for 30 min. The flow-through was discarded again. This spin with PB buffer was repeated at 4500 g and stopped when the probe was concentrate in 250 µl. The probe was recovered and its concentration was measured by Bradford. 250 µl of glycerol was added and the probe was stored at -20°C.

3. Molecular biology

3.1. Cellular transfection and infection

Transfection was used to introduce plasmids into cellular lines. Different methodologies were used.

3.1.1. Lipofectamine 2000 transfection

MDA-MB-231 cells were transfected with lipofectamine 2000. 70,000 MDA-MB-231 cells (80% of confluence) were seeded in poly-L-lysine treated coverslips in 24-well plates. The transfection mix was prepared for each well by mixing solution A and solution B. Both solutions were separately previously vortexed and incubated at RT for 15 min. Solution A contained 49.2 µl of FBS/antibiotic free DMEM with 0.8 µl of lipofectamine 2000 reagent and solution B 500 ng of the plasmid DNA of interest (mCherry-PI(4)P or hCPT1C tagged with mTurquoise2) with the same medium mixed before. The transfection mix was vortexed and left for 15 min at RT and before adding it to the cells drop by drop, wells medium was replaced by fresh antibiotic free DMEM.

3.1.2. Calcium phosphate transfection for lentiviral production

The calcium phosphate transfection method was used in HEK293T cells. This method consists of calcium phosphate precipitation with DNA and attachment of these precipitates to the cell surface and their endocytosis by the cell.

To produce lentiviruses for each condition desired, HEK293T cells at 80% of confluence were transfected with calcium phosphate. Cell medium was removed and fresh medium was added to the plate 2 h before the transfection. For lentivirus production three 100 mm Ø dishes were used per each desired virus. The amount of each plasmid and reagent used for the transfection is summarized in Table 6. The transfection mix was left between 15 and 20 min at RT before being added to the cells drop by drop.

Plasmids	**Lentivirus vector**	45	µg
	pMD2.G	15.9	µg
	psPAX2	29.1	µg
Calcium phosphate transfection reagents	**0.1x TE[1]**	1.3	ml
	Buffered water[2]	0.727	ml
	$CaCl_2$	0.223	ml
	2x HeBS[3]	2.25	ml
	Total volume	4.5	ml
	1.5 ml/dish		

0.1x TE[1]: 1 mM Tris-HCl pH8, 0.1 mM EDTA pH 8.

Buffered water[2]: MQ water supplemented with 2.5 mM HEPES pH 7.3.

2xHBS[3]: 280 mM NaCl, 50 mM HEPES, 1.5 mM $Na_2HPO{\cdot}2H_2O$ pH 7.

Table 6. Reagents calcium phosphate transfection. Amount of each plasmid and reagent used for lentiviral production.

3.1.3. Lentivirus production and infection

The following day of transfection, medium was discarded and replaced by 5 mL of fresh medium. 8 h later, virus-containing medium of each dish was collected and stored at 4 ºC and then replaced by 5 ml of fresh medium. This medium collection was repeated the next day in the morning and at late afternoon. Lentiviruses were finally obtained and concentrated (to 500 µl) by medium centrifugation (1h 30min at 3,000g and 4°C) with filtered tubes (Sartorius VS2042). Afterwards, the viruses were aliquot and stored at -80ºC during a maximum period of 3 months.

The titer of pLVTHM- or pWPI- carrying lentivirus was determined as followed. 30,000 HEK 293T cells were seeded in 24-well plates. The following day, cells were infected with different amounts of viruses (0, 0.03, 0.06, 0.125, 0.25, 0.5, 1 and 2 µl). Two wells were used to count total cells. Three days after the infection, GFP positive cells were counted by using BD FACSCalibur™ through a FL-1 detector. Then, a lineal regression was obtained of infected cells and GFP positive cells. The number of viral particles (TU) per mL was measured as follows:

$$\frac{\text{TU}}{\text{mL}} = \frac{\%\ \text{GFP positive cells x counted cells}}{\mu\text{L of viral solution added in the well}}$$

According to viral titer and MOI test, cancer cell lines used in this work were infected with 7 (SH-SY5Y), 10 (U-87), 20 (MDA-MB-468), 30 (MDA-MB-231) and 40 (MCF7 and BT-474)

MOI's. This titration step was skipped for the virus of psiLVRU6MP plasmid used to silence SAC1 (kindly provided by Maria Casas) because it encodes for the mCherry fluorophore (instead of GFP), which cannot be neither detected or tracked by our FACSCalibur™. For this reason, a trial with different volumes of virus was conducted in MDA-MB-231 cells. SAC1 levels were analyzed by western blot in order to decide which volume would be employed for the experiments. To analyze SAC1 levels, 10^5 cells/well were plated in 6 well-plates and infected with 4, 8, 16 µl. The viral solution volume that better silenced SAC1 with no significant cell death (4 µl) was chosen. Consequently, the same batch of produced viruses was used in all experiments.

3.2. RNA analysis

3.2.1. RNA extraction

Total RNA was isolated from cultured cells using TRIzol™ Reagent (15596018 Thermo-Fisher Scientific) following the manufacturer's instructions. Chloroform was added next to the cellular homogenate leading to three different phases: the upper fraction containing with RNA, an interphase and the lower phase containing DNA and proteins. The upper phase was finally precipitated with isopropanol and washed with ethanol 75%. DEPC water was lastly used to dissolve the extracted RNA. The quantity and quality of the isolated RNA was determined by Multi-Detection Microplate Reader Synergy™HT (Biorad).

3.2.2. Reverse transcription

For gene expression analysis, template cDNA was synthetized from 1 µg of total RNA using a reaction mixture composed of RT buffer (F88903, Lucigen), dNTPs (D7295, Sigma), Random RT primers (309080, Exiqon), M-MuLV reverse transcriptase (30222, bioNova), and Reverse transcriptase (30281-1, bioNova) in a total volume of 20 µl. The mixture was incubated at 37 °C for 1 h. Quantitative PCR was performed using SYBR Green I Master Mix (1725271, BioRad).

3.2.3. Real-Time Quantitative PCR Assays

Of the previous reaction, 2 µl was used with the polymerase chain reaction (PCR) mix SsoAdvanced SYBRGreen Supermix (1725261 BioRad) for quantitative real-time PCR (CFX96 Real-time System; BioRad). The following gene-specific intron-skipping primers (IDT DNA Technologies, Leuven, Belgium) were used at 10 µM: CPT1C (for-GGA CTG ATG GAG AAG ATC AAA GA, rev-CAC AAA CAC GAG GCA AAC AG); and β-actin (for-CGT GAT GGT GGG CAT GGG TC, rev-ACG GCC AGA GGC GTA CAG GG). Relative gene expression was estimated using the comparative Ct (2-ΔΔct) method in relation to β-actin levels.

3.3. Protein analysis

3.3.1. Protein extraction

When 6-well plates reached 90% of confluency, medium was discarded and cells were washed using ice-cold PBS. Ice-cold lysis buffer (10Mm HEPES, 10mM KCl, 1.5 mM $MgCl_2$ with protease inhibitors) was added. The cells were scrapped by using plastic cell scraper and collected in centrifuge tubes. After 10 min on ice, samples were vigorously mixed by vortex and centrifuged at 11,000 rpm for 10 min at 4°C. The supernatant was collected in a fresh tube and placed on ice.

3.3.2. Protein quantification

3.3.2.1. Bradford assay

Bradford assay (500-001 BioRad) is a coomassie dye-binding assay for fast protein quantification. In an acidic environment, proteins bind to coomassie dye. This results in a spectral shift from the reddish brown form of the dye to the blue form. The protocol was performed according to the manufacturer's manual. In a 96-well plate, 100 µl/well of preformulated Coomassie blue G-250 assay reagent was added to duplicates of BSA standard (for standard curve and sample concentration interpolation) and 2 µl/well dilutions of unknown samples and the resultant blue color was measured at 595 nm following 5 min of RT incubation.

3.3.2.2. BCA assay

The BCA protein assay was also used for quantitation of total protein in a sample. The principle of this method is that proteins can reduce Cu^{+2} to Cu^{+1} in an alkaline solution (the biuret reaction) and results in a purple color formation by bicinchoninic acid. Protocol was followed as BCA Protein Kit (23225 Thermo Fisher) manufacturer's instructions. In a 96-well plate, 100 µl/well of BCA reagents was added to duplicates of BSA standard (for standard curve and sample concentration interpolation) and 10 µl/well dilutions of unknown samples and the resultant purple color was measured at 562 nm following 30 min of 37°C incubation.

3.3.3. Western Blot assay

All protein samples were previously diluted with loading buffer (Tris 1M, 20% SDS, 30% glycerol and bromophenol) and heated 5 min at 95ºC for protein denaturalization. Proteins were separated by their molecular weight using 7,5 % or 10 % SDS-PAGE electrophoresis. The composition of the electrophoresis buffer used was 25 mM Tris, 250 mM

Glycine and 0.1% SDS. Once the electrophoresis was performed, the proteins in the gel were transferred to a PVDF membrane (IPVH 00010 Millipore). The transference was conducted at 4ºC for 1h 30min at 400 mA with a transfer buffer (12 mM Tris, 20% Methanol and 96 mM Glycine). In order to avoid unspecific antibody binding, membranes were immersed in blocking solution (5% nonfat milk in 0.1 % Tween 20 in 1X TBS or TBS-T (20 mM Tris, 137 mM NaCl and 3.9 mM HCl)) and incubated for 30 min on an orbital shaker at RT. After membranes were blocked, they were incubated with the appropriate antibody overnight at 4 ºC. The antibodies used in this project were all purchased (Table 7) except for the mouse CPT1C antibody, which was developed at Nuria Casal's group from UIC against the last 14 aminoacids of the mus musculus CPT1C sequence [102] and ABHD6 antibody which was kindly provided by Dr. Ken Mackey. Followed by washing, the membranes were incubated in a 1:20,000 dilution of HRP-tagged correspondent secondary antibody (BioRad) in TBS-T (1 h at RT). Secondary antibody was detected by chemiluminescence reagent Luminata Forte (Millipore WBLUF0500) addition to membrane. Chemiluminescence images were taken using the SYNGENE GBOX and quantified by the ImageJ software.

Antibody	Ref. number	Working dilution	Animal source
Anti-CPT1C (human)	SAB2501194 Sigma-Aldrich	1:500	Goat
Anti-CPT1C (human)	66072-1-Ig ProteinTech	1:500	Mouse
Anti-CPT1C (mouse)	Developed by Dr. Serra's group	1:1000	Rabbit
Anti-SAC1 (human)	13033-1-AP ProteinTech	1:500	Rabbit
Anti-ABHD6 (human)	Dr. Ken Mackey laboratory	1:1000	Rabbit
Anti-β-actin (human)	Ab6276 abcam	1:1000	Mouse
Anti-GAPDH (human)	AM4300 Applied Biosystems	1:50000	Mouse
Anti-tubulin (human)	T5201 Sigma-Aldrich	1:2000	Mouse
Anti-Na^+K^+ATPase (human)	sc-58628 Santa Cruz	1:200	Mouse
Anti-VDAC1-Porin (human)	ab34726 abcam	1:1000	Rabbit
Anti-calreticulin (human)	ab2907 abcam	1:1000	Rabbit

Table 7. Antibodies used in this project. Data of the reference, working dilution and animal source of each antibody are shown.

3.3.4. Ponceau staining

Ponceau S (22001 Biotium) is a rapid and reversible stain for detecting protein bands on Western blot membranes. Ponceau S is a negative stain, which binds to the positively charged amino groups of the protein and it also binds non-covalently to non-polar regions in the protein. In Western blots of experiments performed with treatments (as chemotherapy drugs) that could impair cytoskeletal protein levels, Ponceau staining was used as a loading

control. Membranes were incubated with Ponceau for 1 min and subsequently washed 3 times with water prior to be imaged in SYNGENE GBOX.

3.4. Lipid analysis

3.4.1. Cellular fractionation

In order to obtain a cellular enriched PM-fraction for lipidomic studies, a tissue plasma membrane (PM) isolation protocol of Suski J.M. et al. was optimized for cultured cells [103]. The steps followed are detailed below (Fig. 23). A total of 25 millions of MDA-MB-231 cells of each condition were seeded in 10 plates (150 mm) and cells were allowed to grow for four days. Then, cells were washed with PBS, scrapped with 1 ml of PBS per plate and collected. Lysate was centrifuged at 700g for 5 min at 4°C and supernatant was discarded. Pellet was resuspended in 1 ml of Isolation buffer-1 (225 mM mannitol, 75 mM sucrose, 0.5% (wt/vol) BSA fatty acid-free (126575 Sigma), 0.5 mM EGTA and 30 mM Tris-HCl, pH 7.4, supplemented with protease and phosphatase inhibitor cocktails). Homogenization was performed pipetting 25 times up and down, using dounce homogenizer 25 times loose and 25 times tight, and finally by sonication (25 pulsations at medium power 60 A and 0,6). Then, sample lysate was centrifuged at 800g for 5 min at 4 °C. Supernatant was collected and pellet was newly resuspended with 1 more ml of Isolation buffer-1, and the same homogenization steps described above were repeated. The obtained lysate was unified with the prior separated supernatant and 180 µl of total fraction was collected for lipidomics or in other cases was centrifuged and resuspended with lysis buffer (10mM HEPES, 10mM KCl, 1.5 mM $MgCl_2$ with protease inhibitors) for Western blot analysis. Then, sample lysate was centrifuged at 800g for 5 min at 4 °C. The pellet was discarded (unbroken cells and nuclei) and the supernatant was centrifuged again for 5 min at 800g and 4 °C. This new pellet was discarded (if present) and the supernatant was centrifuged for 10 min at 10,000g and 4 °C. Both the supernatant and the pellet were collected: the supernatant contained PM, microsomes and cytosolic proteins and the pellet contained the crude mitochondrial fraction. The supernatant was centrifuged for 10 min at 10,000g and 4 °C to remove any mitochondrial contamination. The pellet of mitochondrial contamination was discarded and the supernatant was centrifuged for 20 min at 25,000g and 4 °C to obtain the crude PM fraction. Both the supernatant (this is the fraction containing microsomes and cytosolic proteins) and the pellet (containing the crude PM fraction) were collected. The crude PM pellet was gently resuspended in 500 µl of Isolation buffer-1 and centrifuged for 20 min at 25,000g and 4 °C to remove microsomal and cytosolic contamination. The pellet with the crude PM was gently resuspended in 50 µl of Isolation buffer-1 and in other cases this PM-enriched fraction was resuspended with lysis buffer (10mM HEPES, 10mM KCl, 1.5 mM $MgCl_2$ with protease inhibitors) for Western blot analysis.

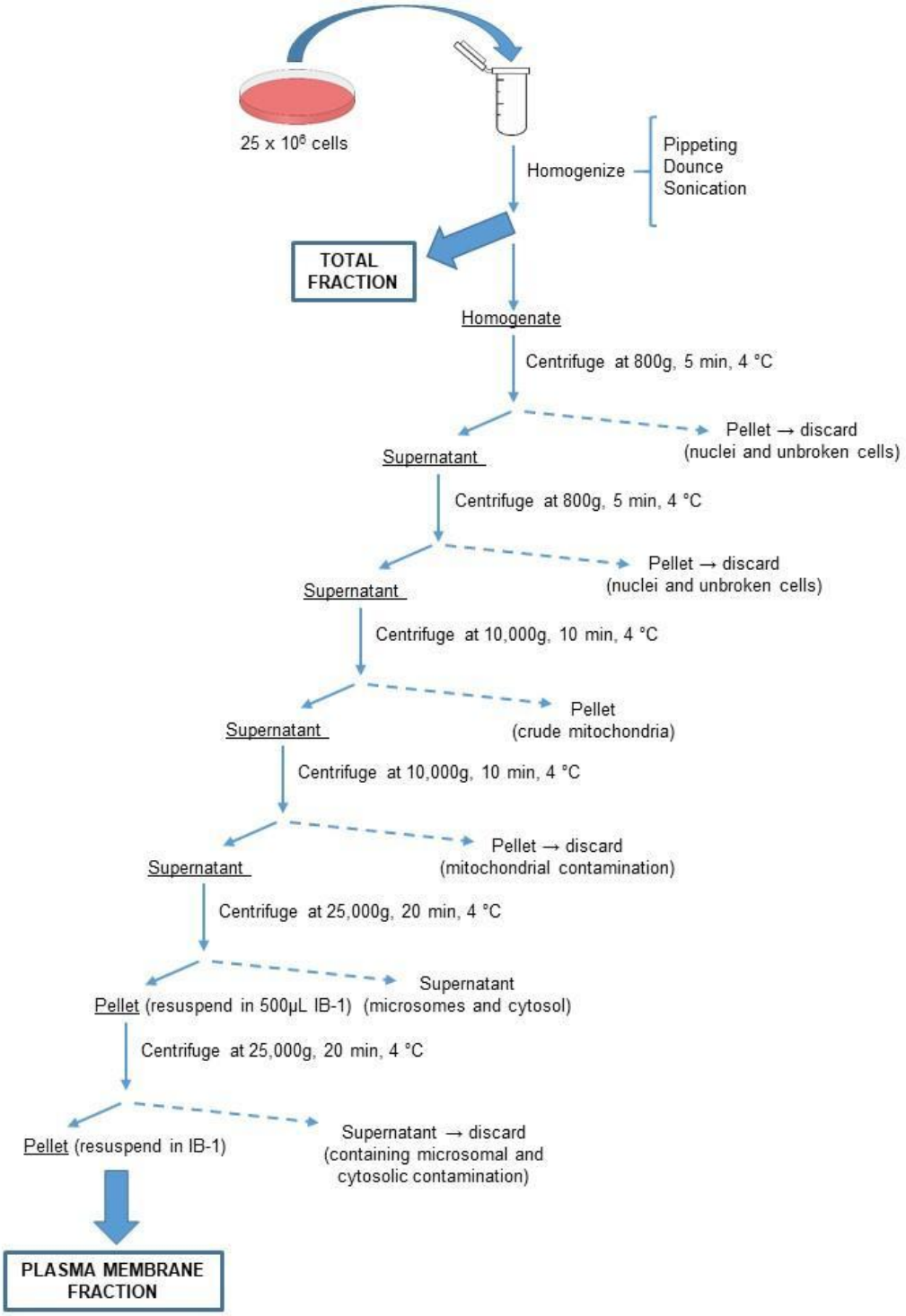

Fig. 23. Timeline and schematic steps for obtaining a PM-enriched fraction from cultured cells.

3.4.2. Lipidomics

In collaboration with Dra Josefina Casas, a complete lipidomic analysis was carried out for the total and plasma-membrane enriched fractions of MDA-MB-231 cells. Samples

were prepared and analyzed by liquid chromatography-high resolution mass spectrometry (LC-HRMS).

4. Flow cytometry

4.1. Chemicals and reagents

5-(N-Ethyl-N-isopropyl)-Amiloride (EIPA) (sc-202458) was from Santa Cruz Biotechnology (Dallas, TX, USA). L-carnitine (C0283), methyl-β-cyclodextrin (C4555) and KT182 (SML1248 Sigma) were from Sigma-Aldrich (St. Louis, MO, USA). All the reagents were diluted in water (except EIPA and KT182, diluted in dimethyl sulfoxide) and used within the efficient pharmacological range of doses obtained from preliminary time-dose studies.

4.2. DOX intracellular accumulation analysis

As DOX is inherently fluorescent, its presence within cells can be directly analyzed by flow cytometry. To measure intracellular DOX accumulation, in indicated times and experiments, MDA-MB-231 cells were treated with 1µg/ml DOX. At the end of the incubation, cells were washed with PBS, pelleted by centrifugation, and analyzed with a FACScalibur Flow Cytometer (Becton Dickinson, Rutherford, NJ, USA). For uptake mechanism study the procedure was the same but in indicated times, MDA-MB-231 cells were also treated (or not) with EIPA (pre-treatment of 30min) as a macropinocytosis inhibitor; L-carnitine as a SLC22A16 competitive inhibitor or methyl-β-cyclodextrin as a Chol-depleting reagent.

- **DOX intracellular accumulation pharmacokinetics analysis**

DOX cell accumulation was analyzed by flow cytometry over time in pulse-chase experiments. Cells were incubated with the drug during 4 h, then medium was changed and cells were incubated with drug-free medium for 20 h more. Values obtained were separated in two different datasets: drug uptake data (from 0h to 4h) and drug release data (from 4h to 24h). The pharmacokinetics analysis was performed by GraphPad Prism 6.0. Before analysis, drug release data was previously normalized by initial DOX cellular content. We used linear regression to fit data sets and successively we automatically tested whether slopes and intercepts differed.

4.3. Plasma membrane cholesterol analysis through mCherry-D4 probe

The mCherry-D4 probe is a fusion between the fluorescent protein mCherry and the D4 fragment of perfringolysin O (referred to as θ toxin), a pore-forming toxin from the bacterium Clostridium perfringens. The D4 fragment of perfringolysin O is able to bind Chol-

rich membranes (>30 mol% Chol) but is devoid of pore-forming activity. Plasma membrane Chol labelling followed by its quantification was performed reproducing the next steps:

- 50,000 cells/ml were plated in 24-well plates.
- 24h later, cells were rinsed with PBS, trypsinized and resuspended in 1ml of medium.
- After centrifugation, pellet was resuspended in 1 ml of PBS and centrifuged again.
- 300 µl of a 1:800 mCherry-D4 2% w/v BSA in PBS dilution were added in each centrifuge tube.
- Samples were incubated for 30 min with gentle shaking (350 rpm) at 37°C.
- Then, samples were centrifuged and supernatants were discarded.
- Pellet was gently resuspended in 500 µl of ice-cold 4% PFA and incubated for 15min on ice.
- Samples were centrifuged again and resuspended in 300 µl of PBS.
- Cells were analyzed with a FACScalibur Flow Cytometer (Becton Dickinson, Rutherford, NJ, USA).

5. Confocal microscopy

5.1. DOX intranuclear accumulation analysis

For the evaluation of DOX intranuclear accumulation, tumor cells grown on poly-L-lysine-coated glass coverslips were treated 2h30min with DOX following the protocol described above. At indicated time, cells were fixed with 3.7% PFA for 15 min at 4°C. Then, cells were washed twice with phosphate-buffered saline (PBS) and stained with Hoechst for 5 min. After two more washings with PBS, slides were mounted in Fluoromount medium. Fluorescence images were acquired with a confocal laser microscopy system with a 60X oil objective (Confocal Leica TCS SP8). Argon lasers with 488 and 568 lines were used. Around 20 stacks with 1 µm-distance were taken per each imaged cell and quantification was done on the reconstructed 3D image made by the IMARIS software. On original images, region of interest (ROI) was selected by Hoechst staining and DOX mean fluorescence intensity was measured inside it.

5.2. Plasma membrane cholesterol levels analysis

MDA-MB-231 were seeded at 25,000 cells/well on poly-L-lysine-treated glass coverslips. After 48 h, cells were incubated with the mCherry-D4 solution (1: 800 in PBS containing 1% BSA) for 30 min at 37°C. Then, cells were quickly washed with 1 ml of PBS at RT and fixed with 3.7% PFA for 15 min at 4°C and washed twice with PBS. The slides were mounted in Fluoromount medium. Fluorescence images were acquired with a confocal laser microscopy system with a 60X oil objective (Confocal Leica TCS SP8). Argon lasers with 488

and 552 lines were used. Around 20 stacks with 0.5 µm-distance, double line average and 1x Zoom were taken per each imaged cell and quantification was done on the reconstructed 3D image made by the IMARIS software. On original images, region of interest (ROI) was selected by GFP staining (whole cell) and mCherry mean fluorescence intensity was measured inside it.

5.3. PI(4)P total levels analysis

A protein that contain lipid domain that specifically recognize PI(4)P was used to quantify cellular total PI(4)P phospholipid. The fluorescent probe was the mCherry-PI(4)P (Hammond, et al.; 2014) kindly gifted by Eamonn Dickson from UCDavis. The mCherry-PI(4)P contains a P4M domain from L. pneumophila SidM fused to the mCherry fluorophore. This PI(4)P probe reveals a localization of PI(4)P both in plasma membrane and Golgi Apparatus pools, as well as a pool associated with LEs and/or lysosomes. The probe was transfected in MDA-MB-231 cells with Lipofectamine 2000. Thirty hours after transfection, cells were fixed with 3.7% PFA for 15 min at 4°C and washed twice with PBS. The slides were mounted in Fluoromount medium. Fluorescence images were acquired with a confocal laser microscopy system with a 60X oil objective (Confocal Leica TCS SP8). Argon lasers with 488 and 552 lines were used. Around 20 stacks with 0.5 µm-distance, double line average and 1.5x Zoom were taken per each imaged cell and quantification was done on the reconstructed 3D image made by the IMARIS software. On original images, region of interest (ROI) was selected by GFP staining and PI(4)P mean fluorescence intensity was measured inside it.

5.4. Co-localization studies

In order to analyze CPT1C intracellular localization, hCPT1C tagged with mTurquoise2 was transfected in MDA-MB-231 cells with Lipofectamine 2000 as it is described above. To stain mitochondria, 48 h later, Mitotracker Orange (200 nM) was added and incubated for 30 min. Then, cells were fixed with 3.7% PFA for 15 min at 4°C and washed twice with PBS. Calnexin (used as ER marker) was detected by immunocytochemistry. This was performed as follows. Cells were permeabilizated with acetone for 5 min at 4 ºC and washed three times with PBS (for 5 min each washing). Blocking was performed incubating coverslips for 20 min at 37ºC with a 2% Goat serum solution. After a PBS washing, coverslips were incubated with 15 µl of primary antibody solution (1:200 anti-calnexin rabbit 22595 abcam) for 1 h at 37ºC in a wet chamber. This incubation was followed by three washes with PBS. Coverslips were incubated with 300 µl of the secondary antibody (1:300 anti-rabbit Alexa A647) for 1 h at 37ºC in a 24 well-plate. This incubation was followed by three washes with PBS. Finally, coverslips were mounted with Fluoromount Aqueous Mounting Medium (F4680 Sigma-Aldrich). CPT1C

intensity was detected inside the ER, mitochondria and ER-Mitochondria (MAMs) co-localized ROIs obtained by Surface tool and Surface-Surface co-localized plugin of Imaris 9.2 Software. Results are given as a percentage obtained from the ratio between sum intensity in each compartment and the sum intensity in the whole cell.

6. Biochemistry

6.1. ABHD6 activity assay

This high sensitive fluorescent hydrolase activity assay based on the ABHD6 ability to hydrolyze the 4-methylumbelliferyl-heptanoate (4-MUH) substrate was developed by Dr. Miralpeix in our laboratory. This method allows studying ABHD6 activity in cells. The assay was performed as follows. A total of 1.5 x 10^5 MDA-MB-231 cells/well were seeded on 6-well plates. After 48h, cells were washed with cooled PBS and collected with 1ml PBS. Samples were centrifuged at 1,000 rpm for 5min at 4°C to discard the remaining PBS and pellet was frozen at -80°C for 10min to break cells. The pellet obtained was resuspended with 200µL of homogenization buffer (50mM Tris, 1mM EDTA pH 7.4) and sonicated briefly (10 pulsations at medium power 60 A and 0,6) to homogenise the cells properly. The amount of protein was quantified using BCA (Pierce) and protein solution was prepared with homogenization buffer. 90µl/well of protein solution (4 µg protein/well) in duplicates was added in black 96-well plates. Samples were incubated with 5µl/well of WWL70 (10011213 Cayman chemical, ABHD6 inhibitor) to a final concentration of 200µM (WWL70 or DMSO as a vehicle) for 30min at 37ºC. A total volume of 5µl/well of 4-MUH (M2514 Sigma) was added to a final concentration of 50µM. Immediately, fluorescence was read at least for 60min every 10min at 37ºC. Excitation filter was selected for 355nm and emission filter for 460nm. ABHD6 activity data was analysed subtracting the absorbance of WWL70-incubated wells to the absorbance of DMSO-incubated wells. In this way, it was possible to distinguish ABHD6 activity from total hydrolase activity. Then, absorbance was represented as an exponential curve of absorbance along time and slopes were compared.

6.2. Total cholesterol levels analysis

The method for the measurement of total Chol in cell lysate involves the use of a monoreagent (1118015 Linear) containing three enzymes: cholesterol esterase (CE), cholesterol oxidase and peroxidase. In the presence of them, the mixture of phenol and 4-aminoantipyrine are condensed by hydrogen peroxide to form a quinoneimine dye proportional to the concentration of Chol in the sample. The procedure was performed in six-replicates in two independent experiments as following. MDA-MB-231 at 10^5 cells/well were seeded on 6-well plates. After 48 h, medium was discarded and cells were washed using ice-cold PBS. 50

µl of ice-cold lysis buffer (10mM HEPES, 10mM KCl, 1.5 mM $MgCl_2$ with protease inhibitors) was added to each well. The cells were scrapped by using plastic cell scraper and collected in centrifuge tubes. After 10 min on ice, samples were vigorously vortexed and stored at -20°C at least for 2 days. The samples were allowed to thaw and sonicated briefly (about 20 pulsations at medium power) to homogenise the cells properly. A volume of 50 µl of each homogenate was mixed with 150 µl of the monoreagent and incubated for 10 min at RT in 96-well plates. Plates were briefly shaked and absorbance was read in Multi-Detection Microplate Reader Synergy™HT (Biorad) at 500nm. Absorbance values were normalized by Bradford protein concentration.

6.3. Fatty acid oxidation assay

FAO to CO_2 and acid-soluble products (ASP; essentially ketone bodies) were measured in MDA-MB-231 cells cultured in 6 well plates. Briefly, cells were washed in KRBH (135 mM NaCl, 3.6 mM KCl, 0.5 mM NaH_2PO_4, 0.5 mM MgSO4, 1.5 mM $CaCl_2$, 2 mM $NaHCO_3$, 10 mM HEPES, and pH 7.4) with 0.1% BSA, pre-incubated for 30 min in KRBH-1% BSA, and then incubated for 3 h with fresh KRBH containing 8 mM carnitine and 300 µM [1-^{14}C] palmitate-BSA (GE Healthcare, Little Chalfont, UK) in a CO_2-free incubator. The flasks were sealed with a stopper supporting a 3-cm length of PVC tubing containing a piece of Whatman GF/B paper soaked in 0.1 N KOH. At the end of the incubation, 40% of perchloric acid was injected into each flask to acidify the medium and liberate the CO_2. After overnight isotopic equilibration, the trapped $^{14}CO_2$ was measured by liquid scintillation counting. FAO into ASP was measured from the perchloric acid–treated medium after centrifugation. Next, supernatants containing the labelled ASP were collected and counted by liquid scintillation. The scintillation values were normalized to the protein content.

7. Bioinformatics analysis

7.1. Kaplan-Meier Plotter analysis

To assess the prognostic value of CPT1C and further functionally linked genes, the online tool kmplot.com (http://kmplot.com/analysis/) [104], a database that integrates gene expression and clinical data to obtain survival information for gastric, lung, breast, and ovarian cancer in relation to expression levels of genes. Gene expression data were obtained through gene-chip data-sources from the databases GEO, EGA, and TCGA and converted into Kaplan-Meier plots. According to the median expression levels of CPT1C, the samples were divided into two groups: high expression group and low expression group [104]. Subsequently, the 95% Confidence Interval (CI), the log-rank P-value and the hazard ratio (HR) were

calculated. In this study were performed relapse-free survival analysis of patients with breast cancer for the next genes: n=1,764 for CPT1C and n=3,951 for SACM1L and ABDH6. The corresponding Affymetrix IDs were 227468_at (CPT1C), 202797_at (SACM1L) and 221552_at, 221678_at, 221679_s_at and 45288_at (ABHD6).

7.2. ROC plotter analysis

ROC Plotter web application (www.rocplot.org) was used in order to link gene expression of CPT1C, SACM1L and ABHD6 with response to therapy using transcriptome-level data of breast cancer patients. We filtered for patients who received anthracycline therapy (breast cancer, n=383) or any chemotherapy (glioblastoma, n=454). Therapy response was determined using relapse-free survival status at 5 years.

7.3. DepMap portal analysis

DepMap (https://depmap.org/portal/depmap/)[105] is a tool that provides a cancer dependency interaction map that describes which genes are necessary for cell viability or proliferation, helping to identify new cancer targets. The cancer dependency (in cancer cell viability or proliferation) across cancer cells lines analyzes cell growth kinetics through gene depletion assays based on CRISPR-Cas9 and shRNA/siRNA approaches. CERES dependency score method is used for CRISPR-Cas9 based depletion assays (from Avana and Sanger datasets), and DEMETER2 score for RNAi depletion assays (from Broad, Novartis, Marcotte datasets). This later infers gene knockdown viability effects screened by shRNA (or siRNA) library containing multiple targets for the same gene. A negative CERES or DEMETER2 score indicates that a gene knock-out or silencing results in a slower growth rate for each cell line. Conversely, in the same conditions, a positive score implies a higher cellular growth rate.

7.4. TNMplot analysis

TNMplot is a pan-cancer analysis webpage that displays the expression range for a selected gene across different tissues in all available normal and tumor RNA Seq data. RNA sequencing data proceeds from the The Cancer Genome Atlas (TCGA), Therapeutically Applicable Research to Generate Effective Treatments (TARGET), and Genotype-Tissue Expression (GTEx) repositories. TCGA and TARGET contain predominantly tumor and metastatic samples from adult and pediatric patients, while GTEx samples are from healthy tissues. Statistical significance is computed using Kruskall-Wallis test [106].

8. Statistical analysis

All results are shown as a mean or median ± standard error (SEM) or standard deviation (SD) Statistical tests were performed using the GraphPad Prism 6.0 sofware. According to normality test, Student test, Mann-Whitney test or Wilcoxon test was used when comparing only two groups and two-way ANOVA was performed with Bonferroni post hoc test if distinct groups including different variables were compared. Analysis of Covariance (ANCOVA) was used to compare linear regression lines.

RESULTS

1. CPT1C expression improves relapse-free survival in breast cancer

To establish whether CPT1C expression could affect breast cancer prognosis, we investigated its relation to patient survival. For this purpose, we used the Kaplan-Meier Plotter. Survival curves for 23-year relapse-free survival (RFS) time were plotted for 1,764 patients with breast cancer. RFS, also called disease-free survival, is defined as the time from randomization until disease recurrence (local, regional, contralateral, or distant) or death from any cause; it is usually employed in the adjuvant (curative) setting [107,108]. Surprisingly, contrary to what has been demonstrated in other cancer tissues [34,35,109], we observed that high CPT1C levels were a protective factor for RFS in patients with breast cancer (Fig. 24).

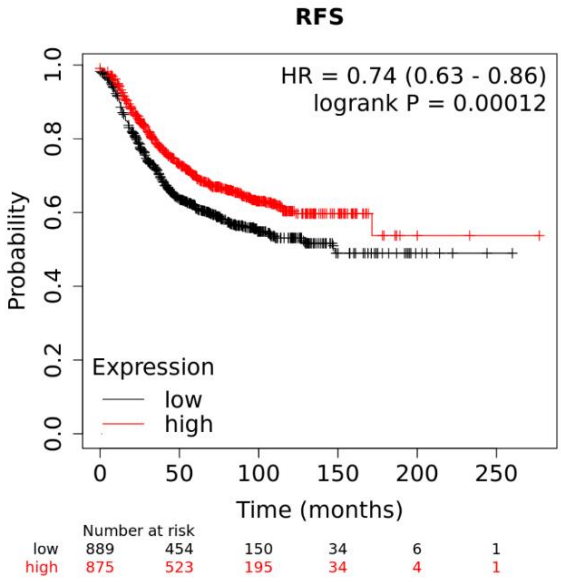

Upper quartile survival

Low expression cohort (months)	High expression cohort (months)
28.8	44.4

Fig. 24. Low expression of CPT1C is associated with poor breast cancer relapse-free survival (RFS). RFS rate for patients with breast cancer with low or high CPT1C gene expression as analyzed with Kaplan-Meier Plotter. Log-rank p-value and hazard ratio (HR; 95% confidence interval in parentheses) are shown. The corresponding Affymetrix ID for CPT1C is 227468_at. Upper quartile survival rates (months) for the low and high expression groups are shown.

The RFS is frequently analyzed when looking at the effects of treatment of a cancer that has a propensity to relapse. This is particularly true with breast cancer, in which late recurrences are common especially in patients that require chemotherapy. In fact, when only systemic-treated patients in the RFS plot were included, differences were exacerbated from 1.54-fold to 1.96-fold (ratio of survival time between high and low CPT1C-expressing tumors) (Fig. 25).

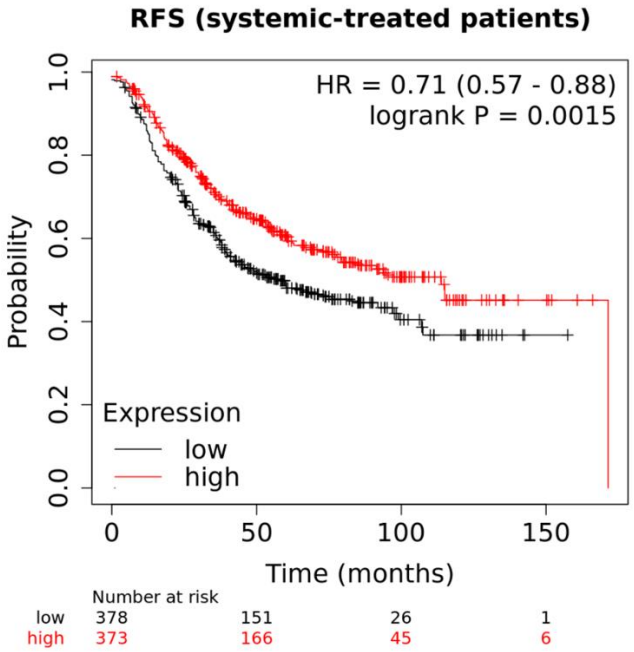

Median survival

Low expression cohort (months)	High expression cohort (months)
58	113.77

Fig. 25. Low expression of CPT1C is associated with poor relapse-free survival (RFS) in systemic-treated patients. RFS rate for patients with breast cancer with low or high CPT1C gene expression as analyzed with Kaplan-Meier Plotter. Only patients that had received systemic treatment were selected. Log-rank p-value and hazard ratio (HR; 95% confidence interval in parentheses) are shown. The corresponding Affymetrix ID for CPT1C is 227468_at. Median survival rates (months) for the low and high expression groups are shown.

To better understand the meaning of the significant differences in RFS linked to CPT1C expression, we tried to limit breast cancer patient selection for Kaplan-Meier analysis according to expression levels of different molecular markers frequently used as predictors of therapy response. Results showed that low CPT1C expression levels was related to worse RFS only in tumors where HER2 was highly expressed (Fig. 26).

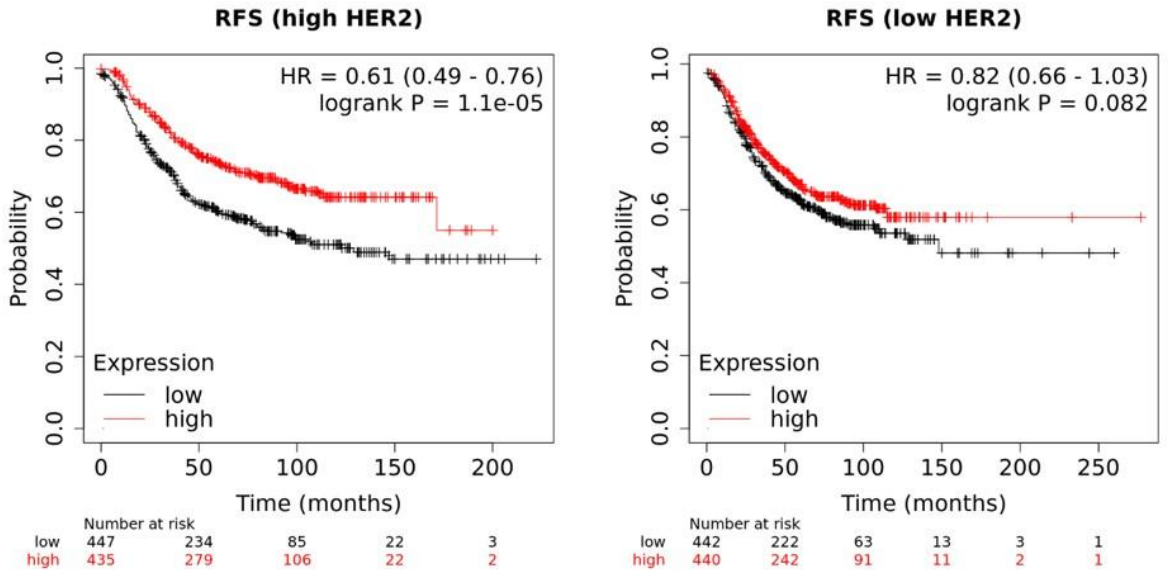

Upper quartile survival

Low expression cohort (months)	High expression cohort (months)
28	53.56

Upper quartile survival

Low expression cohort (months)	High expression cohort (months)
29	38.4

Fig. 26. Low expression of CPT1C is associated with poor relapse-free survival (RFS) only in patients with HER2-high-expressing breast cancers. RFS rate of patients with breast cancer with low or high CPT1C gene expression as analyzed with Kaplan-Meier Plotter. Log-rank p-value and hazard ratio (HR; 95% confidence interval in parentheses) are shown. Patients with breast cancer were previously split by median expression of HER2 in tumors distinguishing between HER2-high (left) and -low (right)–expressing tumors. The corresponding Affymetrix IDs for CPT1C and HER2 are 227468_at and 216836_s_at, respectively. Upper quartile survival rates (months) for the low and high CPT1C expression groups are shown.

Next, we performed a similar analysis considering the expression of hormone receptors. Estrogen receptors, ERα and ERβ, are encoded by ESR1 and ESR2 genes, respectively. We classified breast cancers by ESR1, ESR2 and PR (progesterone receptor) median expression, distinguishing between low and high gene-expressing breast tumors. Low CPT1C expression was shown to be related to worse RFS, especially in patients who had tumors with low ERα, ERβ and PR expression (Fig. 27).

RFS (high ERa)

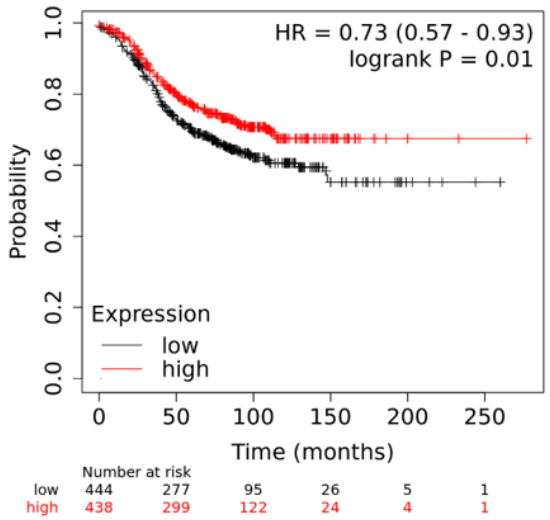

Upper quartile survival

Low expression cohort (months)	High expression cohort (months)
46	57

RFS (low ERa)

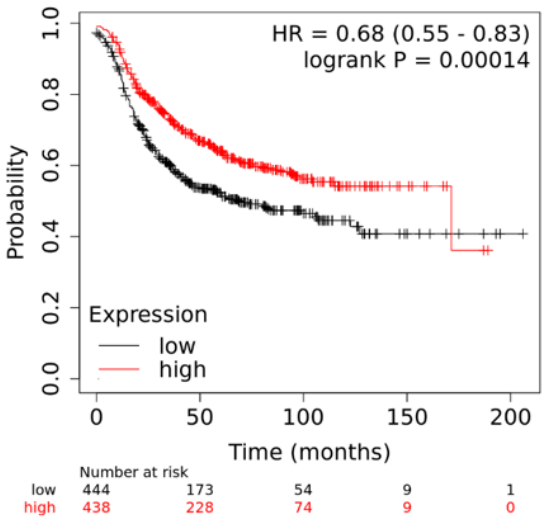

Median survival

Low expression cohort (months)	High expression cohort (months)
69	171.43

RFS (high ERb)

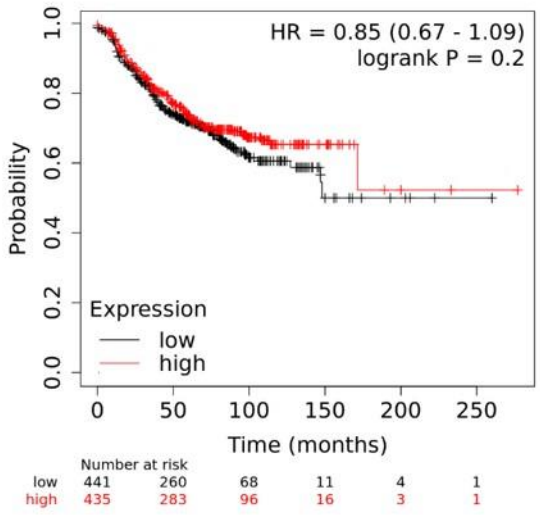

Upper quartile survival

Low expression cohort (months)	High expression cohort (months)
46	57

RFS (low ERb)

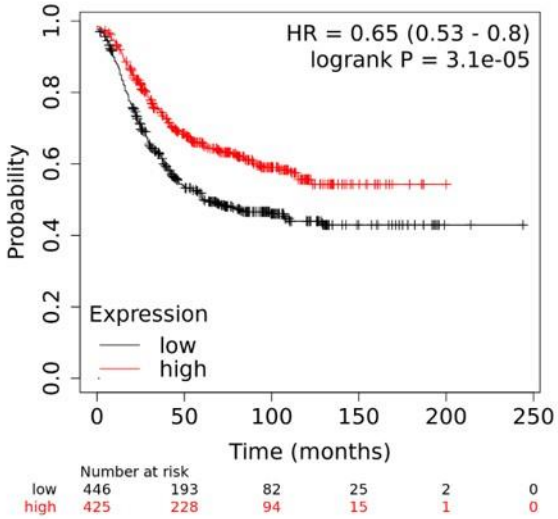

Upper quartile survival

Low expression cohort (months)	High expression cohort (months)
21.6	35.98

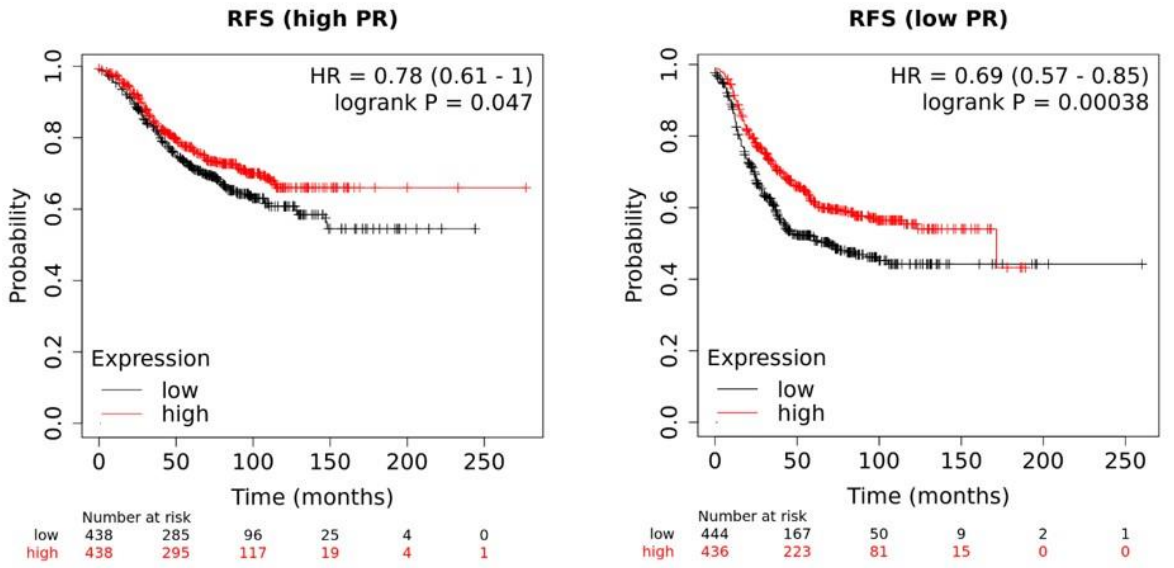

Upper quartile survival

Low expression cohort (months)	High expression cohort (months)
50	68.4

Median survival

Low expression cohort (months)	High expression cohort (months)
69	171.43

Fig. 27. Low expression of CPT1C is more associated with poor relapse-free survival (RFS) in patients with hormone receptor–low-expressing breast tumors. RFS rate of patients with breast cancer with low or high CPT1C gene expression as analyzed with Kaplan-Meier Plotter. Log-rank p-value and hazard ratio (HR; 95% confidence interval in parentheses) are shown. Patients with breast cancer were previously classified according to the median expression of ESR1, ESR2, and PR genes, distinguishing between high (left) and low (right) gene-expressing tumors. The corresponding Affymetrix IDs for CPT1C, ESR1, ESR2, and PR are 227468_at, 205225_at, 210780_at, and 205272_s_at, respectively. Upper quartile and median survival rates (months) for the low and high CPT1C expression groups are shown.

Finally, as mentioned above, CPT1C is a p53 target protein. Although not yet used for the management of breast cancer prognosis, p53 has an obvious central role in cancer [110]. TP53 mutations are the most frequent genetic alterations in breast cancer, observed in 30% of breast carcinomas. Moreover, their distribution is highly associated with molecular tumor subtypes: 26% of luminal tumors (luminal A, 17%; luminal B, 41%); 50% of HER2-amplified tumors; and 88% of basal-like triple-negative carcinomas [111]. Considering TP53 expression, we assigned patients with breast cancer to low and high p53 expressing tumor groups using the Kaplan-Meier database. As expected, a significantly worse RFS related to CPT1C low expression was only found in patients with breast tumors harboring a low p53 expression (Fig. 28).

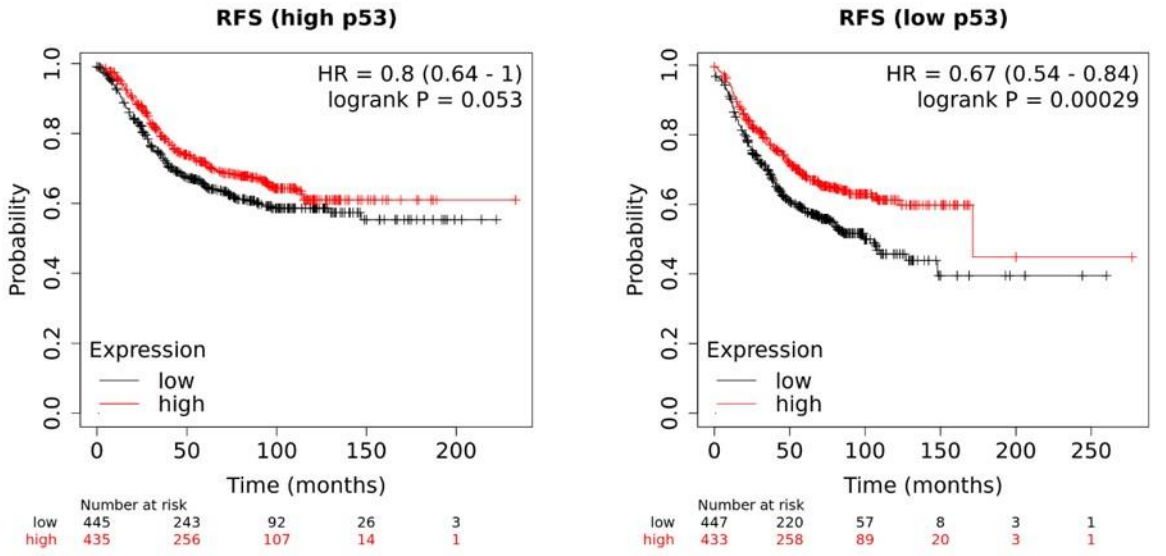

Upper quartile survival

Low expression cohort (months)	High expression cohort (months)
33	43.7

Median survival

Low expression cohort (months)	High expression cohort (months)
99	171.43

Fig. 28. Low expression of CPT1C is associated with poor relapse-free survival (RFS) only in patients with p53-low-expressing breast tumors. RFS rate of patients with breast cancer with low or high CPT1C gene expression as analyzed with Kaplan-Meier Plotter. Log-rank p-value and hazard ratio (HR; 95% confidence interval in parentheses) are shown. Patients with breast cancer were previously classified by median p53 expression in tumors, distinguishing between p53-high (left) and -low (right)–expressing tumors. The corresponding Affymetrix IDs for CPT1C and p53 are 227468_at and 201746_at, respectively. Upper quartile and median survival rates (months) for the low and high CPT1C expression groups are shown.

In summary, the CPT1C effect in RFS appeared to be sharp especially in patients with breast tumors that expressed high levels of HER2, low levels of hormone receptors, and low levels of p53. These three features are especially present in two known subtypes of breast cancer: HER2-positive (hormone receptor negative, HER2+) and triple-negative breast cancers (TNBCs, hormone receptor negative, HER2−).

In the same database, we also analyzed overall survival (OS) and distant metastasis–free survival (DMFS) rates in 626 and 173 patients with breast cancer, respectively. OS was defined as the time from randomization until death from any cause [112]. DMFS is considered as the time interval between the day of reference in the study (depends on the study: date of randomization, date of diagnosis, etc.) and the date of the occurrence of distant metastases or death (all causes), whichever occurs first [113]. Given that RFS is a composite endpoint

comprising locoregional, contralateral breast cancer, distant recurrences, and death from any cause, patients with cancer types that currently have many therapeutic options, such as breast cancer, tend to exhibit slight or no changes in OS studies. This is because over a longer follow-up, an increasing proportion of RFS events are curable (locoregional and contralateral breast cancers) or unlikely to be reduced by adjuvant therapies (death from other causes). Additionally, this may explain why, despite improved RFS, many adjuvant treatments have shown no or low DMFS and OS effect in breast cancer [114]. Thus, as was expected, OS curves did not show significant variation in survival between low or high tumor CPT1C gene expression (Fig. 29). Neither changes were seen in DMFS curves related to CPT1C expression (Fig. 29).

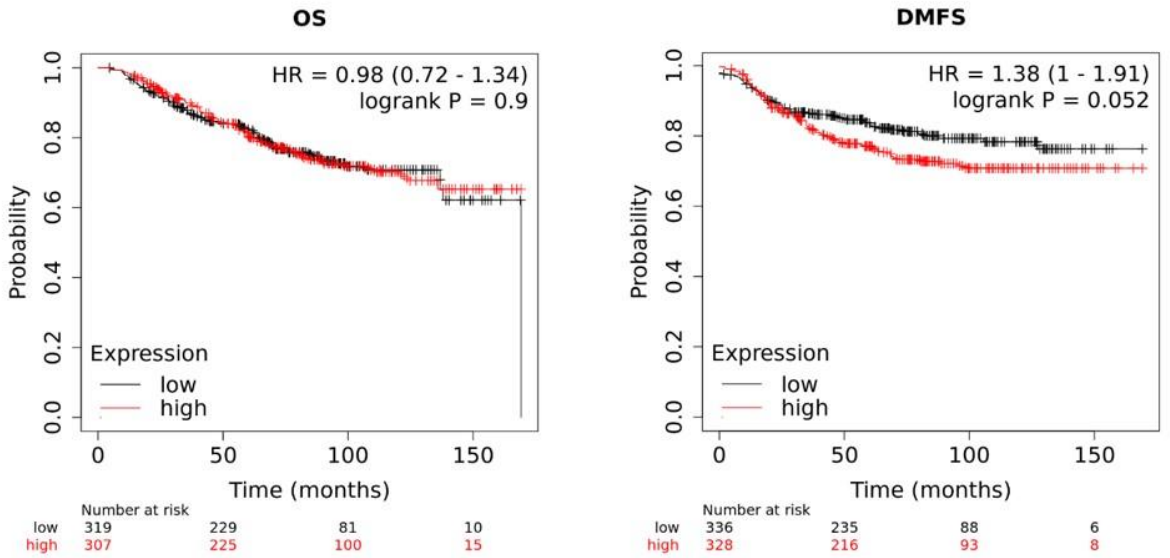

Upper quartile survival

Low expression cohort (months)	High expression cohort (months)
85.2	81.6

Median survival

Low expression cohort (months)	High expression cohort (months)
NA	NA

Fig. 29. Effect of CPT1C expression in breast cancer survival. OS and DMFS rate for patients with breast cancer with low or high CPT1C gene expression as analyzed with Kaplan-Meier Plotter. Log-rank p-value and hazard ratio (HR; 95% confidence interval in parentheses) are shown. The corresponding Affymetrix ID for CPT1C is 227468_at. Upper quartile survival rates (months) for the low and high expression groups are shown. This information was not available for DMFS.

Despite no statistical differences, the tendency observed in the DMFS curves was consistent with data extracted from the pan-cancer TNMplot tool [106]. When compared between tumor and metastatic breast cancer tissues, CPT1C expression tend to be higher in the metastatic tissue (Fig. 30). As explained above with Kaplan-Meier plots, each survival rate focused on different tumor events. Altogether, these findings showed that low CPT1C expression levels are more

closely associated with local or regional than distant tumor recurrences and more related to low treatment response rather than the occurrence of metastasis.

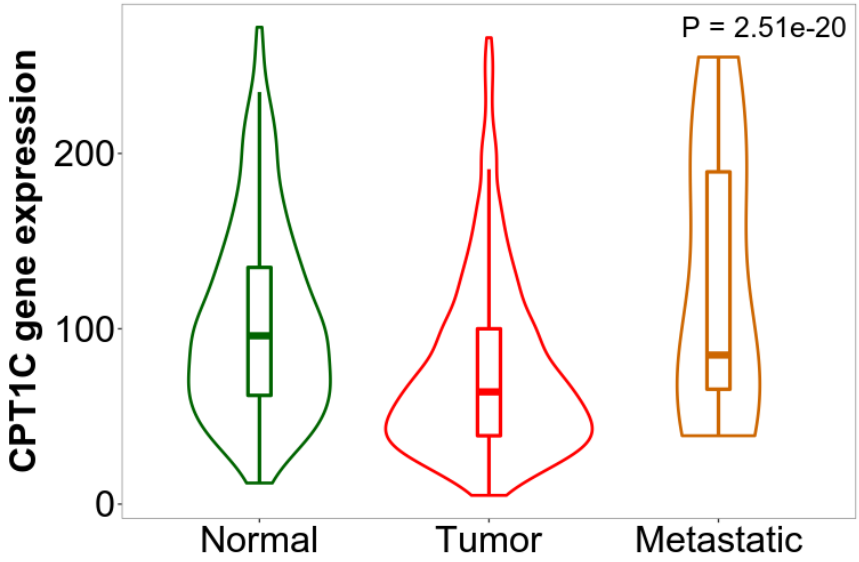

Kruskal.Wallis.p.	Fc.tumor.norm.	Fc.meta.tumor.
2.51E-20	0.76	1.4

Dunn.test.P	Normal-Tumor	Tumor-Metastatic	Normal-Metastatic
	2.12E-21	4.50E-01	5.76E-02

	Min	Q1	Med	Q3	Max	Upper whisker	N
Normal	12	63.5	99	147.5	646	272	403
Tumor	5	40	65	106	1298	204	1097
Metastatic	39	65.5	85	189.5	255	255	7

Fig. 30. Normal, tumor, and metastatic breast tissues differ in CPT1C expression. Violin plot represents CPT1C expression across normal, tumor, and metastatic tissues. Normal tissues were from noncancerous patients. RNA sequencing data were downloaded from TNMplot. The number of tissue samples and fold-change expression levels are shown. Statistical significance was computed using the Kruskall-Wallis and Dunn's test.

2. CPT1C silencing mediates different tumorigenic processes in breast cancer cell lines

Considering the prognostic value of CPT1C, we assessed the effects of this protein in aggressive features of breast cancer cells, such as proliferation, migration, and invasion in vitro. To choose the in vitro model, we considered the gene expression profile of commonly used breast cancer cell lines. Luminal A MCF7 (ER+, PR+, HER2−) was selected as a hormone receptor–positive breast cancer cell line; luminal B BT-474 (ER+, PR+, HER2+), as

a HER2+ breast cancer cell line; and MDA-MB-231 (ER−, PR−, HER2−) and MDA-MB-468 (ER−, PR−, HER2−), as TNBC cell lines.

2.1. CPT1C expression in human breast cancer cell lines

First, we quantified CPT1C protein expression in the selected breast cancer cell lines (Fig. 31). As a comparative, we used neuroblastoma (SH-SY5Y) and glioblastoma (U87 and U373) cell lines, which are known to be high CPT1C-expressing human cancer cell lines. We noted that CPT1C was differentially expressed among different cell lines. The highest expression was found in the ER+ MCF7 cells. For further studies, we selected MDA-MB-231 as a model because it expressed detectable levels of CPT1C, was considered to be a suitable cell line for studies of cell migration and invasion, and is a representative of the breast cancer subtype with worse prognosis. Doublets of CPT1C were detected in the western blot as has been observed in previous works, probably due to post-translational modification or proteolysis [1]. Ponceau staining was used as a loading control because other frequently used loading controls such as proteins related to metabolism (e.g. GAPDH) or cytoskeleton (β-actin and β-tubulin) differed greatly between cell lines.

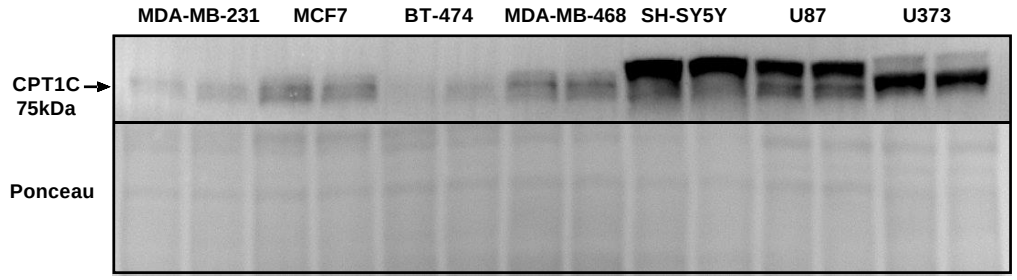

Fig. 31. CPT1C expression in different breast cancer, neuroblastoma and glioblastoma human cell lines. CPT1C expression was measured by western blot in MDA-MB-231, MCF7, BT-474, and MDA-MB-468 breast cancer cell lines and in SH-SY5Y neuroblastoma cell line and U87 and U373 glioblastoma cell lines.

2.2. CPT1C silencing enhances proliferation in breast cancer cells

To further examine the biological effect of CPT1C on breast cancer cells, we silenced the CPT1C gene in MDA-MB-231 cells using two different shRNA engineered with the pLVTHM vector in our laboratory [101]: shLVTHM1-CPT1C (shCPT1C_1) and shLVTHM2-CPT1C (shCPT1C_2) introduced by lentiviral infection. Western blot analysis was used to evaluate the expression levels of CPT1C in the generated cell lines (Fig. 32A). We next investigated cell proliferation in these breast cancer cells by MTS proliferation and colony formation assays. MTS and colony formation assays showed a cell proliferation increase in CPT1C-silenced

MDA-MB-231 cells (Fig. 32B and 32C). Western blot analysis showed lower levels of CPT1C with shCPT1C_2 than shCPT1C_1 (Fig. 32A) and phenotypic results were similar with both shRNA's. Thus, from this point on, we worked with the shRNA shCPT1C_2. Additionally, xCELLigence real-time and BrdU immunofluorescence cell analysis were used to investigate the proliferation of these MDA-MB-231 cells. In line with previous results, the cell index (Fig. 32D) and the number of BrdU-positive cells (Fig. 32E) were higher in silenced cells than in the control cells. Therefore, these findings indicate that CPT1C silencing enhances proliferation in MDA-MB-231 breast cancer cells in vitro.

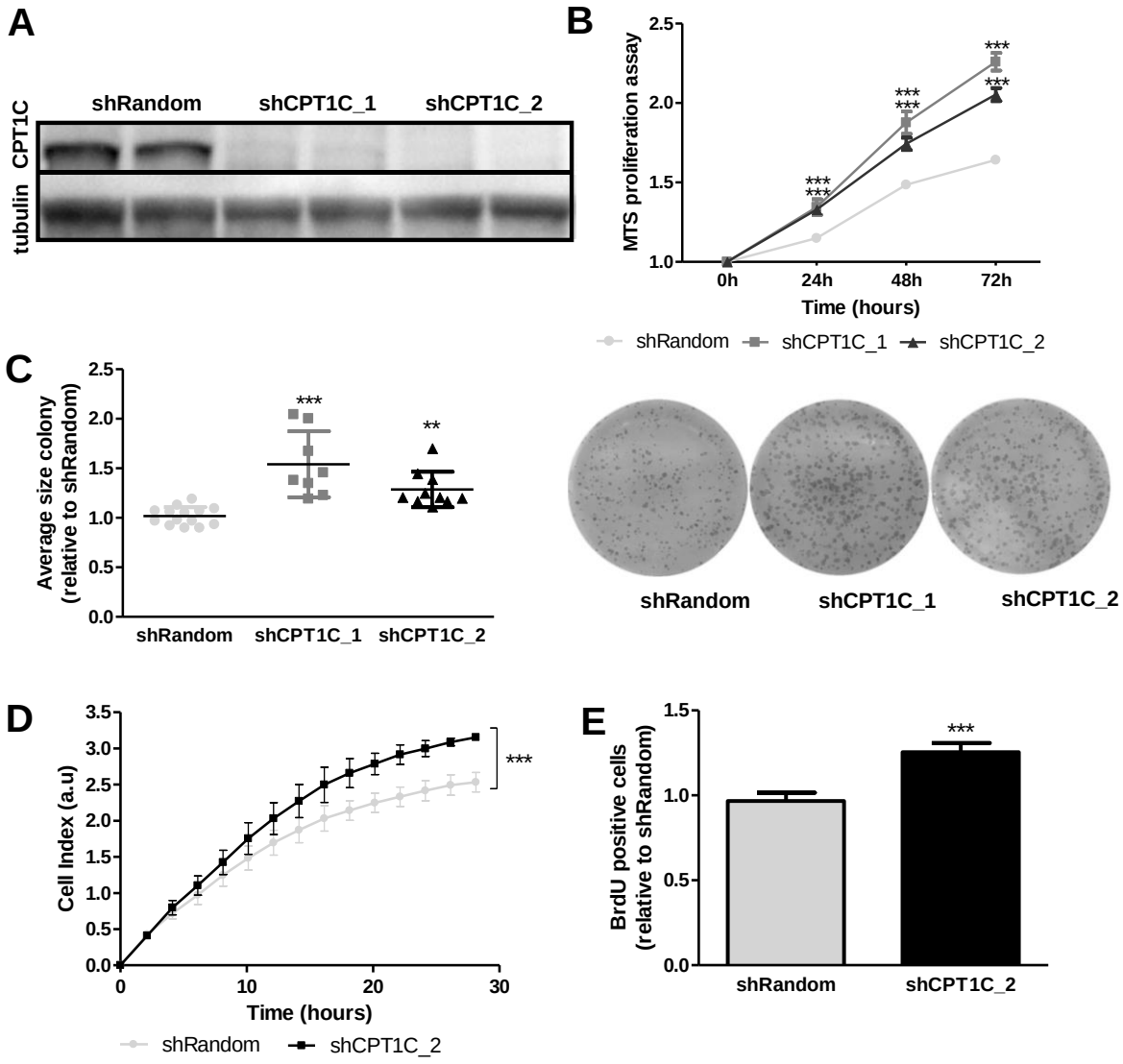

Fig. 32. CPT1C silencing increases cell proliferation in MDA-MB-231 cells. MDA-MB-231 cells were infected with two shCPT1C-carrying lentiviruses (shCPT1C_1 and shCPT1C_2) or a shRandom sequence used as a control. A. CPT1C silencing was confirmed by western blot. Tubulin was used as a loading control. B. MTS cell proliferation was measured at the indicated times. Results are represented as the mean ± SD (n = 6 per condition; two-way ANOVA followed by Bonferroni's multiple comparison test; ***p < 0.001). C. Clonogenic cell proliferation ability. Results are the mean ± SD from

four independent experiments performed with at least three replicates (n = 8-14 per condition; one-way ANOVA followed by Dunn's multiple comparison test; **p < 0.01, ***p < 0.001). D. Proliferation differences were assessed by xCELLigence real-time Cell Analysis DP system. Cell index is a quantitative measure of cell number present in a well. Four independent experiments were performed. A representative result is shown, and the values are given as the mean ± SD of biological duplicates (analysis of covariance for slopes comparation; ***p = 0.0013). E. Proliferation rates analyzed using the BrdU assay. Results are shown as the mean ± SEM of three independent experiments performed with at least three biological replicates (n = 14 per condition; Student's t-test; ***p = 0.0005).

We also checked whether the proliferative effect of CPT1C silencing was something exclusive to MDA-MB-231 cells. For this reason, we silenced CPT1C in the previously selected breast cancer cell lines with shCPT1C_2-lentiviral infection. CPT1C depletion was verified by western blot (Fig. 33A). Then, we compared colony formation ability between control and CPT1C-depleted cell lines (Fig. 33B). The results showed that CPT1C silencing also increased proliferation in BT-474 and MDA-MB-468 cells. However, in luminal A MCF7 cells, CPT1C silencing decreased proliferation. These results indicate that the CPT1C silencing effect on proliferation is cell-line dependent.

A

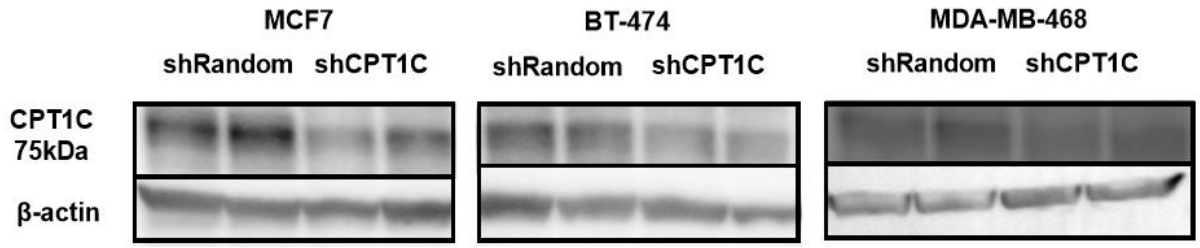

B

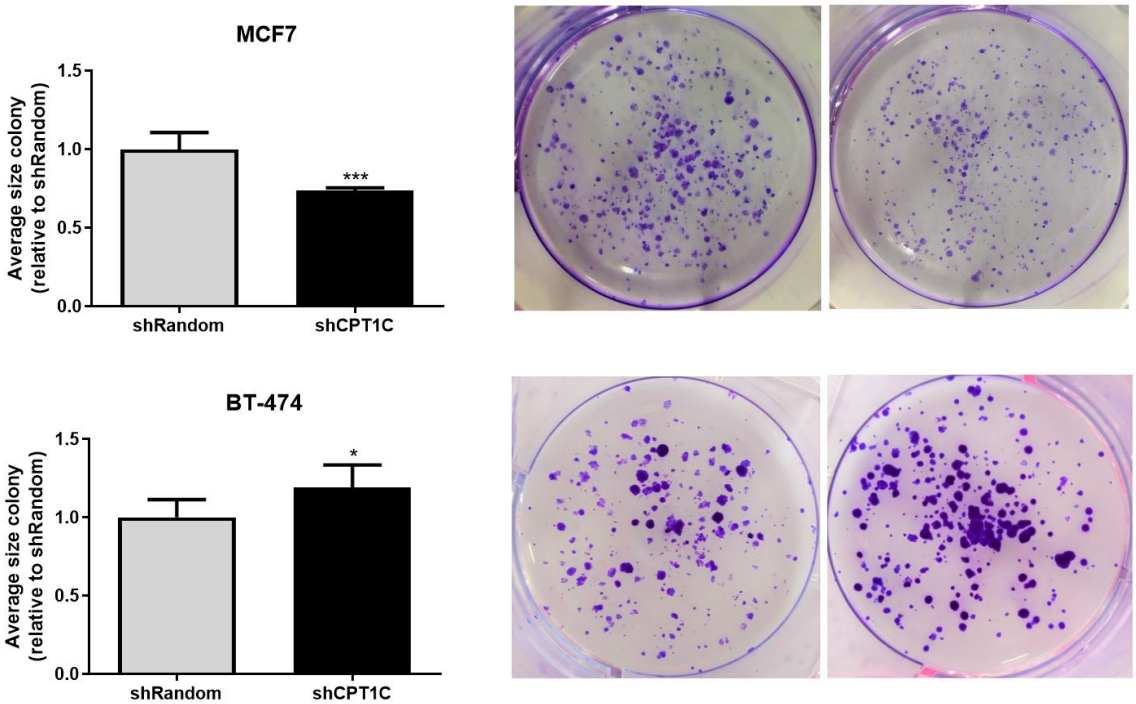

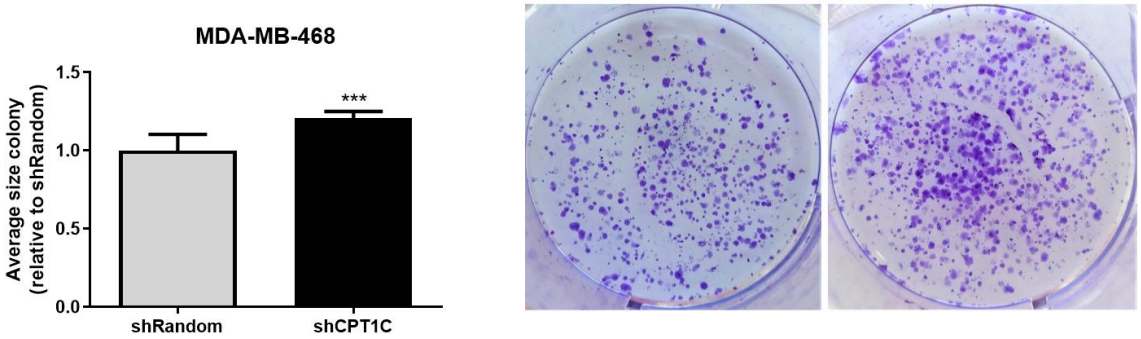

Fig. 33. CPT1C silencing impairs differentially cell proliferation in breast cancer cell lines. A. CPT1C silencing was confirmed by western blot. β-actin was used as a loading control. B. MCF7, BT-474, and MDA-MB-468 breast cancer cells were infected with shRandom- or shCPT1C_2-carrying lentivirus. Clonogenic cell proliferation ability was assayed. 1,500 cells were seeded per well for 9 days, 5 weeks, and 7 days, respectively. Then, colonies were stained with crystal violet and imaged using Fiji Image J software. Results are the mean ± SD from two independent experiments performed with at least three replicates (n = 7-12 per condition; Student's t-test; ***p < 0.0001, *p = 0.0126, ***p = 0.0001, respectively).

The proliferation enhancement seen in MDA-MB-231 breast cancer cells under CPT1C silencing was contradictory to some previous data [41,42,43,53]. For this reason, we contrasted our results with high-throughput screenings databases, such as the DepMap portal. This analysis confirms that CPT1C silencing by CRISPR (Sanger) technology decreases MDA-MB-321 and MDA-MB-468 proliferation and increases MCF7 proliferation (Fig. 34). Nevertheless, the effect of CPT1C on proliferation in most of the breast cancer cell lines was small (<20% of a change), as observed in the in vitro assays (Fig. 32 and 33).

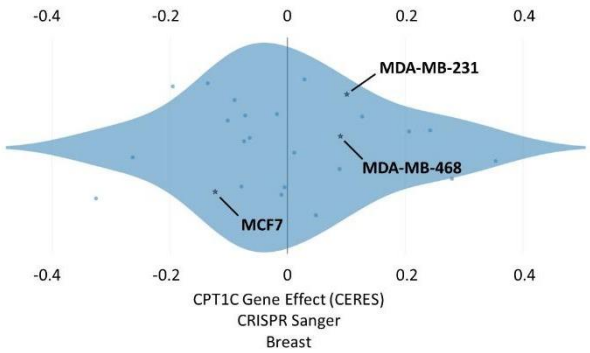

Fig. 34. CPT1C silencing enhances proliferation in MDA-MB-231 and other human breast cancer cells. CPT1C proliferation or survival dependency scores were extracted from the DepMap database considering only breast cancer cell lines. CERES scores of CRISPR Sanger dataset are represented in a violin plot distribution across 25 different breast cancer cell lines, respectively. Higher values indicate more proliferation under gene silencing. Each blue dot represents a single cell line. The cell lines used in our studies are highlighted.

2.3. CPT1C's role in MDA-MB-231 proliferation under metabolic stress conditions

As has been widely described, CPT1C protein is involved in cancer cell proliferation but specifically under metabolic stress conditions. This prosurvival effect of CPT1C has been generally associated with an enhanced fatty oxidation ability of cancer cells. For this reason, we subjected MDA-MB-231 (shRandom and shCPT1C) cells to conditions of nutrient deprivation (glucose and serum) for later survival analysis. Fatty acid oxidation (FAO) levels were measured in both cell lines under glucose deprivation. CPT1C silencing did not have any significant effect on survival under nutrient deprivation conditions in these breast cancer cells (Fig. 35A). However, a decrease of FAO was detected in CPT1C-silenced cells (Fig. 35B), confirming the influence of CPT1C on FAO.

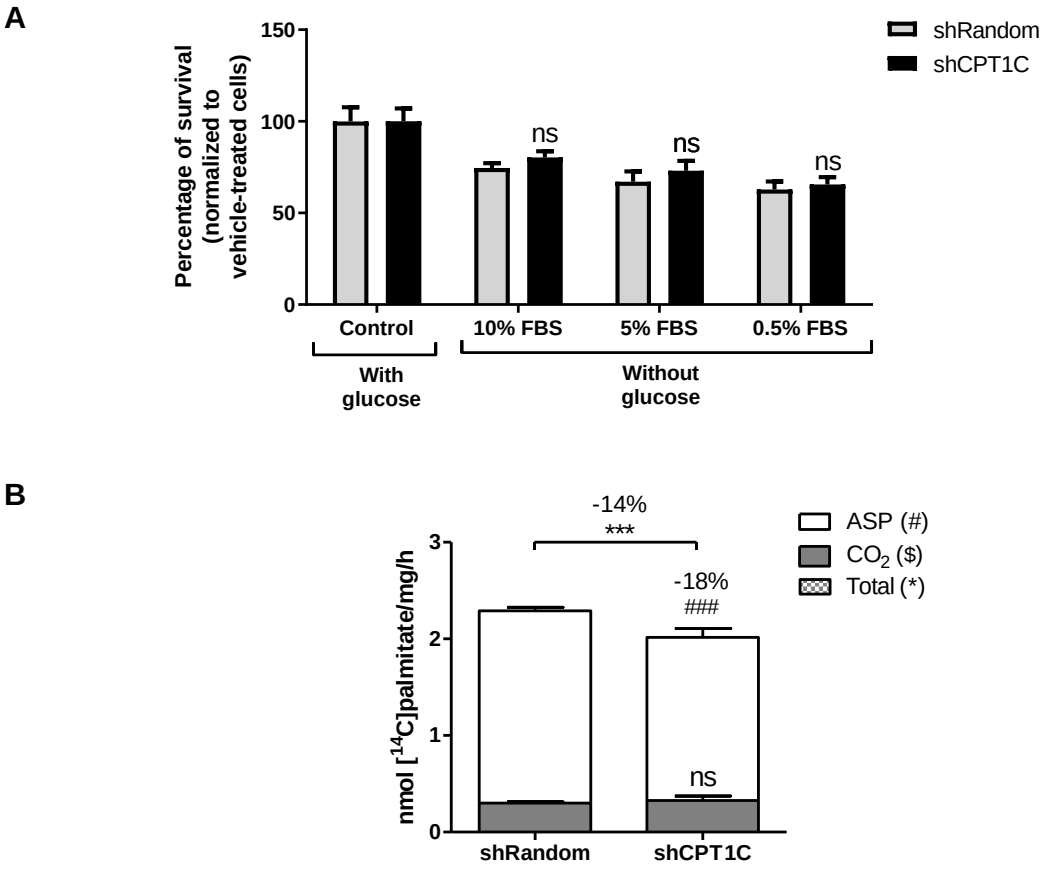

Fig. 35. CPT1C silencing effect on survival and FAO under glucose deprivation in MDA-MB-231 cells. MDA-MB-231 cells were infected with shRandom or shCPT1C-carrying lentivirus. A. Cells were treated in the presence, reduction, or absence of glucose and fetal bovine serum for 9 h. Then, MTT cell proliferation was measured. Results are represented as the mean ± SD (n = 6 per condition; two-way ANOVA followed by Bonferroni's multiple comparison test; $p > 0.05$). B. FAO assay was performed with measuring the nmol (14C)-palmitate/mg/h converted to carbon dioxide and acid-soluble products (ASP). Results are shown as the mean ± SD of quadruplicates from two independent experiments. For the statistical analysis of ASP and CO_2 production, two-way ANOVA followed by Bonferroni's multiple comparisons test was performed (***$p < 0.001$ for total; ###$p < 0.001$ for ASP; $p > 0.05$ for CO_2).

2.4. CPT1C silencing promotes invasion but not migration in MDA-MB-231 cells

As explained previously, MDA-MB-231 is a highly aggressive and invasive breast cancer cell line. Thus, it was considered a good model to study invasive and migratory processes in relation to CPT1C expression. The gelatin degradation assay and the xCELLigence real-time cell invasion analysis were performed to investigate the role of CPT1C on invasion in MDA-MB-231 cells. Both gelatin degradation assay (Fig. 36A) and xCELLigence real-time cell invasion (Fig. 36B) analysis demonstrated that downregulation of CPT1C expression increments the cell invasion ability of MDA-MB-231 cells. These results allowed us to conclude that CPT1C has a negative effect on cell invasion processes in MDA-MB-231 cells.

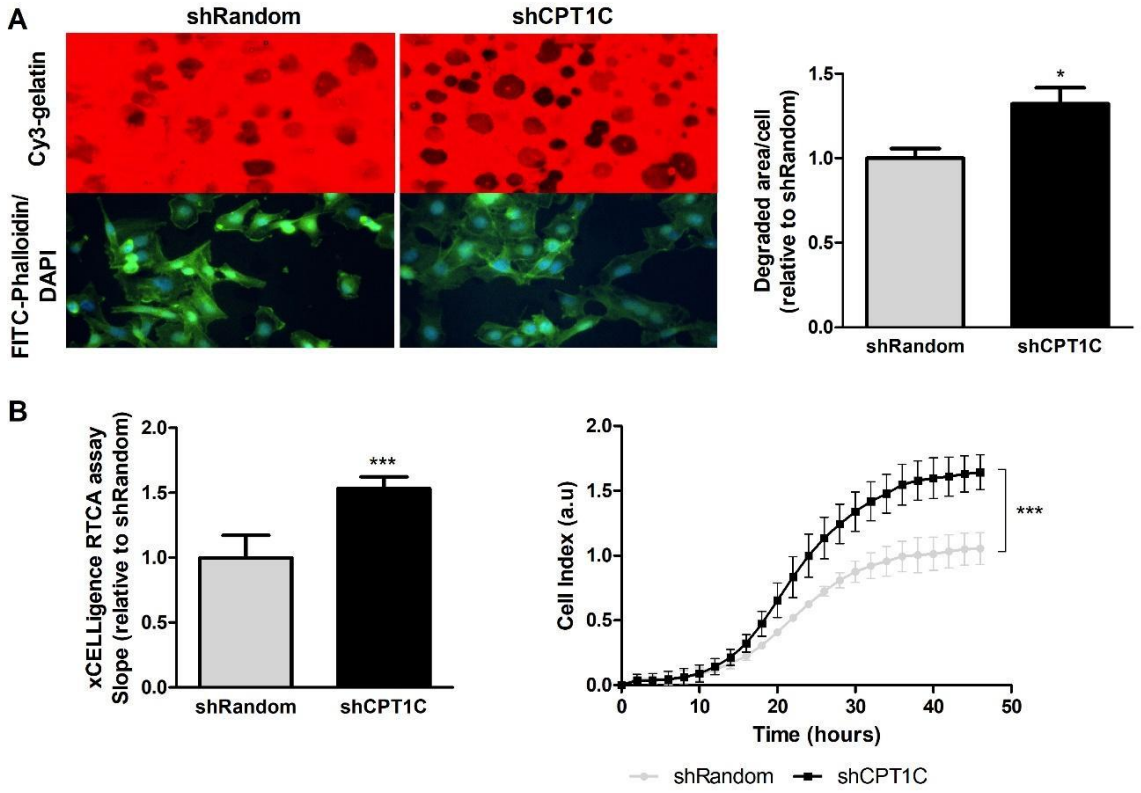

Fig. 36. CPT1C silencing promotes cell invasion in vitro. MDA-MB-231 cells were infected with shRandom or shCPT1C-carrying lentivirus. A. Gelatin degradation assay was assessed 40 h after cell seeding in Cy3-gelatin-coated dishes. Ten random fields were imaged per condition. Gelatin degradation was measured by quantifying the total area of nonfluorescent pixels per cell using Fiji Image J software. Results are the mean ± SEM from two independent experiments performed with four replicates (n = 41-47 cells per condition; Mann-Whitney test; *p = 0.0251). B. Invasion assay with xCELLigence real-time cell analysis system was performed. Cells were added to a Matrigel-coated porous chamber of a CIM-Plate 16. The cell index represents the capacity for cell invasion, and the slope of the curve indicates the invasion velocity of tumor cells. Left panel: Results are shown as the mean of the cell index slope ± SD of two independent experiments performed with at least three biological replicates (n = 9 per condition; Student's t-test; ***p = 0.0005). Right panel: Cell index results are shown from one representative experiment.

To investigate if CPT1C could also exhibit migratory effects, wound healing (Fig. 37A), xCELLigence real-time cell migration analysis (Fig. 37B), and Transwell (Fig. 37C) assays were performed. As shown in Figure 37, the migratory ability of MDA-MB-231 cells was not impaired by CPT1C silencing. These findings suggest that CPT1C is involved in cell invasion but not in cell migration in MDA-MB-231 breast cancer cells.

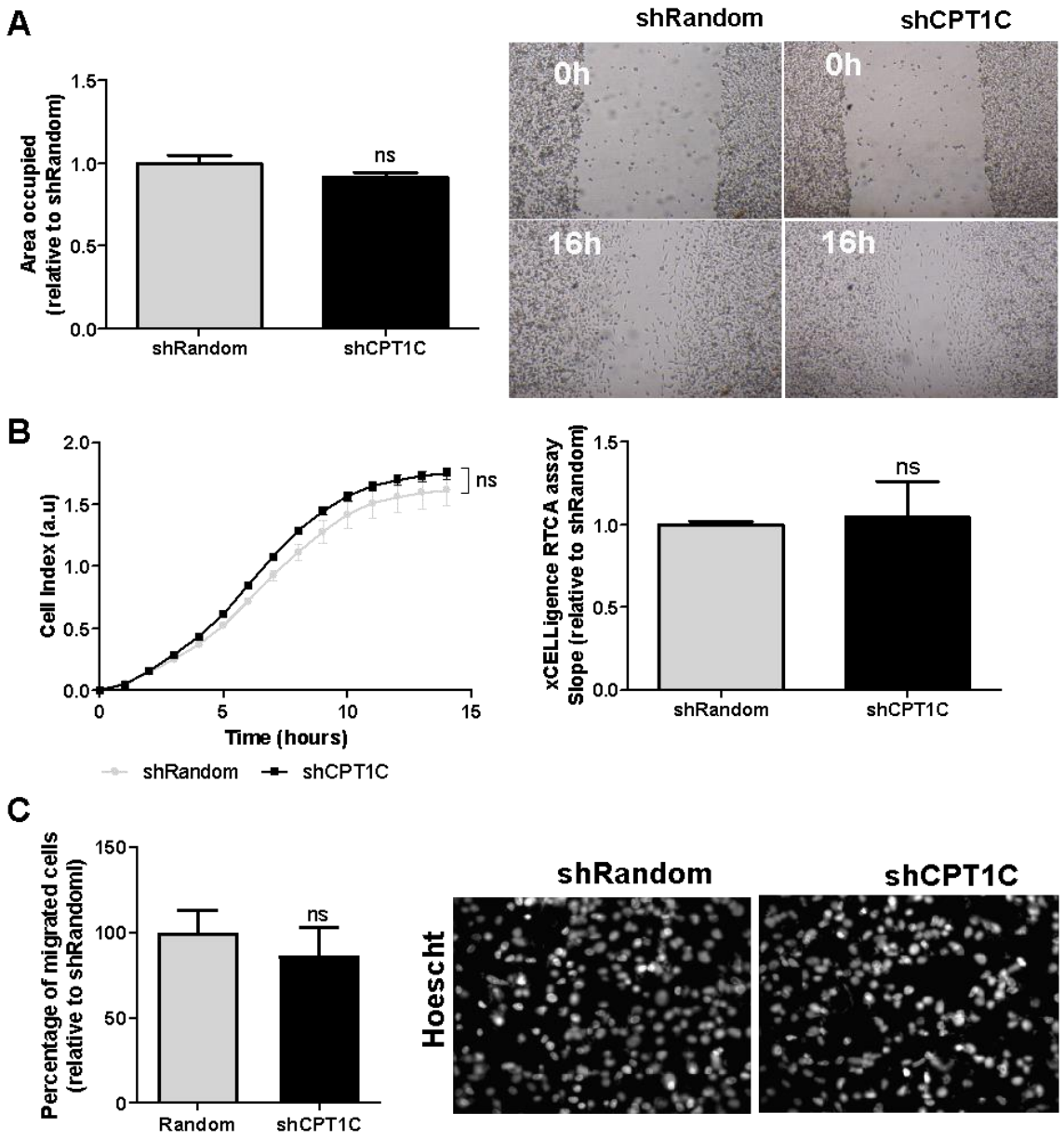

Fig. 37. CPT1C inhibition does not impair cell migration in vitro. MDA-MB-231 cells were infected with shRandom or shCPT1C-carrying lentivirus. A. Results and images at different times during the wound healing assay (magnification, ×10). Cells were seeded into 24-well cell culture plates and cultured to near confluence. The wounded monolayer was incubated in 0.5% FBS DMEM for 16 h. Results represent area gap-closure measured automatically using Fiji Image J software and are shown as the mean ± SEM of four independent experiments performed with six biological replicates (Mann-Whitney test; p = 0.2790). B. Migration assay with xCELLigence real-time cell analysis system. Cells were added to a porous chamber of a CIM-Plate 16. The cell index represents the capacity for cell

migration, and the slope of the curve indicates the migration velocity of tumor cells normalized by proliferation rate. Left panel: Cell index results are shown from one representative experiment. Right panel: Results are shown as the mean of cell index slope ± SD of three independent experiments performed with at least duplicates (Student's t-test; p = 0.5622). C. Results and representative images of transwell chamber assay (magnification, ×20) 14 h after seeding. Cell nuclei were stained with Hoescht. Results are shown as the mean ± SD of two independent experiments performed with four replicates (Student's t-test; p = 0.1001).

Cell proliferation, cell migration, and cell invasion were also assayed in MDA-MB-231 cells under conditions of CPT1C gain-of-function. MDA-MB-231 cells expressing pWPI-CPT1C were generated using lentiviral infection. We performed xCELLigence real-time cell proliferation, migration, and invasion analysis assays with control and CPT1C overexpressing-MDA-MB-231 cells, but no differences were seen between both conditions in any of the three assays (Fig. 38). Hence, all of these results suggest that the loss but not the gain of CPT1C function affects cell proliferation and cell invasion in MDA-MB-231 cells.

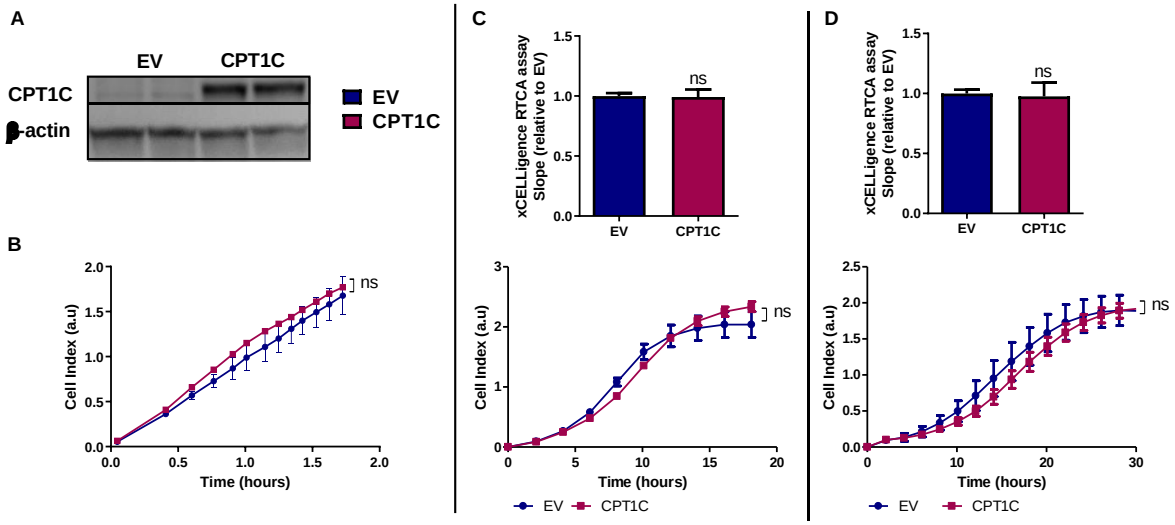

Fig. 38. CPT1C overexpression has no effect on proliferation, migration, and invasion in MDA-MB-231 breast cancer cells. MDA-MB-231 cells were infected with CPT1C-carrying lentivirus or an empty vector (EV) sequence. A. CPT1C overexpression was confirmed by western blot. β-actin was used as a loading control. Proliferation, migration, and invasion differences were assessed by xCELLigence Real-Time Cell Analysis DP system. The cell index is a quantitative measure of the cell number present in a well. B. For the cell proliferation study, four independent experiments were performed. A representative experiment is shown and the values are given as the mean ± SD of biological duplicates (analysis of covariance for slopes comparison; p = 0.4027). C. For migration assay, cells were added to a porous chamber of a CIM-Plate 16. The cell index represents the capacity of cell migration, and the slope of the curve indicates the migration velocity of tumor cells. The slope of the curve was normalized by the proliferation rate of each condition. A representative experiment (bottom) and results (top) are shown as the mean ± SD of three independent experiments performed with at least duplicates (n = 9 per condition; Student's t-test; p = 0. 8150). D. Invasion assay was performed as a migration assay, but the porous membrane was previously coated with Matrigel. A representative experiment (bottom) and results (top) are shown as the mean ± SD of three independent experiments performed with at least duplicates (Student's t-test; p = 0. 6423).

3. CPT1C silencing promotes drug resistance

Previous research has found that CPT1C is related to multidrug resistance in cancer. Therefore, we decided to study the role of CPT1C in drug resistance in breast cancer in vitro.

3.1. CPT1C silencing induces resistance to doxorubicin and paclitaxel treatments in breast cancer cells

Doxorubicin (DOX) and paclitaxel are included in the most commonly used chemotherapy drugs in breast cancer [58]. To determine whether CPT1C affects chemotherapy drug cytotoxicity, MDA-MB-231 cell lines were treated with 1 μM and 2 μM DOX (Fig. 39A) or 100 nM and 200 nM paclitaxel (Fig. 39B) for 24 h and 48 h. Cell viability was measured through the MTT assay. Interestingly, MTT results showed that DOX and paclitaxel resistance was clearly increased under CPT1C-silencing conditions in MDA-MB-231 cells. To confirm that the effect was specific to CPT1C silencing and not to an off-target effect of the shRNA, we overexpressed CPT1C in CPT1C-depleted MDA-MB-231 cells, and coherently, DOX sensitivity was recovered. CPT1C expression was checked by western blot (Fig. 39C).

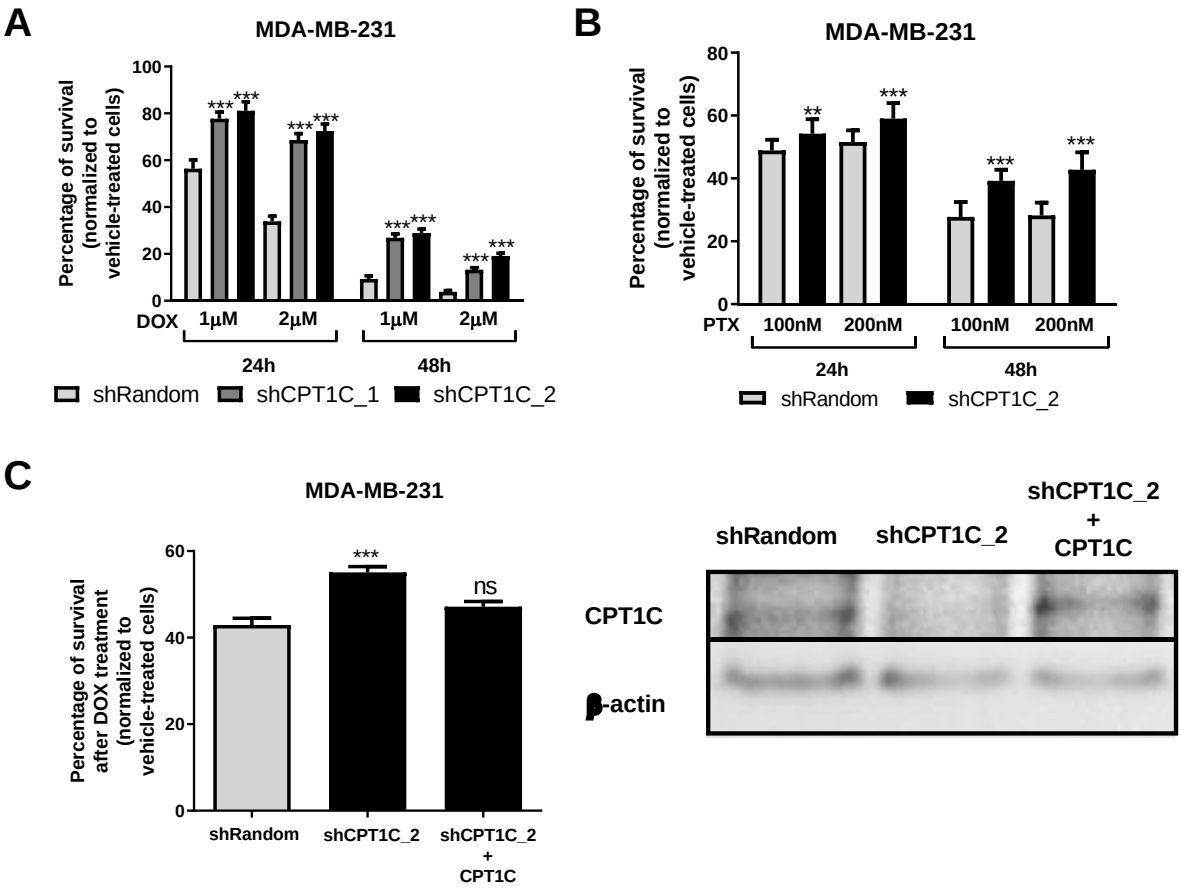

Fig. 39. CPT1C silencing increases doxorubicin (DOX) and paclitaxel resistance in MDA-MB-231 cells. MDA-MB-231 were infected with shRandom or shCPT1C-carrying lentivirus. A, B. MTT assay used to evaluate the chemosensitivity of breast cancer cell lines to DOX and paclitaxel after 24 h or 48 h treatment at the indicated doses. Results are represented as the mean ± SD (A) or ± SEM (B) (n = 4 per condition; two-way ANOVA followed by Bonferroni's multiple comparison test; **p < 0.01, ***p < 0.001). C. MTS cell viability assay was performed by treating cells with 2 μM DOX for 48 h (n = 6 per condition; one-way ANOVA followed by Dunn's multiple comparison test; ***p < 0.001). CPT1C inhibition and overexpression was confirmed by western blot. β-actin was used as a loading control.

Next, we investigated whether this CPT1C drug resistance effect was specific to the MDA-MB-231 cell line. For this purpose, we generated stable cell lines of BT-474 and MCF7 in which CPT1C was downregulated by shCPT1C_2. DOX and paclitaxel cytotoxicity was measured through the MTT assay. The results demonstrated that CPT1C silencing also strongly increased DOX and paclitaxel resistance in BT-474 cells (Fig. 40A). The same effect was demonstrated in MCF7 cells with the exception of those treated with paclitaxel (Fig. 40B).

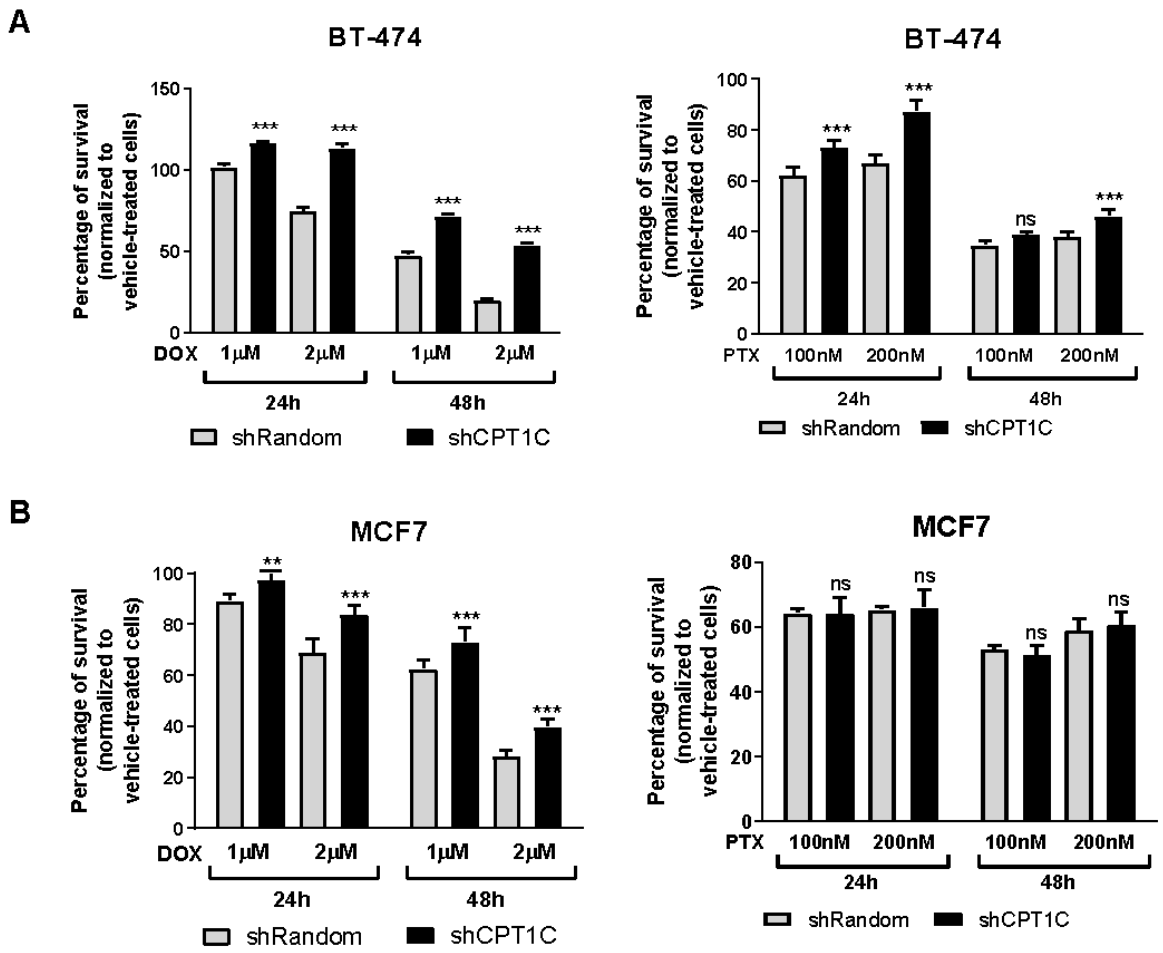

Fig. 40. CPT1C silencing also increases drug resistance in BT-474 and MCF7 cells. BT474 (A) and MCF7 cells (B) were infected with shRandom or shCPT1C-carrying lentivirus. The MTT assay was used to evaluate the chemosensitivity of breast cancer cell lines to doxorubicin (DOX) and paclitaxel after 24 h or 48 h treatment at the indicated doses. Results are represented as the mean ± SD of three experiments for DOX and one or two experiments, respectively, for 24 h or 48 h paclitaxel (n = 4 per condition; two-way ANOVA followed by Bonferroni's multiple comparison test; **p < 0.01, ***p < 0.001).

To investigate CPT1C effects in drug resistance could be extended to other types of cancer, we explored CPT1C-induced chemoresistance in neuroblastoma and glioblastoma cells. Neuroblastoma is the most common extracranial solid tumor appearing in childhood. This is frequently treated with a combination of chemotherapy drugs, which include DOX, carboplatin, cyclophosphamide, and etoposide [115]. In regard to glioblastoma, this is the most common malignant primary brain tumor and has a very poor prognosis. It is treated with temozolomide as a first-line chemotherapy drug; however, there is no established systemic therapy in the second-line setting. Despite not being included in the standard regimens, DOX has been included in some clinical trials in combination with the common regimen for glioblastoma [35,116]. For this reason, we considered it valuable to assess CPT1C-silencing DOX resistance in brain cancer cell lines. SH-SY5Y, a neuroblastoma cancer cell line, and U-87 MG, a glioblastoma cancer cell line, were infected with shRandom or shCPT1C_2-carrying lentivirus, and CPT1C expression was verified using qPCR (Fig. 41A). Then, these brain cancer cells lines were treated at the indicated times and doses with DOX. Surprisingly, CPT1C silencing had no effect (or even the opposite effect) on drug resistance in these brain cancer models, compared to breast cancer cell lines (Fig. 41B). Thus, we concluded that the drug resistance effect triggered by CPT1C downregulation may be specific to breast cancer cells.

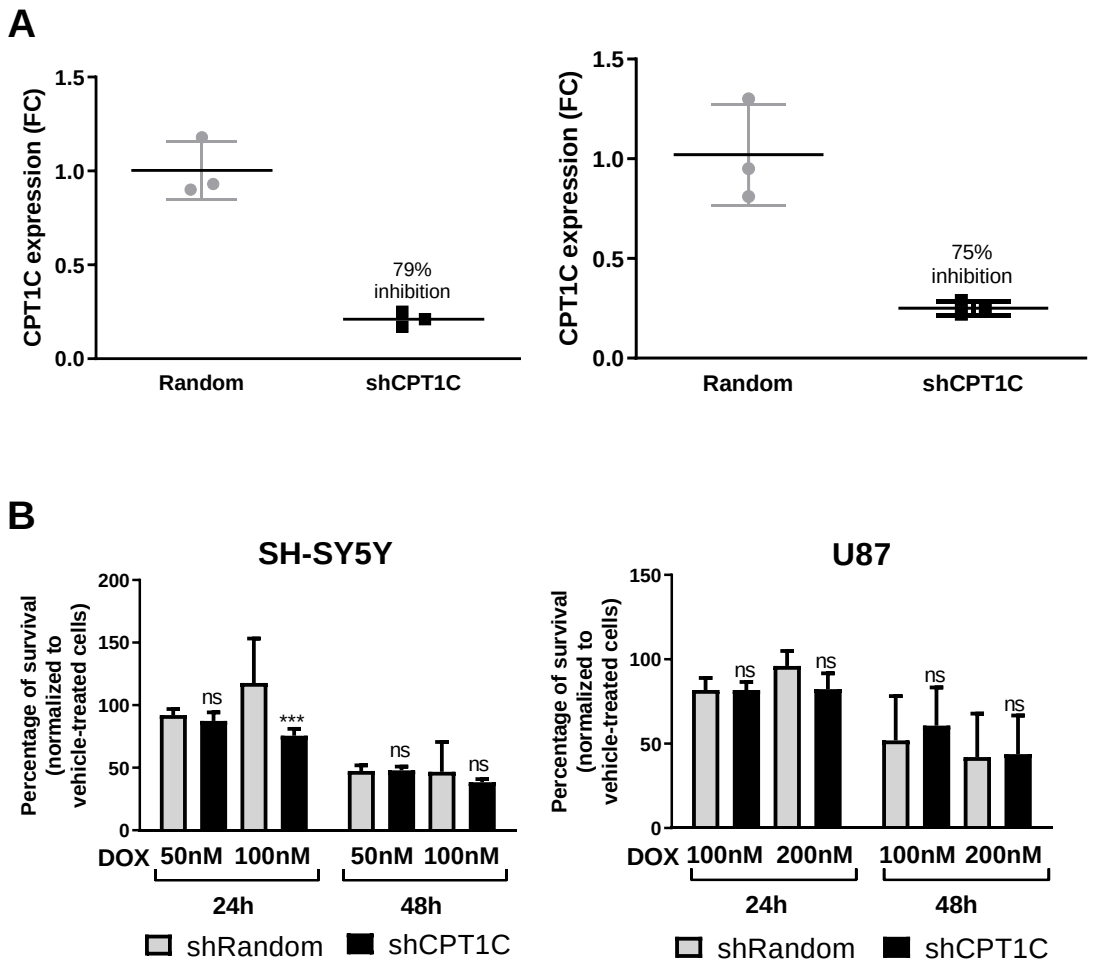

Fig. 41. CPT1C silencing effects on doxorubicin (DOX) resistance in some neuroblastoma and glioblastoma cells in vitro. SH-SY5Y and U87 brain cancer cells were infected with shRandom or shCPT1C-carrying lentivirus. A. CPT1C silencing was confirmed by RT-PCR. β-actin was used as a reference gene. B. MTT cell viability assays were performed to study chemosensitivity to DOX. The experiments were repeated two times independently. Results represent the mean ± SD (n = 4 per condition, two-way ANOVA followed by Bonferroni's multiple comparison test; ***p < 0.001).

To more closely reflect the tumor environment, we formed 3D mammospheres with MDA-MB-231 and BT-474 cells. Drug resistance in mammospheres was ascertained using the CellTiter-Glo® 3D cell viability assay with the same times and doses of DOX used previously for the 2D cultures (Fig. 42). Similar to the results in 2D cultures, CPT1C silencing increased DOX resistance in MDA-MB-231 and BT-474 mammosphere cultures.

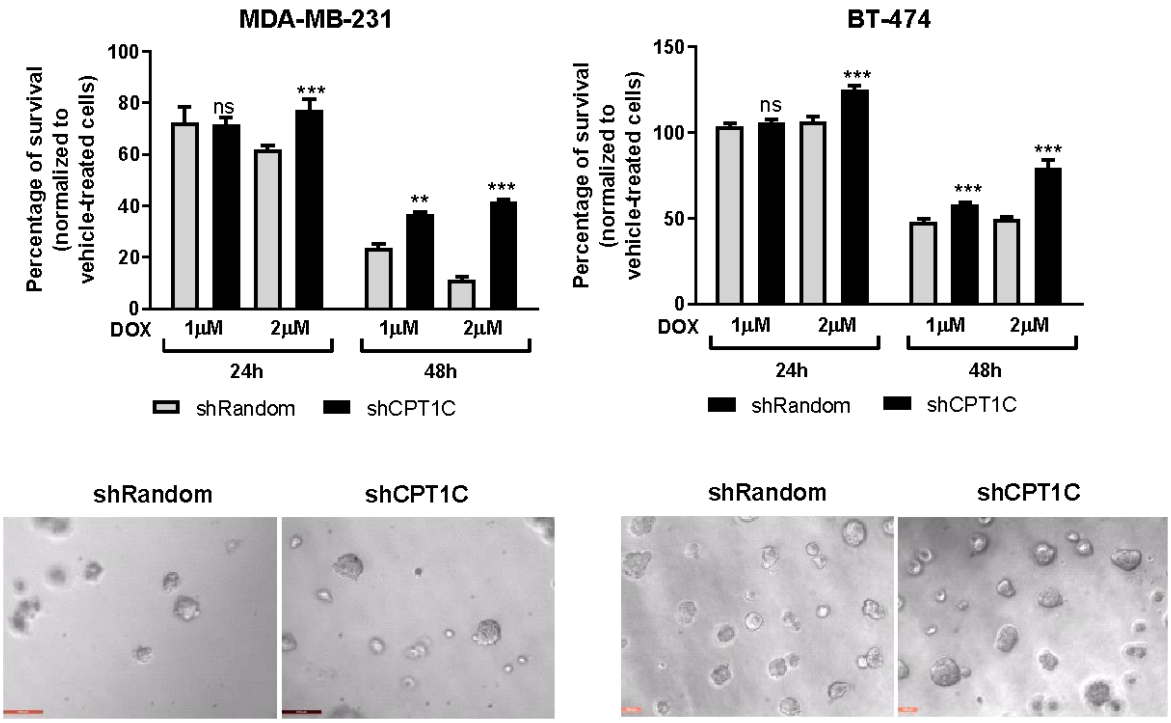

Fig. 42. CPT1C silencing increases doxorubicin (DOX) resistance in breast cancer mammospheres. MDA-MB-231 and BT-474 were infected with shRandom or shCPT1C-carrying lentivirus. Cell viability of MDA-MB-231 and BT-474 mammospheres was determined by CellTiter-Glo® luminescent cell viability assay. Images represent mammospheres at 24 h after DOX treatment. Two independent experiments were performed with each cell line. A representative result is shown, and the values are given as the mean ± SD of biological triplicates (two-way ANOVA followed by Bonferroni's multiple comparison test; **p < 0.01, ***p < 0.001).

3.2. CPT1C is a predictive biomarker of chemotherapy response in patients with HER2+ and TNBC breast cancer subtypes

In cancer treatment, biomarkers can be categorized into two major types: prognostic biomarkers that can provide information about patient survival irrespective of the treatment, and predictive biomarkers that can predict the response to a selected anticancer therapy. Predictive biomarkers help to select a particular treatment over another and to avoid unnecessary adverse effects [117]. Having some evidences of the chemoresistance role of CPT1C silencing in vitro, we determined whether CPT1C could be a predictive marker for patients with breast cancer. For this aim, we took charge of the novel ROC Plotter online server, released in 2019 [117]. The ROC Plotter is the first online transcriptome-level validation tool for predictive cancer biomarkers. This tool is capable of linking gene expression and response to therapy and revealing new biomarkers using transcriptome-level data of 3,104 patients with breast cancer who received chemotherapy. In this database, the patients are assigned to two cohorts (responders and nonresponders to therapy) based on their clinical

characteristics (grade, nodal status, receptor status and molecular subtype). For our study, patients with neoadjuvant chemotherapy were classified according to pathological complete response (pCR). pCR is defined as the disappearance of all invasive cancer in the breast and in axillary nodes after completion of neoadjuvant therapy. Patients with pCR have increased OS and RFS, with the greatest benefits seen in those with HER2+ and TNBC breast cancers [118,119].

We performed a first search across all patients with breast cancer and did not see significant differences in pCR related to CPT1C expression under any chemotherapy treatment. However, as was explained previously, in Kaplan-Meier studies, we observed a strong significative relationship between low CPT1C expression and a worse RFS depending on the expression of some important molecular breast cancers markers (section 1 from results).

For this reason, we ran a ROC Plotter analysis filtering by the HER2 molecular subtype to include patients with breast cancer with ER−, PR−, HER2+ tumors. According to the Kaplan-Meier results, we confirmed that under anthracycline treatment, the pCR was lower and significantly worse in patients with HER2+ breast cancer and low CPT1C expression (Fig. 43). Because patients with HER2+ breast cancer are normally treated with anti-HER2 therapy and chemotherapy, we tested the ROC Plotter for CPT1C expression in patients with HER2+ breast cancer but submitted to anti-HER2 therapy such as trastuzumab anti-HER2 antibody; however, no changes in pCR were associated with CPT1C expression (data not shown).

The ROC server gives a numerical representation of the classifier performance when providing the area under the curve (AUC) value. An AUC of 0.5 corresponds to no classification predictive power of a gene, and an AUC value of 1 denotes a perfect cancer biomarker. With less than 0.6, the effect is small for clinical utility; 0.6-0.7 is considered to be a cancer biomarker with potential clinical utility; 0.7-0.8, a top-quality cancer biomarker; and more than 0.8, a blockbuster biomarker [117]. For CPT1C, pCR in patients receiving anthracycline, the AUC was 0.661. These data revealed the CPT1C gene as a novel and potential predictive biomarker for anthracycline treatment in patients with HER2+ breast cancer.

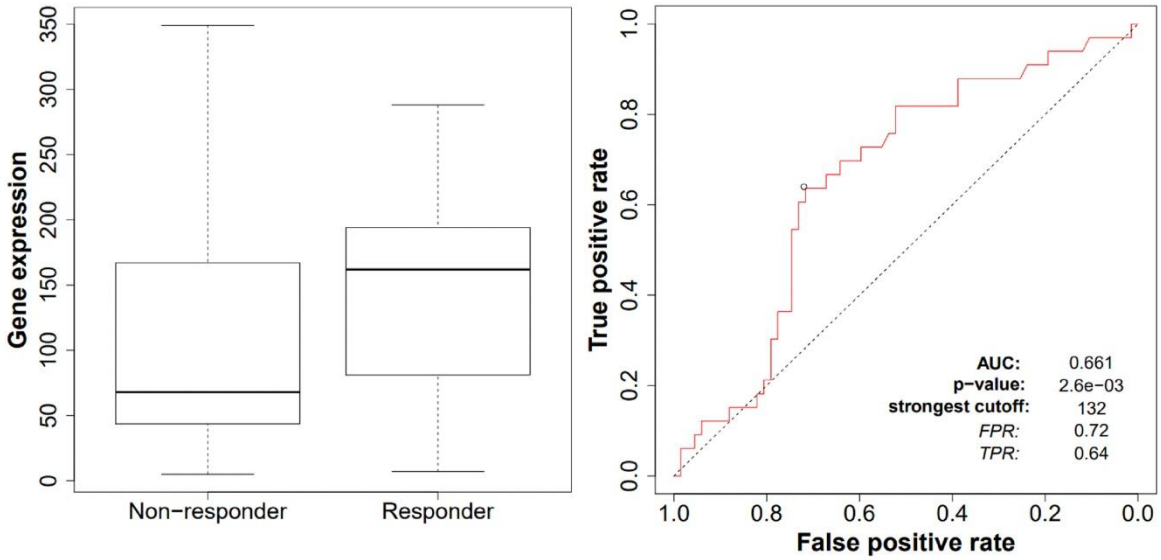

Anthracyclines								
Data							Result	
							AUC	0.661
Patients	N	Mean	SD	Median	Minimum	Maximum	ROC p-value	2.60E-03
Responder	33	176	132	162	7	530	Mann-Whitney test p-value	0.0094
Non-responder	67	125	130	68	5	541	Fold change	1.4

Fig. 43. CPT1C gene is a cancer biomarker with a potential clinical utility as a predictor for chemotherapy treatment in patients with HER2+ breast cancer. The ROC Plotter web application (www.rocplot.org) was used to link CPT1C expression with therapy response using the transcriptome-level data of patients with breast cancer. We filtered for patients with HER2+ who had received anthracycline (n = 100). Response to therapy was determined using complete pathological response. Left panel: Box-and-whisker plots represents the median, minimum and maximum values of CPT1C expression for responding and nonresponding patients according to pCR. Right panel: ROC curve is created by plotting the true positive rate against the false positive rate. It illustrates the diagnostic ability of the binary classifier system. The diagonal divides the ROC space. Points above the diagonal represent good binary classification (in responders and nonresponders) results (better than random) and points below the line represent poor results (worse than random). The p-values, AUC, and the strongest cutoff values capable of best discriminating between responders and nonresponders are shown. Table provides data on the number of patients, pCR (mean, SD), and CPT1C expression (median, minimum, maximum), as well as the data results of ROC analysis (AUC, p-value) and pCR analysis (p-value, FC).

We also considered it interesting to run the ROC Plotter tool in TNBC breast cancers. We examined pCR for all patients with TNBC breast cancer who received anthracycline treatment and did not see differences related to the CPT1C gene, despite a tendency in the expected direction (data not shown). However, when we restricted the analysis to only those patients who were node-positive, the results showed that patients with CPT1C-low-expressing tumors were less likely to achieve a pCR when they received anthracycline treatment (Fig. 44). We did not consider the equivalent data for node-negative TNBC patients as the number of responder patients was too low (n = 5).

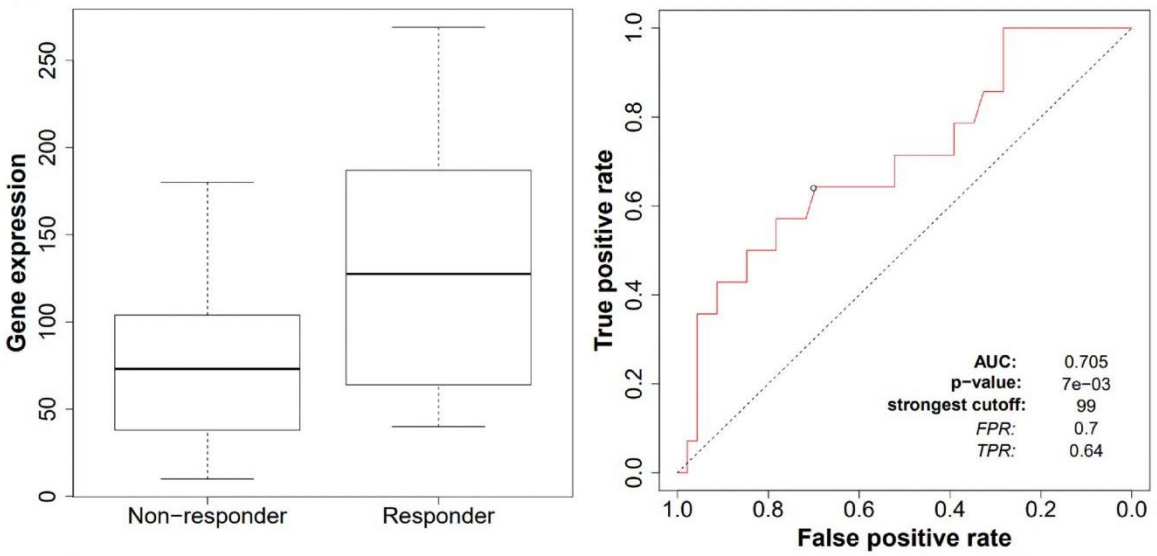

Anthracyclines (node positive)								
Data							Result	
							AUC	0.705
Patients	N	Mean	SD	Median	Minimum	Maximum	ROC p-value	7.00E-03
Responder	14	131	70	128	40	269	Mann-Whitney test p-value	0.022
Non-responder	46	90	85	73	10	542	Fold change	1.5

Fig. 44. The CPT1C gene is a cancer biomarker with potential clinical utility as a predictor for chemotherapy treatment in patients with node-positive TNBC breast cancer. The ROC Plotter web application (www.rocplot.org) was used to link CPT1C expression with therapy response using transcriptome-level data of patients with breast cancer. We filtered for patients with node-positive TNBC who had received anthracycline treatment (n = 60). Response to therapy was determined using complete pathological response. Left: Box-and-whisker plots showing the median, minimum and maximum values of CPT1C expression for responding and nonresponding patients according to pCR. Right: The ROC curve created by plotting the true positive rate against the false positive rate. It illustrates the diagnostic ability of the binary classifier system. The diagonal divides the ROC space. Points above the diagonal represent good binary classification (in responders and nonresponders) results (better than random) and points below the line represent poor results (worse than random). The p-value, AUC, and the strongest cutoff value capable of best discriminating between responders and nonresponders are shown. Table provides data on the number of patients, pCR (mean, SD), and CPT1C expression (median, minimum, maximum), as well as the data results of ROC analysis (AUC, p-value) and pCR analysis (p-value, FC).

3.3. Drug resistance in CPT1C-silenced MDA-MB-231 cells is due to an impairment in DOX uptake

Once the drug resistance increasing effect of CPT1C silencing was confirmed in breast cancer cell lines, we wondered which mechanism was responsible for this phenotype. Taking advantage of the inherent fluorescent properties of DOX, we directly analyzed its cell accumulation using flow cytometry with pulse-chase experiments in control and CPT1C-silenced MDA-MB-231 cells. We incubated the cells with the drug for four hours, then changed the medium and incubated the cells with drug-free medium for 20 hours more. As expected,

intracellular DOX accumulation increased during the first four hours and decreased after the medium change in a time-dependent manner. The DOX accumulation flow cytometry graph revealed that CPT1C silencing significantly reduced DOX accumulation in MDA-MB-231 cells (Fig. 45A). The pharmacokinetics analysis allowed us to separate flow cytometry DOX accumulation information in two different datasets: drug uptake (from 0 h to 4 h) and drug release (from 4 h to 24 h). For the analysis of drug release, data were previously normalized by initial DOX cellular content. By comparing the uptake and release slopes of both cell lines, we were able to conclude that the reduced DOX accumulation of CPT1C-silenced MDA-MB-231 cells primarily corresponded to an impairment in drug uptake rather than to drug release (Fig. 45B). To see whether cell DOX accumulation was due to accumulation in the nucleus which is the drug target, we investigated its subcellular distribution by confocal microscopy. Nuclear accumulation of DOX was analyzed in fixed cells at 2 h 30 min after drug treatment, as this point corresponded to a time slot where drug uptake was higher than drug release. Coherent with results mentioned above, CPT1C silencing decreased DOX nuclear accumulation in MDA-MB-231 breast cancer cells (Fig. 45C). All these results that CPT1C could play a role in the uptake of some chemotherapy drugs, such as DOX, in breast cancer cells.

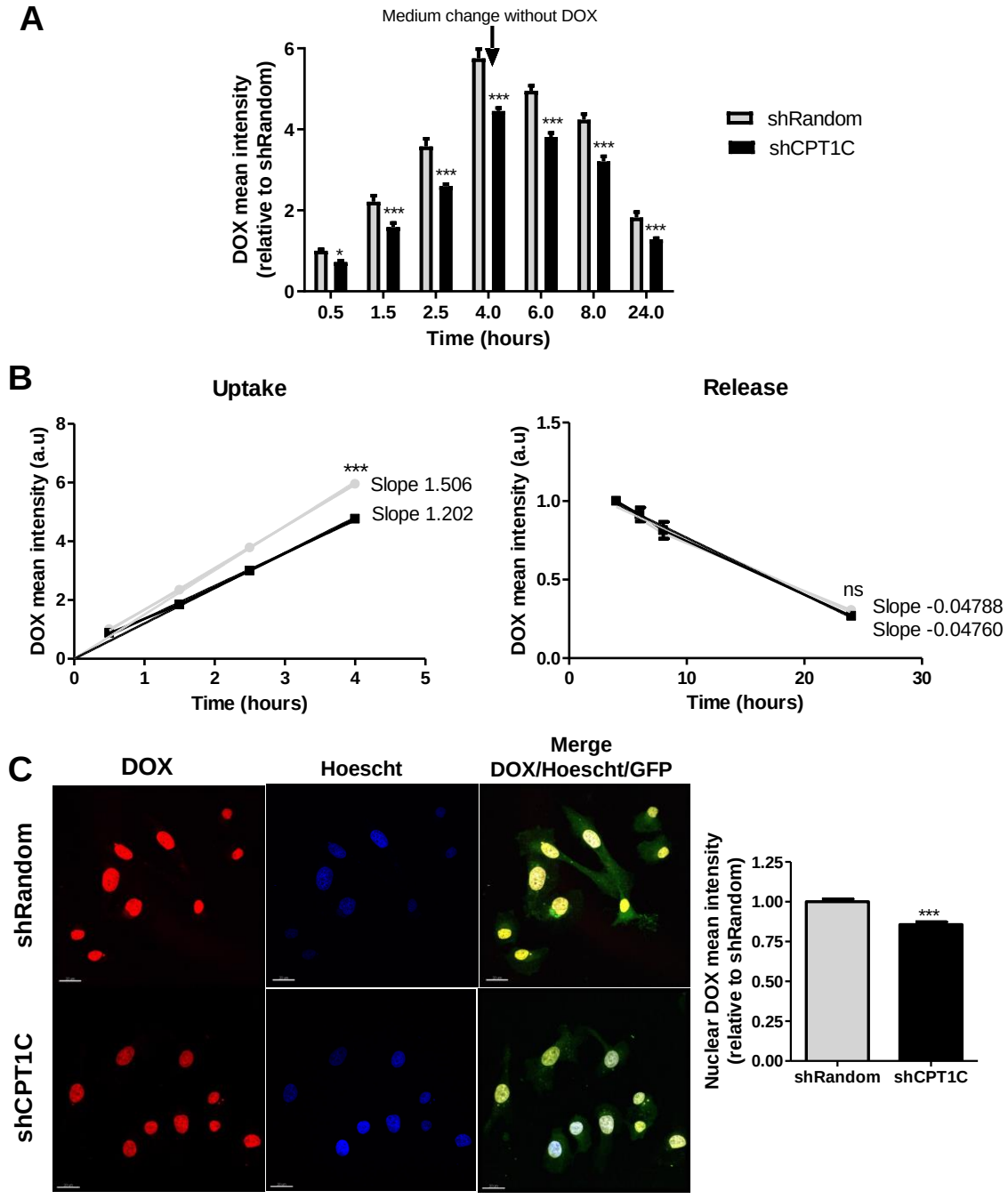

Fig. 45. CPT1C silencing decreases cellular and nuclear accumulation doxorubicin (DOX) by decreasing its uptake. MDA-MB-231 cells were infected with shRandom or shCPT1C-carrying lentivirus. A. Quantification of intracellular DOX at the indicated times detected by flow cytometry. Cells were treated with 1 µg/ml DOX for 4 h, and then, a medium change was made for DOX removal to study drug release until 24 h. Two independent experiments were performed. A representative result is shown, and the values are given as the mean ± SD of four replicates (two-way ANOVA followed by Bonferroni's multiple comparison test; *p < 0.05, ***p < 0.001). B. DOX accumulation kinetics (uptake and normalized release) from both flow cytometry experiments. Slopes of both conditions were compared (n = 8, analysis of covariance for slopes comparation; uptake p*** < 0.0001 and release p = 0.5063). C. Left panel: Intracellular localization of DOX visualized by confocal microscopy at 2 h 30 min after DOX exposure. Nuclei were labeled with Hoescht (scale bars, 20 µm). Right panel: Quantification of fluorescence intensity (DOX) in the nuclei. Results are shown as the mean ± SEM of two independent experiments performed with four biological replicates (n = 154-183 cells per condition were analyzed; Mann-Whitney test; ***p < 0.0001).

3.4. Identification of the mechanism underlying DOX resistance in CPT1C-silenced cells

The next question was to elucidate which mechanism of uptake was modulated by CPT1C deficiency. Free chemotherapy drugs can enter the cells through different pathways. DOX enters cells via passive diffusion and is rapidly distributed and retained in nucleated cells due to its lipophilicity and DNA-binding capacity. Additionally, DOX can enter cells by the plasma membrane (PM) transporter SLC22A16, a transporter of L-carnitine. Finally, the free DOX can enter the cell by endocytosis, and specifically, by a nonspecific endocytosis such as macropinocytosis. In fact, this process is frequently increased in cancer cells. Thus, we assessed how representative these three DOX uptake mechanisms are in our model of MDA-MB-231 cells.

3.4.1. Identification of the DOX uptake mechanism in MDA-MB-231 breast cancer cells

We started studying DOX uptake through the PM transporter SLC22A16. When we treated MDA-MB-231 wild-type cells at the same time with DOX and increasing doses of L-carnitine as a competitive inhibitor, DOX uptake was progressively decreased (Fig. 46A). This result confirmed that part of DOX enters the cell through the SLC22A16 transporter.

The second pathway to explore was endocytosis. In breast cells, endocytosis can be categorized into four major types: clathrin-mediated endocytosis, caveolae-mediated endocytosis, clathrin- and caveolae- independent endocytosis, and macropinocytosis. The latter type is characterized by engulfment of extracellular fluids and solutes, and thus, we considered it most relevant for free-DOX uptake. EIPA (5-[N-ethyl-N-isopropyl] amiloride), a Na+/H+ exchanger inhibitor that specifically blocks macropinocytosis, was used to confirm that DOX uptake occurred via macropinocytosis. MDA-MB-231 cells were treated with DOX at increasing doses of EIPA, and DOX uptake was measured using flow cytometry. Effectively, DOX uptake was reduced under macropinocytosis inhibition. These results also confirmed that DOX enters cells through macropinocytosis (Fig. 46B).

The last pathway that we explored was passive diffusion. Because one of the lipids known to decrease free drug uptake by passive diffusion is cholesterol (Chol), we reduced PM Chol levels in MDA-MB-231 cells with methyl-beta-cyclodextrin (MBCD) to see whether this reduction could increase DOX uptake. Additionally, we treated cells with MBCD-Chol complexes as a control of MBCD-Chol depletion efficacy. As expected, PM Chol reduction

increased DOX uptake, as revealed by flow cytometry results (Fig. 46C). Thus, we confirmed that DOX partially crosses the PM by passive diffusion.

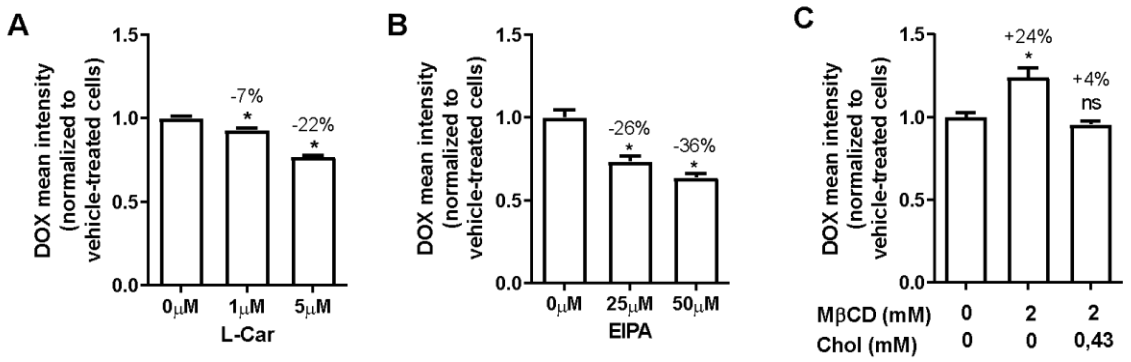

Fig. 46. Doxorubicin (DOX) drug uptake study in breast cancer cells. Flow cytometry analysis of intracellular DOX accumulation after 1 h 30 min of treatment in wild-type MDA-MB-231 cells. A. Cells were cotreated with L-carnitine as a competitive inhibitor of the SLC22A16 transporter. B. Cells were cotreated with EIPA as a specific macropinocytosis inhibitor. C. Cells were cotreated with methyl-beta-cyclodextrin (MBCD) as a PM Chol disruptor. MBCD-Chol complex treatment was used to recover/replete Chol content in the PM. All results are shown as the mean ± SD of experiments performed with four biological replicates (Mann-Whitney test was applied comparing pairs of columns; *$p < 0.05$).

3.4.2. Identification of the mechanism underlying DOX resistance in CPT1C-silenced cells

Once the participation of the three DOX uptake mechanisms were confirmed in MDA-MB-231 cells, we aimed to determine in which uptake mechanism CPT1C could be involved. For this aim, we repeated the experiments explained above but compared control and CPT1C-silenced MDA-MB-231 cells. The inhibition of the transporter SLC22A16 decreased DOX uptake in the same percentage in both conditions (Fig. 47A), indicating that CPT1C expression does not affect this mechanism. Similar results were obtained through macropinocytosis inhibition (Fig. 47B). However, MBCD Chol depletion only increased DOX uptake in control MDA-MB-231 cells, not in CPT1C-depleted cells (Fig. 47C). These results suggested that Chol levels are not responsible for the chemoresistance derived from CPT1C depletion, as CPT1C-silenced cells, under Chol depletion, did not increased DOX uptake at a higher level than control cells. However, these data suggested that CPT1C was partially modulating PM Chol levels.

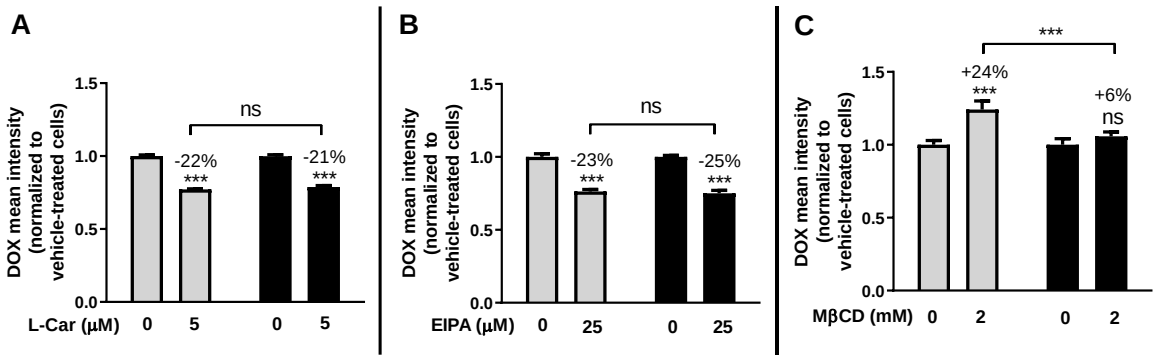

Fig. 47. Drug uptake mechanism study. MDA-MB-231 cells were infected with shRandom or shCPT1C-carrying lentivirus. Quantification of intracellular DOX 1 h 30 min after treatment was detected by flow cytometry. Cells were treated with 1 μg/ml DOX together with DOX uptake disruptors such as L-carnitine (A), EIPA (B), and MBCD (C). Percentage differences under different treatments are shown. Percentage of DOX uptake disruption was compared. All results are shown as the mean ± SD of experiments performed with four biological replicates (two-way ANOVA followed by Bonferroni's multiple comparison test; *p < 0.05, **p < 0.001, ***p < 0.001).

3.4.2.1. Cholesterol analysis

To study whether PM Chol levels were regulated by CPT1C, we decided to start quantifying total Chol levels in shRandom- and shCPT1C-MDA-MB-231 cells. We tackled this issue by measuring total Chol in cell lysates of shRandom- and shCPT1C-MDA-MB-231 cells. The results clearly showed that no changes in total cellular Chol levels were found between both conditions (Fig. 48).

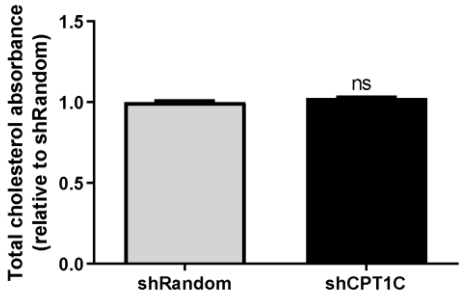

Fig. 48. Total Chol levels were unchanged under CPT1C silencing. MDA-MB-231 cells were infected with shRandom or shCPT1C-carrying lentivirus. Cell lysates were mixed with Chol reagent for 10 min. Then, absorbance was read at 500 nm. Two independent experiments were performed. A representative result is shown, and the values are given as the mean ± SD of six biological replicates (Student's t-test; p = 0.2894).

After ensuring that no changes in global Chol were observed between control- and shCPT1C-MDA-MB-231 cells, we proceeded to measure PM Chol levels using the specific probe mCherry-D4. Coherently with DOX uptake results, shCPT1C-MDA-MB-231 cells showed significantly less mCherry-D4 staining at the PM than control cells, observed by confocal microscopy (Fig. 49A) and flow cytometry (Fig. 49B). Therefore, we concluded that the increased resistance of CPT1C silenced-MDA-MB-231 cells to DOX treatment was not due to increased PM Chol.

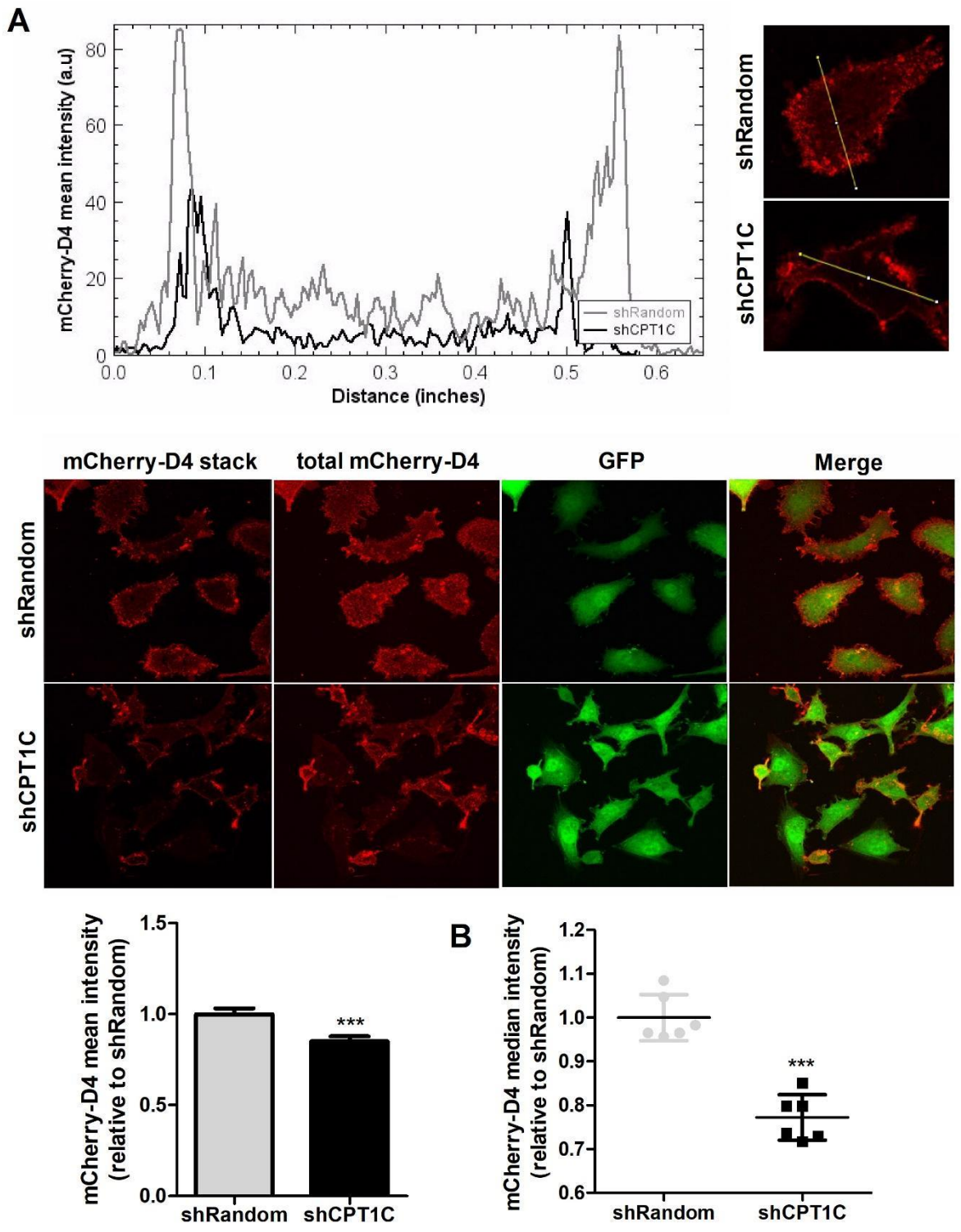

Fig. 49. PM Chol levels in CPT1C-silenced MDA-MB-231 cells. MDA-MB-231 cells were infected with shRandom or shCPT1C-carrying lentivirus. PM Chol staining with the mCherry-D4 probe was quantified. A. Fluorescence confocal analysis of labeled cells with mCherry-D4 recombinant protein. GFP intensity was used as an infection control. Live cells were seeded, then stained with the mCherry-D4 probe and fixed. Representative histograms display PM Chol staining (top left) from a line across cell (top right). Representative images of cells with GFP-D4 staining and GFP as a cell marker. Scale bar: 20 µm (middle). Quantification of mCherry-D4 mean intensity per cell using IMARIS imaging software (bottom). Two independent experiments were performed. A representative result is shown and

the values are given as the mean ± SEM of four biological replicates (n = 99-120 cells per condition were analyzed; Mann-Whitney test; ***p = 0.0003). B. Flow cytometry analysis of PM Chol staining with the mCherry-D4 probe. Cells were stained with the probe and fixed, and mCherry-D4 staining median intensity was analyzed by flow cytometry. Two independent experiments were performed. A representative result is shown, and the values are given as the mean ± SD of six biological replicates (Student's t-test; ***p < 0.0001).

3.4.2.2. Complete lipidomic analysis

Having ruled out Chol as directly responsible for decreased PM permeability in CPT1C-silenced breast cancer cells, we decided to explore other lipids that could be also involved in the biophysical properties of the PM. Thus, in collaboration with Dr. Josefina Casas, we decided to analyze total and PM lipids by liquid chromatography–high resolution mass spectrometry (LC-HRMS). The PM-enriched cellular fraction was obtained by cellular fractionation as explained previously (Methodology Section 3.4.1.). PM enrichment was confirmed by western blot (Fig. 50). Indeed, a 2.60- and 2.81-fold change in PM marker intensity was observed in PM-enriched fractions relative to total fraction in shRandom- and shCPT1C-MDA-MB-231 samples, respectively. Additionally, PM enrichment led to a slight increase in ER (endoplasmic reticulum) markers, which could be attributed to membrane contact sites between PM and ER fractions.

Organelle marker	shRandom		shCPT1C	
	T	PM	T	PM
PM marker NaKATPase protein			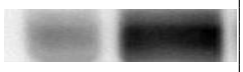	
Concentration (FC)	1.00	2.60	1.00	2.81
Other markers				
Mitochondrial marker VDAC-1 protein			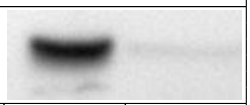	
Concentration (FC)	1.00	0.08	1.00	0.10
ER marker Calreticulin protein			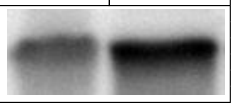	
Concentration (FC)	1.00	1.54	1.00	1.69
Cytosolic marker GAPDH protein				
Concentration (FC)	1.00	0.00	1.00	0.24

Fig. 50. PM enrichment in the isolated fractions (PM) compared with total lysate (T). Na+/K+-ATPase, VDAC1/Porin, calreticulin, and GAPDH were selected as PM, mitochondria, ER, and cytosolic protein markers, respectively. Comparing PM with T samples, plots show a clear enrichment in the PM, an almost complete removal of mitochondrial and cytosolic fractions, and a slight increase in ER fraction.

Known differences between the lipid profiles of total lysate and PM-enriched fractions were reflected in average percentages of cellular lipid species. Additionally, remarkable oscillations in lipid content were detected under CPT1C silencing in MDA-MB-231 cells (Fig. 51). The following subsections provide more details about these lipid changes.

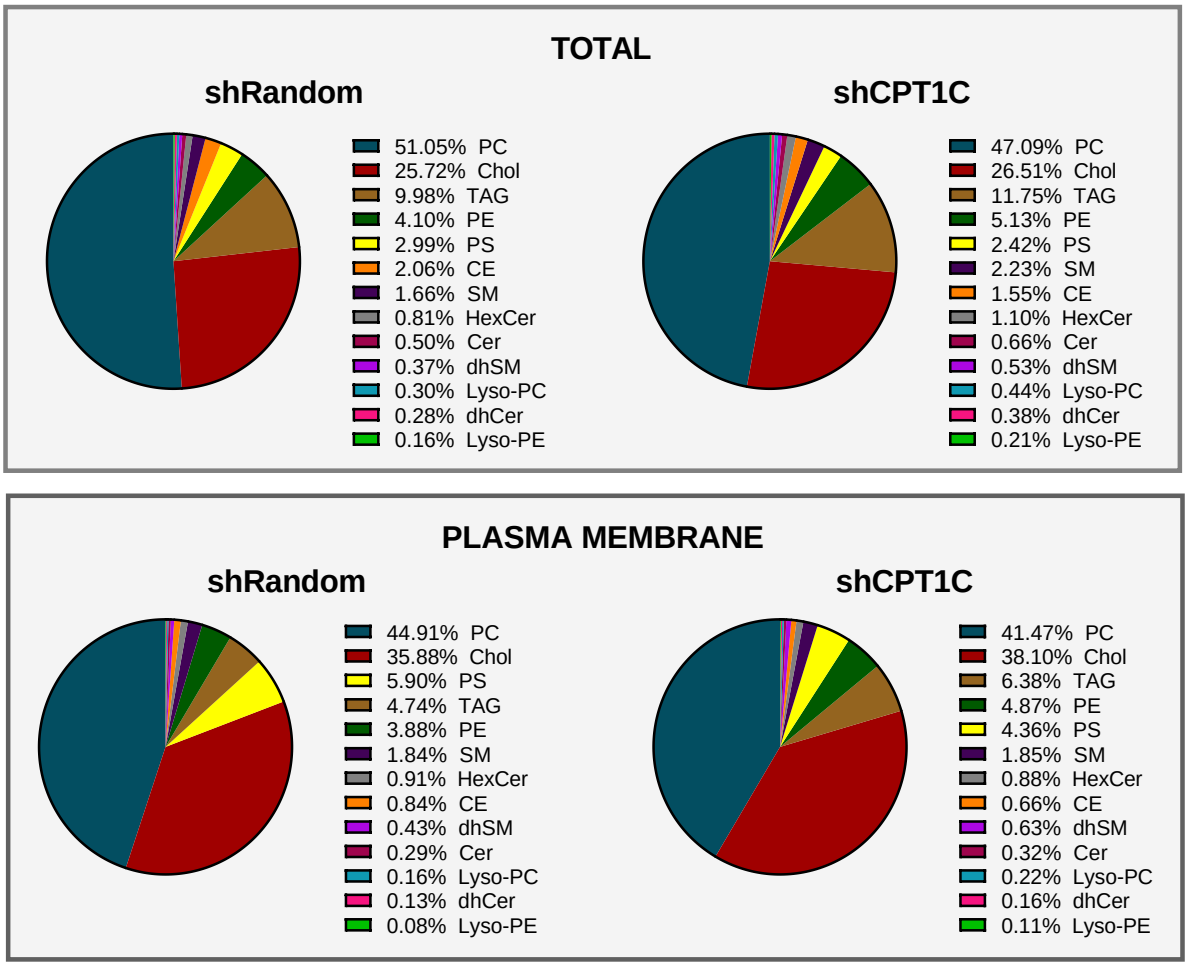

Fig. 51. Average percentages of lipid species in control and CPT1C-silenced MDA-MB-231 cells by LC-HRMS. MDA-MB-231 cells were infected with shRandom or shCPT1C-carrying lentivirus. Pie charts display the percentage distribution of the primary lipid species in total lysate (top) and PM-enriched fractions (bottom). In the right side of each chart, average percentage of each detected species is shown. PC: Phosphatidylcholine; Chol: cholesterol; TAG: Triglycerides; PE: Phosphatidylethanolamine; PS: Phosphatidylserine; CE: cholesteryl esters; SM: sphingomyelin; HexCer: hexosylceramide; Cer: ceramide; dhSM: dihydrosphingomyelin; LPC: Lysophosphatidylcholine; dhCer: dihydroceramide; LPE: Lysophosphatidylethanolamine.

3.4.2.2.1. Free-cholesterol

Next, we measured free-Chol levels in the PM and total lysate of MDA-MB-231 cells using LC-HRMS, but no changes were detected (Fig. 52).

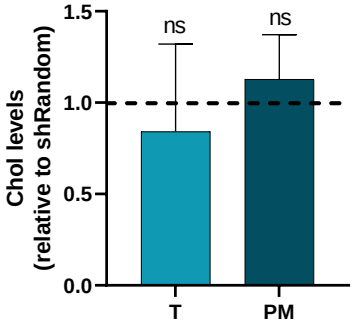

Fig. 52. Relative abundance of free-Chol in CPT1C-silenced MDA-MB-231 cells by LC-HRMS. MDA-MB-231 cells were infected with shRandom or shCPT1C-carrying lentivirus. Chol levels in CPT1C-silenced MDA-MB-231 cells normalized by shRandom. Results are shown as the mean ± SD (Wilcoxon signed-rank test; p-values were 0.7500 and 0.7500).

3.4.2.2.2. Phospholipids

3.4.2.2.2.1. Glycerophospholipids

We proceeded to analyze glycerophospholipids. Different species of glycerophospholipids were quantified by acyl chain length and the degree of saturation in total and PM-enriched fraction of MDA-MB-231 cells. We analyzed the most abundant phospholipids in all mammalian cell membranes: phosphatidylcholine (PC) and phosphatidylethanolamine (PE). We found a significant relationship between CPT1C expression and fatty acids saturation degree in PC lipid species. PCs with polyunsaturated fatty acids were decreased in CPT1C-silenced MDA-MB-231 cells. By contrast, PCs with saturated and monounsaturated fatty acids were increased in their PM-enriched fractions (Fig. 53B1). In addition, a positive correlation was found between fatty acid length and CPT1C silencing (Fig. 53C and D).

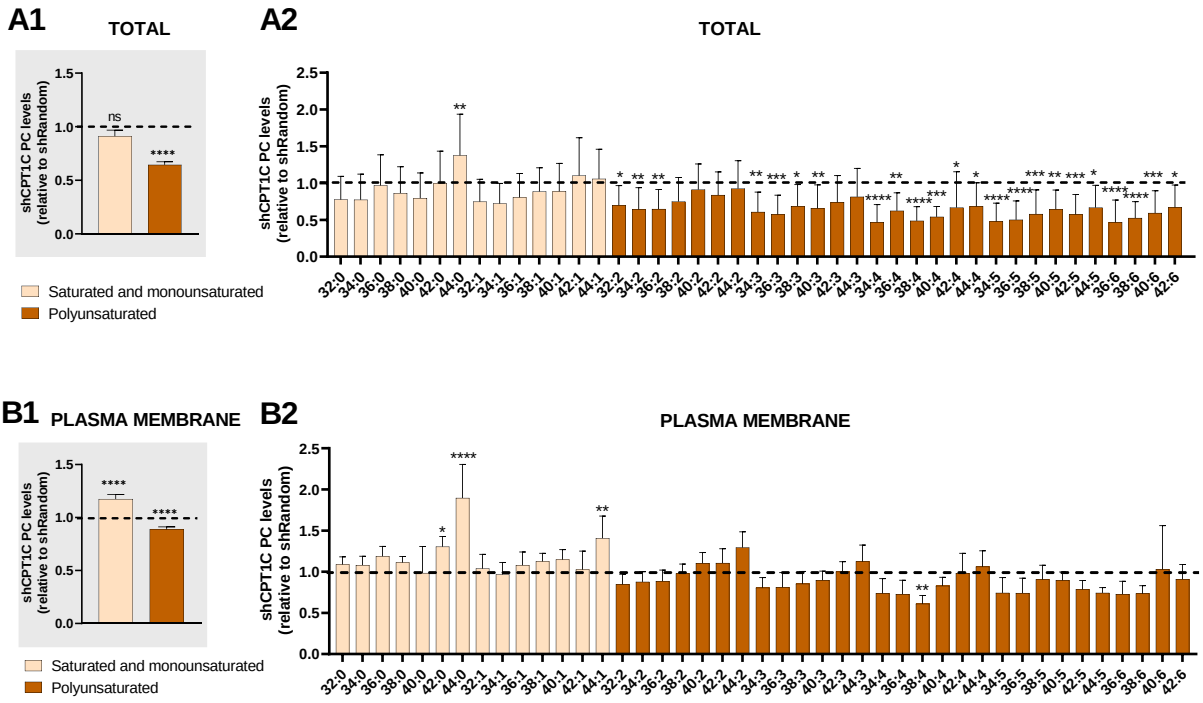

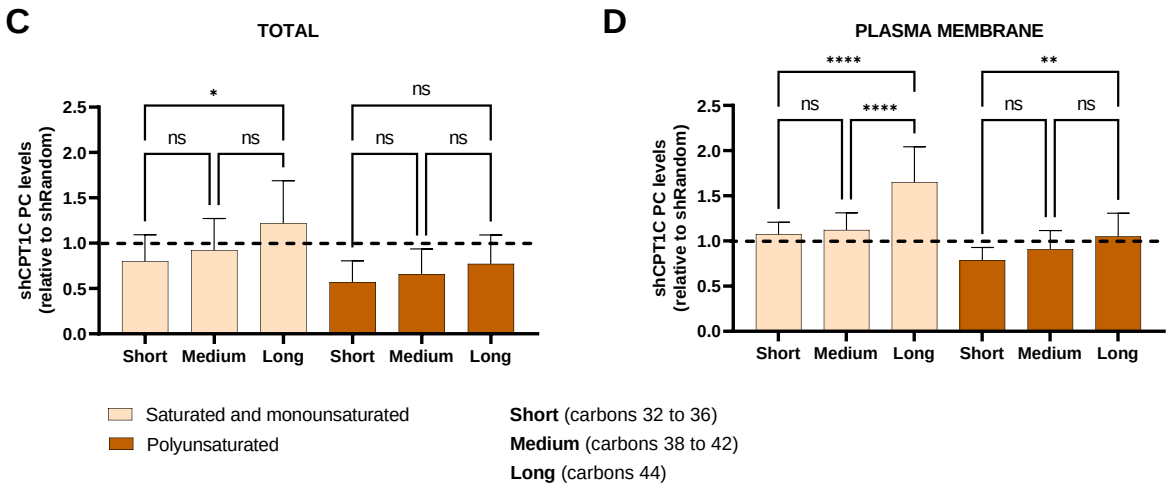

Fig. 53. Relative abundance of phosphatidylcholine (PC) molecular species in CPT1C-silenced MDA-MB-231 cells by LC-HRMS. MDA-MB-231 cells were infected with shRandom or shCPT1C-carrying lentivirus. Values from total lysate (A) and PM–enriched fraction (B) are shown. A1, B1. PC levels in CPT1C-silenced MDA-MB-231 cells normalized by shRandom. Values are grouped by fatty acid (FA) saturation degree. Results are shown as the mean ± SEM (Wilcoxon signed-rank test; p-values were 0.1662 and ****<0.0001). A2, B2. Levels of each PC molecular species in CPT1C-silenced MDA-MB-231 cells normalized by shRandom. Numbers (C:N) indicate the number of carbon atoms (C) and double bonds (N) in the fatty acid side chains of the different molecular species. Results are shown as the mean ± SD of three independent experiments (two-way ANOVA followed by Dunnett's multiple comparison test; *p<0.05, **p<0.01, ***<0.001 ****<0.0001). C, D. PC levels in CPT1C-silenced MDA-MB-231 cells normalized by shRandom. Values are grouped by fatty acid length and saturation degree from total lysate (C) and PM-enriched fractions (D). Results are shown as the mean ± SEM (Wilcoxon signed-rank test; *p < 0.05, **p < 0.01, ***<0.001 ****<0.0001).

Similar results were obtained in PE lipid species. PEs with polyunsaturated fatty acids were decreased in total fraction of CPT1C-silenced MDA-MB-231 cells. By contrast, PEs with saturated and monounsaturated fatty acids were increased in their PM-enriched fractions, compared with control cells (Fig. 54).

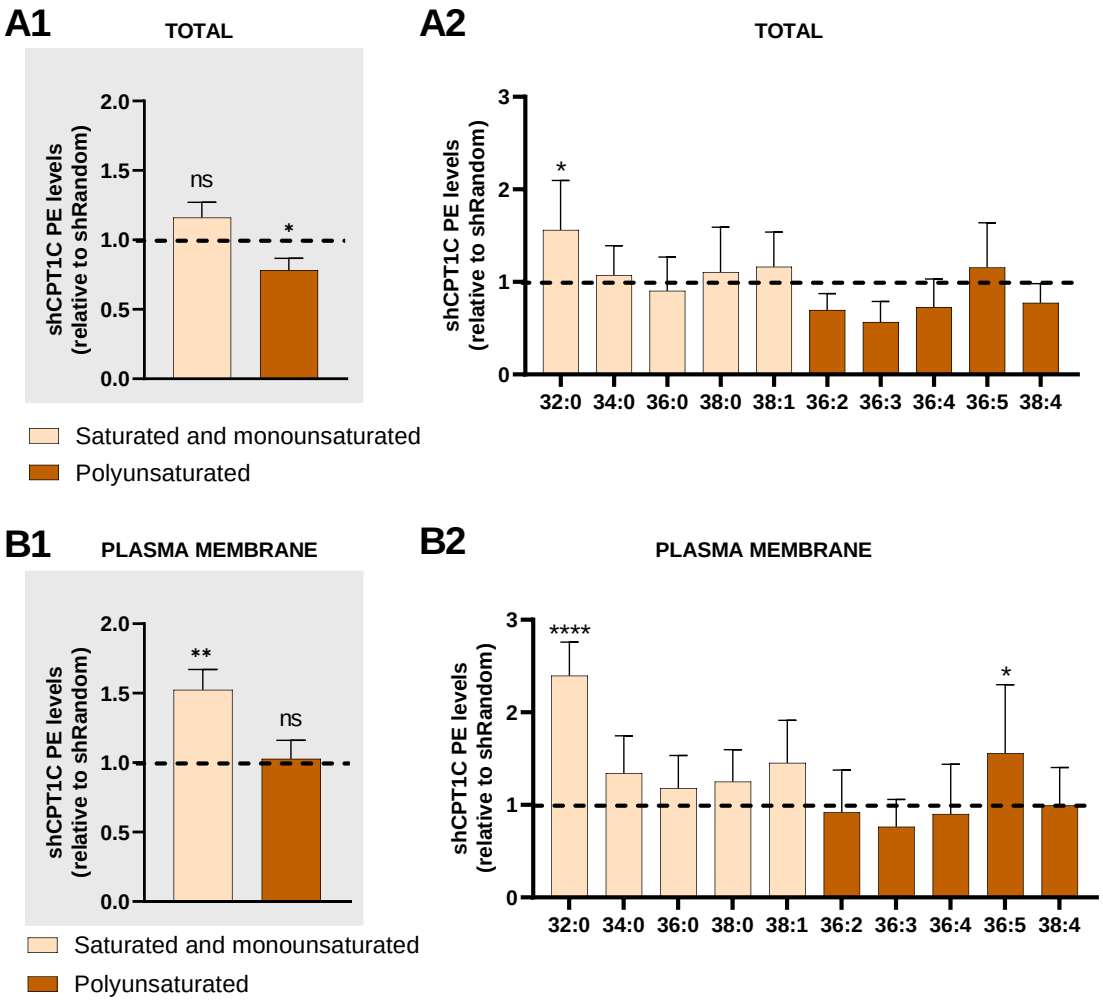

Fig. 54. Relative abundance of phosphatidylethanolamine (PE) molecular species in CPT1C-silenced MDA-MB-231 cells by LC-HRMS. MDA-MB-231 cells were infected with shRandom or shCPT1C-carrying lentivirus. Values from total lysate (A) and PM–enriched fraction (B) are shown. A1, B1. PE levels in CPT1C-silenced MDA-MB-231 cells normalized by shRandom. Values are grouped by fatty acid (FA) saturation degree. Results are shown as the mean ± SEM (Wilcoxon signed-rank test; p-values were 0.2347 and *0.0203 for total lysate and **0.0026 and 0.9019 for PM fraction). A2, B2. Levels of each PE molecular species in CPT1C-silenced MDA-MB-231 cells normalized by shRandom. Numbers (C:N) indicate the number of carbon atoms (C) and double bonds (N) in the fatty acid side chains of the different molecular species. Results are shown as the mean ± SD of three independent experiments (two-way ANOVA followed by Dunnett's multiple comparison test; *$p < 0.05$, ****$p < 0.0001$).

The saturation degree and length of glycerophospholipid acyl chains are important determinants of many membrane characteristics such as fluidity and permeability. In general, shorter length and higher unsaturation of phospholipid fatty acyl chains is associated with more fluid membranes [120]. Our results showed that PM-enriched fractions of CPT1C-silenced MDA-MB-231 cells present higher levels of saturated lipids and lower levels of polyunsaturated lipids (PCs and PEs, respectively). Moreover, in these cells, the acyl chains

of PCs are longer. Considering that PCs and PEs are by far the most abundant lipids in the PM, these results suggested that CPT1C silencing could decrease PM fluidity in MDA-MB-231 cells.

To reinforce our prior results, we calculated the PC/PE ratio. Coherently, we found that CPT1C silencing significantly decreased the PC/PE ratio in MDA-MB-231 cells, corresponding again with a less fluid membrane (Fig. 55).

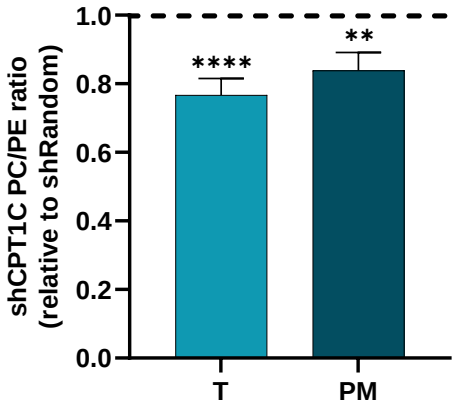

Fig. 55. PC/PE ratio in CPT1C-silenced MDA-MB-231 cells by LC-HRMS. A. Schematic representation of PC and PE structure modified from [130]. B. PC/PE ratio in CPT1C-silenced MDA-MB-231 cells normalized by shRandom. MDA-MB-231 cells were infected with shRandom or shCPT1C-carrying lentivirus. Values from total lysate and PM–enriched fractions are shown as the mean ± SEM (Wilcoxon signed-rank test; p-values were ****<0.0001 and **0.0061).

The next lipid we analyzed was phosphatidylserine (PS). Under CPT1C silencing, PS was significantly decreased independent of fatty acid saturation degree (Fig. 56). At physiological pH, PC and PE are neutral molecules that behave as zwitterions. However, PS has a net negative charge and behaves as an acid. Thus, a lower presence of PS in shCPT1C-MDA-MB-231 cells correlates with a less negative charge in the PM, and consequently, less interaction with positive-charged drugs such as DOX.

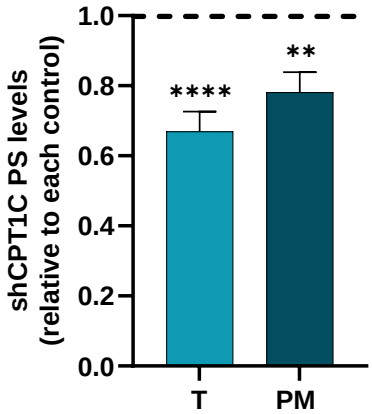

Fig. 56. Relative abundance of phosphatidylserine (PS) in CPT1C-silenced MDA-MB-231 cells by LC-HRMS. MDA-MB-231 cells were infected with shRandom or shCPT1C-carrying lentivirus. PS levels in CPT1C-MDA-MB-231 silenced cells normalized by shRandom. Values from total lysate and PM-enriched fractions are shown as the mean ± SEM (Wilcoxon signed-rank test; p-values were ****<0.0001 and **0.0014).

In each glycerophospholipid molecule, one of the two fatty acids can be hydrolyzed by phospholipase A2, resulting in lysoderivatives formation as lysophosphatidylcholines (LPCs) and lysophosphatidylethanolamines (LPEs). In cells, lysoglycerophospholipid concentration is

low compared to their corresponding phospholipids. By contrast, this concentration is high in interstitial fluids and plasma [52]. Additionally, their amphipathic characteristics allows some of them to be secreted extracellularly and act as important signaling molecules [121]. Similar to their corresponding precursors, saturated and monounsaturated lysoglycerophospholipids were increased in the PM-enriched fractions of shCPT1C-MDA-MB-231 cells, supporting a stiffening of the PM [48] (Fig. 57).

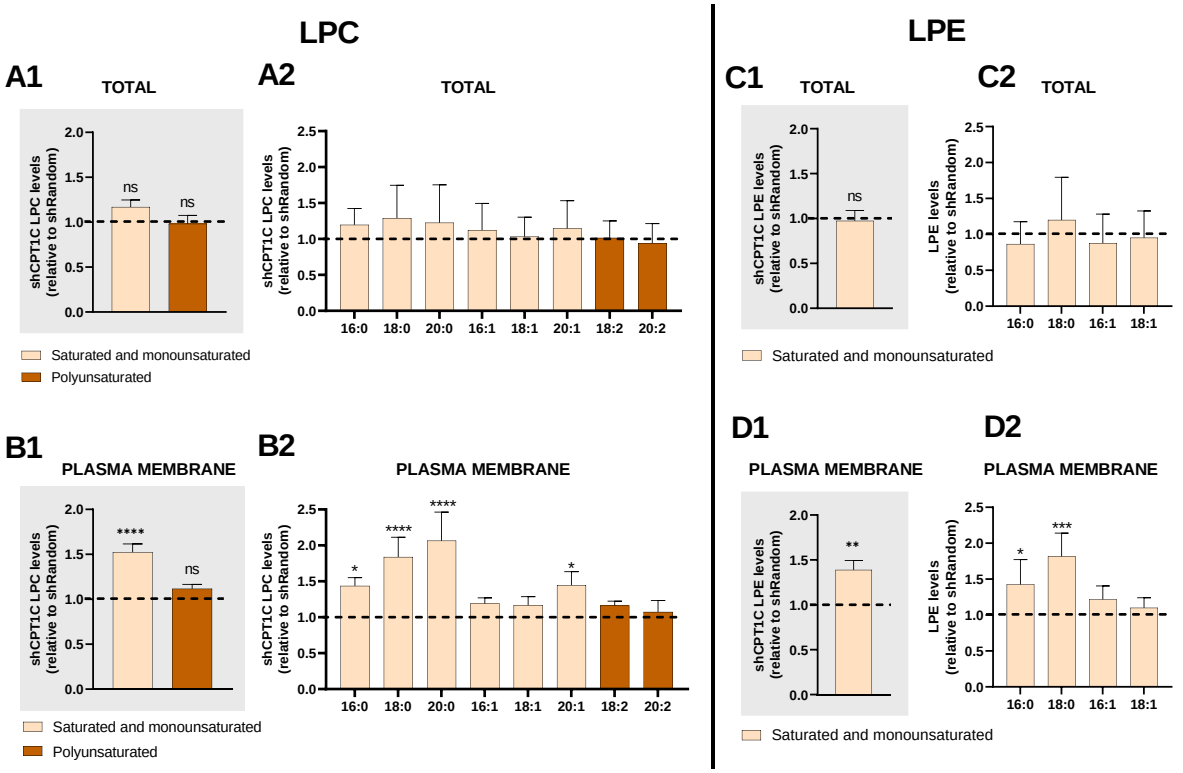

Fig. 57. Relative abundance of PC and PE lyso-derivatives molecular species in CPT1C-silenced MDA-MB-231 cells by LC-HRMS. MDA-MB-231 cells were infected with shRandom or shCPT1C-carrying lentivirus. Values from total lysate (A, C) and PM–enriched fractions (B, D) are shown. A1, B1, C1, D1. LPC (left) and lysophosphatidylethanolamines (LPE) (right) levels in CPT1C-silenced MDA-MB-231 cells normalized by shRandom. Values are grouped by fatty acid saturation degree. Results are shown as the mean ± SEM (Wilcoxon signed-rank test; LPC p-values were 0.1291 and >0.9999 for total lysate and ****<0.0001 and 0.1563 for PM fractions; LPE p-values were 0.6221 for total lysate and **0.0020 for PM fraction). A2, B2, C2, D2. Levels of each LPC (left) and LPE (right) molecular species in CPT1C-silenced MDA-MB-231 cells normalized by shRandom. Numbers (C:N) indicate the number of carbon atoms (C) and double bonds (N) in the fatty acid side chains of the different molecular species. Results are shown as the mean ± SD of three independent experiments (two-way ANOVA followed by Dunnett's multiple comparison test; *p<0.05, ***<0.001, ****<0.0001).

3.4.2.2.2.2. Sphingophospholipids or sphingolipids

The other subgroup of phospholipids that we analyzed were sphingophospholipids. Ceramide (Cer) is the basic structure of sphingolipids. It is present in smaller proportions in cell membranes, wherein they occur primarily as intermediates in the metabolism of the more

complex sphingolipids and play an important role in cell signaling [122]. Sphingomyelin (SM) is the most abundant sphingolipid and an important component of cell membranes. Additionally, the related dihydro-derivatives such as dihydroceramides (dhCer) and dihydrosphingomyelins (dhSM) are found but in lower levels in cell membranes. In these species, the double bond in the sphingosine base is reduced to a single-bond linkage. Sphingolipids could also be modified with a sugar. The most abundant in higher animals are glycosphingolipids, primarily cerebrosides and gangliosides (e.g., hexosylceramide [HexCer]). We measured lipid levels of these sphingolipids mentioned above. We found no changes in Cer and dhCer levels in CPT1C-silenced MDA-MB-231 cells compared to control cells (Fig. 58A and B). However, dhSM and HexCer species were increased in the PM under CPT1C silencing (Fig. 58D and E). Considering that dhSM forms more condensed and ordered membrane domains than SM via effective hydrogen bond formation [123], we could conclude that increased dhSM levels contributed to a more rigid PM in CPT1C-silenced MDA-MB-231 cells. Both impaired dhSMs and HexCers are lipid constituents of lipid rafts microdomains. Moreover, dhCer/Cer and dhSM/SM ratios were quantified to investigate whether CPT1C silencing could be affecting the saturation degree of sphingosine backbone. CPT1C silencing did not increased the dhCer/Cer ratio (Fig. 58F); however, an increased dhSM/SM ratio was detected in MDA-MB-231 cells (Fig. 58G). Finally, the proportion of SM and Cer was measured but remained unchanged in PM fractions (Fig. 58H).

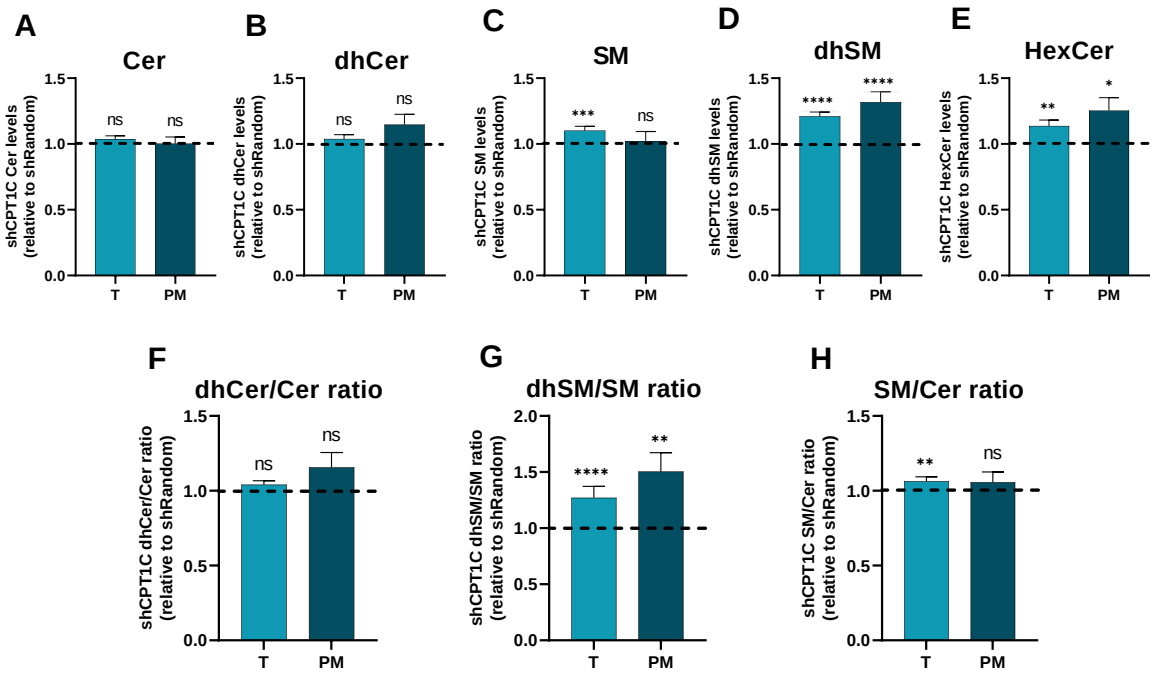

Fig. 58. Relative abundance of sphingolipid molecular species in CPT1C-silenced MDA-MB-231 cells by LC-HRMS. MDA-MB-231 cells were infected with shRandom or shCPT1C-carrying lentivirus. Top panel: Sphingolipid levels (Cer, dhCer, SM, dhSM, and HexCer) in CPT1C-silenced MDA-MB-231

cells normalized by shRandom. Values from total lysate and PM–enriched fractions are shown as the mean ± SEM (Wilcoxon signed-rank test; p-values were 0.2906 and 0.6695 for Cer; 0.4770 and 0.1109 for dhCer; ***0.0004 and 0.6933 for SM; ****<0.0001 for dhSM; **0.0029 and *0.0203 for HexCer). Bottom panel: Sphingolipid ratios (dhCer/Cer, dhSM/SM and SM/Cer) in CPT1C-silenced MDA-MB-231 cells normalized by shRandom. Values from total lysate and PM-enriched fractions are shown as the mean ± SEM (Wilcoxon signed-rank test; p-values were 0.1898 and 0.1573 for dhCer/Cer ratio; ****<0.0001 and **0.0022 for dhSM/SM ratio; and **0.0070 and 0.5147 for SM/Cer ratio). Cer: ceramide; dhCer: dihydroceramide; SM: sphingomyelin; dhSM: dihydrosphingomyelin; HexCer: hexosylceramide.

3.4.2.2.3. Lipid droplets

Lipid droplets are cytoplasmic lipid-enriched organelles delimited by a monolayer of phospholipids, which surrounds a hydrophobic core containing neutral lipids, primarily triacylglycerol (TAGs) and cholesteryl esters (CEs), with a diverse content of proteins. TAGs are formed by a glycerol joined to three fatty acids. Instead, CEs are the storage form of Chol and synthesized by acyl coenzyme A: cholesterol acyltransferase [124]. Lipidomic results demonstrated that under CPT1C silencing TAGs were increased in the PM fraction, especially those containing saturated and monounsaturated fatty acids (Fig. 59). Meanwhile, polyunsaturated CE levels were significantly reduced.

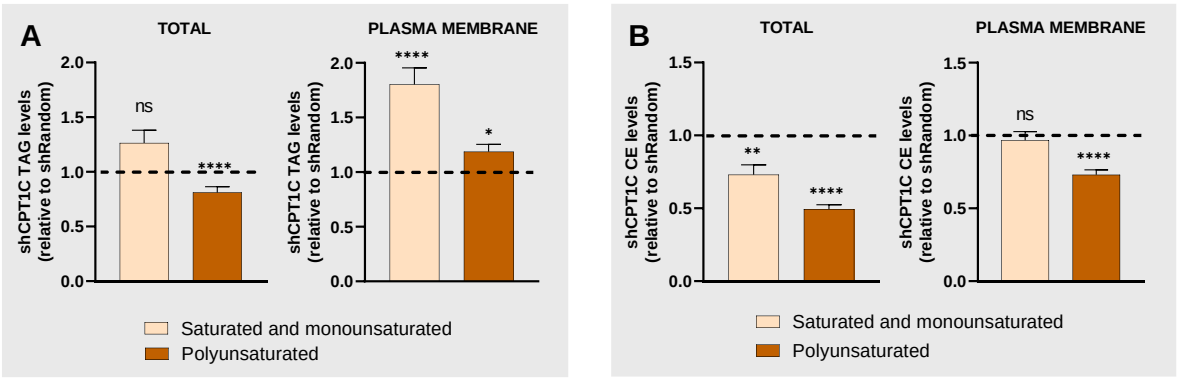

Fig. 59. Relative abundance of TAGs and CEs in CPT1C-silenced MDA-MB-231 cells by LC-HRMS. MDA-MB-231 cells were infected with shRandom or shCPT1C-carrying lentivirus. TAG (A) and CE (B) levels of total lysate and PM fractions in CPT1C-silenced MDA-MB-231 cells normalized by shRandom. Values are grouped by fatty acid saturation degree. Results are shown as the mean ± SEM (Wilcoxon signed-rank test; p-values were 0.1127 and ****<0.0001 (total), and ****<0.0001 and *0.0325 (PM) for TAG; **0.0011 and ****<0.0001 (total), 0.5154, and ****<0.0001 (PM) for CE.

4. Exploring the role of CPT1C interactors in chemoresistance

In parallel with lipidomic studies, we decided to study whether the chemoresistance effect of CPT1C silencing was occurring through the recently established CPT1C protein interactors: ABHD6 and SAC1. In fact, both proteins are phospholipid (BMP and PI4P) hydrolases that modulate cellular lipid sorting and lipid transport to the PM. For this reason, our working

hypothesis was that CPT1C silencing disturbs PM permeability to drugs through a deregulation of ABHD6 and SAC1 activity.

4.1. CPT1C is primarily located in ER

As explained before, CPT1C has been described to be an ER-integral protein in neurons and to interact with protrudin, SAC1, and ABHD6, which are ER-resident proteins. Because we wanted to study whether CPT1C was impairing PM lipid composition through its interactors, we decided to elucidate whether CPT1C was located in the ER in breast cancer cells. For this reason, we decided to overexpress human CPT1C tagged with the fluorescence protein mTurquoise2 (hCPT1C-mTurq) in MDA-MB-231 cells. ER was stained with anti-calnexin and mitochondria with Mitotracker. ER-mitochondria contact sites (also known as mitochondria-associated membranes) were identified by colocalization of calnexin with Mitotracker. Our results showed that CPT1C is primarily located in the ER of these cells but also exists in a small proportion in the mitochondria (Fig. 60). The fact that CPT1C is present in ER-mitochondria contact sites with the same percentage as in mitochondria suggested that CPT1C is located on the ER side of these contacts.

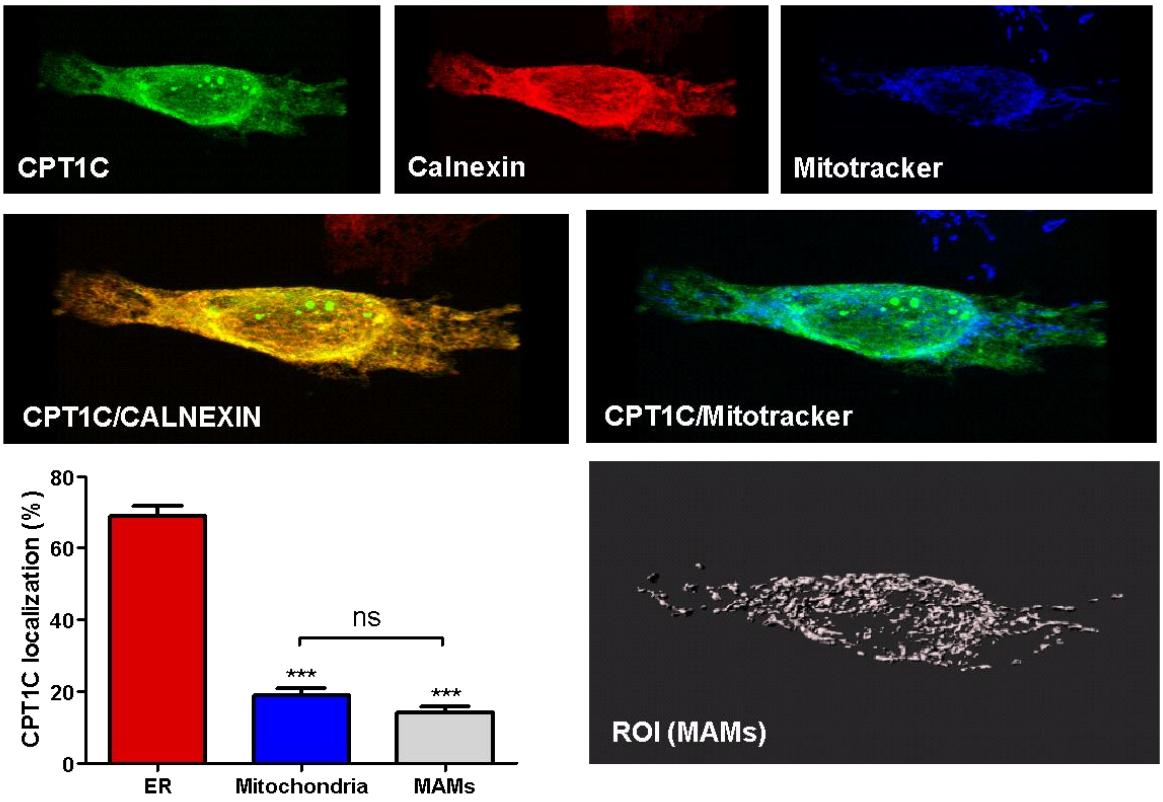

Fig. 60. CPT1C is localized in the ER and mitochondria-associated membranes (MAMs). MDA-MB-231 cells were transfected with lipofectamine to drive the expression of human CPT1C tagged by mTurquoise2 (hCPT1C-mTurq). Mitotracker Orange was used to stain mitochondria while calnexin (an ER marker) was detected by immunocytochemistry. The graph shows the percentage of CPT1C inside the ER, in the mitochondria, or on the surface of MAMs (region of interest, ROI) defined by the colocalization of the ER with the mitochondria. Values of a representative experiment are expressed as the mean ± SEM (16 randomly selected cells per coverslips were analyzed, one-way ANOVA followed by Dunn's multiple comparison test; scale bar 10 μm. ***$p < 0.0001$).

4.2. The involvement of ABHD6 in drug uptake and resistance

CPT1C has the ability to modulate ABHD6 hydrolase activity depending on the energy status of the cell. Interestingly, ABHD6 has been related to tumor and metastatic features. Moreover, ABHD6 has been demonstrated to regulate the sensitivity to chemotherapy drugs in vitro through control of BMP levels, a glycerophospholipid present in small amounts in most tissues and highly enriched in the ILVs of LEs.

We examined whether ABHD6 expression could affect the changes in breast cancer RFS caused by CPT1C expression. For this aim, we stratified patients with breast cancer by ABHD6 median expression, distinguishing between low and high ABHD6-expressing breast tumors. In both groups, we analyzed the role of CPT1C in breast cancer RFS (Fig. 61A). Our results suggest that in breast cancer tumors the expression of ABHD6 does not affect the role of CPT1C in RFS.

Nevertheless, because CPT1C has been demonstrated as an inhibitor of ABHD6 activity [9], we expected that CPT1C silencing would increase ABHD6 activity. To confirm this, we measured the ability of ABHD6 to hydrolyze the 4-methylumbelliferyl-heptanoate substrate through a high sensitive fluorescent hydrolase activity assay comparing control and CPT1C-silenced MDA-MB-231 cells. Because cells can contain other hydrolases for 4-methylumbelliferyl-heptanoate, ABHD6 specific activity was verified by its selective inhibitor WWL70. Our results showed that ABHD6 activity is increased in CPT1C-silenced MDA-MB-231 cells compared with the control ones, as expected (Fig. 61B).

Next, we aimed to see whether the more activated status of ABHD6 in shCPT1C-MDA-MB-231 cells was partly responsible for the higher chemoresistance in these cells. For this purpose, first, we checked whether ABHD6 could modulate DOX uptake. We treated wild-type MDA-MB-231 cells with different concentrations of KT182, another specific inhibitor of ABHD6 hydrolase more suitable for cell culture, and measured DOX uptake by flow cytometry (Fig. 61C). Effectively, we could confirm an ABHD6 role in DOX uptake. At increasing doses of the ABHD6 inhibitor, DOX uptake was enhanced, suggesting that DOX resistance in CPT1C-silenced cells could be mediated by increased ABHD6 activity.

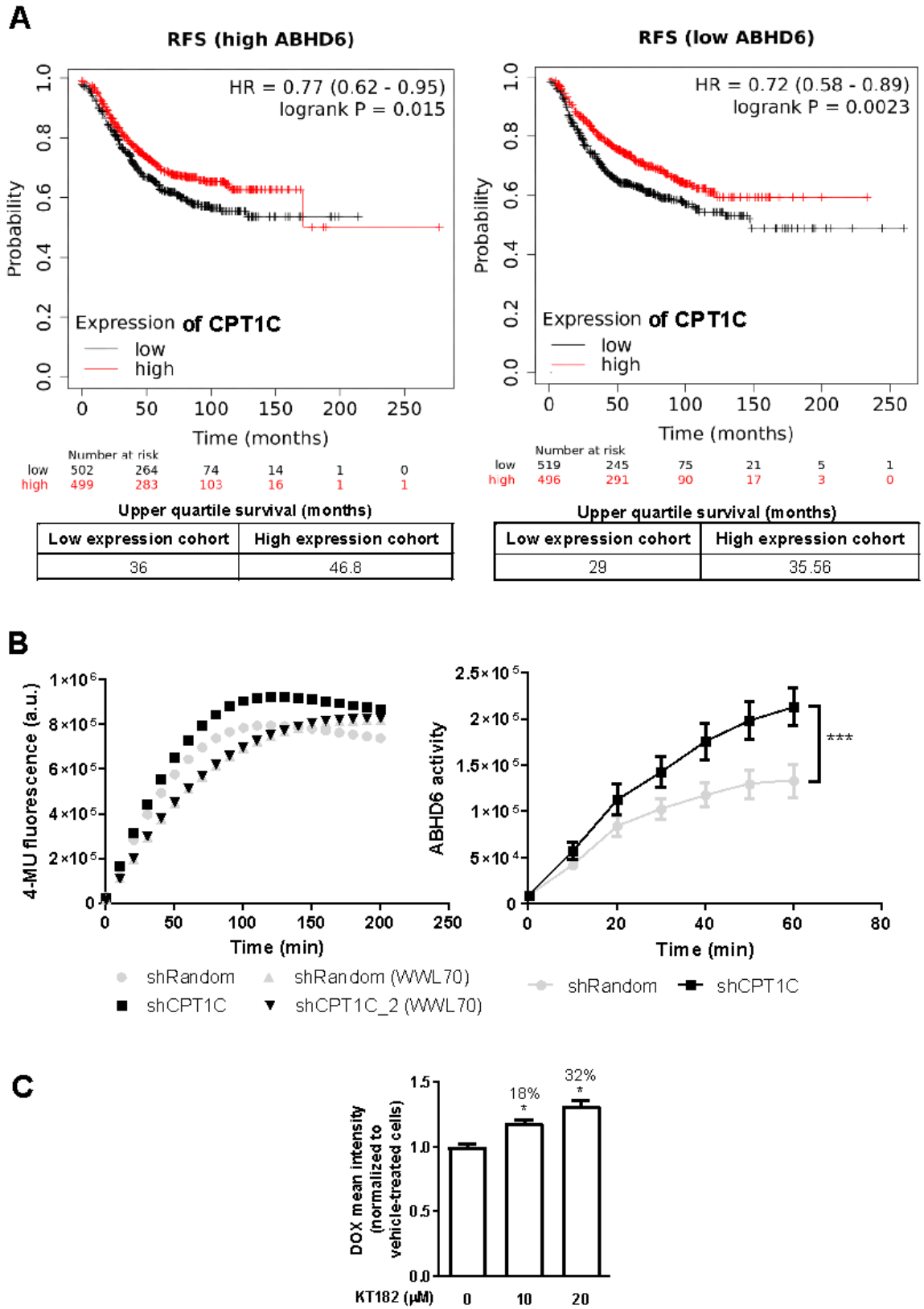

Fig. 61. ABHD6 depletion increases DOX uptake. A. RFS rate for patients with breast cancer with low or high CPT1C gene expression analyzed with Kaplan-Meier Plotter. Log-rank p-value and hazard ratio (HR; 95% confidence interval in parentheses) are shown. Patients with breast cancer were stratified by median expression of ABHD6 in tumors, distinguishing between high (left) and low (right)

ABHD6-expressing tumors. The corresponding Affymetrix IDs for CPT1C and ABHD6 is 227468_at and 221552_at, respectively. Upper quartile survival rates (months) for the low and high ABHD6 expression groups are shown. ABHD6 is not involved in DOX resistance mediated by CPT1C. B. MDA-MB-231 cells were infected with shRandom or shCPT1C-carrying lentivirus. ABHD6 activity assay was studied by measurement of 4-methylumbelliferylheptanoate (MUH) consumption, a substrate for this enzyme. A total of 4 µg protein for samples was needed. Cell lysates were treated with or without WWL70 (ABHD6 inhibitor) for 30 min, and consecutively, MUH was added as a substrate. Fluorescence increase was read every 10 min for at least 60 min total at 37ºC. Absorbance was represented as an exponential curve of absorbance along time, and the slopes were compared. Left panel: Total hydrolase activity with or without ABHD6 inhibition. Right panel: ABHD6 activity is shown, and data were analyzed subtracting the absorbance of WWL70-incubated wells to the absorbance of DMSO-incubated wells. Two independent experiments were performed. A representative result is shown, and the values are given as the mean ± SD of biological duplicates (analysis of covariance for slopes comparation; ***$p < 0.001$). C. DOX uptake was detected by flow cytometry after treating MDA-MB-231 cells with or without KT182 (ABHD6 inhibitor). Two independent experiments were performed. Results are shown as the mean ± SD of experiments performed with four biological replicates; Mann-Whitney test was applied comparing pairs of columns; *$p<0.05$.

To study whether ABHD6 increased activity was mediating CPT1C silencing in in vitro chemoresistance, we repeated the DOX uptake experiment comparing shCPT1C and control MDA-MB-231 cells at increasing doses of KT182 (an inhibitor of ABDH6). We expected to see KT182 treatment reverse the drug resistance mediated by CPT1C silencing. However, KT182 treatment did not produce a significantly higher increase in DOX uptake in CPT1C silenced cells compared to control cells (Fig. 62A). Coherently, KT182 treatment did not sensitize shCPT1C-MDA-MB-231 cells to DOX compared to control cells in the MTT survival assay (Fig. 62B), but even a contrary effect was seen. So, we could conclude that ABHD6 is involved in DOX uptake and anthracycline resistance in breast cancer cells, but it is not responsible for the chemoresistant effect of CPT1C silencing.

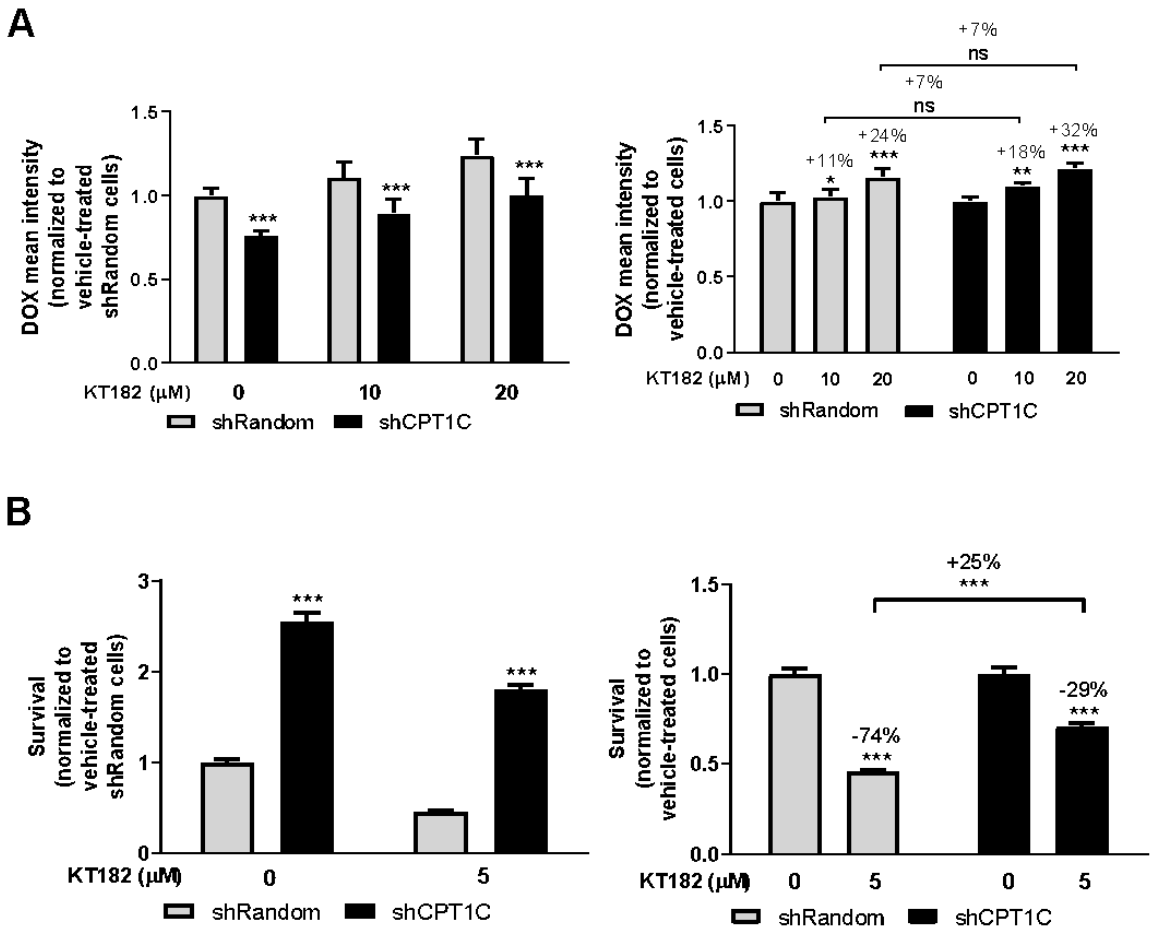

Fig. 62. ABHD6 activity is not involved in CPT1C-dependent chemoresistance. MDA-MB-231 cells were infected with shRandom or shCPT1C-carrying lentivirus. A. Doxorubicin (DOX) uptake was detected by flow cytometry after treating cells with or without KT182 (ABHD6 inhibitor). Two independent experiments were performed. Results are shown as the mean ± SD of experiments performed with four biological replicates. Two-way ANOVA followed by Bonferroni's multiple comparison test was applied; *p < 0.05, ***p < 0.01, ***p < 0.001. B. MTT assay was used to evaluate the effect of KT182 in DOX sensitivity. Cells were pretreated with 5 μM KT182 for 24 h and then cotreated with 1 μM DOX and 5 μM KT182 for 24 h more. Results are represented as the mean ± SD (n = 4 per condition, two-way ANOVA followed by Bonferroni's multiple comparison test; ***p < 0.001).

4.3. SAC1 mediates drug resistance but independently of CPT1C

Having confirmed that CPT1C-silencing DOX resistance in MDA-MB-231 cells was not mediated by ABHD6 protein, we investigated if SAC-1 was playing a role in the related lipid membrane dynamics. This phosphatase is an ER-integral membrane protein that dephosphorylates PI4P to PI and controls Chol and phospholipid pools across different organelle membranes. It is crucial for vesicular transport-both secretion and endocytosis. Casas et al. proved that CPT1C is an inhibitor of SAC-1 activity.

First, we checked how SAC-1 expression could affect the changes in breast cancer RFS caused by CPT1C expression. For this aim, we stratified patients with breast cancer by median SAC-1 expression, distinguishing between low and high SAC1-expressing breast tumors. In both groups, we analyzed the role of CPT1C in breast cancer RFS (Fig. 63A). Low CPT1C expression levels was shown to be related to worse RFS only in the tumors where SAC1 was highly expressed. This suggests that the effect of CPT1C in breast cancer RFS is dependent on SAC-1 presence.

The next step was to confirm that CPT1C is an inhibitor of SAC1 in MDA-MB-231 cells. For this purpose, we measured total cellular levels of PI4P (SAC1 substrate) in our model. Contrary to what we expected, CPT1C-silenced MDA-MB-231 cells presented increased PI4P levels compared with the control cells, indicating a more inactivated status of SAC1 (Fig. 63B).

Then, we studied the role of SAC-1 in MDA-MB-231 cell viability under chemotherapy treatment. We infected MDA-MB-231 cells with shSAC-1 lentivirus and confirmed protein inhibition by western blot. We treated cells with DOX at the indicated times and doses and measured cell survival. Our results clearly show an increased chemosensitization to DOX in SAC-1-depleted cells (Fig. 63C). At this point, we ruled out that the chemoresistance of CPT1C-silenced cells was dependent on SAC1 activity.

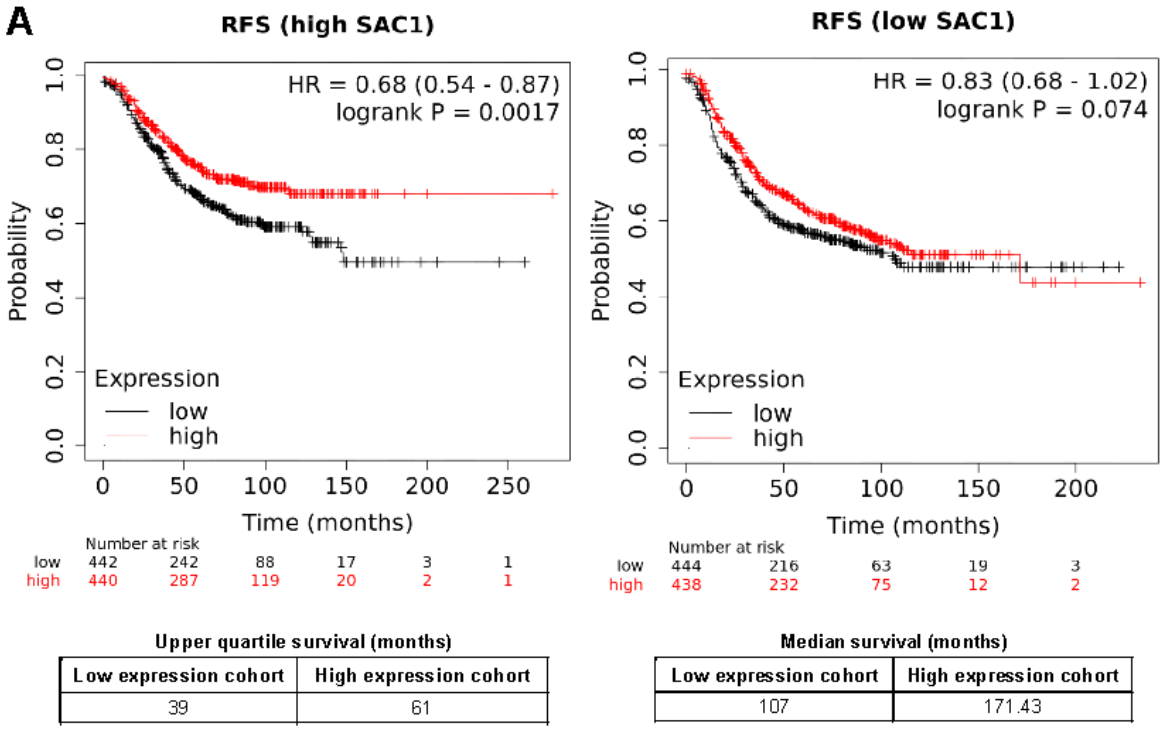

Upper quartile survival (months)

Low expression cohort	High expression cohort
39	61

Median survival (months)

Low expression cohort	High expression cohort
107	171.43

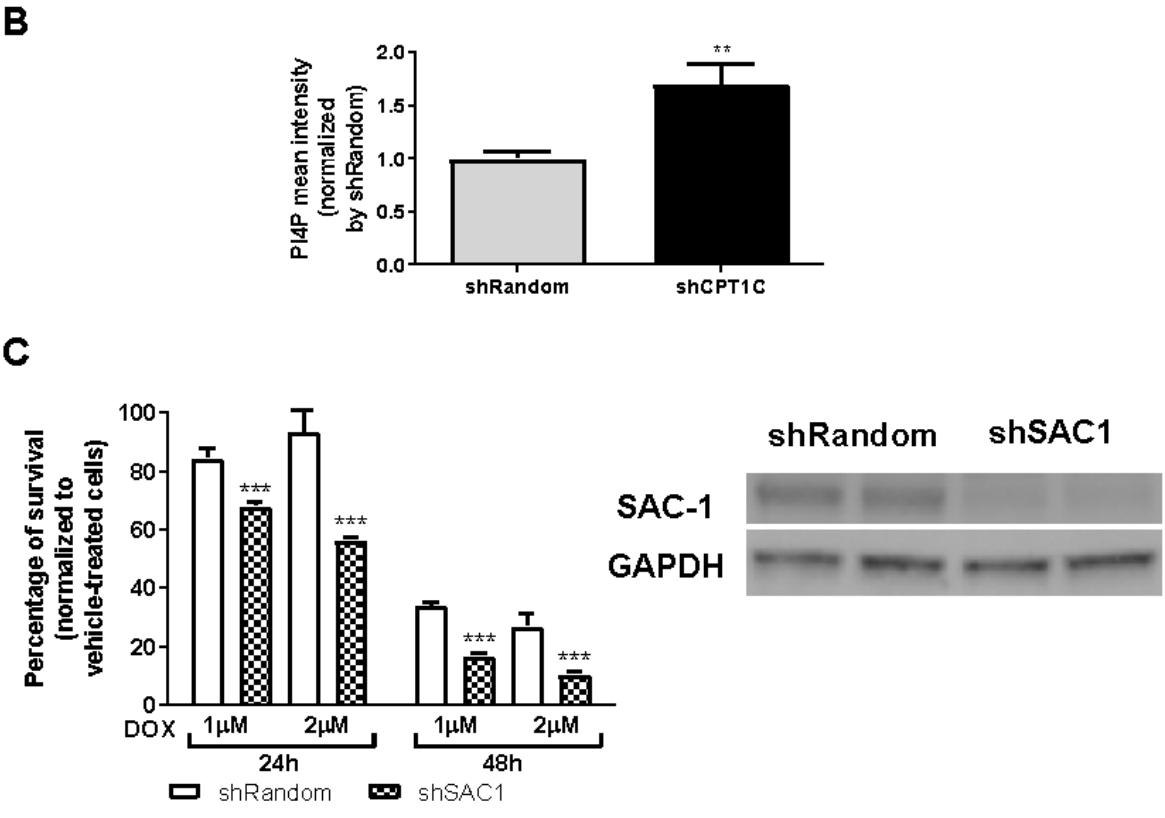

Fig. 63. SAC-1 depletion increases DOX sensitivity. A. Relapse-free survival (RFS) rate for patients with breast cancer with low or high CPT1C gene expression analyzed with Kaplan-Meier Plotter. Log-rank p-value and hazard ratio (HR; 95% confidence interval in parentheses) are shown. Patients with breast cancer were previously stratified by median expression of SAC-1 in tumors, distinguishing between high (left) and low (right) SAC-1-expressing tumors. The corresponding Affymetrix IDs for

CPT1C and SAC-1 are 227468_at and 202797_at, respectively. Upper quartile and median survival rates (months) for the low and high SAC1 expression groups are shown. Other figures: MDA-MB-231 cells were infected with shRandom or shCPT1C or shSAC1-carrying lentivirus. B. Total PI(4)P was measured by confocal microscopy. Cells were transfected with the P4M probe, then fixed and imaged. Two independent experiments were performed. A representative result is shown, and the values are given as the mean ± SEM of four biological replicates (Mann-Whitney test; $p = 0.1267$). C. SAC1 silencing was confirmed by western blot. GAPDH was used as a loading control. The MTT assay was used to evaluate the chemosensitivity of cells to DOX after 24 h of treatment at the indicated doses. Results are represented as the mean ± SD (n = 4 per condition; A: two-way ANOVA followed by Bonferroni's multiple comparison test; ***$p < 0.001$; B: Mann-Whitney test; *$p = 0.0294$).

In summary, these results demonstrate that CPT1C silencing promotes chemoresistance in breast cancer cells by increasing PM rigidity and drug impermeability. This is a consequence of a PM lipid remodeling that is principally characterized by an enhancement in the saturation degree and length of the fatty acids that constitute phospholipids. However, the molecular mechanism underlying this lipid membrane restructuring does not occur through the CPT1C protein interactors, ABHD6 and SAC1.

DISCUSSION

DISCUSSION

In the last few years, metabolic reprogramming has come to be considered a major hallmark in malignancy. Cancer cells adapt their metabolism to support early stages, as well as tumor development, including survival in harsh conditions, invasion, metastasis, chemoresistance and recurrence. Over the past 10 years, an array of publications have demonstrated how CPT1C provides cancer cells the ability to resist stressful conditions such as hypoxia and glucose deprivation [38,40]. This acquired competency has been attributed to increased fatty acid oxidation (FAO), theoretically due to its carnitine palmitoyl transferase activity [38,40,41]. Nevertheless, the exact mechanism by which CPT1C may exert this function is unknown.

CPT1C in cancer cells has usually been studied in tumorigenesis. The involvement of CPT1C in lipid metabolism elicited our interest to study its role in breast cancer because this tumor type develops in a lipid enriched environment. Based on previous findings we focused on the role of CPT1C in different tumor processes including proliferation, migration, invasion, and drug resistance in breast cancer.

CPT1C and cancer cell proliferation

First, we conducted proliferation studies because these have been frequently explored in the published literature. Using cell proliferation assays, we demonstrated that CPT1C silencing increases proliferation in different breast cancer cell lines such as MDA-MB-231, BT-474, and MDA-MB-468. However, the opposite effect was observed in MCF7 cells. Interestingly, across the four cell lines, only MCF7 expresses the wild-type form of TP53 gene. The other three cell lines harbor TP53 mutations. Most of these TP53 mutations in cancers are missense mutations, which produce the full-length mutant p53 protein with only single-amino acid substitutions. In addition to losing wild-type tumor-suppressive function, many mutated p53 proteins (as those present in MDA-MB-231, MDA-MB-468, and BT-474 cells) [125] acquire gain of function with new oncogenic activities to promote cancer progression. Mutant TP53 gain-of-function activities include promoting cell growth kinetics, metastasis, metabolic reprogramming, and resistance to therapy in cancer [126]. In terms of proliferation, wild-type p53 plays a critical role in the suppression of cancer cell growth through different mechanisms, such as cell cycle arrest, senescence, and apoptosis. By contrast, gain-of-function mutant p53 promotes cancer cell proliferation. Similar opposite effects have been found regarding cell invasion and chemoresistance. This contradictory effect has been related to AMPK activation

(Fig. 64). Once activated, AMPK stimulates catabolism while inhibiting anabolism. AMPK achieves these effects by targeting many downstream metabolic enzymes such as acetyl-CoA carboxylase. The activation of wild-type p53 by AMPK signaling is believed to suppress cell growth under conditions of metabolic stress. Moreover, once activated, wild-type p53 can, in turn, increase AMPK activity through transcriptional activation of the gene, providing a positive feedback effect. By contrast, gain-of-function p53 mutants directly inhibit AMPK activation, which increases anabolic growth and contributes to gain-of-function properties of p53 mutants [127]. As CPT1C has been located downstream of p53 and AMPK signaling, TP53 mutation status could be the explanation of the opposite effect in the proliferation of CPT1C silencing in different breast cancer cell lines.

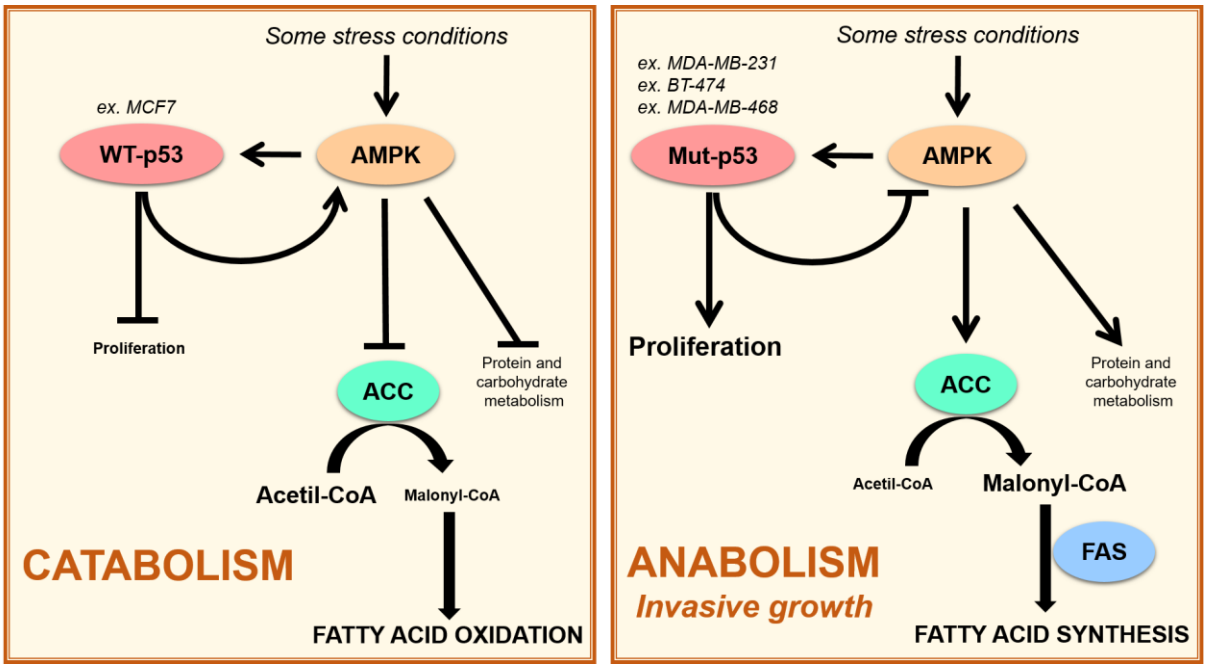

Fig. 64. Schematic representation of AMPK pathway signaling according to TP53 mutation status in cancer cells. ACC: acetyl-CoA carboxylase; FAS: fatty acid synthase (extracted from [125],[126]).

An orthotopic mammary xenograft of MDA-MB-231 was designed to study the effect of CPT1C silencing on proliferation in vivo (data not shown). Unfortunately, results obtained were inconclusive. Tumor samples were processed after the in vivo experiment. CPT1C-silenced tumors presented a reduction in the protein silencing respect the original cells. The lessening of silencing and the contribution of stromal effects could explain the proliferative phenotype that we obtained. It would be desirable to repeat the experiment but depleting CPT1C expression by CRISPR to obtain a better and long-term silencing.

Despite commonly being associated with increased proliferation in gastric, thyroid, colon, lung, pancreatic, and even breast cancer cells, CPT1C overexpression has been often assessed under metabolic stress conditions, such as hypoxia and glucose deprivation [38,40]. However, this pro-proliferative effect of CPT1C is also exhibited in normal conditions [34,37,42,43,46, 53,128]. Given the discrepancy between our results and those published by Huichang Bi's group indicating that CPT1C silencing decreases cell proliferation, we contrasted our results with databases from high-throughput screenings, such as those present in the DepMap portal. In agreement with our experimental results, Sanger database showed a pro-proliferative effect of CPT1C knock-out in MDA-MB-231 and MDA-MB-468 cells. CERES score, which is the parameter used in this portal, is generally considered relevant beyond 0.4. In our particular case, the corresponding CERES scores for CPT1C are primarily approximately 0.3 in breast cancer cells. Taken together, we concluded that the role of CPT1C in breast cancer cell proliferation in normal conditions is small or negligible. Again, this could explain the absence of an effect in the in vivo experiment, harboring the large deviations.

Regarding the mechanism of action, published data linked CPT1C-mediated enhanced proliferation to increased FAO [38,40,41]. CPT1C belongs to the carnitine palmitoyl transferase proteins, a family of enzymes that are widely known (especially CPT1A) for their presence in mitochondria, where they enter long-chain fatty acids to be further oxidized as an energy source. However, CPT1C was reported to not maintain this carnitine palmitoyl transferase activity [1]. Moreover, CPT1C mostly resides in the ER in both brain and mesenchymal stem cells [101,102]. In the field of cancer, studies assumed that CPT1C is a mitochondrial protein that directly mediates fatty acid entering to the organelle and, thus, FAO. For this reason, we confirmed CPT1C location in the ER rather than mitochondria in MDA-MB-231 cells. Colocalization studies demonstrated that CPT1C is primarily located in the ER, but it was also present in ER-mitochondria contact sites, where it could indirectly mediate FAO. The question that arises from these results is how CPT1C depletion could decrease FAO in MDA-MB-231 cells, as proved in this thesis in line with published results. Two hypotheses are contemplated. On the one hand, preliminary homoFRET results suggest a direct interaction between CPT1C and CPT1A, which could explain FAO changes under the modulation of CPT1C expression. On the other hand, the explanation might rely on the retained ability of CPT1C to bind malonyl-CoA, as other CPT isoforms do. This second explanation appears to be more likely. A decrease in CPT1C protein levels due to silencing might raise the availability of malonyl-CoA, which would bind and inhibit CPT1A and cause a decrease in FAO.

Concerning metabolic stress resistance, it was surprising that CPT1C silencing did not impair cell viability under glucose and serum starving, due to decreased FAO. Possibly, in these

conditions, cancer cells would be using alternative energy sources, such as glutamine. In fact, glutaminolysis plays a central role especially in TNBC cell lines, like MDA-MB-231 [129].

CPT1C and cancer cell invasion

Metabolic reprogramming is required in tumor progression processes, such as invasion, metastases, and resistance to treatments. This thesis has suggested CPT1C involvement in cell invasion. A previous study reported that CPT1C silencing increases the expression of metalloproteases (MMPs; MMP-1, MMP-3, and MMP-10) in lung MRC-5 cell lines [128]. In the report, Chen P. et al. linked this increase with senescence. However, metalloproteases are considered major players of cell invasion. Indeed, exosomes secreted by MDA-MB-231 cells are found highly enriched in MMPs [130].

Moreover, lipid rafts play a key role in cell invasion. Lipid rafts are liquid-ordered PM subdomains that primarily contain Chol, SM, gangliosides (e.g. HexCer), and saturated phospholipids [131]. Alterations in raft structure can change the activity of membrane-signaling proteins, such as CD44 which serves as a platform for MMPs and thus promotes tumor invasion [132]. Despite not directly measuring lipid rafts content, we found impaired PM lipid composition in MDA-MB-231 cells under CPT1C silencing (high levels of saturated phospholipids, dhSM, and HexCer), suggesting a disruption of these subdomains.

Also related to cell invasion, Tang et al. demonstrated that ABHD6 silencing suppresses lung cancer cell invasion [29]. They do not describe the mechanism (it may be related to the exosomes derived from the BMP-enriched ILV), but these data would match the increased cell invasion that we observed in CPT1C-depleted MDA-MB-231 cells, wherein ABHD6 was more active.

CPT1C and chemoresistance in breast cancer cells

Our findings also relate CPT1C with chemotherapy resistance, probably one of the greatest challenges in current breast cancer treatment. We showed evidences of how CPT1C depletion produces resistance to chemotherapy drugs such as DOX and paclitaxel, both commonly used in clinical practice, in several breast cancer cell lines. We found that this drug chemoresistance was a consequence of disrupted drug uptake. Our interest in deepening the understanding of the mechanisms by which chemotherapy drugs enter cancer cells brought us to draft a revision on this topic, which is already published and summarized in the Introduction. We confirmed that CPT1C participates in passive diffusion.

Passive diffusion is impaired mostly through modifications in lipid composition of the PM. The decrease in chemotherapy drug uptake by passive diffusion is generally attributed to Chol increase in the PM. However, in shCPT1C-silenced MDA-MB-231 cells, we showed that Chol is not responsible for these alterations. In fact, the specific PM Chol probe mCherry-D4 even detected a decrease in this lipid in CPT1C-silenced cells. However, lipidomic results allowed us to conclude that PM free-Chol remained unchanged. The Chol decrease observed with the probe was probably due to the reduced CEs levels (also present in the PM, although to a much lesser extent), because mCherry-D4 probe is not able to distinguish between CEs and free-Chol [133]. Results from this thesis suggests that the composition of other PM lipids, different from Chol, could be determinant for PM rigidity/permeability. Thus, they could regulate drug transport through passive diffusion, which agrees with previous reports describing that phospholipids are able to modulate PM fluidity, independent of Chol [50].

DOX and paclitaxel establish hydrophobic (involving lipids that modulate membrane fluidity) and electrostatic interactions (involving charged lipids) with the PM. PM fluidity is particularly influenced by the saturation degree, length, and polar head size of phospholipids, as well as by Chol and SM content.

Lipidomic results suggest that increased rigidity in CPT1C-silenced MDA-MB-231 cells is due to an increased saturation degree and length of fatty acids. This was especially noticeable in PC species, which constitute almost 45% of all PM lipids. Moreover, the decreased PC/PE ratio contributes to this rigidity. Given that the synthetic pathways of PC, PE, and PS are so interrelated, changes in one of these phospholipids give rise to alterations in the others.

Another question that arises is how we could explain these changes in fatty acid saturation degree. First, it could be attributed to decreased FAO seen in our model. Mitochondria oxidize primarily saturated and monounsaturated fatty acids, and among them importantly, palmitate. For this reason, under CPT1C silencing, a reduced FAO activity might partially explain the rise in saturated and monounsaturated species. Furthermore, because palmitate is the precursor for sphingolipids synthesis, a higher availability of this molecule would explain the general increase in sphingolipids observed when CPT1C is depleted. Second, polyunsaturated fatty acids are more unstable and easily oxidized. In the literature, it is well known that in cancer cells including MDA-MB-231 CPT1C silencing provokes an increase in ROS [41,53]. In addition, it was demonstrated that in KO-CPT1C brain, oxidized glutathione levels are duplicated [134]. Furthermore, under CPT1C silencing, a rise in oxidized fatty acids was detected MDA-MB-231 cells [53]. Therefore, we could expect a higher rate of oxidation and faster degradation of polyunsaturated fatty acids in our model, leading to an increase in the percentage of saturated phospholipids. Finally, these changes in lipid saturation degree could derive from an

impairment in the catalytic activity of desaturases. These enzymes, which introduce double bonds to fatty acids, are located in the ER, and some, concretely in mitochondria-associated membranes. The significant elevation of the dhSM/SM ratio and the same tendency in the dhCer/Cer ratio under CPT1C silencing points to a possible disruption in the desaturase activity of the sphingosine backbone. The same applies to glycerophospholipids, as the saturation degree of acyls is much greater in CPT1C-deficient cells. Enzymes that catalyze this reaction are varied and act as complexes. Thus, CPT1C depletion could be negatively modulating this desaturase activity and, thus, the saturation of fatty acids in general.

This modified saturation is evident even in triglyceride composition. Triglycerides together with CEs constitute lipid droplets that are lipid storage organelles used later for membrane synthesis and energy production. In CPT1C-silenced MDA-MB-231 cells, we found an enhanced saturation degree of the fatty acids that form triglycerides, reflecting the higher saturation of PM phospholipids.

Regarding drug-PM electrostatic interactions, the ionization degree of drugs and their partition coefficient (access) to membranes is determined by the pH of the medium and the drug's pKa. DOX (pKa~7.2-8.2) is an amphiphilic molecule that contains an aminosugar, which at acid pH (as in the tumor environment) becomes positively charged. In fact, this amino group is responsible for the electrostatic interactions with cellular membranes. The PM contains some negatively charged lipid species that might be involved in this interaction, such as phosphatidic acid, phosphatidylglycerol, PS, and phosphatidylinositol. In MDA-MB-231 cells, the first two are the 0.5% of PM lipid content while the latter two each represent 4% of membrane lipids [135]. The literature has paid special attention to PS because this lipid is located on the inner leaflet of the PM in normal cells and translocates to the external leaflet in cancer cells. In our study, we confirmed that CPT1C silencing decreases PS in the PM, which in turn would correlate with a decreased interaction between DOX and the PM, reducing DOX uptake. For paclitaxel, a very hydrophobic molecule, electrostatic interaction is less representative. This could explain why in chemoresistance experiments, we found some differences between DOX and paclitaxel in MCF7 cells.

We explored the mechanism by which CPT1C is involved in PS presence in the PM. As stated in the Introduction, PS enrichment in the PM (against gradient) requires PI4P hydrolysis that SAC1 catalyzes in the ER. We know that CPT1C depletion reduces SAC1 activity in our model cells. An abolished SAC1 activity would prevent PS transference to the PM and then its accumulation in the ER, arresting PS production. Altogether, this would agree with the diminished PS levels detected in the PM and in total lysate in CPT1C-depleted MDA-MB-231 cells. However, it is harder to explain how CPT1C silencing leads to a decrease in SAC1

activity in MDA-MB-231 because it has actually been demonstrated and reported by our group that CPT1C is a negative modulator of SAC1 [136]. This probably occurs through an indirect mechanism that takes place in the absence of CPT1C. For example, Brechet et al. described in the brain that CPT1C deletion markedly reduces the interaction of SAC1 to the GluA1 protein [137]. In the same way, the absence of CPT1C in cancer cells could change SAC1 interaction with other partners, modulating in turn its activity. In addition, Zhong et al. confirmed an allosteric activation of SAC1 by anionic phospholipids as PS. Thus, the decreased levels of PS in CPT1C-silenced MDA-MB-231 cells could also decrease SAC1 activity [138].

Our results have also suggested that SAC1 and ABHD6 play a role in chemoresistance by CPT1C-independent mechanisms.

In summary, we propose that chemotherapy resistance derived from CPT1C silencing associates with a more rigid and less negative charged PM as a result of lipid composition remodeling (summarized in Fig. 65). This chemotherapy could be the result of the modulation of CPT1C through different proteins. In normal conditions CPT1C inhibits ABHD6 activity and somehow modulates SAC1, desaturase, and CPT1A activity. Conversely, CPT1C silencing results in the impairment of these proteins' activities. First, it leads to the inhibition of SAC1, which avoids PS translocation from the ER to the PM. The reduced PS presence in the PM decreases the electrostatic interaction between DOX and the PM. Second, CPT1C silencing can reduce desaturase activity, increasing the amount of saturated fatty acids. Finally, the absence of CPT1C provokes a decrease in FAO through CPT1A, which in turn increases saturated and monounsaturated fatty acid content and, concretely, palmitate content. This palmitate, as a precursor, will increase cellular sphingolipid synthesis. The enhanced amount of saturated and monounsaturated fatty acids and sphingolipids will result in a more rigid membrane less permeable to DOX, leading to chemoresistance. In addition, this lipid remodeling disrupts lipid rafts structure together with a more activated ABHD6 status contributes to cell invasion. More experiments are needed to corroborate this model. We are performing more experiments to deeper demonstrate this hypothesis.

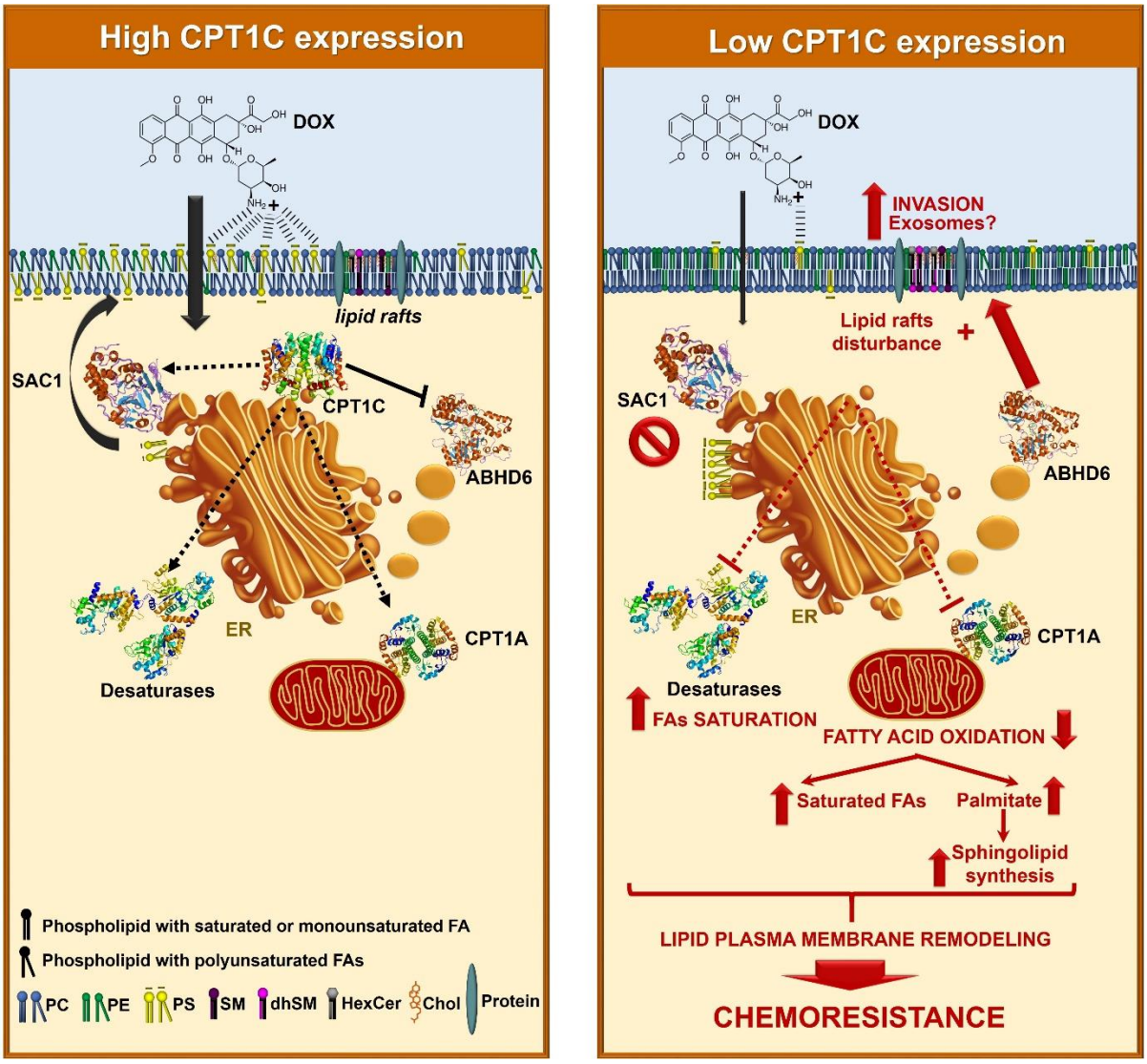

Fig. 65. Suggested molecular mechanism of breast cancer chemoresistance mediated by CPT1C silencing. Doxorubicin (DOX) uptake in control- (left panel) or shCPT1C- (right panel) MDA-MB-231 breast cancer cells. ER: endoplasmic reticulum; FA: fatty acid; PC: Phosphatidylcholine; PE: Phosphatidylethanolamine; PS: Phosphatidylserine; SM: sphingomyelin; dhSM: dihydrosphingomyelin; HexCer: hexosylceramide; Chol: cholesterol.

Clinical relevance of the results derived from this work

We have proposed that the relationship between p53 and CPT1C in chemoresistance has a potential prognostic value. In fact, the two tumor subtypes that have a higher prevalence of TP53 mutation, TNBC (80%) and HER2+ (72%) [139], are precisely those where we have seen that CPT1C plays a major role in response prediction to anthracycline treatment (pCR from ROC Plotter) and in survival (RFS of Kaplan-Meier Plotter). Nowadays, in clinical practice, TP53 mutation status is not generally considered given that its possible role in predicting response to chemotherapy in cancer patients remains inconclusive. In this thesis, we

demonstrated that the CPT1C gene may be a potential predictor gene in response to neoadjuvant anthracycline treatment, but it must be evaluated together with TP53 mutation status. Therefore, CPT1C has a prognostic value in TNBC and HER2-positive tumors depending on p53 levels.

One point has not been addressed in the experimental portion of this thesis but was mentioned in the Introduction. CPT1C silencing is directly related to the activation of senescence in cancer cells. The different stages of tumor progression can be summarized as presented in Figure 66.

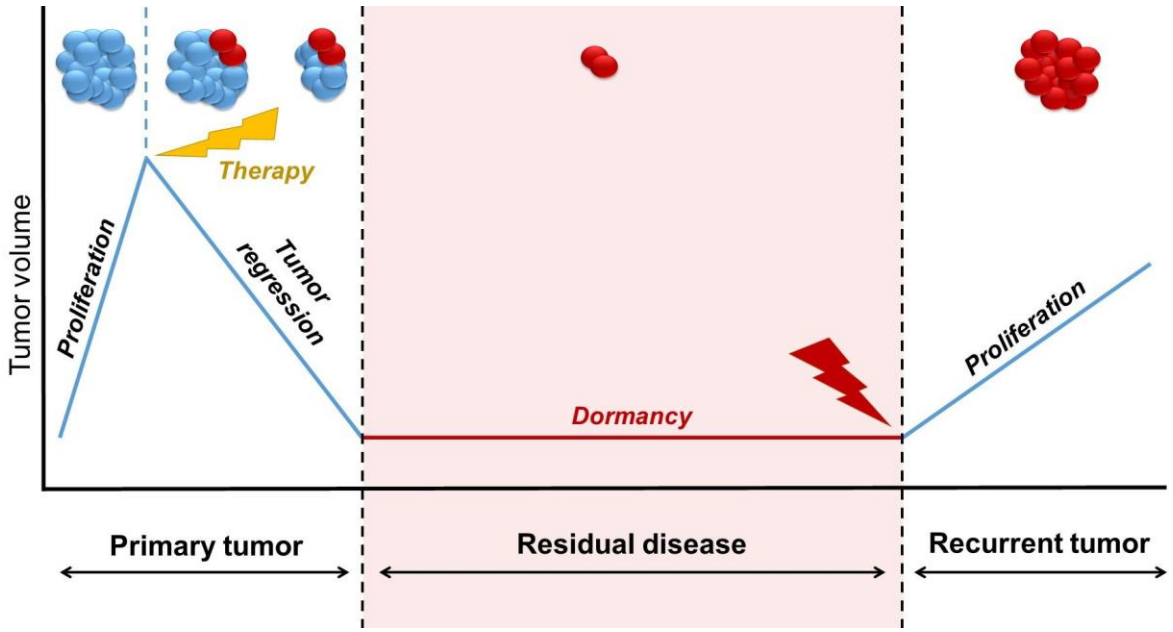

Fig. 66. Schematic representation of the different stages in cancer progression.

Normal breast cells can be transformed and become malignant through the activation of proliferation, leading to a tumor. Depending on the tumor type, this patient would be treated with chemotherapy drugs to provoke cell death, especially of proliferative cells. Unfortunately, some subpopulations of nonproliferative tumor cells are already present at the beginning of the tumor or as a consequence of the therapy, and they could remain in the body as quiescent/dormant/senescent/stem cells (to date, it is still not easy to distinguish among them). Precisely, these cells are commonly responsible for a later recurrence and relapse of tumors, as they are probably more resistant to initial therapy and subsequent treatments. The metabolic state of the tumor along the different stages is completely different because each stage highly differs in metabolic and energetic requirements. For example, proliferative cells do not need the same nutrients, nor they are subjected to the same oxidative stress as a

quiescent cell. Regarding the tumor microenvironment, a cancer cell located in the hypoxic center of a solid tumor will metabolically respond very differently than a cancer cell surrounded by a highly lipid-enriched metastatic environment, as in the brain or breast. Therefore, the proteins that regulate metabolism, as sensor proteins of energetic cell status like CPT1C, appear to be an interesting objective for development of targeted therapy. Given that CPT1C is a very downstream protein compared with others such as transcription factors, its modulation is more unlikely to lead to adverse effects in cancer and normal cells. It is crucial to know the specific characteristics of each tumor stage in order to develop more targeted therapeutic strategies and avoid the undesirable effects of repeated treatment doses.

The latest published papers about CPT1C and cancer propose CPT1C silencing as a potential strategy for cancer treatment to induce senescence to stop tumor proliferation. However, dormancy or senescence states have been clearly related to chemoresistance [140,141], which is one of the more evident causes of relapse in breast cancer. DOX, in fact, is known as an inductor of senescence and chemoresistance. Therefore, senescence stimulation by CPT1C depletion does not seem to be the most appropriate strategy for preventing recurrence in breast cancer.

Our findings point to the importance of a deeper knowledge of chemoresistance mechanisms for a better development of targeted drugs as nanoparticles. Additionally, our results demonstrate the key role of lipid membrane composition of cancer cells in chemotherapy resistance. This work suggests CPT1C as a good prognostic marker for neoadjuvant chemotherapy treatment approach in breast cancer.

CONCLUSIONS

CONCLUSIONS

The conclusions are that:

1. Low CPT1C expression is related to poor relapse-free survival in HER2+ and triple-negative breast cancer patients.
2. CPT1C silencing slightly enhances proliferation in normal conditions but not under glucose deprivation in breast cancer cells.
3. CPT1C silencing promotes invasion but not migration in MDA-MB-231 cells.
4. Depletion of CPT1C induces chemoresistance to DOX and paclitaxel in different breast cancer cells in 2D and 3D in vitro models. This chemoresistance associates with a diminished drug uptake in breast cancer cells.
5. CPT1C triggers lipid plasma membrane remodeling that results in a more rigid membrane which explains the reduced permeability to drugs and this is independent of SAC1 and ABHD6 activity.
6. CPT1C gene is a potential prognostic biomarker for neoadjuvant anthracycline treatment in HER2+ and triple-negative breast cancer patients.

REFERENCES

REFERENCES

1. Price NT, Van Der Leij FR, Jackson VN, et al. A novel brain-expressed protein related to carnitine palmitoyltransferase I. *Genomics*. 2002;80(4):433-442. doi:10.1006/geno.2002.6845

2. Casals N, Zammit V, Herrero L, Fadó R, Rodríguez-Rodríguez R, Serra D. Carnitine palmitoyltransferase 1C: From cognition to cancer. *Prog Lipid Res*. 2016;61:134-148. doi:10.1016/j.plipres.2015.11.004

3. Wolfgang MJ, Kurama T, Dai Y, et al. The brain-specific carnitine palmitoyltransferase-1c regulates energy homeostasis. *Proc Natl Acad Sci U S A*. 2006;103(19):7282-7287. doi:10.1073/pnas.0602205103

4. Fadó R, Rodríguez-Rodríguez R, Casals N. NC-ND license The return of malonyl-CoA to the brain: Cognition and other stories. *Prog Lipid Res*. 2021;81:101071. doi:10.1016/j.plipres.2020.101071

5. Schwenk J, Harmel N, Brechet A, et al. High-Resolution Proteomics Unravel Architecture and Molecular Diversity of Native AMPA Receptor Complexes. *Neuron*. 2012;74(4):621-633. doi:10.1016/j.neuron.2012.03.034

6. Brechet A, Buchert R, Schwenk J, et al. AMPA-receptor specific biogenesis complexes control synaptic transmission and intellectual ability. *Nat Commun*. 2017;8(1):1-14. doi:10.1038/ncomms15910

7. Palomo-Guerrero M, Fadó R, Casas M, et al. Sensing of nutrients by CPT1C regulates late endosome/lysosome anterograde transport and axon growth. *Elife*. 2019;8. doi:10.7554/eLife.51063

8. Casas M, Fadó R, Domínguez JL, et al. Sensing of nutrients by CPT1C controls SAC1 activity to regulate AMPA receptor trafficking. *J Cell Biol*. 2020;219(10). doi:10.1083/jcb.201912045

9. Miralpeix C, Reguera AC, Fosch A, et al. CPT1C negatively regulates the endocannabinoid hydrolase ABHD6 depending on nutritional status. *Br J Pharmacol*. January 2021:bph.15377. doi:10.1111/bph.15377

10. Rinaldi C, Schmidt T, Situ AJ, et al. Mutation in CPT1C associated with pure

autosomal dominant spastic paraplegia. *JAMA Neurol*. 2015;72(5):561-570. doi:10.1001/jamaneurol.2014.4769

11. Gao XF, Chen W, Kong XP, et al. Enhanced susceptibility of Cpt1c knockout mice to glucose intolerance induced by a high-fat diet involves elevated hepatic gluconeogenesis and decreased skeletal muscle glucose uptake. *Diabetologia*. 2009;52(5):912-920. doi:10.1007/s00125-009-1284-0

12. Rodríguez-Rodríguez R, Miralpeix C, Fosch A, et al. CPT1C in the ventromedial nucleus of the hypothalamus is necessary for brown fat thermogenesis activation in obesity. *Mol Metab*. 2019;19:75-85. doi:10.1016/j.molmet.2018.10.010

13. Pozo M, Rodrguez-Rodrguez R, Raḿrez S, et al. Hypothalamic regulation of liver and muscle nutrient partitioning by brain-specific carnitine palmitoyltransferase 1c in male mice. *Endocrinology*. 2017;158(7):2226-2238. doi:10.1210/en.2017-00151

14. Carrasco P, Sahún I, McDonald J, et al. Ceramide levels regulated by carnitine palmitoyltransferase 1C control dendritic spine maturation and cognition. *J Biol Chem*. 2012;287(25):21224-21232. doi:10.1074/jbc.M111.337493

15. Fadó R, Soto D, Miñano-Molina AJ, et al. Novel regulation of the synthesis of α-Amino-3-hydroxy-5-methyl-4-isoxazolepropionic Acid (ampa) receptor subunit glua1 by carnitine palmitoyltransferase 1C (CPT1C) in the Hippocampus. *J Biol Chem*. 2015;290(42):25548-25560. doi:10.1074/jbc.M115.681064

16. Gratacòs-Batlle E, Yefimenko N, Cascos-García H, Soto D. AMPAr interacting protein CPT1C enhances surface expression of GLuA1-containing receptors. *Front Cell Neurosci*. 2015;8(FEB). doi:10.3389/fncel.2014.00469

17. Carrasco P, Jacas J, Sahún I, et al. Carnitine palmitoyltransferase 1C deficiency causes motor impairment and hypoactivity. *Behav Brain Res*. 2013;256:291-297. doi:10.1016/j.bbr.2013.08.004

18. Mesmin B, Bigay J, Moser Von Filseck J, Lacas-Gervais S, Drin G, Antonny B. XA four-step cycle driven by PI(4)P hydrolysis directs sterol/PI(4)P exchange by the ER-Golgi Tether OSBP. *Cell*. 2013;155(4):830. doi:10.1016/j.cell.2013.09.056

19. Nagashima S, Tábara LC, Tilokani L, et al. Golgi-derived PI(4)P-containing vesicles drive late steps of mitochondrial division. *Science (80-)*. 2020;367(6484):1366-1371. doi:10.1126/science.aax6089

20. Del Bel LM, Brill JA. Sac1, a lipid phosphatase at the interface of vesicular and nonvesicular transport. *Traffic*. 2018;19(5):301-318. doi:10.1111/tra.12554

21. Waugh MG. The Great Escape: How phosphatidylinositol 4-kinases and PI4P promote vesicle exit from the Golgi (and drive cancer). *Biochem J*. 2019;476(16):2321-2346. doi:10.1042/BCJ20180622

22. Ijuin T, Takeuchi Y, Shimono Y, Fukumoto M, Tokuda E, Takenawa T. Regulation of CD44 expression and focal adhesion by Golgi phosphatidylinositol 4-phosphate in breast cancer. *Cancer Sci*. 2016;107(7):981-990. doi:10.1111/cas.12968

23. Tokuda E, Itoh T, Hasegawa J, et al. Phosphatidylinositol 4-phosphate in the golgi apparatus regulates cell-cell adhesion and invasive cell migration in human breast cancer. *Cancer Res*. 2014;74(11):3054-3066. doi:10.1158/0008-5472.CAN-13-2441

24. Poursharifi P, Madiraju SRM, Prentki M. Monoacylglycerol signalling and ABHD6 in health and disease. *Diabetes, Obes Metab*. 2017;19:76-89. doi:10.1111/dom.13008

25. Hullin-Matsuda F, Luquain-Costaz C, Bouvier J, Delton-Vandenbroucke I. Bis(monoacylglycero)phosphate, a peculiar phospholipid to control the fate of cholesterol: Implications in pathology. *Prostaglandins Leukot Essent Fat Acids*. 2009;81(5-6):313-324. doi:10.1016/j.plefa.2009.09.006

26. Pribasnig MA, Mrak I, Grabner GF, et al. Î±/Î² Hydrolase Domain-containing 6 (ABHD6) Degrades the Late Endosomal/Lysosomal Lipid Bis(monoacylglycero)phosphate*. *J Biol Chem*. 2015;290:29869-29881. doi:10.1074/jbc.M115.669168

27. Li F, Fei X, Xu J, Ji C. An unannotated α/β hydrolase superfamily member, ABHD6 differentially expressed among cancer cell lines. *Mol Biol Rep*. 2009;36(4):691-696. doi:10.1007/s11033-008-9230-7

28. Grüner BM, Schulze CJ, Yang D, et al. An in vivo multiplexed small-molecule screening platform. *Nat Methods*. 2016;13(10):883-889. doi:10.1038/nmeth.3992

29. Tang Z, Xie H, Heier C, et al. Enhanced monoacylglycerol lipolysis by ABHD6 promotes NSCLC pathogenesis. *EBioMedicine*. 2020;53:102696. doi:10.1016/j.ebiom.2020.102696

30. Makino A, Ishii K, Murate M, et al. D-threo-1-phenyl-2-decanoylamino-3-morpholino-1-

propanol alters cellular cholesterol homeostasis by modulating the endosome lipid domains. *Biochemistry*. 2006;45(14):4530-4541. doi:10.1021/bi052104y

31. Luquain-Costaz C, Lefai E, Arnal-Levron M, et al. Bis(monoacylglycero)phosphate accumulation in macrophages induces intracellular cholesterol redistribution, attenuates liver-X receptor/ATP-binding cassette transporter A1/ATP-binding cassette transporter G1 pathway, and impairs cholesterol efflux. *Arterioscler Thromb Vasc Biol*. 2013;33(8):1803-1811. doi:10.1161/ATVBAHA.113.301857

32. Reilly PT, Mak TW. Molecular pathways: Tumor cells Co-opt the brain-specific metabolism gene CPT1C to promote survival. *Clin Cancer Res*. 2012;18(21):5850-5855. doi:10.1158/1078-0432.CCR-11-3281

33. Nath A, Chan C. Genetic alterations in fatty acid transport and metabolism genes are associated with metastatic progression and poor prognosis of human cancers. *Sci Rep*. 2016;6. doi:10.1038/srep18669

34. Chen T, Wu G, Hu H, Wu C. Enhanced fatty acid oxidation mediated by CPT1C promotes gastric cancer progression. *J Gastrointest Oncol*. 2020;11(4):695-707. doi:10.21037/jgo-20-157

35. Cirillo A, Di Salle A, Petillo O, et al. High grade glioblastoma is associated with aberrant expression of ZFP57, a protein involved in gene imprinting, and of CPT1A and CPT1C that regulate fatty acid metabolism. *Cancer Biol Ther*. 2014;15(6):735-741. doi:10.4161/cbt.28408

36. Kim WT, Yun SJ, Yan C, et al. Metabolic pathway signatures associated with urinary metabolite biomarkers differentiate bladder cancer patients from healthy controls. *Yonsei Med J*. 2016;57(4):865-871. doi:10.3349/ymj.2016.57.4.865

37. Wang R, Cheng Y, Su D, et al. Cpt1c regulated by AMPK promotes papillary thyroid carcinomas cells survival under metabolic stress conditions. *J Cancer*. 2017;8(18):3675-3681. doi:10.7150/jca.21148

38. Sanchez-Macedo N, Feng J, Faubert B, et al. Depletion of the novel p53-target gene carnitine palmitoyltransferase 1C delays tumor growth in the neurofibromatosis type i tumor model. *Cell Death Differ*. 2013;20(4):659-668. doi:10.1038/cdd.2012.168

39. Ijuin T. Phosphoinositide phosphatases in cancer cell dynamics—Beyond PI3K and PTEN. *Semin Cancer Biol*. 2019;59:1044-1579. doi:10.1016/j.semcancer.2019.03.003

40. Zaugg K, Yao Y, Reilly PT, et al. Carnitine palmitoyltransferase 1C promotes cell survival and tumor growth under conditions of metabolic stress. *Genes Dev*. 2011;25(10):1041-1051. doi:10.1101/gad.1987211

41. Wang Y, Chen Y, Guan L, et al. Carnitine palmitoyltransferase 1C regulates cancer cell senescence through mitochondria-associated metabolic reprograming. *Cell Death Differ*. 2018;25(4):733-746. doi:10.1038/s41418-017-0013-3

42. Chen Y, Wang Y, Huang Y, et al. PPARα regulates tumor cell proliferation and senescence via a novel target gene carnitine palmitoyltransferase 1C. *Carcinogenesis*. 2017;38(4):474-483. doi:10.1093/carcin/bgx023

43. Chen Y, Zhou Y, Han F, et al. A novel miR-1291-ERRα-CPT1C axis modulates tumor cell proliferation, metabolism and tumorigenesis. *Theranostics*. 2020;10(16):7193-7210. doi:10.7150/thno.44877

44. Wu Y, Sarkissyan M, Mcghee E, Lee S, Vadgama J V. Combined inhibition of glycolysis and AMPK induces synergistic breast cancer cell killing. *Breast Cancer Res Treat*. 2015;151(3):529-539. doi:10.1007/s10549-015-3386-3

45. Wang B, Kohli J, Demaria M. Senescent Cells in Cancer Therapy: Friends or Foes? *Trends in Cancer*. 2020;6(10):838-857. doi:10.1016/j.trecan.2020.05.004

46. Guan L, Chen Y, Wang Y, et al. Effects of carnitine palmitoyltransferases on cancer cellular senescence. *J Cell Physiol*. 2019;234(2):1707-1719. doi:10.1002/jcp.27042

47. Lesko J, Triebl A, Stacher-Priehse E, et al. Phospholipid dynamics in ex vivo lung cancer and normal lung explants. *Exp Mol Med*. 2021;53(1):81-90. doi:10.1038/s12276-020-00547-x

48. Raynor A, Jantscheff P, Ross T, et al. Saturated and mono-unsaturated lysophosphatidylcholine metabolism in tumour cells: A potential therapeutic target for preventing metastases. *Lipids Health Dis*. 2015;14(1):69. doi:10.1186/s12944-015-0070-x

49. Cullis PR, Hope MJ. Chapter 1 Physical properties and functional roles of lipids in membranes. *New Compr Biochem*. 1991;20(C):1-41. doi:10.1016/S0167-7306(08)60329-4

50. Fajardo VA, McMeekin L, Leblanc PJ. Influence of phospholipid species on

membrane fluidity: A meta-analysis for a novel phospholipid fluidity index. *J Membr Biol*. 2011;244(2):97-103. doi:10.1007/s00232-011-9401-7

51. Ortega-Anaya J, Jiménez-Flores R. Symposium review: The relevance of bovine milk phospholipids in human nutrition—Evidence of the effect on infant gut and brain development. In: *Journal of Dairy Science*. Vol 102. Elsevier Inc.; 2019:2738-2748. doi:10.3168/jds.2018-15342

52. Tan ST, Ramesh T, Toh XR, Nguyen LN. Emerging roles of lysophospholipids in health and disease. *Prog Lipid Res*. 2020;80:101068. doi:10.1016/j.plipres.2020.101068

53. Zhang H, Wang Y, Guan L, et al. Lipidomics reveals carnitine palmitoyltransferase 1C protects cancer cells from lipotoxicity and senescence. *J Pharm Anal*. April 2020. doi:10.1016/j.jpha.2020.04.004

54. Maeda O, Ando T, Ohmiya N, et al. Alteration of gene expression and DNA methylation in drug-resistant gastric cancer. *Oncol Rep*. 2014;31(4):1883-1890. doi:10.3892/or.2014.3014

55. Wang Y, Yu T, Zhou Y, et al. Carnitine palmitoyltransferase 1C contributes to progressive cellular senescence. *Aging (Albany NY)*. 2020;12(8):6733-6755. doi:10.18632/aging.103033

56. Vert A, Castro J, Ribó M, Vilanova M, Benito A. Transcriptional profiling of NCI/ADR-RES cells unveils a complex network of signaling pathways and molecular mechanisms of drug resistance. *Onco Targets Ther*. 2018;11:221-237. doi:10.2147/OTT.S154378

57. Siegel RL, Miller KD, Jemal A. Cancer statistics, 2019. *CA Cancer J Clin*. 2019;69(1):7-34. doi:10.3322/caac.21551

58. Waks AG, Winer EP. Breast Cancer Treatment: A Review. *JAMA - J Am Med Assoc*. 2019;321(3):288-300. doi:10.1001/jama.2018.19323

59. Sridharan S, Howard CM, Tilley AMC, et al. Novel and Alternative Targets Against Breast Cancer Stemness to Combat Chemoresistance. *Front Oncol*. 2019;9:1003. doi:10.3389/fonc.2019.01003

60. Muley H, Fadó R, Rodríguez-Rodríguez R, Casals N. Drug uptake-based

chemoresistance in breast cancer treatment. *Biochem Pharmacol*. 2020;177. doi:10.1016/j.bcp.2020.113959

61. Peetla C, Vijayaraghavalu S, Labhasetwar V. Biophysics of cell membrane lipids in cancer drug resistance: Implications for drug transport and drug delivery with nanoparticles. *Adv Drug Deliv Rev*. 2013;65(13-14):1686-1698. doi:10.1016/j.addr.2013.09.004

62. Hankins HM, Baldridge RD, Xu P, Graham TR. Role of Flippases, Scramblases and Transfer Proteins in Phosphatidylserine Subcellular Distribution. *Traffic*. 2015;16(1):35-47. doi:10.1111/tra.12233

63. Alves AC, Ribeiro D, Nunes C, Reis S. Biophysics in cancer: The relevance of drug-membrane interaction studies. *Biochim Biophys Acta - Biomembr*. 2016;1858(9):2231-2244. doi:10.1016/j.bbamem.2016.06.025

64. Bernardes N, Fialho AM. Perturbing the dynamics and organization of cell membrane components: A new paradigm for cancer-targeted therapies. *Int J Mol Sci*. 2018;19(12). doi:10.3390/ijms19123871

65. Li Q, Shu Y. Role of solute carriers in response to anticancer drugs. *Mol Cell Ther*. 2014;2(1):15. doi:10.1186/2052-8426-2-15

66. Schulte RR, Ho RH. Organic anion transporting polypeptides: Emerging roles in cancer pharmacology. *Mol Pharmacol*. May 2019:490-506. doi:10.1124/mol.118.114314

67. Koepsell H, Lips K, Volk C. Polyspecific organic cation transporters: structure, function, physiological roles, and biopharmaceutical implications. *Pharm Res*. 2007;24(7):1227-1251. doi:10.1007/s11095-007-9254-z

68. Salatin S, Yari Khosroushahi A. Overviews on the cellular uptake mechanism of polysaccharide colloidal nanoparticles. *J Cell Mol Med*. 2017;21(9):1668-1686. doi:10.1111/jcmm.13110

69. Manzanares D, Ceña V. Endocytosis: The nanoparticle and submicron nanocompounds gateway into the cell. *Pharmaceutics*. 2020;12(4). doi:10.3390/pharmaceutics12040371

70. Behzadi S, Serpooshan V, Tao W, et al. Cellular uptake of nanoparticles: Journey

inside the cell. *Chem Soc Rev*. 2017;46(14):4218-4244. doi:10.1039/c6cs00636a

71. McMahon HT, Boucrot E. Molecular mechanism and physiological functions of clathrin-mediated endocytosis. *Nat Rev Mol Cell Biol*. 2011;12(8):517-533. doi:10.1038/nrm3151

72. Large DE, Soucy JR, Hebert J, Auguste DT. Advances in Receptor-Mediated, Tumor-Targeted Drug Delivery. *Adv Ther*. 2019;2(1):1800091. doi:10.1002/adtp.201800091

73. Chatterjee M, Ben-Josef E, Robb R, et al. Caveolae-mediated endocytosis is critical for albumin cellular uptake and response to albumin-bound chemotherapy. *Cancer Res*. 2017;77(21):5925-5937. doi:10.1158/0008-5472.CAN-17-0604

74. Donahue ND, Acar H, Wilhelm S. Concepts of nanoparticle cellular uptake, intracellular trafficking, and kinetics in nanomedicine. 2019. doi:10.1016/j.addr.2019.04.008

75. Prieto-Vila M, Takahashi R-U, Usuba W, Kohama I, Ochiya T. Drug Resistance Driven by Cancer Stem Cells and Their Niche. *Int J Mol Sci*. 2017;18(12). doi:10.3390/ijms18122574

76. Kou L, Sun J, Zhai Y, He Z. The endocytosis and intracellular fate of nanomedicines: Implication for rational design. *Asian J Pharm Sci*. 2013;8(1):1-10. doi:10.1016/j.ajps.2013.07.001

77. Gomes L, Sorgine M, Passos CLA, et al. Increase in fatty acids and flotillins upon resveratrol treatment of human breast cancer cells. *Sci Rep*. 2019;9(1):13960. doi:10.1038/s41598-019-50416-5

78. Finicle BT, Jayashankar V, Edinger AL. Nutrient scavenging in cancer. *Nat Rev Cancer*. 2018;18(10):619-633. doi:10.1038/s41568-018-0048-x

79. Palm W. Metabolic functions of macropinocytosis. *Philos Trans R Soc B Biol Sci*. 2019;374(1765):20180285. doi:10.1098/rstb.2018.0285

80. Ha KD, Bidlingmaier SM, Liu B. Macropinocytosis exploitation by cancers and cancer therapeutics. *Front Physiol*. 2016;7(SEP). doi:10.3389/fphys.2016.00381

81. Reif R, Adawy A, Vartak N, et al. Activated ErbB3 translocates to the nucleus via clathrin-independent endocytosis, which is associated with proliferating cells. *J Biol Chem*. 2016;291(8):3837-3847. doi:10.1074/jbc.M115.686782

82. Kettler K, Veltman K, van de Meent D, van Wezel A, Hendriks AJ. Cellular uptake of nanoparticles as determined by particle properties, experimental conditions, and cell type. *Environ Toxicol Chem*. 2014;33(3):481-492. doi:10.1002/etc.2470

83. Northfelt DW, Allred JB, Liu H, et al. Phase 2 trial of paclitaxel polyglumex with capecitabine for metastatic breast cancer. *Am J Clin Oncol Cancer Clin Trials*. 2014;37(2):167-171. doi:10.1097/COC.0b013e31826e0550

84. Fletcher JI, Williams RT, Henderson MJ, Norris MD, Haber M. ABC transporters as mediators of drug resistance and contributors to cancer cell biology. *Drug Resist Updat*. 2016;26:1-9. doi:10.1016/j.drup.2016.03.001

85. Mao Z, Shen K, Zhu L, et al. Comparisons of Cardiotoxicity and Efficacy of Anthracycline-Based Therapies in Breast Cancer: A Network Meta-Analysis of Randomized Clinical Trials. *Oncol Res Treat*. 2019;42(7-8):405-413. doi:10.1159/000500204

86. Shrestha B, Pokhrel AR, Darsandhari S, Parajuli P, Sohng JK, Pandey RP. Engineering Streptomyces peucetius for Doxorubicin and Daunorubicin Biosynthesis. In: Springer, Cham; 2019:191-209. doi:10.1007/978-3-030-01881-8_7

87. Fraguas-Sánchez AI, Martín-Sabroso C, Fernández-Carballido A, Torres-Suárez AI. Current status of nanomedicine in the chemotherapy of breast cancer. *Cancer Chemother Pharmacol*. 2019;84(4):689-706. doi:10.1007/s00280-019-03910-6

88. Peetla C, Bhave R, Vijayaraghavalu S, Stine A, Kooijman E, Labhasetwar V. Drug resistance in breast cancer cells: Biophysical characterization of and doxorubicin interactions with membrane lipids. *Mol Pharm*. 2010. doi:10.1021/mp100308n

89. Liu H, Liu Y, Zhang JT. A new mechanism of drug resistance in breast cancer cells: Fatty acid synthase overexpression-mediated palmitate overproduction. *Mol Cancer Ther*. 2008;7(2):263-270. doi:10.1158/1535-7163.MCT-07-0445

90. Fan S, Niu Y, Tan N, et al. LASS2 enhances chemosensitivity of breast cancer by counteracting acidic tumor microenvironment through inhibiting activity of V-ATPase proton pump. *Oncogene*. 2013;32(13):1682-1690. doi:10.1038/onc.2012.183

91. Tavares-Valente D, Baltazar F, Moreira R, Queirós O. Cancer cell bioenergetics and pH regulation influence breast cancer cell resistance to paclitaxel and doxorubicin. *J Bioenerg Biomembr*. 2013;45(5):467-475. doi:10.1007/s10863-013-9519-7

92. Wessely R, Schömig A, Kastrati A. Sirolimus and paclitaxel on polymer-based drug-eluting stents: Similar but different. *J Am Coll Cardiol*. 2006;47(4):708-714. doi:10.1016/j.jacc.2005.09.047

93. Fong A, Durkin A, Lee H. The Potential of Combining Tubulin-Targeting Anticancer Therapeutics and Immune Therapy. *Int J Mol Sci*. 2019;20(3):586. doi:10.3390/ijms20030586

94. Krens SD, Mcleod HL, Hertz DL. Pharmacogenetics, enzyme probes and therapeutic drug monitoring as potential tools for individualizing taxane therapy. *Pharmacogenomics*. 2013;14(5):555-574. doi:10.2217/pgs.13.33

95. Buxhofer-Ausch V, Secky L, Wlcek K, et al. Tumor-Specific Expression of Organic Anion-Transporting Polypeptides: Transporters as Novel Targets for Cancer Therapy. *J Drug Deliv*. 2013;2013:1-12. doi:10.1155/2013/863539

96. Dorman SN, Baranova K, Knoll JHM, et al. Genomic signatures for paclitaxel and gemcitabine resistance in breast cancer derived by machine learning. *Mol Oncol*. 2016;10(1):85-100. doi:10.1016/j.molonc.2015.07.006

97. Zhao M, Lei C, Yang Y, et al. Abraxane, the Nanoparticle Formulation of Paclitaxel Can Induce Drug Resistance by Up-Regulation of P-gp. Leggas M, ed. *PLoS One*. 2015;10(7):e0131429. doi:10.1371/journal.pone.0131429

98. Hisano T, Ono M, Nakayama M, Naito S, Kuwano M, Wada M. Increased expression of T-plastin gene in cisplatin-resistant human cancer cells: identification by mRNA differential display. *FEBS Lett*. 1996;397(1):101-107. doi:10.1016/s0014-5793(96)01150-7

99. Ma Y, Lai W, Zhao M, et al. Plastin 3 down-regulation augments the sensitivity of MDA-MB-231 cells to paclitaxel via the p38 MAPK signalling pathway. *Artif Cells, Nanomedicine, Biotechnol*. 2019;47(1):684-694. doi:10.1080/21691401.2019.1576707

100. Leroy B, Girard L, Hollestelle A, Minna JD, Gazdar AF, Soussi T. Analysis of TP53 Mutation Status in Human Cancer Cell Lines: A Reassessment. *Hum Mutat*. 2014;35(6):756-765. doi:10.1002/humu.22556

101. Roa-Mansergas X, Fadó R, Atari M, et al. CPT1C promotes human mesenchymal stem cells survival under glucose deprivation through the modulation of autophagy.

Sci Rep. 2018;8(1). doi:10.1038/s41598-018-25485-7

102. Sierra AY, Gratacós E, Carrasco P, et al. CPT1c is localized in endoplasmic reticulum of neurons and has carnitine palmitoyltransferase activity. *J Biol Chem*. 2008;283(11):6878-6885. doi:10.1074/jbc.M707965200

103. Suski JM, Lebiedzinska M, Wojtala A, et al. Isolation of plasma membrane-associated membranes from rat liver. *Nat Protoc*. 2014;9(2):312-322. doi:10.1038/nprot.2014.016

104. Győrffy B, Lanczky A, Eklund AC, et al. An online survival analysis tool to rapidly assess the effect of 22,277 genes on breast cancer prognosis using microarray data of 1,809 patients. *Breast Cancer Res Treat*. 2010;123(3):725-731. doi:10.1007/s10549-009-0674-9

105. Shimada K, Muhlich JL, Mitchison TJ. A tool for browsing the Cancer Dependency Map reveals functional connections between genes and helps predict the efficacy and selectivity of candidate cancer drugs. *bioRxiv*. December 2019:2019.12.13.874776. doi:10.1101/2019.12.13.874776

106. Bartha Á, Győrffy B. TNMplot.com: a web tool for the comparison of gene expression in normal, tumor and metastatic tissues. doi:10.1101/2020.11.10.376228

107. Korn EL, Freidlin B. Clinical Trial Designs in Oncology. In: *Abeloff's Clinical Oncology*. Elsevier; 2020:296-307.e2. doi:10.1016/B978-0-323-47674-4.00018-9

108. Administration D. *Clinical Trial Endpoints for the Approval of Cancer Drugs and Biologics Guidance for Industry*.; 2018. https://www.fda.gov/Drugs/GuidanceComplianceRegulatoryInformation/Guidances/default.htmand/orhttps://www.fda.gov/BiologicsBloodVaccines/GuidanceComplianceRegulatoryInformation/Guidances/default.htm. Accessed March 11, 2021.

109. Wu B, Tao L, Yang D, Li W, Xu H, He Q. Development of an Immune Infiltration-Related Eight-Gene Prognostic Signature in Colorectal Cancer Microenvironment. *Biomed Res Int*. 2020;2020. doi:10.1155/2020/2719739

110. Hanahan D, Weinberg RA. Hallmarks of cancer: The next generation. *Cell*. 2011;144(5):646-674. doi:10.1016/j.cell.2011.02.013

111. Koboldt DC, Fulton RS, McLellan MD, et al. Comprehensive molecular portraits of human breast tumours. *Nature*. 2012;490(7418):61-70. doi:10.1038/nature11412

112. Administration D. *Clinical Trial Endpoints for the Approval of Cancer Drugs and Biologics Guidance for Industry*.; 2018. https://www.fda.gov/Drugs/GuidanceComplianceRegulatoryInformation/Guidances/default.htmand/orhttps://www.fda.gov/BiologicsBloodVaccines/GuidanceComplianceRegulatoryInformation/Guidances/default.htm. Accessed February 25, 2021.

113. Distant Metastasis Free Survival - an overview | ScienceDirect Topics. https://www.sciencedirect.com/topics/medicine-and-dentistry/distant-metastasis-free-survival. Accessed February 25, 2021.

114. Algorashi I, Goldvaser H, Ribnikar D, Cescon DW, Amir E. Evolution in sites of recurrence over time in breast cancer patients treated with adjuvant endocrine therapy. *Cancer Treat Rev*. 2018;70:138-143. doi:10.1016/j.ctrv.2018.08.009

115. National Cancer Institute. Neuroblastoma Treatment PDQ. *PDQ*. 2012;(Md):1-81. https://www.cancer.gov/types/neuroblastoma/hp/neuroblastoma-treatment-pdqtoma/HealthProfessional. Accessed February 12, 2021.

116. Ananda S, Nowak AK, Cher L, et al. Phase 2 trial of temozolomide and pegylated liposomal doxorubicin in the treatment of patients with glioblastoma multiforme following concurrent radiotherapy and chemotherapy. *J Clin Neurosci*. 2011;18(11):1444-1448. doi:10.1016/j.jocn.2011.02.026

117. Fekete JT, Győrffy B. ROCplot.org: Validating predictive biomarkers of chemotherapy/hormonal therapy/anti-HER2 therapy using transcriptomic data of 3,104 breast cancer patients. *Int J Cancer*. 2019;145(11):3140-3151. doi:10.1002/ijc.32369

118. Spring LM, Fell G, Arfe A, et al. Pathological complete response after neoadjuvant chemotherapy and impact on breast cancer recurrence and survival: a comprehensive meta-analysis. 2020. doi:10.1158/1078-0432.CCR-19-3492

119. Cortazar P, Zhang L, Untch M, et al. Pathological complete response and long-term clinical benefit in breast cancer: The CTNeoBC pooled analysis. *Lancet*. 2014;384(9938):164-172. doi:10.1016/S0140-6736(13)62422-8

120. van Blitterswijk WJ, Hilkmann H, van der Meer BW. Quantitative Contributions of Cholesterol and the Individual Classes of Phospholipids and Their Degree of Fatty Acyl (Un)Saturation to Membrane Fluidity Measured by Fluorescence Polarization. *Biochemistry*. 1987;26(6):1746-1756. doi:10.1021/bi00380a038

121. Sommer SG. The role and clinical applications of bioactive lysolipids in ovarian cancer. *J Soc Gynecol Investig*. 2001;8(1):1-13. doi:10.1177/107155760100800101

122. Goñi FM, Alonso A. Biophysics of sphingolipids I. Membrane properties of sphingosine, ceramides and other simple sphingolipids. *Biochim Biophys Acta - Biomembr*. 2006;1758(12):1902-1921. doi:10.1016/j.bbamem.2006.09.011

123. Kinoshita M, Kyo T, Matsumori N. Assembly formation of minor dihydrosphingomyelin in sphingomyelin-rich ordered membrane domains. *Sci Rep*. 2020;10(1):11794. doi:10.1038/s41598-020-68688-7

124. Cruz ALS, Barreto E de A, Fazolini NPB, Viola JPB, Bozza PT. Lipid droplets: platforms with multiple functions in cancer hallmarks. *Cell Death Dis*. 2020;11(2):1-16. doi:10.1038/s41419-020-2297-3

125. Mirzayans R, Andrais B, Scott A, Murray D. New insights into p53 signaling and cancer cell response to DNA damage: Implications for cancer therapy. *J Biomed Biotechnol*. 2012;2012. doi:10.1155/2012/170325

126. Zhang C, Liu J, Xu D, Zhang T, Hu W, Feng Z. Gain-of-function mutant p53 in cancer progression and therapy. *J Mol Cell Biol*. 2020;12(9):674-687. doi:10.1093/jmcb/mjaa040

127. Zhou G, Wang J, Zhao M, et al. Gain-of-Function Mutant p53 Promotes Cell Growth and Cancer Cell Metabolism via Inhibition of AMPK Activation. *Mol Cell*. 2014;54(6):960-974. doi:10.1016/j.molcel.2014.04.024

128. Chen P, Zhang Q, Zhang H, et al. Carnitine palmitoyltransferase 1C reverses cellular senescence of MRC-5 fibroblasts via regulating lipid accumulation and mitochondrial function. *J Cell Physiol*. 2021;236(2):958-970. doi:10.1002/jcp.29906

129. Wang Z, Jiang Q, Dong C. Metabolic reprogramming in triple-negative breast cancer. *Cancer Biol Med*. 2020;17(1):44-59. doi:10.20892/j.issn.2095-3941.2019.0210

130. Kruger S, Elmageed ZYA, Hawke DH, et al. Molecular characterization of exosome-like vesicles from breast cancer cells. *BMC Cancer*. 2014;14(1). doi:10.1186/1471-2407-14-44

131. Pike LJ. Lipid rafts: Bringing order to chaos. *J Lipid Res*. 2003;44(4):655-667. doi:10.1194/jlr.R200021-JLR200

132. Raghu H, Sodadasu PK, Malla RR, Gondi CS, Estes N, Rao JS. Localization of uPAR and MMP-9 in lipid rafts is critical for migration, invasion and angiogenesis in human breast cancer cells. *BMC Cancer*. 2010;10(1):647. doi:10.1186/1471-2407-10-647

133. Rudolf M, Mohi A, Dettbarn MC, et al. Detection of esterified cholesterol in murine bruch's membrane wholemounts with a perfringolysin O-based cholesterol marker. *Investig Ophthalmol Vis Sci*. 2014;55(8):4759-4767. doi:10.1167/iovs.14-14311

134. Lee J, Wolfgang MJ. Metabolomic profiling reveals a role for CPT1c in neuronal oxidative metabolism. *BMC Biochem*. 2012;13(1). doi:10.1186/1471-2091-13-23

135. Szlasa W, Zendran I, Zalesińska A, Tarek M, Kulbacka J. Lipid composition of the cancer cell membrane. *J Bioenerg Biomembr*. 2020;52(5):321-342. doi:10.1007/s10863-020-09846-4

136. Casas M, Fadó R, Domínguez JL, et al. Sensing of nutrients by CPT1C controls SAC1 activity to regulate AMPA receptor trafficking. *J Cell Biol*. 2020;219(10). doi:10.1083/jcb.201912045

137. Brechet A, Buchert R, Schwenk J, et al. AMPA-receptor specific biogenesis complexes control synaptic transmission and intellectual ability. *Nat Commun*. 2017;8(1):1-14. doi:10.1038/ncomms15910

138. Zhong S, Hsu F, Stefan CJ, et al. Allosteric activation of the phosphoinositide phosphatase Sac1 by anionic phospholipids. *Biochemistry*. 2012;51(15):3170-3177. doi:10.1021/bi300086c

139. Koboldt DC, Fulton RS, McLellan MD, et al. Comprehensive molecular portraits of human breast tumours. *Nature*. 2012;490(7418):61-70. doi:10.1038/nature11412

140. Wang B, Kohli J, Demaria M. Senescent Cells in Cancer Therapy: Friends or Foes? *Trends in Cancer*. 2020;6(10):838-857. doi:10.1016/j.trecan.2020.05.004

141. O'Reilly EA, Gubbins L, Sharma S, et al. The fate of chemoresistance in triple negative breast cancer (TNBC). *BBA Clin*. 2015;3:257-275. doi:10.1016/j.bbacli.2015.03.003